UNIVERSITY OF SOUTHAMPTON

FACULTY OF ENGINEERING, SCIENCE AND MATHEMATICS

School of Engineering Sciences

SIMULATION OF TISSUE DIFFERENTIATION IN UNCEMENTED HIP IMPLANTS BASED ON A MECHANOREGULATORY HYPOTHESIS

by

Pramod Kumar Puthumanapully

Thesis for the degree of Doctor of Philosophy

October 2010

UNIVERSITY OF SOUTHAMPTON

ABSTRACT

FACULTY OF ENGINEERING, SCIENCE AND MATHEMATICS
SCHOOL OF ENGINEERING SCIENCES

Doctor of Philosophy

SIMULATION OF TISSUE DIFFERENTIATION IN UNCEMENTED HIP IMPLANTS BASED ON A MECHANOREGULATORY HYPOTHESIS

By Pramod Kumar Puthumanapully

The proportion of uncemented implant procedures carried out annually worldwide is increasing, with improved clinical outcomes for young and old patients alike. However, their success depends largely on their ability to achieve good initial stability and long term bone ingrowth. There are a number of factors that govern this process and failure to integrate with surrounding bone could lead to loosening. Implant design factors are important with respect to implant/bone integration, and their shape, size and, if there is a coating present, the nature of coating, may be optimised to promote bone ingrowth around the implant. To this end, novel preclinical testing tools have been developed using computational methods, with the aim of predicting the response of bone to the implant.

This thesis describes the development and application of a novel algorithm that simulates tissue differentiation around implants using finite element methods, to study design features that could promote bone formation at the interface. To illustrate the capabilities of the algorithm, a series of case studies were undertaken which focussed on the porous coating and implant geometries. The results were then compared to clinical data for corroboration. The effect of implant geometry was investigated by simulating tissue differentiation around short stemmed and long stemmed implants. For short stemmed implants, the beneficial role of shape, size and specific design features such as the lateral flare were highlighted. For conventional, diaphyseal filling long stemmed implants, tissue differentiation around the implant, and the influence of different porous coating lengths on bone formation at the interface was investigated. It was predicted that bone formation occurs more on the distal aspects of the stem and did not vary much with coating length. No added advantage in terms of the bone formation was observed for proximal coated implants. Given the relatively similar performance, using the porous coating over the entire length of the implant was favoured in light of the increased surface area available for ingrowth. As a final case study, the algorithm was employed in a microscale study of a sintered beaded coating, to investigate the effect of micromotion on tissue differentiation. The results suggested that micromotion had a strong influence on bone formation at the interface. In addition, it was found that a two layered porous structure appeared to promote more bone formation than the typically used three layered coatings for similar micromotion levels.

The results obtained from the aforementioned case studies corroborated well with clinical data and clearly demonstrated the efficacy of the algorithm in simulating tissue differentiation around uncemented implants and highlighted the importance of design features in promoting bone ingrowth and securing a stable fixation.

TABLE OF CONTENTS

LIST OF FIGURES

LIST OF TABLES

GLOSSARY OF TERMS AND ABBREVIATIONS

Anastomosis	Connection of structures (mostly blood vessels)
Anisotropy	Material properties that vary depending on the orientation of the specimen
Aseptic	Of not relating to microbes like bacteria
Atrophy	Loss in density or size of a region (in this case bone)
BW	Body weight
BMD	Bone mineral density
CT	Computer tomography
Chondrogenesis	Process of forming cartilage
Deviatoric stress	Stresses that act to distort the original volume
Diaphysis	Mid section of a long bone
Dilatational stress	Stresses that act to change the original volume
DOF	Degrees of freedom
Endosteum	Inner surface of bone in contact with the implant
Epiphysis	Rounded sections at the ends of a long bone that encompasses part of a joint
FE	Finite element
Fibrogenesis	Process of forming fibrous tissue
HA	Hydroxyapatite
Haematoma	Localised collection of blood as a result of haemorrhage
Haematopoiesis	Formation of blood cells (especially in the marrow)
Haematopoietic	Of relating to blood
Homeostasis	Metabolic equilibrium through internal regulation
Hypertrophy	Densification/enlargement of a region
Hypoxia	Shortage of oxygen
Lamellar bone	Bone laid down after woven bone
Lysis	Death of cells in a region
Metaphysis	Wide region of a long bone that lies between the epiphysis and diaphysis
MSC	Mesenchymal stem cells
Ossification	Process of bone formation

Osteotomy	Cutting of bone to change its size and shape
Periosteum	Outer surface of bone in contact with soft tissues
ROM	Range of motion
THA	Total hip arthroplasty
THR	Total hip replacement
Tissue differentiation	The change of a specific type of tissue to form other tissues
TJR	Total joint replacement
Woven bone	Newly laid down bone

DECLARATION OF AUTHORSHIP

I, **Pramod Kumar Puthumanapully,** declare that the thesis entitled "**Simulation of Tissue Differentiation in Uncemented Hip Implants based on a Mechanoregulatory Hypothesis"** and the work presented in the thesis are both my own, and have been generated by me as the result of my own original research. I confirm that:

- This work was done wholly or mainly while in candidature for a research degree at this University;
- Where any part of this thesis has previously been submitted for a degree or any other qualification at this University or any other institution, this has been clearly stated;
- There I have consulted the published work of others, this is always clearly attributed;
- Where I have quoted from the work of others, the source is always given. With the exception of such quotations, this thesis is entirely my own work;
- I have acknowledged all main sources of help;
- Where the thesis is based on work done by myself jointly with others, I have made clear exactly what was done by others and what I have contributed myself;
- Parts of this work have been published, as stated in Chapter 9 (APPENDIX F)

Signed: ……..

Date: ……..

ACKNOWLEDGEMENTS

Where do I start? Hmmm... One of the many questions I asked myself at the start of the PhD and although I've pretty much gone through the five W's (mostly the WHY's) in varying degrees over the last 4 years, I always managed to find a way, and so I do so now. There are many people whose support and help has been invaluable to the production of this fine, awe-inspiring work; yes, you are all equal contributors to this and accountable if it fails to create the necessary scientific impact.

Firstly, mom and dad, for being THE best support structure ever (feeding me, educating me, putting up with my whims and tantrums, allowing me to be here, etc....well you know best the associated traumas having known me the longest [1]). Bro, my never ending source of inspiration and the reason I'm doing this. My Sis 'n law & Tikki (in your special 3 year old way) who've been nothing but caring and supportive through some traumatic times. Special mention of Juno, for all the unconditional barks and slobbering love showered on me when I go back home every year; thanks for missing me and making me feel special.

Now that the entrees are done, I can concentrate on thanking the people involved in this project and my life here in wonderful Southampton. My supervisors, Dr. Martin "the boss/bossman" Browne, the absolute best a student can ask for. I would've given up at various stages (mostly years 1, 2, 3 and 4) if not for your support and guidance. Andy New, the Ansys guru for setting it all up. My colleagues in the office; I did promise I was going to mention each of you by name with an appropriate addendum so here goes. Alex, my main hombre and partner in numerous shenanigans. Mon-Thurs would've been an absolute drag if not for your "mini" and the back rows of Cineworld. Catherine, for the constant encouragements and forwarding important emails that'd mysteriously been deleted by me. Becky, for coining the now renowned and revered moniker "Prammy". Caro, for putting up with my version of Spanish. Hamid 'I'll let you know' Alidousti and Hatice 'holiday' Ozturk for being your wonderful selves and not ever making me feel like the only strange and crazy one in the office, and for the innumerable awesome times and culinary escapades (& Asa, et tu, for aforementioned and the crazy hair and hours in front of the tiniest TV ever). Pete, my back would be sore everyday if not for your loving fingers. Mike, for excessive gaming and surpassing my specialness. Mav, for a number of things that I dare not mention here. Francis, resident food connoisseur and creator extraordinaire of Cake Friday. Aida and Gav, for the many masterplans and their epic aftermaths. Mari, for the countless hugs and the Rhubarb cake. Fayester, for being equally gym crazy and fellow companion in getting injured, and Sibbles for putting a roof over my head, bringing back people to my room at 4am and general merriment. Not to forget, all the newbie lot, Orestis, Fede, Jon and the team at Glen. You guys are all LEGEN, wait for it...DARY. Special thanks to all the admin staff, Gwyneth, Alessia, Julia, Sally, and also the finance ladies, Glenda, Dawn and Sonya for putting up through my troublemaking efforts.

Last but not the least, to the little yellow canary who has been an integral part of my life through most of this, a heartfelt thank you for all the encouragement, support and chirps you gave me. Oh, and well done me too (pat on the back) for the enormous effort and pulling through... eventually.

1. Parents et al., (1982-present). Life of Pramod, the triumphs, tribulations and craziness. Incomplete article. To be published, circa 2050.

CHAPTER 1

INTRODUCTION

This section introduces the background behind the research and provides an overview of the research encompassed in this thesis along with its relevance and importance to current implant designs.

Quality of life has improved considerably over the years thanks to advances in medicine and living conditions. However, many diseases and ailments still exist and some are even on the rise, reducing and hindering the quality of life, especially among people aged 50 and older. In this age group, one of the most prevalent afflictions is arthritis, which involves the wear, tear and degradation of joint surfaces. Arthritis is thought to be associated with old age, obesity, infection, a faulty immune system and lifestyle among other factors. The hip and the knee are the most frequently affected joints, where the condition can be very painful and debilitating.

The hip joint in particular is one of the most vulnerable to diseases and impairment. This is mainly due to the range of movement and extensive use of the joint in daily activities. In addition, the whole of the body weight is transferred through the joint, making it highly susceptible to failure. Total hip replacements (THR) or hip arthroplasties have been sporadically performed since the early 1900's in various forms but have only come in to prominence as a safe and tested method since the 1960's. The Swedish joint register, one of the oldest joint registers, records that in the late 1960's there were only 6 operations carried out in Sweden as opposed to 14,000+ operations in 2007, clearly indicating the success of the procedure through the years [1]. Traditionally, hip replacements have been used for the older patient population (>60 years). As an example, the same register also states that between 1992 and 1999, there were 5 times more procedures for patients over 60 years as opposed to those younger than 60 years. However, this trend is changing, with the number of younger patients undergoing THRs increasing every year [2].

There are two main methods of fixation of THRs, cemented fixation and uncemented fixation. Cemented implants use bone cement as a grout and filler to fix and hold the implant in position. Uncemented implants do not use bone cement and rely primarily on a mechanical interlock with the surrounding bone for initial stabilization, coupled with bone ingrowth or osseointegration after a few months to secure a stable fixation. Cementing has been the preferred choice of surgeons, especially since the advent of bone cement and its successful use by Sir John Charnley in the late 1960s. For the older patient demographic, cemented techniques offer increased longevity and less need for revision [1-4]. This is for the most part due to the age group and the level of activity the patient engages in. An older patient would typically not have a very active lifestyle, and considering the poor bone stock associated with the demographic in that age group, the use of cement would be the best choice. In addition, the long term detrimental effects of using bone cement such as thermal and chemical necrosis, cement particle osteolysis and interface debonding would not be as prevalent as in younger patients.

Uncemented or cementless implants, introduced in the 1980s, rely on a good interference fit and frictional interlock with the surrounding bone to achieve primary stability. They are then stabilized further by bone ingrowth. This is achieved through certain design features such as roughened or porous surfaces, porous coatings, or osteoconductive coatings to encourage bone to grow into them to form a continuous interface from the surrounding bone to the implant. If successful, long term

stability should then achieved, and avoid the many problems associated with bone cement. It is on this premise that cementless implants are being used increasingly for younger patients who need the implants to last considerably longer than older patients. In addition, young patients also have better quality of bone which is suitable for this type of fixation. However, a major concern remains: if bone ingrowth cannot be achieved, there is a high possibility that the interface could weaken over time, leading to implant failure. Whether the implantation is cemented or uncemented, aseptic loosening has been the leading cause of implant failure and subsequent revision for many years [1,2].

A combination of mechanical and biological factors governs the type of tissues formed at the implant-bone interface. Mechanical factors have been researched extensively, with retrieval studies and supplementary animal studies carried out to formulate hypotheses that can provide a qualitative if not quantitative description of the tissue formation process [5-8]. Biological factors such as hormone regulation, cell migration, differentiation, proliferation, cell death etc. are less well documented clinically due to the difficulty in obtaining data specifically related to tissue formation at the interface.

Regarding mechanical factors, it has been hypothesised that high levels of micromotion, almost always leads to the formation of fibrous tissue at the interface [7]. Fibrous tissue is an interface tissue that has weak mechanical properties and may not be able to sustain continued loading on the hip, leading to implant loosening. Additional mechanical parameters such as high strains, stresses, and pressure are also believed to lead to the formation of this weak tissue and compromise the stability of the implant [9]. Bone and other stronger tissues only permeate or grow on to the surface of the implant if there is a low mechanical stimulus at the interface. Studies have confirmed new bone formation at very low stimuli [6,7,10,11]. Therefore it is imperative that for cementless implants, bone ingrowth or the formation of stronger tissues is encouraged by lowering the mechanical stimulus at the interface. To this end, there have been many studies conducted on uncemented implants, looking at the type of coatings used, be it a simple roughened grit blasted surface or a complex network of fibres of beads [12-14]. In addition, there have also been implant design factor studies that have aimed to reduce interface stresses and micromotion to encourage the formation of osseous tissue at the interface. Some of the more popular resultant design changes include the addition of a proximal collar, long stems to engage the diaphysis and provide better fit in the femoral canal, short stemmed implants to engage the proximal femur and flare designs to reduce micromotion due to torque and fit the metaphysis.

Pre-clinical testing of implants can be a useful tool to evaluate key design features and their clinical relevance [15]. Originally, testing was restricted to experimental setups, but with the advent of high end computing, computational finite element (FE) methods can provide more flexible and diverse methods of testing the implant. FE methods have become commonplace in biomechanics since the 1990s and exhaustive studies have been carried out on implant designs, especially of the hip and

the knee. They have also been combined with musculoskeletal models, which can represent the influence of muscle forces acting on the hip and the femur [16]. Most of the data from these musculoskeletal models have come from gait analysis data. Gait analysis using telemetrised implants and force plates have helped understand forces acting on the femur and the implant during activities such as normal walking, stair climbing and jogging [17,18]. These models also allow different parameters to be changed and tested with ease, which would normally take a lot longer in an experiment. In addition, it's now possible to apply non-homogenous material properties to tissues using non-invasive scan techniques such as magnetic resonance imaging (MRI) and computed tomography (CT) [19], allowing an alternative to the linear isotropic material properties that have historically been used for tissues in FE models. Such non-invasive techniques can also help recreate an accurate geometry for the bone. Thus, a better understanding of the functioning of the implant in the body may be achieved and the effects of specific design features of the implant may be ascertained.

FE models have also been used to study bone response to mechanical stimuli [20-22]. These models come under the field of mechanobiology, which can be broadly defined as the study of the effects of mechanical or physical conditions on regulating biological tissues. This concept was first postulated in the 1800's by Roux, as part of the theory of functional adaptation and has been researched ever since. Mechanobiology can be addressed on four main levels, the molecular, cellular, tissue and organ levels. Bone would thus come under the tissue level, with stimuli such as stress, strain, fatigue and pressure influencing its regulation and properties. An apt and frequently used example would be the process of fracture healing; with good stabilisation and immobilisation a fracture would heal quicker which implies that mechanical stimuli should be low. Various types of fracture healing hypotheses have been studied, with emphasis on the type and influence of individual stimuli acting at the fracture site to reproduce the clinical scenario. The hypotheses have varied from treating bone as an isotropic single phase tissue to a biphasic tissue with fluid and solid components [8,23,24]. Most of these hypotheses are based on rules of specific stimuli acting at the site and have been able to simulate fracture healing accurately. The steps involved in bone healing still hold generally for when a joint prosthesis is implanted, including the formation of a haematoma, invasion of cells and formation of fibrous tissue. The concept of fracture healing can thus be applied and modified to simulate the formation of different types of tissues around the implant. This is particularly important in the case of uncemented implants as bone ingrowth is essential for longevity and the avoidance of implant loosening.

Research specifically dealing with tissue differentiation around implants has been limited, and the focus of the present work is focussed to extend the knowledge obtained from previous fracture healing hypotheses to simulate tissue differentiation. The work presented in this thesis aims to simulate bone formation and tissue differentiation around uncemented hip implants by employing finite element methods in combination with a mechanoregulatory hypothesis. A new algorithm is developed based on a mechanoregulatory hypothesis to simulate tissue differentiation. The

algorithm is then applied in a series of case studies that look at design features that have been postulated as affecting bone ingrowth. The first study focuses on a recent development in uncemented implant design, that of short stemmed implants, as applied to young patients with good bone quality in the proximal femur. These types of implant are proposed to provide improved loading on the femur and increased osseointegration, Specific design features are investigated and the results corroborated with clinical studies. The second study focuses on a well known and clinically successful uncemented implant and investigates the factors that contribute to the types of tissues formed around the implant, including the design, extent of the porous coating and the use of a long stem for distal fixation. A third study focuses on a popular type of porous coating used in uncemented implants and provides a microscale model of tissue differentiation at that level. The influence of using multiple layers for the porous coating is also investigated as in a separate case study.

All of the aforementioned studies have aimed to present a clearer picture of tissue differentiation around uncemented implants through the use of computational methods. Design factors that would usually warrant rigorous experimental investigations through animal and clinical studies are explored and their inclusion or exclusion in an implant, justified. The computational approach described in this thesis allows the evaluation of uncemented implant design with regards to osseointegration at the conceptual stage and the possible elimination of dubious and faulty design before mechanical testing.

CHAPTER 2

LITERATURE REVIEW

Simulating tissue differentiation at the bone-implant interface is a complex process and involves a number of factors. The following literature review aims to inform the reader as to what factors can affect the tissue differentiation process through a progressive explanation from the basics of bone anatomy, the femur and the functioning of the hip joint, through to a description of hip replacements, with emphasis on uncemented implants and the design features they employ to secure fixation. The concept of mechanobiology and the underlying premise of fracture fixation, both crucial to simulating tissue differentiation at the interface are then detailed and the theory behind them explained.

2.1 BONE

2.1.1 INTRODUCTION

Bone is a complex, highly organised and specialised connective tissue. It is characterised physically by its hardness, rigidity and strength, and microscopically by cellular and intercellular substance formed of mineralized fibres. Bone tissue performs a multitude of functions that could be mechanical, for example, providing the basic framework of the body, support, protection for internal organs, movement etc or physiological functions like mineral homeostasis, blood cell production through haemopoiesis, and triglyceride storage. In terms of shape, there are five different bone types in the body:

Long bones – are bones that have their lengths greater than their widths and associated with large movement. They are long and cylindrical with a shaft (diaphysis) and two expanded ends (epiphyses). They act as levers to transmit forces. The epiphyses have cartilage at their ends to articulate with other bones. The outer layer of the bone is hard, and is called "compact bone". The inside of the bone is spongy, called "cancellous bone". Examples of long bones include the femur, the humerus and the phalanges.

Short bones – are smaller bones and often cube shaped, associated with smaller more complex movements. They do not possess a shaft like structure like the long bones and are normally made of cancellous bone with a thin layer of compact bone at the outer surface. They provide strength and help transmit longitudinal forces. Examples of short bones include the carpals of the hand and the tarsals of the feet.

Flat bones – are flat and plate shaped. They are extremely thin and their functions include providing attachment points for muscles and protection to internal organs. They normally consist of cancellous bone sandwiched between two layers of compact bone. Most of the bone marrow in adults is formed in flat bones. Examples of flat bones include the cranial bones, ribs, sternum, scapula and the pelvic girdle.

Sesamoid bones – are special bones that develop in some tendons in locations where there is considerable friction, tension, and physical stress. They primarily act to protect the tendon. They do so by increasing the moment arm by altering the location of the tendon further away from the centre of the joint. Examples of Sesamoid bones include the patella or the knee cap and the Sesamoid bones of the feet.

Irregular bones- are peculiar shaped bones that cannot be grouped into any of the above-mentioned categories. They serve unique purposes in the body like protection, attachment

sites for muscles and support. Examples of these bones include the vertebrae, sacrum, hyoid etc.

2.1.2 BONE COMPOSITION

Bone tissue consists of an organic component, an inorganic component, cells and water. The inorganic component account for 60-75% of the weight, about 45% of the total volume and is mostly the mineral Hydroxyapatite. The organic phase of the bone tissue is mainly the matrix, which consists of collagen and noncollagenous proteins. It accounts for 30-35% of the volume. The rest of the tissue, around 25% of the volume is made of water of which 60% is bound to collagen and around 40% is free.

2.1.2.1 ORGANIC COMPONENT

The organic component of bone, the matrix provides the form and structure for the deposition and crystallisation of inorganic salts. The matrix primarily consists of collagen (98% of its volume) of which type I collagen accounts for 90%. Collagen is a fibrous protein, formed in other tissues by fibroblasts and in the bone by osteoblasts, the bone forming cells. It is more densely packed in the bone than in other tissues. The collagen gives the bone its inherent toughness and strength and the architectural arrangement of fibres within osteons and trabeculae of the bone are conducive to great strength. The remainder of the organic component consists of noncollagenous proteins, proteoglycans, phospholipids, glycoproteins and phosphoproteins and is commonly referred to as the 'ground substance'

2.1.2.2 MINERAL COMPONENT

The mineral content of bone serves as a reservoir for ions and contributes to the regulation of extracellular fluid composition. The inorganic component of bone is mostly a complex form of calcium and phosphate in the form of the mineral Hydroxyapatite $Ca_{10}(PO4)_6(OH)_2$ among lesser proportions of carbonate, citrate, potassium, sodium, magnesium, strontium and other materials as constituents of the crystal lattice or on the crystal surface. They are mostly in the form of small crystals in the shape of needles, plates, and rods located within and between collagen fibres.

2.1.3 BONE ANATOMY

The outer surface of bone is dual layered consisting of a sheet of fibrous connective tissue called the periosteum and an inner osteogenic cambial layer of undifferentiated cells. The central medullary cavity is lined by a thin layer of bone cells called the endosteum. Both layers are well populated by blood vessels. With reference to the different types of bone tissue, there are two; cortical or

compact bone tissue and cancellous (spongy) or trabecular bone tissue. All bones in the body consist of both cancellous and cortical bone in varying proportions. A coronal section through the proximal region of the femur and the microstructure of cortical bone identifying the different parts that make up its structural composition is shown in figure 2.1.

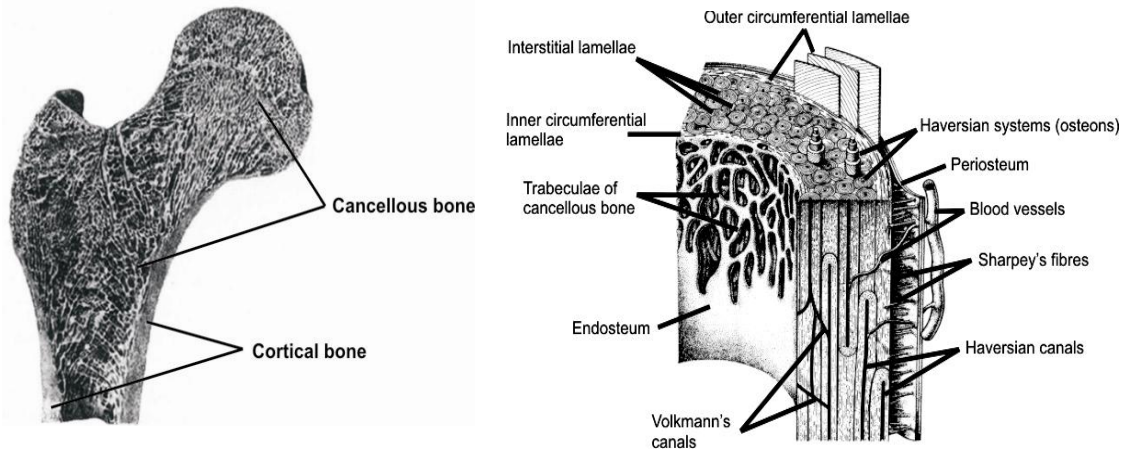

Figure 2.1: Coronal section through the proximal region of the adult femur revealing the internal structure (left) and the microstructure of cortical bone (right) [25].

The two bone types differ significantly in their distribution, structure and properties. The distribution of cancellous and cortical bone is different in different bones in the body depending on their location and function. The volume of the ulna for example is 90% cortical and 10% cancellous whereas the vertebra consists of around 60% cortical and 40% cancellous bone. A similar difference in distribution would be found in other regions. The differences between the cortical and cancellous bone in their development, architecture, blood supply etc are summarised in table 2.1.

PROPERTY	***CORTICAL BONE***	***CANCELLOUS BONE***
Skeletal mass	80%	20%
Bone surface	33%	67%
Soft tissue	~10%	~75%
Adult tissue	Secondary osteons/haversian systems/lamellae	Curved plates, rods, interstitial lamellae
Porosity	Low	High
Development	Intramembranous ossification	Endochondral ossification
Turnover	Slow	Fast
Function	Support/Protection	Support/homeostasis

Table 2.1: Properties of cortical and cancellous bone [26].

Cortical bone is found in the diaphysis and cancellous bone in the epiphysis and most parts of the metaphysis. Cortical bone is a dense solid mass containing very few spaces. Its main functions are to provide protection and support. It forms around 80% of the bone mass. The basic unit of cortical bone is the osteons or the haversian system. Osteons form around 1/3rd of the cortical bone volume, the remaining of which is interstitial bone consisting of circumferential subperiosteal (outer) and subendosteal (inner) lamellae. The lamellae are rings of hard calcified matrix. The osteons are cylindrically shaped measuring 200-250μm in diameter. The wall of the osteons is made of 20-30 concentric lamellae and cement lines separate the osteons individually. Between these lamellae are small spaces called the lacunae that contain osteocytes and their cytoplasmic processes. The lacunae containing these entrapped cells are connected by small channels called the canaliculi. The osteocytes in adjacent lacunae communicate using these small channels. Canaliculi that open to extracellular fluid and bone surfaces form an anastomosing network for nutrition and metabolic activities of the osteocytes. Diffusion through the lamellae is very slow and hence the canalicular system is essential. The osteons themselves have a central haversian canal that consists of numerous blood vessels, lymphatic vessels and nerves. The haversian canals of the osteons are interconnected by transverse channels called Volkmann's canals. These canals running longitudinally provide a path from the endosteum up to the periosteum and consist of blood vessels.

Trabecular or cancellous bone forms around 20% of the bone mass. It has very low density and high surface area. It consists of an irregular lattice network of thin columns and rods of bone called trabeculae and do not contain any osteons. As mentioned earlier, cancellous bone is mainly found in the epiphysis and metaphysis of bone and may form a thin layer in the endosteum of the diaphysis. The gaps between the trabeculae are filled with bone marrow. The trabeculae form the basic units of cancellous bone. It is crescent shaped in cross section, measures 1200μm in diameter, and is 1mm long. It is metabolically more active and more susceptible to mechanical variations than cortical bone and its remodelling rate is higher. The trabeculae are not organised like the osteons but are oriented in the direction of the stress to transfer force and load without breaking. The macro and microstructure of cancellous bone is shown in figure 2.2.

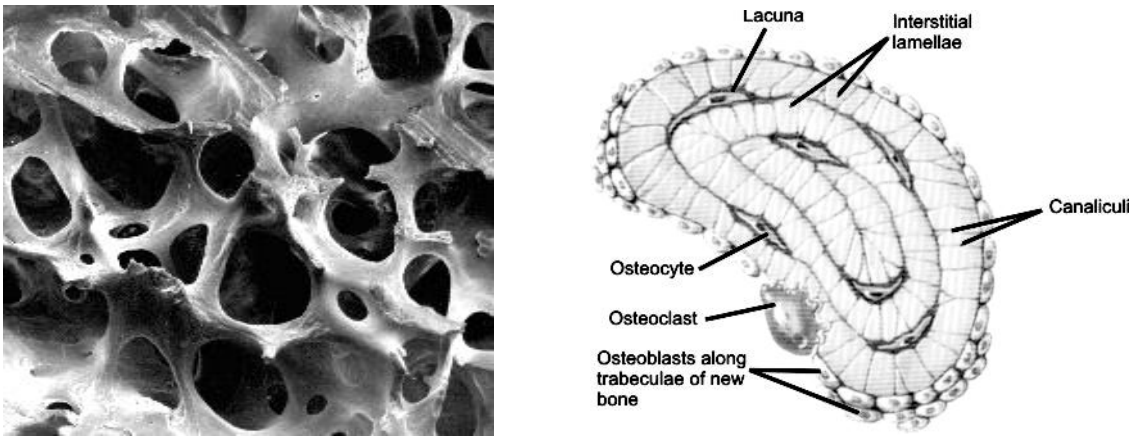

Figure 2.2: Section through cancellous bone showing trabeculae (left) and microstructure (right) [27].

Cortical and cancellous bone can be further categorised as being woven or lamellar. Woven bone is usually found in the developing embryo and is short lived. It consists of a matrix of interwoven coarse collagen fibres with randomly distributed osteocytes. It is later resorbed and replaced by lamellar bone. Woven bone is also the bone initially laid down during fracture healing. It can be formed by either the process of intramembranous or endochondral ossification. Lamellar bone is more mature and consists of layers of concentric circular rings called lamellae. The rings contain collagen fibres that are oriented in a unique direction within lamellae.

2.1.4 BONE CELLS

There are four main bone cells, each with specific functionalities. They are the osteoblasts, osteocytes, osteoclasts and the bone lining cells. The general shape of these cells is shown in figure 2.3.

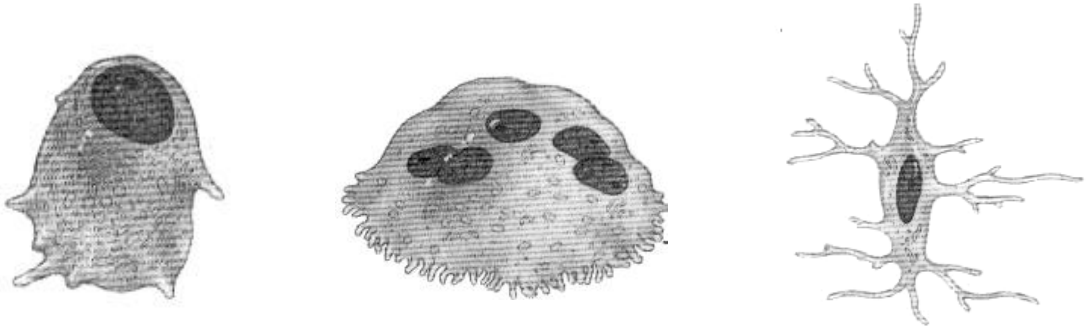

Figure 2.3: The osteoblast (left), osteoclast (centre) and the osteocyte (right) [27].

2.1.4.1 OSTEOBLASTS

Osteoblasts are round, organelle rich bone forming cells responsible for ossification and secreting the unmineralized bone matrix otherwise known as osteoid. They also participate in the calcification and resorption process and regulate the flux of calcium and phosphate in and out of bone. Osteoblasts occur as a layer of contiguous cells, which in their active state are cuboidal measuring 15-30 μm.

2.1.4.2 OSTEOCLASTS

The osteoclasts are the bone breaking or resorbing cells. They are giant multi-nucleated cells that are formed by the fusion of 1-50 monocytes and contain as many nuclei. They appear foamy in appearance due to the large number of vesicles, ribosomes, mitochondria and vacuoles present on its surface. Osteoclasts are derived from cells of the mononuclear lineage of the hematopoietic marrow. They range from around 20μm to 100 μm in diameter.

2.1.4.3 OSTEOCYTES

Osteocytes are mature bone cells and form the bulk of the cells in bone tissue. They are formed when osteoblasts form new bone and get left behind in the newly formed osteoid. The osteoblasts in the lacunae then differentiate into osteocytes by losing their organelles but forming becoming long, slender processes that connect with other osteocytes, bone lining and periosteal cells through the canalicular network. They are regarded to be the main cells that sense the magnitude and distribution of mechanical loading. The main functions of osteocytes are in the areas of homeostatic, morphogenetic and restructuring processes.

2.1.4.4 BONE LINING CELLS

The surface of bone is often the centre of regular activity by the osteoblasts and the osteoclasts constantly modelling and remodelling the bone. However, during quiescent periods, the osteoblasts become inactive, thin elongated cells on the surface of the bone and are called bone lining cells. The bone lining cells might be involved in homeostatic, morphogenetic and restructuring processes that regulate bone mass, mineral content and hematopoietic process. They do not multiply but can secrete growth factors that trigger osteoblastic activity. Networks of bone lining cells and osteocytes make junctional communication with each other to sense the shape of bone and reaction to mechanical factors like stress and strain and transmit these signals to the bone surface where new bone formation and resorption could occur.

2.1.5 BONE FORMATION

Osteogenesis or ossification is the process of forming bone and occurs mainly through two methods, intramembranous ossification and endochondral ossification. The process is normally based on an existing template, with bone previously present and is site-specific. Both methods involve replacing existing connective tissue and do not differ in the final structure of the bone formed.

2.1.5.1 INTRAMEMBRANOUS OSSIFICATION

Intramembranous ossification as the name suggests, involves bone forming directly on or within fibrous connective tissues and is the simpler process as compared to endochondral ossification. The process usually forms the bulk of future cortical bone and examples of the bones formed are the bones of the skull and the mandible. The process starts with the formation of a centre of ossification where mesenchymal cells gather and differentiate into the osteogenic pathway resulting in osteoblast formation. Matrix deposition takes place and osteocytes are formed. Calcification starts and the matrix begins to harden. As the matrix matures, trabeculae form and blood vessels occupy the spaces between them and on the surface. They continue to increase in thickness and enlarge by deposition at their free ends. Compact bone begins to form when the spaces begin to fill on the outer surface with primary osteons and haversian canals, and as bone matures, it is replaced by secondary systems. The bone at the centre remains cancellous.

2.1.5.2 ENDOCHONDRAL OSSIFICATION

Endochondral ossification involves replacing cartilage by bone and forms the bulk of future cancellous bone. It is the most common process of bone formation and the long bones in the body are formed in this manner. In contrast to intramembranous ossification, the mesenchymal cells gather in the shape of the bone to be formed, but in this case differentiate into chondroblasts. They secrete cartilage matrix and produce a hyaline cartilage model. A membrane called perichondrium forms around this. Chondrocytes are soon surrounded by the matrix they secrete. The cartilage model grows by repeated cell division by the osteocytes and results in an increase in length. As the model grows, chondrocytes in the mid region hypertrophy and burst, which changes the pH and triggers calcification.

As chondrocytes die, lacunae begin to form. A primary ossification centre forms when a nutrient artery penetrates the perichondrium in to the mid region stimulating osteogenic cells in the perichondrium to differentiate into osteoblasts. Once the perichondrium begins to form bone, it develops into a periosteum. At the centre of the model, periosteal capillaries grow into the disintegrating calcified cartilage and forms the primary ossification centre. At this stage, bone tissue

replaces the cartilage. Bone matrix is then deposited over the cartilage remnants forming trabeculae. As the centre grows, osteoclasts resorb the trabeculae, forming the medullary cavity. Secondary ossification centres develop around the time of birth, when epiphyseal arteries invade the epiphyses. Ossification proceeds outwards from the centre to the surface of the bone. No cavities are formed during the process. The hyaline cartilage covering the epiphysis becomes articular cartilage and the cartilage between the diaphysis and epiphysis becomes the growth plate, responsible for lengthwise growth.

2.2 THE HIP JOINT

2.2.1 ANATOMY OF THE HIP

The hip joint is one of the largest joints in the human body. It is a simple, multi-axial, ball and socket synovial joint formed by the articulation of the head of the femur against the acetabulum of the pelvis. The pelvis is a bowl shaped structure, made of two irregular bones that form the sides of the pelvis called the innominate bones and are joined to each other anteriorly at the pubic symphysis. Each of these bones is formed by the fusion of three bones, the ilium (largest), ischium and the pubis (smallest). At the junction of the fused bones is a hemispherical depression or socket known as the acetabulum. The acetabulum is surrounded on its outer surface by a layer of cartilage, which forms one half of the articulating surface of the joint (figure 2.4).

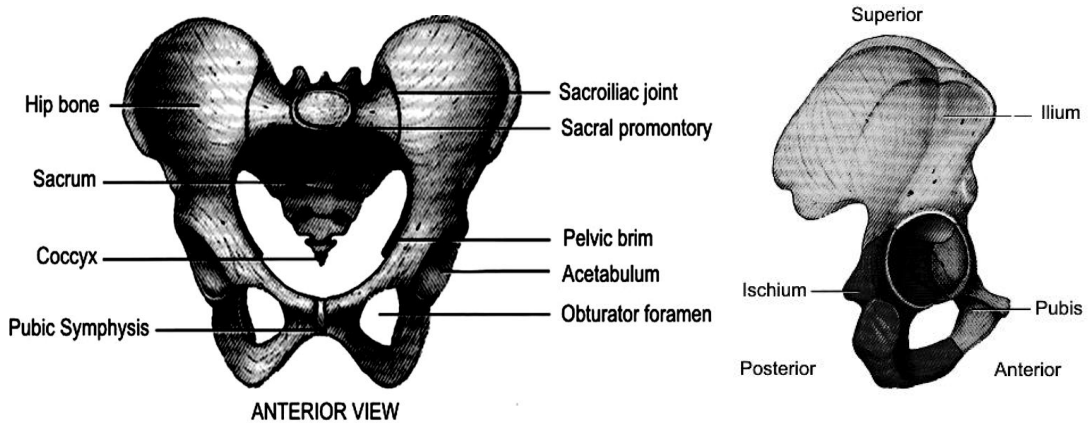

Figure 2.4: Front (left) and lateral (right) views of the pelvis. The three bones forming the acetabulum are also shown [27].

The other half of the articulation is provided by the cartilage on the head of the femur. The femur or the thigh-bone is the longest, heaviest and strongest bone in the body. The proximal part of the femur comprises of the femoral head, the neck and the greater and lesser trochanters. The femoral head is spherical in shape, forming approximately two-thirds of a sphere. A small depression in the centre of the head, called the fovea capitis is a ligament attachment point which also houses a blood

vessel that supplies blood to the femoral head. A constricted flattened pyramidal section known as the femoral neck connects the head to the main body of the femur.

The greater trochanter is located laterally at the junction of the femoral head and neck with the lesser trochanter located medially just under the neck. The trochanters are muscle attachment sites. The main body or shaft of the femur is bowed anteriorly with the distal end of the femur forming the medial and lateral condyles that articulate with the tibia. The medial condyle is larger and locks the knee while walking. Two superior aspects, known as the epicondyles for both the medial and lateral condyles are the sites for muscle attachment (figure 2.5).

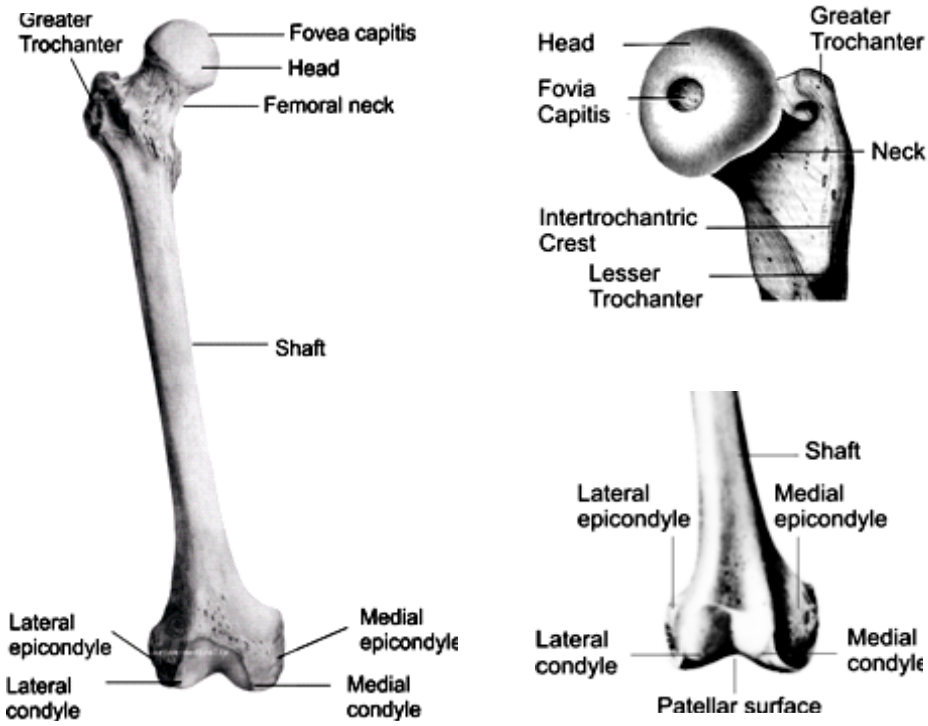

Figure 2.5: Anterior view of the femur (left). Close up of the proximal part (top-right) and distal end (bottom-right) of the femur [1].

The hip joint is a synovial joint, which means it allows the greatest range of movement compared to other non synovial joints. After the knee joint, it has the largest range of movement and yet supports the weight of the body, arms and the head. It is also extremely stable, surrounded by a strong fibrous capsule filled by a clear or slightly yellow viscous fluid known as the synovial fluid. Its main function is to provide a fluid medium within the joint, provide nutrition and lubricate the joint. The fluid also has a cellular component consisting of leukocytes, lymphocytes, monocytes,

[1] http://www.artem-medicalis.com

phagocytes and other synovial cells. The phagocytes are responsible for the removal of wear debris that arises due to joint use. The other cells are responsible for replenishing the synovial fluid. The surrounding capsule is also reinforced by three ligaments; the iliofemoral, pubocapsular and the ischiocapsular ligaments. The iliofemoral ligament is a Y shaped ligament and covers the anterior portion of the joint, attached to the ilium on the hip and at the intertrochateric line on the femur. It assists in preventing hyperextension at the joint. The pubocapsular ligament is situated inferiorly, attached to the pubis and is separated from the iliofemoral ligament by the iliopsoas tendon. The ischiocapsular is the least developed of the three ligaments and runs across the posterior aspect of the joint. The ligaments are shown in figure 2.6.

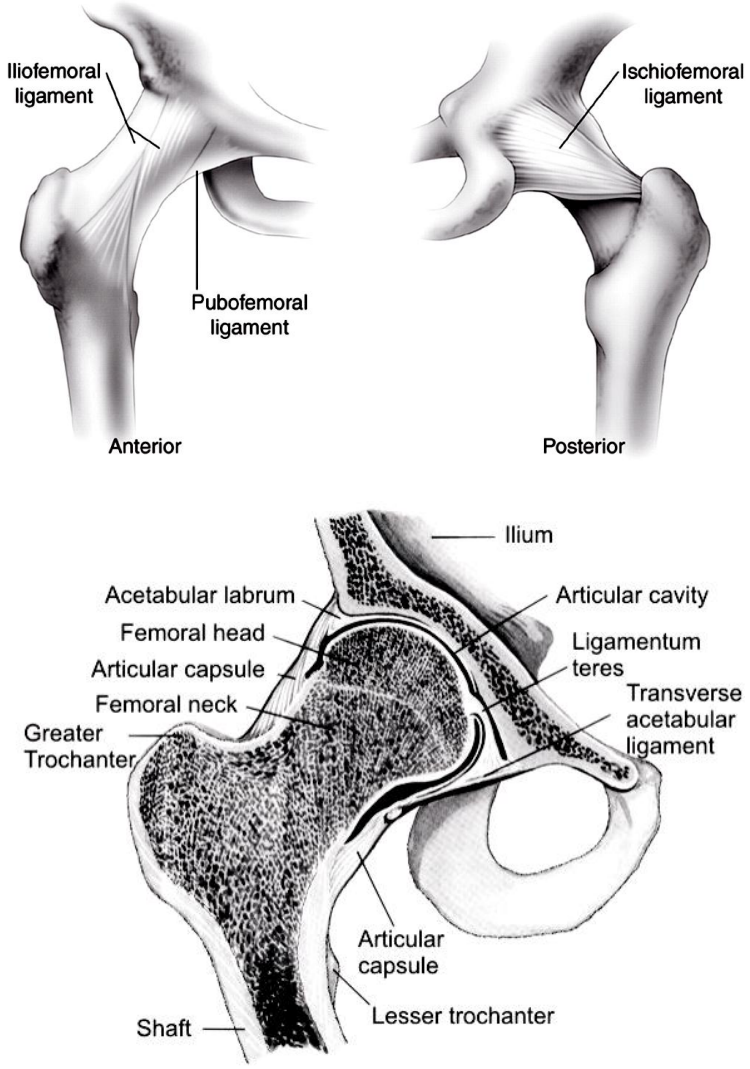

Figure 2.6: The ligaments of the hip (top)[2]. Mid-coronal section of the hip joint showing structure and assisting ligaments (bottom)[3].

[2] Anatomy of the human body, Gray, H 1918

[3] http://ajs.sagepub.com/content/31/6/1020/F1.large.jpg

2.2.2 BIOMECHANICS OF THE HIP

2.2.2.1 RANGE OF MOTION

The hip joint allows a large number of movements across multiple axes due to the powerful surrounding muscles which form a ring around the joint. They stabilise the joint and also allow normal activities like walking, stair climbing, running etc. Specifically, the motions permitted at the hip are flexion-extension, abduction-adduction, cricumduction, and internal-external rotation (figure 2.7).

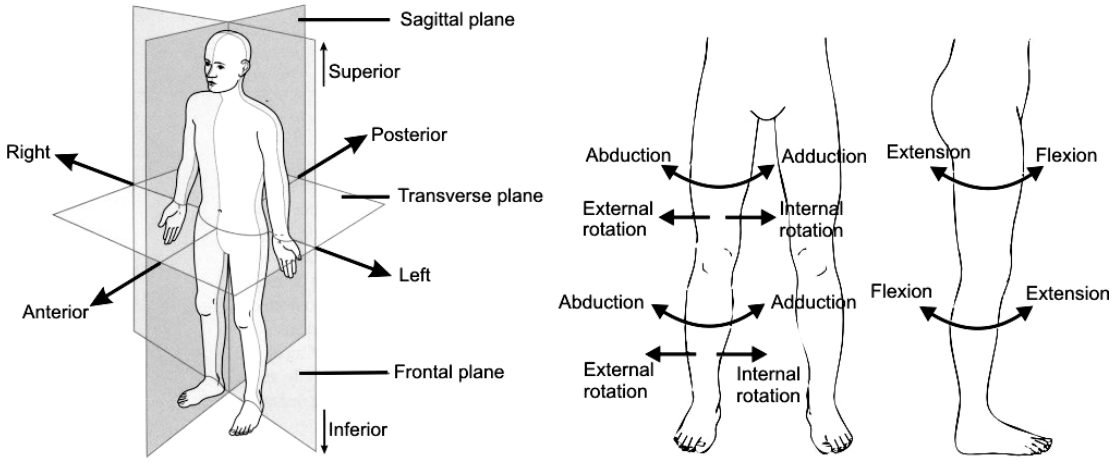

Figure 2.7: Anatomical planes of the body (left) and the motions permitted at the hip and knee joints (right) [28].

The degree of movement possible in each case differs; flexion can be described as the anterior motion of the femur in the sagittal plane. The muscles can be classified by the type of movement and orientation around the joint. The hip can achieve around 120°-140° of flexion. The posterior motion in the same plane is known as extension and is limited to around 20° of motion. Abduction is the lateral movement of the leg in the coronal plane of which the hip can produce 30°- 45° of movement. Adduction is the opposite of abduction, and the hip can produce around 30° of movement. Lastly, internal and external rotation which when combined can contribute to 90° of movement.

The specific muscles (figure 2.8) used for each of the aforementioned movements are the:

Rotators - External Rotation/Internal rotation - These muscles are responsible for lateral rotation of the hip. The muscles are small and include the piriformis, obdurator internus and externus, gamellus superior and inferior and the quadratus femoris.

Abductors – These muscles move the leg away from the midline of the body (abduction). They lie laterally to the joint in the lateral gluteal region. The muscles of this group include the gluteus medius and minimus and the tensor fasciae latae.

Adductors - This group consist of the muscles of the groin that move the legs toward the midline of the body (adduction) and lie medially to the joint. The muscles of this group are the pectineus and the adductor brevis, longus and magnus.

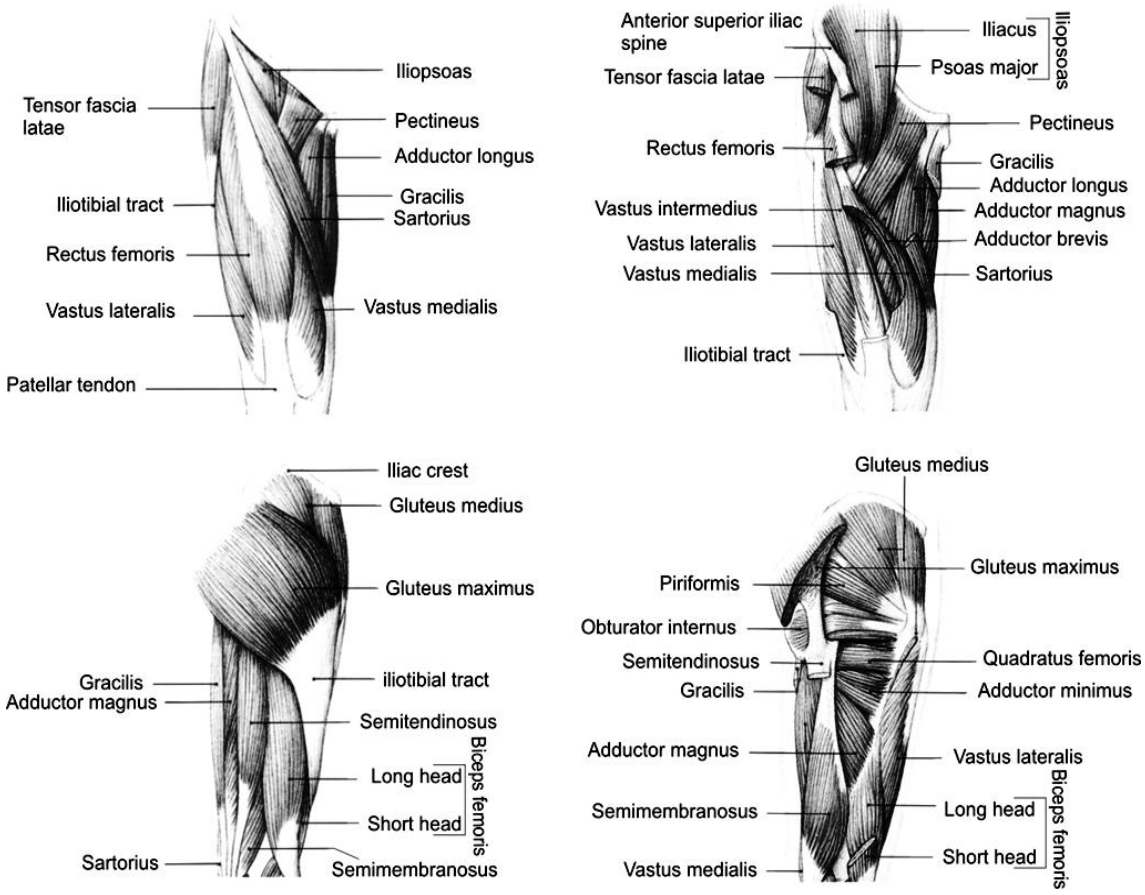

Figure 2.8: The muscles acting at the hip showing the anterior and posterior views (top and bottom) and the deep cut muscles that are not visible superficially [29].

Flexors - This group allows the hip to flex (move the thigh toward the chest) and oppose the muscles of the extensor group and include the iliopsoas (iliacus and psoas parts), rectus femoris, pectineus, sartorius and the tensor fasciae latae.

Extensors – These muscles allow the hip to extend (move the thigh backward) and oppose the flexion muscles. The main muscle is the gluteus maximus, assisted by the hamstring muscles (semitendinosus, the biceps femoris and the semimembranosus).

Even though the muscles have their distinctive groups, they blend together during movement and may be involved in just one movement. For example, the tensor fasciae latae abducts, flexes and medially rotates the joint and the pectineus assists in flexion and adduction.

2.2.2.2 NECK-SHAFT ANGLE AND DEGREE OF ANTEVERSION

Two important angular relationships between the femoral neck and the shaft are the neck shaft angle and the degree of anteversion. These two factors can alter gait and impose restrictions on the movement allowed at the hip joint. Neck-shaft angle can be defined as the angle of inclination of the neck to the shaft in the frontal plane. This angle in adults is around 125°, but can vary. An angle less than 125° refers to a condition known as coxa vara and the hip is said to be in varus. Similarly, an angle more than 125° refers to a condition known as coxa valga and the hip is said to be in valgus (figure 2.9).

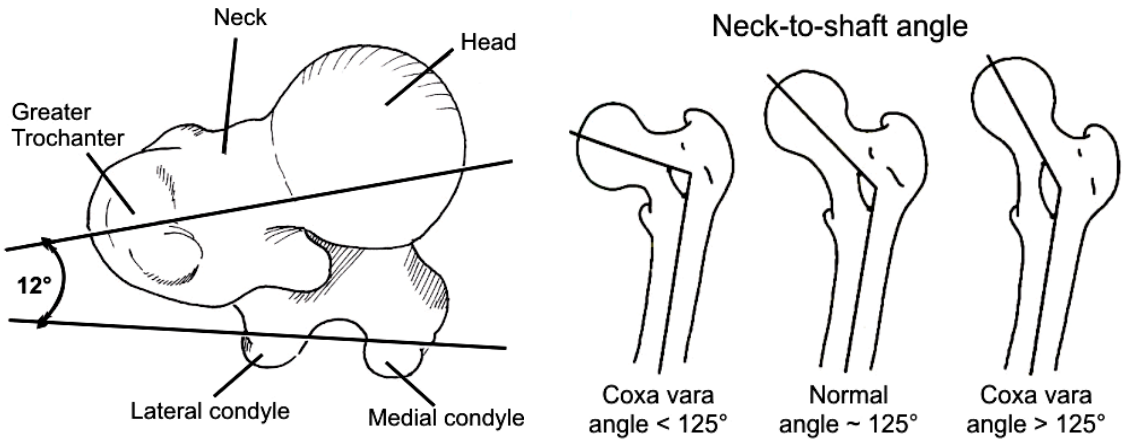

Figure 2.9: The angle of anteversion formed by the intersection of the long axis of the femoral head and the transverse axis of the condyles (left) and the neck-to-shaft angle that shifts the hip into a varus, normal or valgus position (right) [30].

Either of these conditions changes the how the load is distributed through the femur and also affects the surrounding muscles. Anteversion refers to the angle created if a transverse axis is drawn at the femoral condyles relative to the axis at the femoral head. This angle is normally around 12° but can vary. An angle exceeding this can result in the internal rotation of the leg during normal gait to stop the femoral head slipping out of the acetabular socket. An angle lesser than this, called retroversion, can cause external rotation of the leg.

2.2.2.3 GAIT ANALYSIS

The human gait can be defined as cyclic, bipedal locomotion requiring complex interactions and coordination among most of the major joints in the body. The hip and the knee play a big part and during this, the hip joint experiences flexion-extension on the medio-lateral axis, abduction-adduction along the antero-posterior axis and internal-external rotation around the longitudinal axis. Together, these movements form a circular arc of movement called circumduction. Each gait cycle (a single sequence of functions by one limb) can be split into two phases, the stance and the swing phase (figure 2.10). The stance phase is the period of time when the limb under consideration is in contact with the floor and occupies around 60% of the cycle. It also has two periods of double limb support (when both feet are in contact with the floor). The swing phase is the period of time when the limb under consideration is not in contact with the floor and occupies around 40% of the cycle [31].

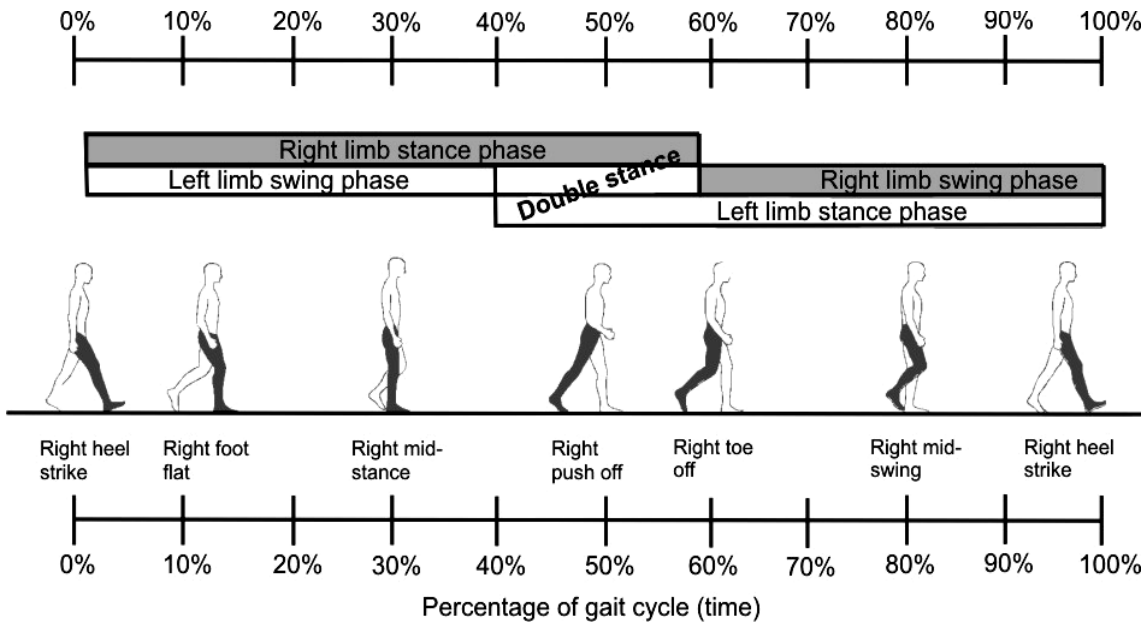

Figure 2.10: Phases and sequences of the gait cycle with their timings.

The stance phase is the most complex phase of the gait and consists of the following sequences, namely,

- Heel strike or the initial contact
- Foot flat (initial contact of forefoot with the ground)
- Mid-stance
- Heel off or the terminal stance
- Push off

- Toe off or the pre-swing

In the swing phase, the swinging limb moves in front and forward motion takes place. The sequences involved in this are,

- Acceleration or the initial swing
- Mid-swing (the swinging limb overtakes the limb in stance)
- Deceleration or the terminal swing

It is also interesting to note that if the walking speed is increased, there will be a marked decrease in the stance phase and a corresponding increase in the swing phase. This is more pronounced while running where the swing phase occupies a larger period of the gait cycle compared to the stance phase. Double support is also missing while running. Ground reaction forces using forceplates have shown that vertical, anterior-posterior and medio-lateral forces act between the foot and the floor during normal gait. The vertical forces are the most pronounced with the smaller anterior-posterior and medio-lateral forces mainly used for stability, cushioning and shock absorption. Figure 2.11 shows the ground reaction forces for a normal gait.

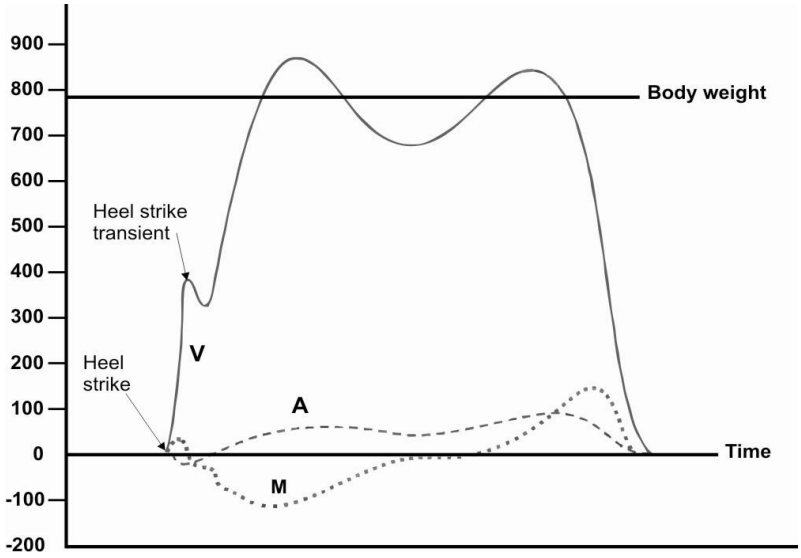

Figure 2.11: The ground reaction forces for a normal adult gait. V is the vertical force, A the anterior-posterior force and M the medial/lateral force [32].

A number of studies have been conducted to study the human gait, normal and pathological. Various methods have been employed to this end. Some of the more popular ones include force platforms [33], gyroscopes [34], accelerometers [35], electromyography [36], Energy systems [37], kinematic systems [38] or combinations of the aforementioned methods. Cadaver studies have been used in the past with the advantage of studying internal joint motions but have been unable to reproduce normal loading patterns. However, gait studies have diametrically opposite problems. A

way around is to combine one or more methods to get more information from gait studies. One such method is to extend gait analysis to also calculate joint reaction forces. This is done using inverse dynamics as shown by Paul (1976) using a combination of kinematics data from force plates and acceleration data measurements from filming. Gait analysis can be a useful tool for investigating and determining abnormalities in gait, like pathological, post prosthetics and orthotics, or post surgical conditions after lower limb arthroplasties. Telemetrised prostheses are used in conjunction with aforementioned methods to investigate muscle forces and changes in gait after implantation. This has been done in quite a few studies [17,18,39-43]

The most comprehensive study has been done by Bergmann et al., measuring hip contact with instrumented implants and synchronous analyses of gait patterns and ground reaction forces for daily and frequent activities. It was found that during normal walking, the hip joint was loaded with 238% of body weight (BW). This happened mainly at heel strike during the stance phase and with little force acting during the swing phase. A smaller force compared to the force at heel strike was found at toe-off. During stair ascent and descent, the peak forces were between 250-260% BW. Similar values for normal walking and stair climbing have been reported by Davy et al [39] . A summary of the peak hip contact force in terms of BW is shown in figure 2.12. The high inter-patient variability is seen. Bergmann et al [18] also measured the peak forces during stumbling loads, which were found to be highest at 870% BW. The peak hip contact forces for different activities are also shown in figure 2.12. However, considering the average patient would not stumble frequently, it can be safely concluded from the data that stair climbing and normal/fast walking would contribute the most to the peak contact forces and should be an integral part of implant stability testing. Normal walking and stair climbing are also one of the most frequent activities performed by patients post hip arthroplasties [44]. For young patients with higher activity levels, running or jogging where the hip contact forces exceed 3 times BW can also be studied to check implant stability.

Soft tissues play an important role in maintaining the equilibrium of the femur during gait. However, the contribution of soft tissues to the forces acting on the femur is extremely difficult to measure directly. Electromyogrpahy can be a useful tool to study the activation of different muscles during normal gait but force information cannot be obtained by this method. They can be calculated using limb displacement theory combined with forceplate forces and limb inertial properties as shown by Pederseon et al. [45] for measuring pelvic and acetabular contact forces during gait.

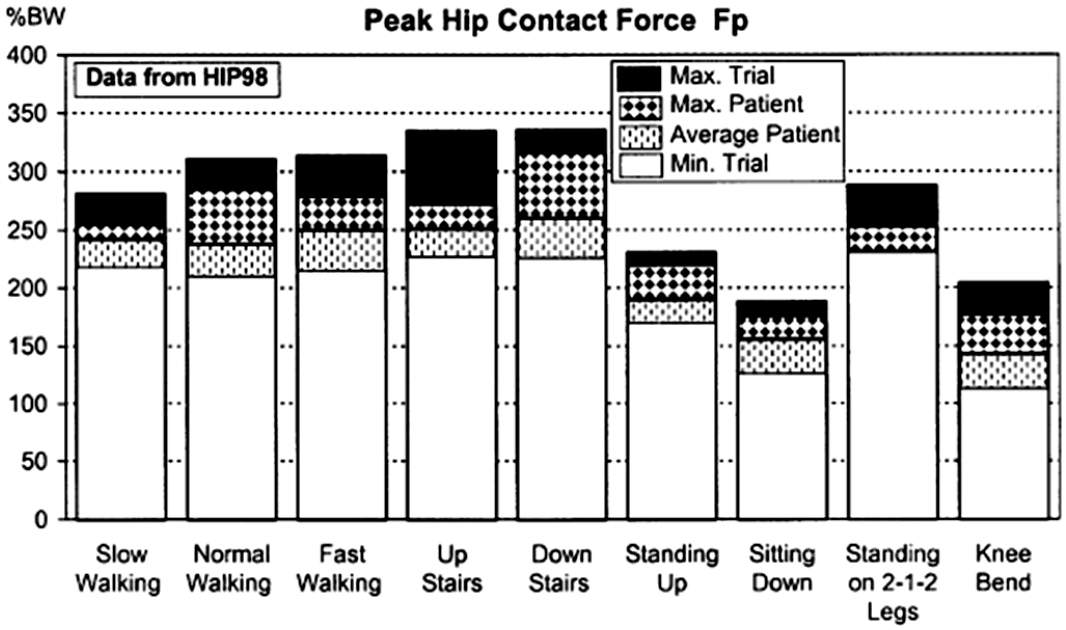

Figure 2.12: Peak hip contact forces in terms of BW for 9 different activities [18].

Duda et al [46] provided a more complex model by using the inverse dynamics approach to construct a three dimensional model that included the muscles of the thigh , body weight and the contact forces from the hip, knee and patella-femoral joints. The concept of mechanical equilibrium at the thigh was applied to a free body analysis based on the equilibrium of forces and moments as shown in equation 1 and equation 2.

Equation 1

Equation 2

Where , & were the muscle forces, ligament forces and incremental weight of the thigh; were the hip contact force, the patella-femoral contact force and knee contact force; a free moment arm. , and were the corresponding moment arms.

The influence of different groups of muscles on the forces acting on the femur was also studied and it was found that the abductors and the vasti group had the largest influence on force in the femoral

part of the femur. If other smaller muscle groups like the obturators, or the iliopsoas were considered, the forces on the femur were reduced, especially at the distal end. Muscle forces have also been employed in finite element (FE) models to study different boundary conditions by Speirs et al [47] like the influence of the individual muscle groups under different boundaries and constraints. High strains were recorded in the mid diaphysis of the femur in the models that had poor boundary conditions and fewer muscle forces. This agrees well with the studies of Brand et al [48,49], where the contribution of muscle forces to avoid overestimating strains in the femur was elucidated. It was found that for these models to be accurate, all muscle groups had to be included with relevant physiological constraints to reach equilibrium and model physiological deflections correctly. The relevance of including relevant muscle groups for measuring implant micromotion, which further determines implant stability by regulating tissue differentiation at the interface, is also extremely crucial. Major muscle groups should be included in modelling, if a parallel is to be drawn with conditions *in vivo.*

2.3 HIP REPLACEMENTS

2.3.1 INTRODUCTION

The hip joint is one of the most vulnerable joints to diseases and impairment. This is mainly due to the range of movement and extensive use in daily activities that it is subjected to. The whole of the body weight is transferred through the joint, and there is a high risk that the joint could be damaged, or fail due to biological factors, mechanical factors or a combination of both. In any of these cases, the most popular and widely adopted method to relieve the patient of pain is through a hip arthroplasty, otherwise known as a hip replacement. Usually advocated when physiotherapy and pain killers are inadequate, this operation has become increasingly popular in the last ten years or so in a number of countries [1,3,4,50,51]. Figure 2.13 shows the incidence of primary hip replacement in England and Wales since 2003 according to the National Joint Register.

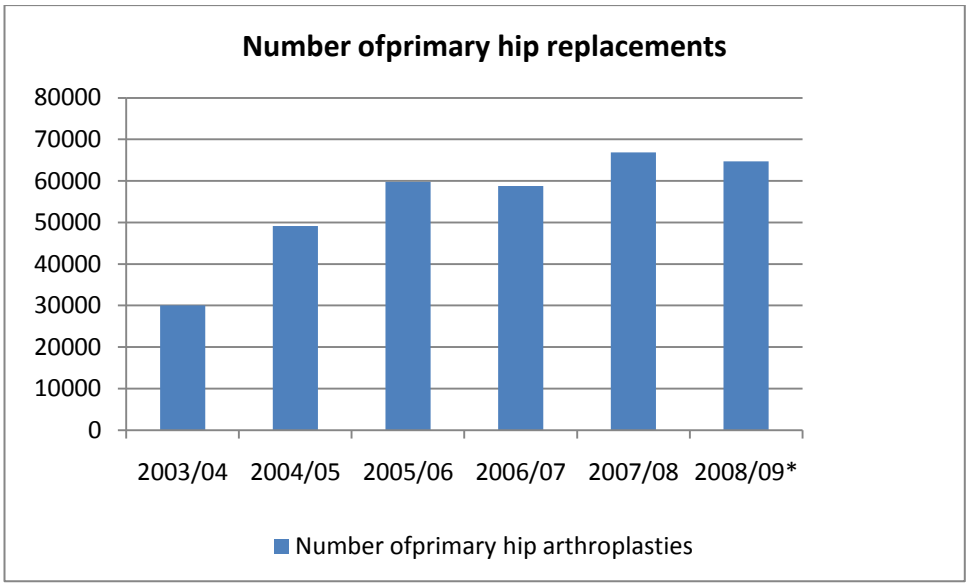

Figure 2.13: The number of primary hip replacements in England and Wales for different years [51].

2.3.2 REASONS/INDICATIONS FOR A HIP REPLACEMENT

There are a number of indications for hip replacements. Some of the most common are pain, functional limitations, joint stiffness, radiographic changes etc. [52]. These problems are often indicators of more serious underlying problems like osteoarthritis (OA), rheumatoid arthritis (RA), osteonecrosis (ON), fractures or infection.

2.3.2.1 OSTEOARTHRITIS (OA) [53,54]

OA is one of the most common critical and crippling conditions that usually affect the older population. It is characterised by pain at the thigh and the buttocks, sometimes radiating to the knee, accompanied by stiffness and limited movement at the joint. OA is chronic, progressive and a degenerative disease caused by an abnormality in the chondrocyte metabolism . It is distinguished by the degeneration of the articular cartilage over time resulting in the articulation of the bony surfaces which causes acute pain. OA is also a dynamic process and involves the surrounding capsule, ligaments and muscles in addition to the cartilage and bone at the joint. The main pathological changes include the loss of the cartilage and remodelling of the adjacent bone with new bone formation, especially at the joint margins (figure 2.14). These new bone sprouts are called osteophytes. The synovial membrane and the joint capsule thicken, with reduced joint space and sometimes an increase in the amount of fluid in the joint. Inflammation then follows. Normally, joint repair involves replacing the worn out articular cartilage and is signalled by trauma at the joint. Many a time, this process is successful, especially for low tissue trauma. However, when this

process slows down or is overwhelmed by the extensive damage, the repair potential is compromised and results in continuing tissue damage and the rubbing of the bony surfaces. This process can take many years to develop and the exact causes unknown. However, some key risk factors have been identified. Some of these factors are age, sex, genetic factors, heredity, obesity, joint injuries and trauma. There is currently no cure for arthritis, but common methods for relieving pain in the joints include reducing stress in the joints (reducing weight, pacing daily activities, special shoes and soles etc.), activity and exercise (strengthening, aerobic), pain medications and intra-articular injections (corticosteroids, hyaluroans etc). For severe cases of arthritis, joint replacements are recommended.

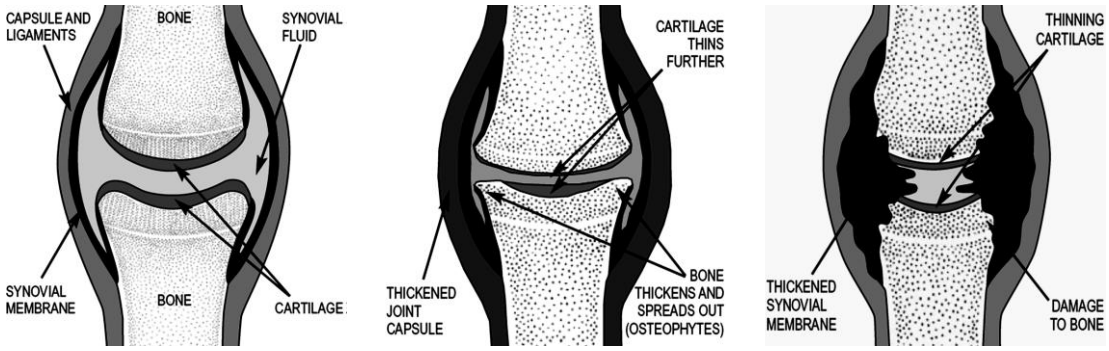

Figure 2.14: A normal synovial joint (left), osteoarthritic (middle) and a rheumatoid arthritic joint [53,55].

2.3.2.2 RHEUMATOID ARTHRITIS (RA) [55,56]

RA is the most debilitating form of chronic arthritis and can affect men and women of all age groups. RA involves inflammation of the synovial membrane that lines the joint capsule, the tendon sheaths and the bursae causing acute pain, inflammation and stiffness at the joint. RA is an autoimmune disease in which the body's immune system (specifically T cells) attacks the joint cartilage instead of protecting it. The general symptoms include fatigue, fever and anemia which proceeds on to joint specific symptoms. In RA, there is a large increase in the blood flow to the joint, proliferation of the synovial membrane with an increase in synovial fluid and pain, resulting in the rapid loss of muscle around the joint (Figure 2.14). The condition is progressive with the increasing damage to the joint caused by the release of protein degrading enzymes from inflammatory cells. This then interferes with the nourishment of the cartilage, slowly destroying it and replacing it with fibrous tissue. In extreme cases, this fibrous tissue can get calcified forming a bony union and eliminating the joint completely. Joint replacement procedures to treat RA were common, but non surgical alternatives like therapy and drugs (antirheumatics, anti-inflammatory, analgesics) are effective, reducing the need for surgery.

2.3.2.3 OSTEONECROSIS (ON)

ON, also known as avascular, aspetic or ischemic necrosis is a disease of impaired blood flow commonly affecting the epiphysis of long bones like the femur and the humerus [57]. ON can be categorised into traumatic and non-traumatic (figure 2.15), with the former mostly involving trauma to the joint, mostly in the form of a fracture or a dislocation. Nontraumatic ON has a variety if etiological associations and can be related to excessive alcohol use, corticosteroids, renal failure, hypersensitivity reactions, sickle cell diseases etc.

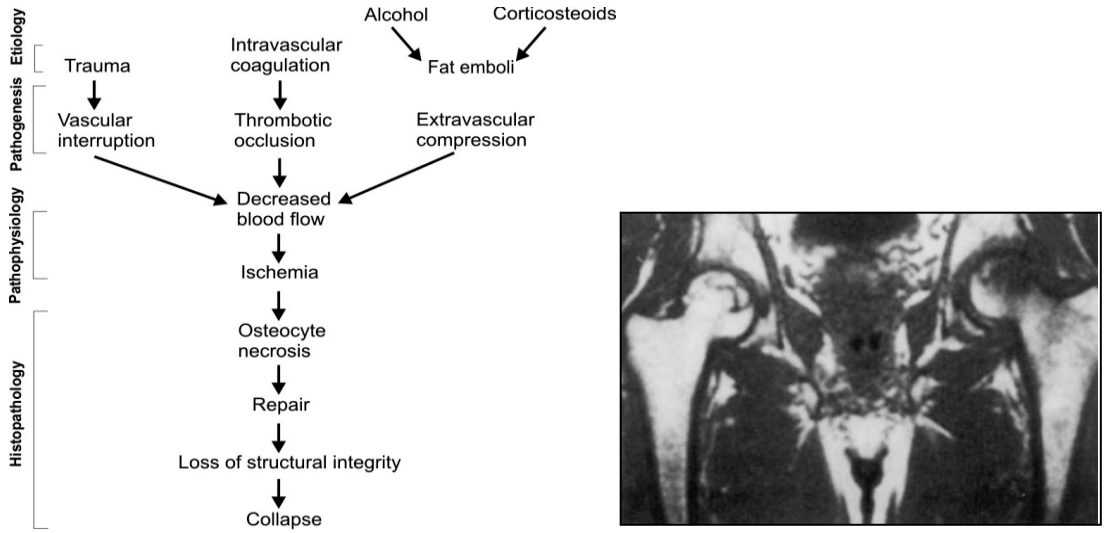

Figure 2.15: hypothesised pathogenesis of ON (left); a weighted MRI demonstrating a small osteonecrotic lesion on the left and a large lesion on the right [57].

During ON, the death of the bone and marrow occurs due to the reduction or loss of blood supply, which hinders nutrient and oxygen transport. In ON, unless the region is small, the repair mechanisms are ineffective and a mature healing response of osteoblastic and osteoclastic activity is absent [58]. ON is not easy to diagnose at first, and is most often not picked up till it has progressed. Common symptoms of ON include pain in the groin, stiffness, decreased range of motion, an antalgic gait (slight limp to avoid pain) and clicking in the hip when the necrotic fragment has collapsed. Radiographs were commonly used to diagnose the condition but have been replaced by MRI's for more accuracy (figure 2.15, right). Treatment for ON include core depression, where the intraosseous pressure is reduced in the femoral head by creating a hole and removing part of the bone. However, for more severe cases, osteotomy, bone grafting and joint replacements are widely used. Hip arthroplasty in cases of osteonecrosis of the femoral head is the most widely recommended method for providing relief and restoring functionality at the joint. This can either be a surface replacement, a femoral replacement or a total hip replacement, with or without the use of cement and has been shown to be very successful [57].

2.3.2.4 OTHER FACTORS

Other commonly cited reasons for a hip replacement are infection, fractures, trauma congenital dislocation, inflammation and other diseases [1,51]. Although some of these may not always warrant a hip replacement and can be dealt with by administration of drugs or condition specific osteotomies, for severe cases, a hip replacement may be the only way to provide long term relief to the patient.

2.3.3 HIP REPLACEMENT PROCEDURE

In a hip replacement, the articulating surface or surfaces are replaced by artificial equivalents, usually metals or ceramics for the femoral components and either ceramic, metal or polyethylene for the acetabular component. Figure 2.16 shows a replaced joint compared to a normal hip joint. Note that the position of the implant is such as to least alter the normal functioning of the joint. There are a wide range of hip replacements used today but traditionally, the femoral component consists of a metallic implant with a stem that extends to the diaphysis of the femur, with a small neck and a part spherical implant head to replicate the motions of the femoral head. The head is usually metallic or ceramic.

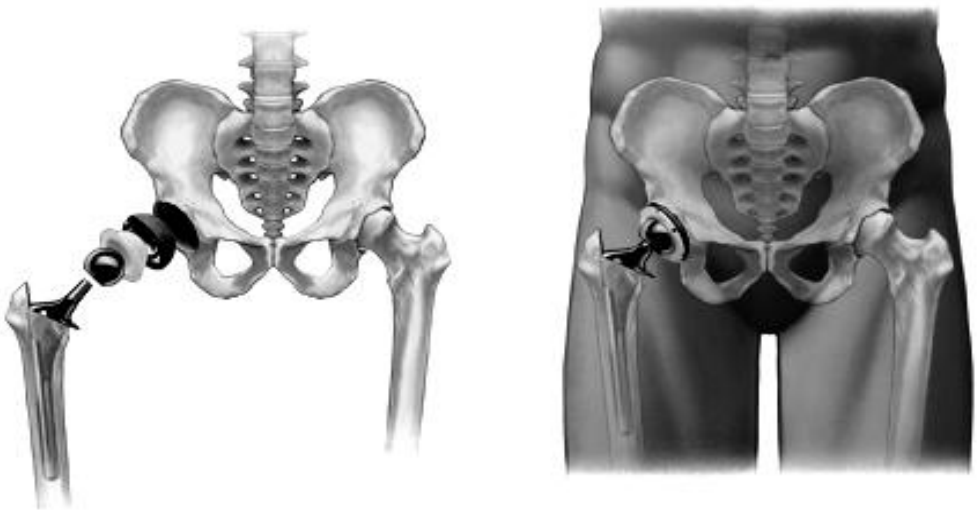

Figure 2.16: A total hip replacement and its components (left) and the complete assembly in the body (right)[4].

On the acetabular side, a hemispherical component made of metal, plastic or ceramic is encompassed by a metal or ceramic backing, with or without a liner in between the parts. There

[4] http://www.zimmer.co.uk

may also be situations where, due to the presence of healthy cartilage at one of the surfaces, only one component needs to be replaced, in which case it is referred to as a hemi arthroplasty. This is most often done keeping the acetabular component and replacing only the femoral side. For younger patients with good bone quality, a hip resurfacing arthroplasty can also be considered. In this case, only the femoral head is replaced by cutting and resizing and a lot of the bone is preserved. In case of failure, a conventional hip replacement may be performed later on. Some typical hip prostheses are shown in
figure 2.17.

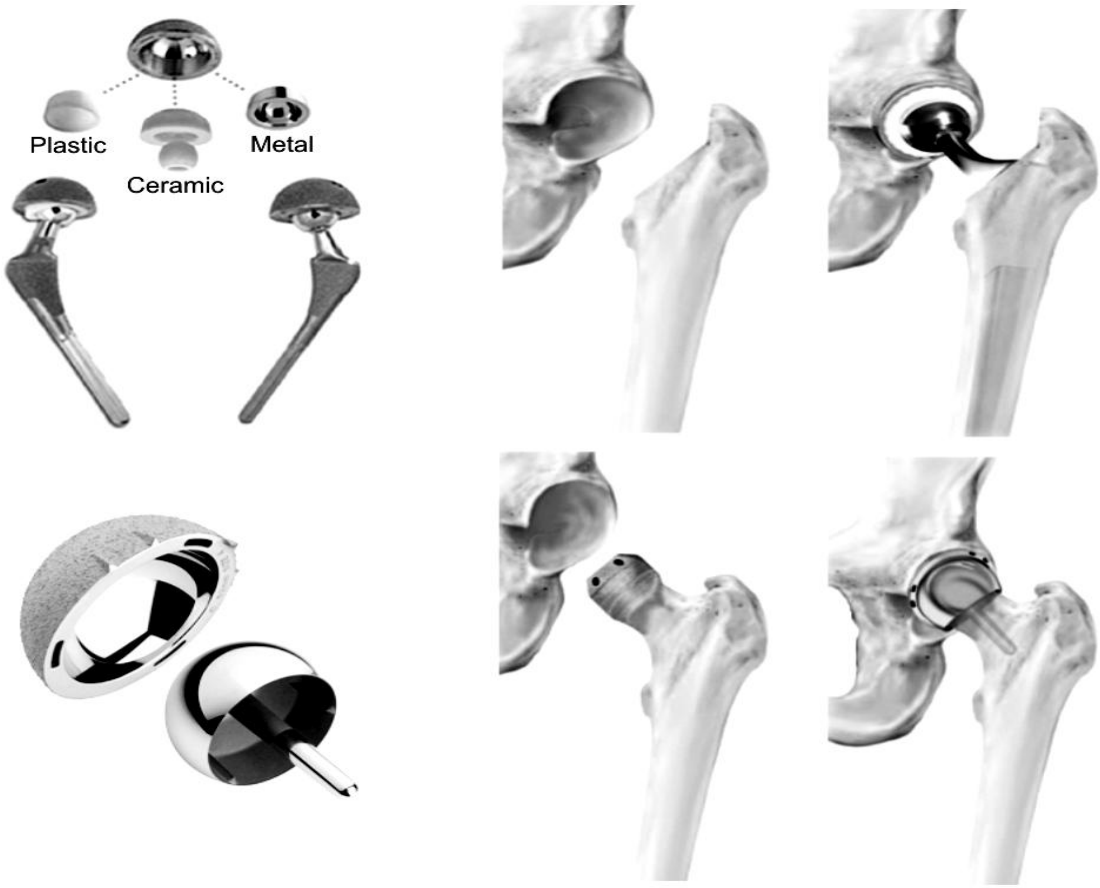

Figure 2.17: Different types of hip prosthesis used in total hip arthroplasty with their implantation strategy. Traditional THR's and their implantation (top)[5]. Hip resurfacing and implantation (bottom)[6].

As mentioned before, hip replacements are highly varied in the type of material used, size, shape, fixation etc. A single type of implant may not be suitable for all patients, hence the need for different implants. For example, an implant chosen for an 80 years old patient with low activity levels may not be ideal for a 50 year old with an active lifestyle. Similarly, an implant chosen for a sportsperson

[5] http://www.wmt.com and http://www.coringroup.com

[6] http://activejointsortho.com/BHR_web_images/hip_compare2.jpg

could be different from a patient leading a largely sedentary lifestyle. The choice of implants and materials used has been a topic of debate for many years and will continue to be as long as variability in the patient population exists. Hip arthroplasty currently is a safe and tested surgical intervention with few complications, and aims to improve mobility and relieve pain in patients otherwise confined to a hip affliction.

2.3.4 FAILURE OF HIP REPLACEMENTS

Although hip replacements have enjoyed long-term success of up to 10-15 years [59], there are many complications that can arise post-implantation. Follow-ups and revision surgeries are good indicators of the performance and life of the implant. Revision surgeries cause additional trauma to the patient and involve replacing failed components. These surgeries can be complicated and time consuming considering the quality of the bone at the site may not be the same as when the original procedure took place. In addition, removing the implant to replace it can be cumbersome and if the patient is old, this may prove risky. Some of the many problems that can lead to failure of hip replacements are described below.

2.3.4.1 ASEPTIC LOOSENING

Aseptic loosening remains the single most cause of failure of hip replacements according to joint registry data from different countries (figure 2.18). Aseptic loosening can be defined as loosening of the components of a hip replacement through factors not associated with infection.

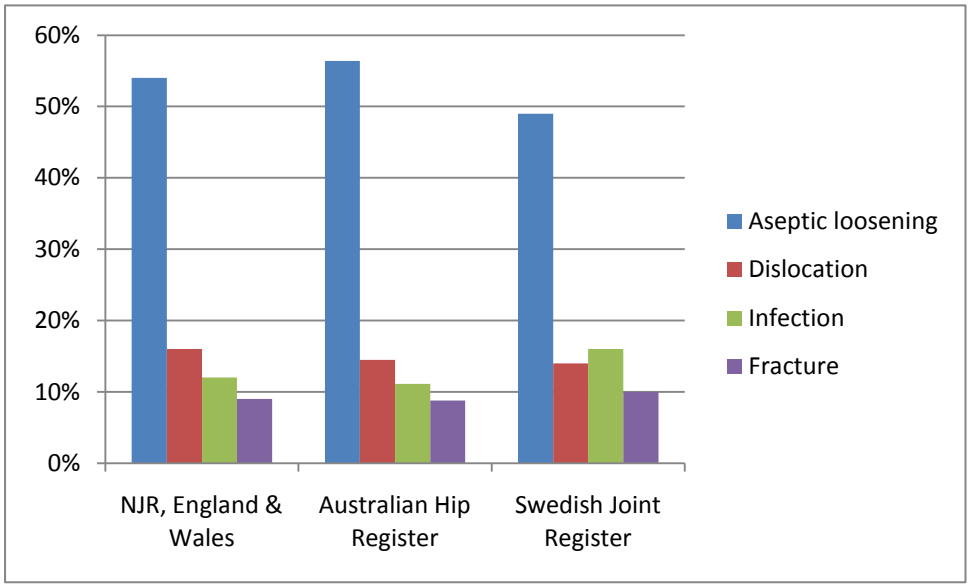

Figure 2.18: Causes of failure of hip replacements in different joint registers [4,59,60].

Aseptic loosening is a multi-factorial process, and can be induced by factors such as debonding, wear, micro fractures, fatigue failure and stress shielding or their combinations. Loosening exacerbates problems at the joint by making the joint unstable and causing pain and a return of symptoms to the patient. Some of these factors are elucidated below:

Debonding

Debonding is a failure process associated with cemented and uncemented implants alike and signifies the loss of the fixation in parts or the whole of the interface. In cemented implants, this can refer to the interface between the implant and the cement and also between the cement and the bone. Studies have shown that debonding often precedes clinical failure of the component, with shear stresses at the interface responsible for failure, starting at the distal end of the implant and proceeding to the proximal regions [61]. Debonding of the implant from the cement mantle can also lead to elevated stress level and in addition, provide a pathway for wear debris to reach the interface [62,63]. Residual stresses in the cement can also cause debonding by causing damage [64,65]. For uncemented implants that normally employ a porous coating to provide a rough interlock with the bone and also encourage bone ingrowth, debonding can take place when ingrowth fails to occur. These coatings require secondary stabilization through ingrowth to achieve stability, and factors like micromotion and high stresses and strains at the interface can prove detrimental. Research has shown that only extremely low levels of micromotion at the interface will encourage formation of bone with higher levels of micromotion will lead to the formation of the fibrous tissue [10]. Fibrous tissue, with weaker mechanical properties can loosen the implant. In addition, debonding can also result in particulate debris from the coating, leading to osteolysis [66].

Damage accumulation and fatigue failure

Damage accumulation can be defined as the gradual accumulation of mechanical damage in materials and interfaces due to repetitive dynamic loading. For a joint replacement, the damaging process proliferates eventually to disruption of the implant from the bone, bone resorption, interface micromotion, formation of fibrous tissue and gross loosening as described by Huiskes, 1993 [67]. These processes affect both cemented and uncemented implants but are associated more with cemented implants. For a cementless implant, a possible mechanism could be the formation of cracks at the interface bonds between implant and bone due to fatigue, which would produce high levels of micromotion leading to the formation of fibrous tissue and thus, failure of the interface. For cemented implants, the process of cementing can lead to the formation of pores and voids if not mixed correctly. These tiny voids can initiate cracks under fatigue loading and lead to gross loosening of the implant through damage accumulation. Cracks have been shown to develop at the cement-bone interface before loading, and located entirely in the cement after cyclic loading, showing the distributed cracking that occurs continuously under fatigue loading [68]. Crack initiation at pores has also been shown in other studies [69] where with higher stresses, more

cracks developed per pore. In addition a relationship between damage accumulation, loading cycles, and stress levels has also been formulated based on their interdependence in contributing to failure of the interface.

Osteolysis and Wear

Osteolysis and wear are closely associated in the loosening of implants. Osteolysis is an asymptomatic, time dependent process that arises from the inflammatory reaction of macrophages and osteocytes against wear debris. Wear by itself cannot loosen an implant, but the particle debris generated during articulation and other mechanisms can lead to o steolysis. Osteolysis is more pronounced in implants using polyethylene (PE) as the bearing surface due its poor wear characteristics, but can also be caused by cement particles (PMMA) and metallic debris. It has been shown that PE wear debris travel away from the articulating surfaces, assisted by the joint fluid and causes osteolysis at the interface leading to implant loosening [70]. The problem is exacerbated in cases of poorly fixed implants because of the larger interface gap that facilitates wear debris particle movement deeper into the interface. Metallic titanium particles have also been found to stimulate osteoclastic activity [71] and having systemic effects by affecting the liver, spleen, and abdominal lymph nodes of THR patients. Even mechanically stable, well-fit implants have shown signs of osteolysis due to particles of PMMA present in the surrounding tissues [72].

Stress shielding

Stress shielding follows Wolff's law, which states that bone is a living, dynamic material that will adapt to loads that it is placed under; it changes its external and internal architecture in response to the stresses acting on it [73]. This means that if the loading on the hip is high or low, it will remodel to adapt to the new loading environment. In stress shielding, due to the presence of the stiffer implant, the majority of the load is transferred through the implant rather than the bone. This results in bone adapting to the new environment and the removal of bone surrounding the femoral cortex [74]. The degree of stress shielding is dependent mainly on the stiffness of the implant, with stiffer materials resulting in more stress shielding compared to implants of lower stiffness. The degree of stress shielding is also more in uncemented implants due to their bulky nature and their tight fit in the medullary canal [75]. Other factors that can influence stress shielding are the fit and positioning of the implant, the bonding with the surrounding bone and quality of host bone. Stress shielding mostly affects the cortical bone. A variant of stress shielding is stress bypass where the seating of the implant becomes paramount. If an implant relies mainly on distal fixation and has a tight fit in the diaphysis, this would result in stress bypass to the diaphysis, shielding the proximal regions of the bone from experiencing any loads [67]. This would again result in the resorption of bone in the proximal regions. Hence, the shape and the seating of the implant in the bone become important.

Infection

Immediately following surgery, there is a high risk of infection to the tissues surrounding the implant. The National joint registry of England and Wales reports high percentage (12%), revision operations performed due to infection in 2008. Infection can cause pain and loosening of the prosthesis and can set early (early infections) or even after a year (late infections) following the operation. Infection can be acquired either during the operation itself due to unsterile conditions or outside through cross infection. Studies have shown that discharge from the wound site during healing, absence of prophylactic antibiotics, previous operations, remote infections and even the type of prostheses contribute to infection [76]. Infections at the replaced joint can also arise from other septic locations in the body, transported by the blood stream [77]. A number of precautionary measures, like those advocated by Sir John Charnley of using prophylactic antibiotics, laminar flow, and a body-exhaust system can help reduce the incidence of infection. Laminar, filtered airflow can significantly lower infection rate as shown by Salvati et al [78]. Loosening associated with infection can closely mimic those of purely mechanical loosening and can be extremely difficult to notice on radiographs. The difference is that in the case of infection, the implant has to be removed and an antibiotic course administered before revision can proceed [79]. Hence extreme care should be employed during and after surgery to prevent this condition.

Dislocation

A dislocation at the hip takes place when the implant head is displaced from the acetabular socket. According to the Swedish hip registry, dislocation is one of the three main factors responsible for revision surgery [1]. Dislocations can happen for a variety of reasons but are often caused due to the loosening of the muscles surrounding the joint post surgery. These muscles are important to maintain stability at the joint and any loosening can cause instability at the joint during articulation. Other factors include malpositioning of the femoral and acetabular components, the influence of previous surgeries and the recovery time after surgery [80,81]. Surgical approach is an important determinant in the positioning of the components and a faulty angle of implantation, especially of the acetabular component can lead to dislocations. Neuromuscular problems can also cause dislocations in some cases, along with the bad designs of the implants, surgeon experience, size of the femoral head and a long femoral neck also contributing [82]. A large femoral head is said to resolve this problem without compromising on the range of movement allowed at the joint [83].

Pulmonary embolism (PE) and deep vein thrombosis (DVT)

Both of these inter-related problems come under a more general term, venous thromboembolism (VTE). A DVT occurs when there is a blockage, partial or complete, by a blood clot in one of the deep veins [84,85]. PE is when this clot breaks off from its location and travels to the lungs through the blood streams. Large clots can cause death, and smaller clots damaging the lungs or the heart.

Problems arising due to PE after hip arthroplasties have been well documented [85], with even loose particles from the reaming of the bone contributing to the occlusion of the capillaries [86]. Some of the causes of DVT include limited activity and bed rest, smoking, fractures, obsesity etc. Blood thinning agents are often used which stop clots from forming. Surgery in extreme cases is also carried out.

Pain

These make up a few percentages of all failures according to the joint registries. Pain is usually associated with debonding of the stem from the cement mantle for cemented implants but is not necessarily the case with cementless implants. For cementless implants, thigh pain could be associated with the bulky nature and tight fit of the implant in the medullary canal. Other factors like subsidence, bead shedding and distal periosteal reactions are also said to cause thigh pain [87].

Fractures

Fractures of the implant itself are uncommon and occur only in extreme cases. Periprosthetic femoral fractures are more common and are mostly associated with trauma or a loose implant [88]. The same paper also found a close association of implant related factors like design and malpositioning contributing to fractures. It can be reasoned that a loose implant can cause stress concentrations in specific locations in the bone and under cyclic loading, cause fractures.

2.4 FIXATION OF IMPLANTS

2.4.1 INTRODUCTION

The method of fixation, along with the choice of bearing surfaces for articulation, are two of the main dilemmas faced by surgeons planning a joint replacement. The type of fixation for implants can be classified into two main categories, cemented and uncemented. Cemented fixations use polymethylmethacrylate or bone cement to fix the component in place whereas uncemented implants use a rough frictional interlock coupled with osseointegration to achieve stability. Figure 2.19 provides a description of the interface in both cases. More on this will be explained in the following sections. The rationale behind the use of either type of fixation is influenced by various factors like the implant type, their fit and fills characteristics, patient factors and also the surgeon's preference. A total hip replacement can be made of both components being cemented or uncemented or with one component cemented and the other uncemented, in which case it's called a hybrid fixation. In most cases of hybrid fixations, the femoral component is usually cemented with the acetabular side left uncemented.

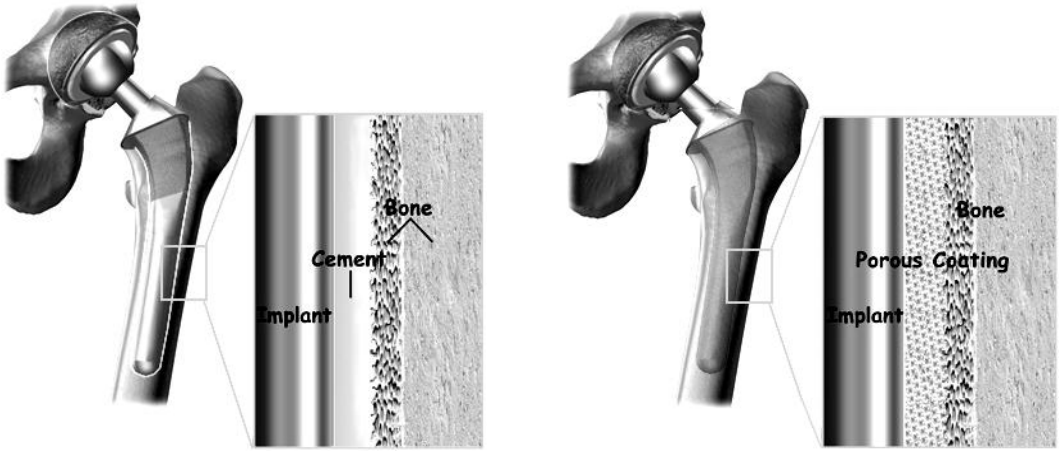

Figure 2.19: Schematic of the bone implant interface in a typical cemented (left) and uncemented fixation (right)[7].

2.4.2 CEMENTED IMPLANTS

Cemented implants, as the name suggests, are implanted using bone cement, commonly polymethylmethacrylate (PMMA). Before its advent in arthroplasty, it was used in dentistry [89]. Cemented fixation of implants became popular after being pioneered by Sir John Charnley in the 1960's but it wasn't the first case of the use of bone cement for hip arthroplasty. It was reported as early as 1953 when a fast setting dental acrylic was used to fix a femoral component [90]. However, it was still Sir John Charnley who popularised and revolutionized the use of bone cement for the fixation of implants [91].

2.4.2.1 BONE CEMENT

Bone cement is made of two main components, with an additional smaller percentage of other substances used to improve specific characteristics of it. The cement is supplied as two components, a PMMA powder component, and a monomer methyl methacrylate component which combine and through polymerisation form bone cement. Bone cement acts as a grout and holds the implant firmly in place. It should be noted that the cement does not provide adhesive properties, and merely conforms to the gaps and spaces and fills them accurately.

[7] http://www.eorthopod.com

2.4.2.2 BASIC DESIGNS

Considering cemented implants, there are two main designs based on the surface finish that are commonly used. The surface can be smooth and polished, or roughened-matt textured. The smooth and polished like the Charnley cemented stem is a force closed design with a tapered edge, which minimises shear stresses but increase compressive radial stresses. The incidence of initial migration is high in these designs. In contrast, the roughened matt finished stems are shape-closed designs and provide a better mechanical interlock with the cement that prevents initial migration, but transmit high shear stresses to both interfaces [92]. An example of a cemented stem that comes in a matt finished and a polished version is the Exeter stem. In an extensive study done on this stem, it was found that the rate of revision was almost four times higher than found with the polished stems over 20 years [93]. Osteolysis was found to be the biggest problem, with matt surfaced stems showing more abrasive wear on its surface. This contributed to the wear of the internal surface of the cement mantle and enlargement of the interface gap, providing a way for particle debris to be transported by joint fluid. This has also been supported in other studies [94-96].

2.4.2.3 ADVANTAGES

Cemented implants have been the popular choice in many countries and also among surgeons. Cementing has been called the “gold standard” due to their excellent clinical history and their ease of use. Cementing provides a number of a advantages. Firstly, the cementing procedure is very forgiving in terms of preparing the bone for implantation. The surgeon can afford to make small deviations from a precise operating technique. The preparation of the femoral canal need not be a perfect fit for the implant because the bone cement acts as a grout or filler. The bed cut can be much larger than the prosthesis and the cement would fill out the incongruities. It also allows the surgeon to make minor modifications to the positioning of the implant, while the cement is still curing. Another advantage of the use of bone cement is that weight bearing is possible in a shorter period as compared to cementless implants. The strength of the cement reaches its peak at the end of the operation and weight bearing would be possible in 2-3 days following the operation. The recovery time would only be restricted to the healing of the soft tissues around the hip following the operation. This would imply that patients would be able to resume normal activities in a shorter period as compared to the weeks of immobilization that would ensure following a cementless implant. Infection, normally associated with any hip arthroplasty can also be minimised by the addition of antibiotics in the bone cement.

Cemented implants also help in transmitting the loads acting at the joint over a larger surface area as compared to uncemented implants [91]. This is due to the interlocking of the cement between the trabeculae of the cancellous bone. Moreover, due to the cement conforming to the shape of the implant, the chances of stress shielding and bypass are also drastically reduced and there is more

uniform stress distribution. Cemented implants do not have the limitations of uncemented implants with respect to the quality of bone and can be used in older patients safely, without compromising on the stability of the implant.

2.4.2.4 PROBLEMS OF BONE CEMENT

There are a number of problems with the use of bone cement, both mechanical and biological, that can lead to complications. Bone cement fixation results in the formation of two interfaces: cement-bone and the cement-implant. Results for femoral components have shown that the incidence of loosening at the two interfaces is evenly divided, as described by Gruen et al and shown in figure 2.20. The mechanical aspects tend to be largely causative of the problems associated with the cement-bone interface and the biological aspects at the bone cement interface.

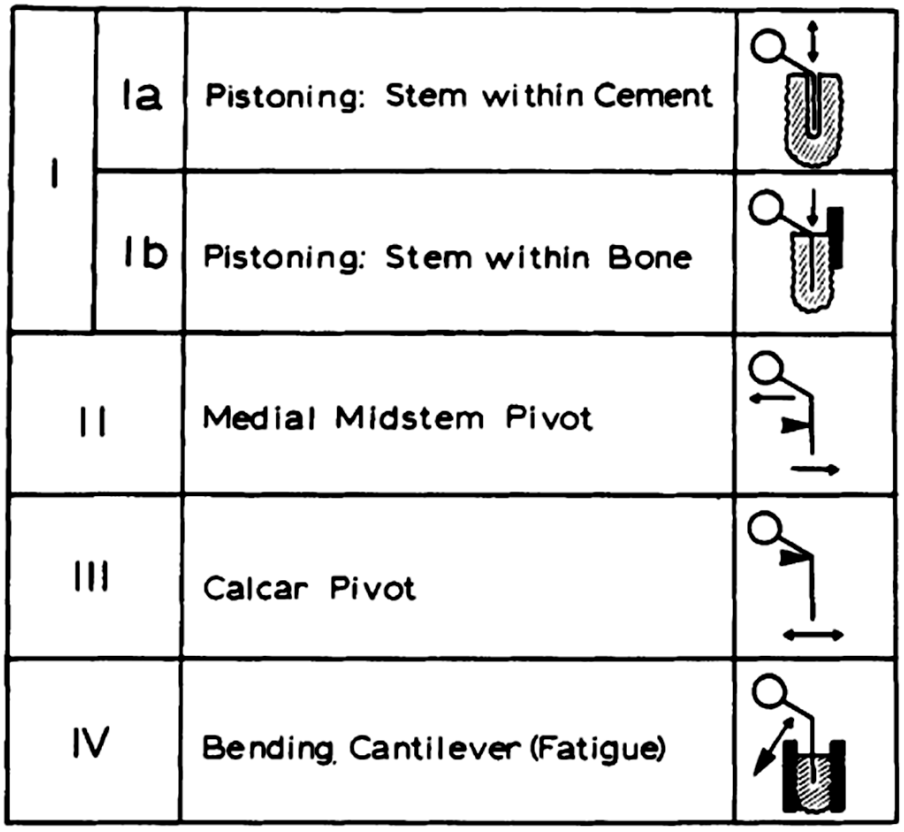

Figure 2.20: The four modes of failure as described by Gruen et al [97] .

Loosening of a cemented component on a purely mechanical basis has been explained by the same authors based on four principal modes of failure through loosening, namely

- Pistoning behavior of the stem with the cement, and the cement with the bone that results in the formation of radiolucent zones.

- Medial midstem pivot characterized by the medial migration of the proximal stem coupled with lateral migration of the distal stem tip.
- Calcar pivot defined by the medial-lateral toggle of the distal end of the stem due to the lack of support in the region.
- Bending cantilever fatigue characterized by the partial or complete loss of proximal support followed by the medial migration of the proximal stem with the distal end remaining fixed.

The specific problems associated with loosening are discussed as follows:

Debonding

Cement-stem debonding is one of the most common forms of failure in cemented implants. Debonding of the stem-cement interface affects the damage process in the stem and the cement considerably. Debonding has been directly linked to high strains and stress on the cement mantle at the proximal and distal tip of prosthesis and also with crack initiation at the debonded surface of pores in the cement surrounding the debonding [98]. These cracks are said to be formed due to stress changes secondary to debonding. Bone cement has another property that has adverse consequences. Its shear strength is only one-third of its tensile strength. Hence if the cement is subjected to shear forces, like the rotation of the stem, it would not be able to resist the load. Finite element studies by Verdonschot et al [61,63] have also shown that debonding is governed by the shear stress component at the interface. Debonding was found to start at the tip region and the proximal, medial anterior region. These debonded regions expanded until the whole interface was debonded, hence causing implant loosening. Debonding is also one of the primary causes of aseptic loosening. This can be explained by the phenomenon of accumulation of wear debris. The debonded stem produces a pathway for debris during loading or normal motion. The formation of the pathway can be adjudged by the interface area that was in contact with the cement. This pathway where debris can accumulate and cause damage can be considered as a possible cause of aseptic loosening.

Another clinical implication is the excessive fatigue caused due to the debonding. The high stress regions are more likely sites for failure initiation. Fatigue cracks often originated from the stem surface. This might be associated with the sharp corners in the stem geometry where high stresses were found [99]. Fretting wear, as a result of primary debonding, could also cause implant loosening in cemented femoral stems [100]. The cement relies on mechanical bonding in order to adhere to the interior of the femur, and also on the chemical bonding to secure the stem within the femur. If the stem manages to loosen from the (primarily chemical) bond of the cement, it rubs and wears against the fairly brittle cement sleeve, resulting in particulates of metal and cement.

Osteolysis

Bone cement can fail under various factors, the most common being damage accumulation under constant dynamic and repetitive loading. When the cement mantle fails, through the defects in the cement mantle, wear particles have been reported to be transported from the stem-cement interface to the cement-bone interface. This process was found to be enhanced when the stem debonds from the cement mantle and a pathway forms to transport particles from the joint space to the fractured sites, activating macrophages and hence osteolysis [101]. Osteolysis almost always follows after loosening of the stem but has also been reported around stable well-fixed cemented implants by Jasty et al and Maloney et al [72,102]. Jasty et al reported that loosening of the implant is not an absolute prerequisite to lysis around cemented hip replacements. It was speculated that osteolysis was a reponse to particulate debris from the articulating surfaces on acrylic wear debris. The osteolytic regions were found to be remote from the joint and PMMA particulate material was found with macrophages and giant cells in the reactive tissue. Maloney et al also reported similar results of lysis being caused by foreign body reaction to particulate PMMA (
figure 2.21). It was also concluded that small amounts of PMMA stimulated endosteal erosion and localized osteolysis. Hypersensitivity has also been reported as a possible cause of osteolysis [103,104].

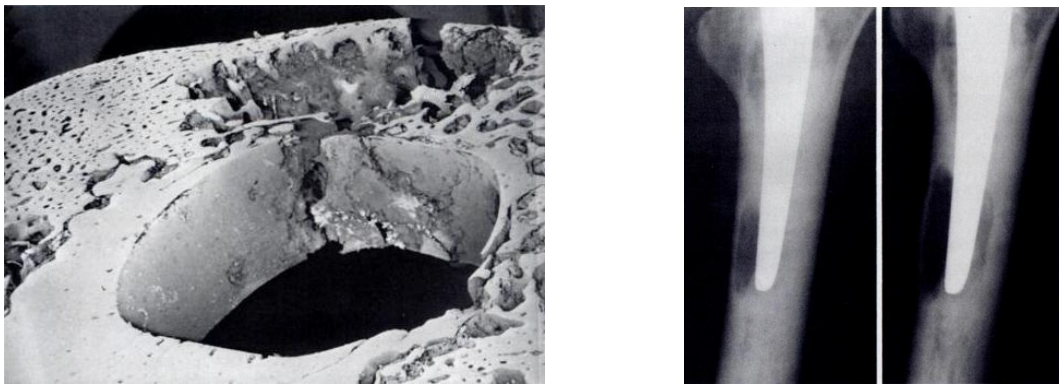

Figure 2.21: SEM showing multiple fractures in the cement mantle with fragmentation of the cement adjacent to a focal area of bone lysis (left) and osteolysis at 102 and 134 months [102].

Residual and shrinkage stresses

Residual stresses are often used in conjunction with shrinkage stresses and are formed in the cement mantle during the polymerization of bone cement. Normal stresses at the stem–cement interface are developed resulting in a press-fit problem. Nearing the end of the process, when polymerization takes place in contact with the cortical bone, which has impermeable surfaces, the residual radial stresses always remain compressive at the stem–cement interface due to the cement

expansion [105]. A finite element study by the same author concluded that residual stresses affected the cement stress distributions at the stem–cement interface. Residual stresses are influenced by shrinkage stresses. To separate shrinkage stresses from residual stresses a separate description follows.

Bone cement shrinkage is yet another factor that contributes to the loosening of an implant. In order to improve the fatigue life of bone cement, vacuum mixing has been favoured to hand mixing as this has been shown to reduce the number of pores formed in the cement [106]. However, the volume of vacuum mixed cement may reduce by as much as 7–8% on curing, compared with only 1–2% in hand mixed cement [107,108]. This is a consequence of the greater content of air bubbles in hand mixed cement expanding during polymerization to counteract shrinkage. The Residual stresses explained earlier are influenced by the shrinkage stresses. Experiments undertaken by Orr et al [109] to investigate shrinkage stresses and its effect on the residual stresses (figure 2.22) have shown that in some cases, the shrinkage stresses neared and sometimes exceeded the tensile strength of bone cement. This could prove detrimental to the stability of the cement mantle and cracks would initiate.

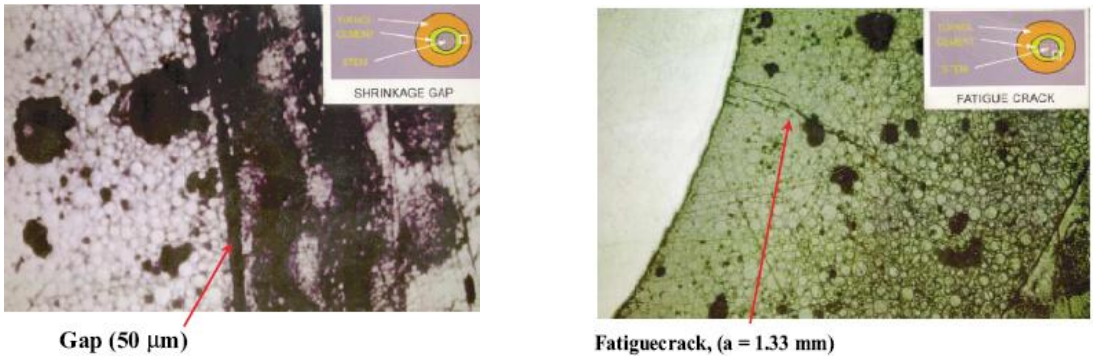

Figure 2.22: Shrinkage gap at the cement-bone interface (left) and the radial fatigue crack at the cement-prosthesis interface (right) [109].

The studies by Lennon et al [64,65]summarise the importance of residual and shrinkage stress. They conclude that residual stress is a factor in pre-load cracking of cement mantles of orthopaedic joint replacements but requires additional factors, such as porosity, stress concentrations, or excessive heat generation, to initiate large cracks. Also, the peak temperature reached for a given region of cement has a significant effect on the level of residual stress that occurs, indicating that control of polymer/monomer ratios as well as ambient conditions during polymerization are critical in controlling the phenomenon of preload cracking due to shrinkage.

Thermal and Chemical necrosis

Since the inception of bone cement in the fixation of orthopaedic implants, there have been concerns about the detrimental effects of the polymerization reactions of the cement in close apposition to the bone. Thermal and chemical reactions produced by the reaction have been reported to cause bone necrosis thus resulting in loosening [110,111]. Homsy et al. [112] and charnley [113,114] have also reported substantial trauma at the implant bone interface. Figure 2.23 shows the extent of damage found after the insertion of cement in the same study. However, the latter has attributed the necrosis to the processes associated with the implantation; broaching, rasping and polymerization combined rather than just on the process of thermal and chemical changes as stated by the former. The rationale behind the possible necrosis is that the heat evolved during the change of the high-energy unstable monomer molecule to the low-energy polymer causes the surrounding bone to die. In addition, the amount of heat produced depends on the amount of the monomer polymerizing and the temperature reached at any given site depends on the rate of production and ease of escape [115,116]. Work by the two separate authors also concluded that the highest temperature at the cement/bone interface is achieved in those cases in which large amounts of acrylic are used. Stanczyk et al [116] in his finite element study concluded that trabeculae extending deep into cement are exposed, for short duration, to temperatures in excess of 70^{o}C and are in a prolonged contact with the volume of cement containing substantial monomer leftover. This could result in bone necrosis. It was also found by the same author that bone tissue that is subjected to the highest temperatures is also subjected to high leftover monomer concentration. Furthermore, the maximum bone temperature is reached relatively early, when monomer content in the neighbouring cement is still quite high thus unlikely that cells subjected to the conditions will survive resulting in necrosis and hence, loosening.

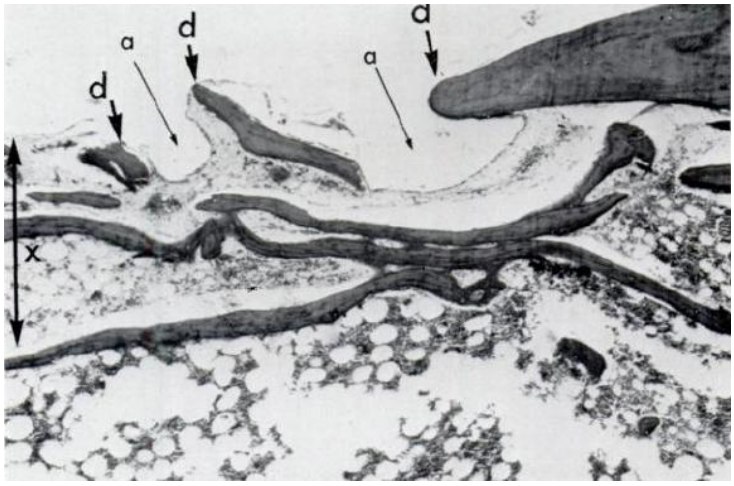

Figure 2.23: Photomicrograph of the interface seventeen days after the insertion of cement. 'a' represents the cement bulges, d the original trabeculae and x is the depth of tissue damaged by cement [114].

Necrosis due to chemical aspects can be well explained by the fact that insertion of the cement brings into contact with bone a powerful fat solvent. Monomers and fat are miscible and also, the cement dough contains free radicals that are formed during activation and are chemically reactive. Chemical damage can damage cell walls can cause protein coagulation [115]. However, it has been a common consensus among the articles reviewed that thermal necrosis in itself is not as detrimental as compared to the mechanical, vascular and chemical trauma that occurs [113,114,116,117].

Cement pores

High cement porosity compromises the cement's mechanical strength and lessens its fatigue life. Pores or other inclusions concentrate stress in the material, often initiating fatigue cracks. These cracks ultimately lead to mechanical or aseptic loosening and implant failure. Reports show that fatigue fractures always occur at the largest macropores [118,119]. Figure 2.24 shows pores in the cement mantle after hand mixing of the cement. Cement fracture and subsequent premature loosening are directly related to the strength of the cement mantle, which acts as an interface between the bone and the prosthetic component. It has been shown that acrylic bone cement is weakened by its porosity, which promotes the formation of micro-cracks that contribute to major crack propagation. It has been observed that mixing procedures play a significant role in determining the quality of bone cement produced [107-109].

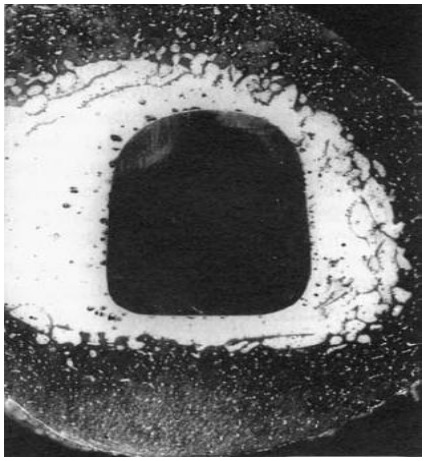

Figure 2.24: Pores formed in the cement mantle after hand mixing [120].

The sources of porosity are in the mixing and delivery stage:

- Trapped air initially surrounding the powder and between the powder beads as the powder becomes wet.
- Trapped air in the cement during mixing.

- Trapped air in the cement during transfer from mixing container to application device.

Hand mixing bone cement in an open bowl allows for the greatest possibility of these occurrences. Large voids and flaws within the cement may lead to a cement mantle fracture caused by rapid crack propagation. Because macroporosity has been shown to be a cause of reduced fatigue strength and mechanical failure, reduction of cement porosity is a logical step [121]. There is strong evidence that cracks in the cement are initiated at voids which act as stress risers, particularly at the cement-stem interface. The preferential formation of voids at the site results from shrinkage during polymerization and the initiation of this process at the warmer cement-bone interface, which causes bone cement to shrink away from the stem [120]. In the same study, it has also been concluded that when a stem at room temperature is implanted into bone which is at approximately body temperature, the polymerization of bone cement will progress from the bone towards the stem. This induces pore formations in the cement mantle near and at the cement-stem interface. The pores decrease the static strength of the cement-stem interface and affect the fatigue strength.

2.4.3 UNCEMENTED IMPLANTS

Uncemented implants can refer to any implant that does not require the use of bone cement for fixation. These implants rely on their rough surface and close apposition to the surrounding bone to provide secure fixation following implantation. Most uncemented implants are press-fit, which implies that the prepared bed for implantation is often undersized compared to the implant. This allows the implant to be firmly fixed in place, and coupled with the interlock provided by the coating, help provide good primary stability.

Uncemented implants, based on the surface in contact with the surrounding bone, can be of three main types: Implants having roughened surfaces with no porous structures, implants with porous coatings and implants with osteoconductive coatings applied to the roughened/porous surface. Implants with just roughened surfaces rely entirely on their proximity to the surrounding bone to provide a good frictional interlock. Additional screws and nails are also used occasionally to provide stability. Porous coated implants use porous structures on the implant surface to initially provide frictional interlock with the surrounding bone and also allow bone formation into or onto the surface. This formation of bone from the endosteum to the surface or specifically into the pores of the coating is often referred to as bone ingrowth or osseointegration [122] . The rationale behind the use of these implants is that if bone grows into the porous surfaces, it can provide a secondary and more stable long-term fixation. A dedicated section on porous coated implants follows in chapter 3. Uncemented implants also use additional osteoconductive coatings like hydroxyapatite and bioactive glass to promote bone ingrowth on to the surface of the implant [123]. These coatings can be applied on the roughened surface of the implant or the porous surface without affecting the porosity by much. These coatings allow bone to grow on their surface. The rationale behind their

use is that bone formation could be stimulated on the surface of the implants, with the coatings gradually being resorbed.

Traditionally, uncemented implants have been large and bulky, with the emphasis being on the fit and fill principle for maximum contact with the surrounding bone, including the diaphysis to encourage more osseointegration with the implant. The anatomic medullary locking (AML) and the porous coated anatomic (PCA) are two such implants that employ this principle and engage the diaphysis for fixation. However, a constant concern regarding uncemented implants, and specifically those that rely on distal fixation has been the stress shielding of the proximal regions of the femur; causing atrophy and loosening of the implant proximally [74,124]. To this end, more recent developments in uncemented implants have relied on engaging the proximal regions of the femur, either through using roughened surfaces/porous coatings only in the proximal half of the implant or through designs that load the proximal femur effectively, including reducing the size of the implant or using the stem as a alignment tool rather than for fixation [125-133]. Other concerns arising from the uncemented implants have been incidence of thigh pain, attributed to the tight fit or with failing fixation [87,134], loosening and wear of the coating [135,136] or fracture of the femur during implantation or at later stages.

2.4.4 CURRENT TRENDS IN FIXATION TYPE

The choice of cemented and uncemented implants for primary hip replacement varies from one country to the next. Traditionally, Europe has always been pro-cement use, with countries like Sweden and England contributing to the large number of cemented procedures. For example, the Swedish hip arthroplasty register [1] records no uncemented implants used in 1979 and very few used till around 2000. However, the use of cemented implants is on the decline, even in these countries that have traditionally been inclined to using cement. For example, there was a sharp decline in the use of cement in the last 10 years in Sweden and a similar trend of late observed in England and Wales (figure 2.25).

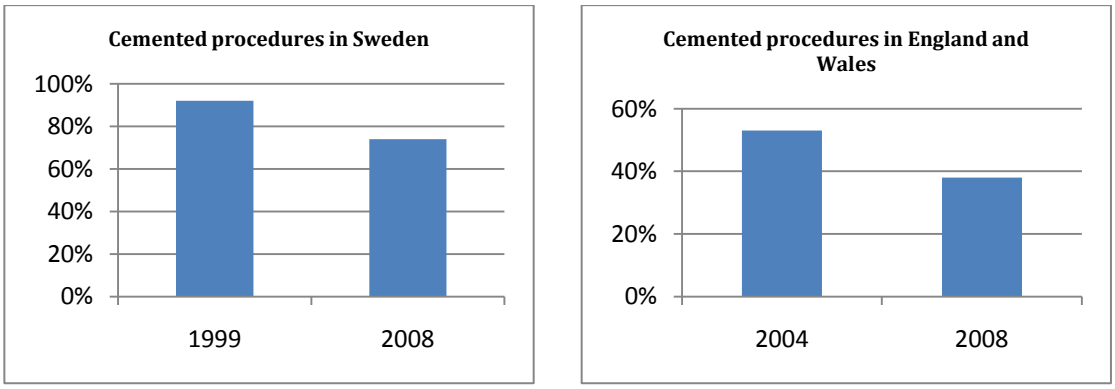

Figure 2.25: The fall in the use of cemented procedures in two different countries [1,51].

The decline in the use of cemented implants has been due to a corresponding increase in the use of uncemented implants. There could be a number of reasons for this; the minimum age of the population requiring hip arthroplasties has drastically reduced, there is renewed belief in the advantages of using uncemented implants for these young patients, surgeons are now getting more experienced with their use and using them for patients who would normally have had a cemented procedure etc. For example, between 1992 and 2007, the average age of patients using uncemented implants has gone up from 45 years to 57 years with little change in the age group for cemented implants [59]. In New Zealand, the last 9 years has seen the most change, with the number of cemented and uncemented implants swapping places (figure 2.26). A similar rise is seen in the national joint registry of England and Wales through the last 4 years.

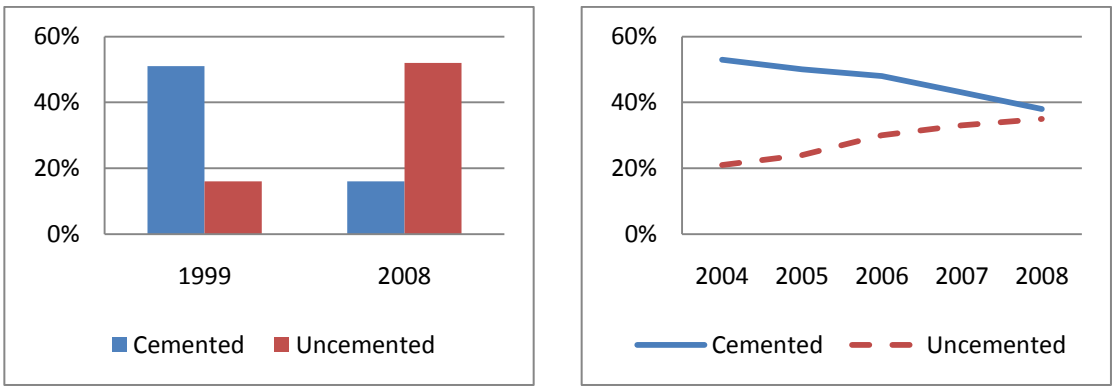

Figure 2.26: The rise in the use of uncemented implants in New Zealand, and England and Wales for different years [1,51].

Other countries like Australia, Canada and North America have had a preference for uncemented implants and their use is always on the rise [3,137]. The hip registers of Australia and Canada report the percentage of uncemented implants used at ~62% and 71% for 2008. The use of cemented implants was as low as 3% in Canada.

Based on the joint registry data from the aforementioned countries, there is no doubt that the use of uncemented implants is always on the rise and the focus is on more natural integration with the surrounding bone than the use of artificial substances for the fixation of implants. Uncemented implants are advocated for patients under the age of 60, who have good bone stock and do not suffer from severe osteoporosis. Above this age group, the use of uncemented implants declines, and are used only in few cases where the surgeon can justify their use over their cemented counterparts. The national joint registry of England and Wales highlights this fact, with the age range for the use of cemented implants between 68 and 80 years, with uncemented between 59 and 73 years. The higher activity level of these young patients may also warrant an additional revision

surgery at a later point, but on a comparative note, uncemented stems in particular have been found to function better than cemented stems for a period exceeding 10 years [59]. For countries that have traditionally been inclined to uncemented implants, the numbers are promising, with the percentage of revised femoral components on the decline in the last few years as show in figure 2.27.

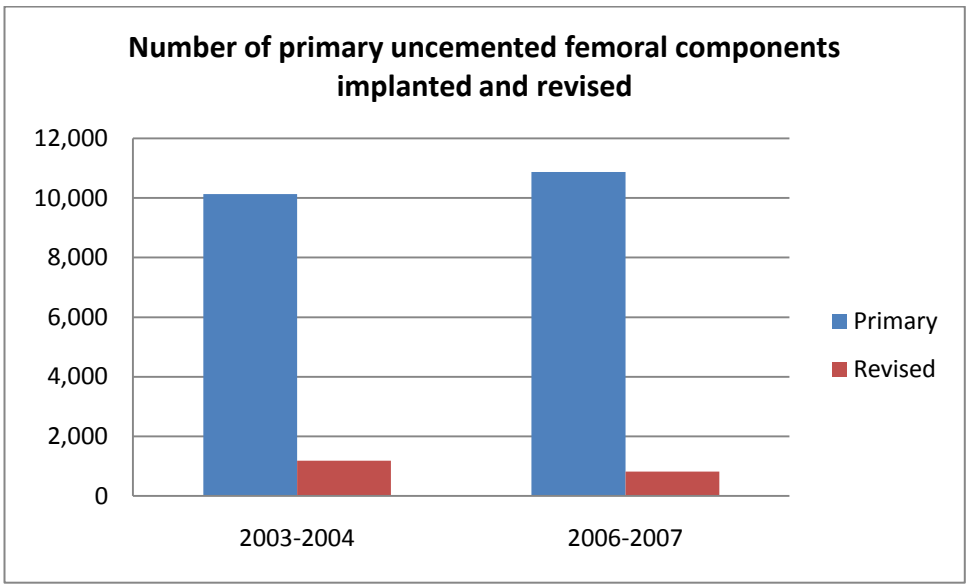

Figure 2.27: The number of primary uncemented femoral stems used and their revised numbers for specific years [3].

Considering the number of problems associated with the use of cement, the use of uncemented implants has seen a rationalised increase in many countries. The promise of a biological interface, if achieved, could result in a safer, more stable interface increasing the longevity of the fixation and reducing the chances of interface failure, especially due to aseptic loosening.

2.5 POROUS COATINGS FOR UNCEMENTED IMPLANTS

2.5.1 INTRODUCTION

The concept of implant fixation by bone ingrowth arose in the early 1900's for a conceptual artificial tooth root. The idea, developed by Greenfield, consisted of a metallic cage-like framework which bone would grow into and around and securely fix it in position. However, it was following the 1950's that the idea really came into prominence with the use of polyvinyl sponges for bone reconstruction [138,139]. In the 1970's, the use of metallic porous surfaces in the form of cobalt chrome and titanium beads came into use followed by titanium fibre mesh coatings. The trend to use metallic coatings has continued through the years. An important aspect regarding the choice of

porous coating for implants is that the performance is dependent on the amount of bone ingrowth it can achieve, which in turn is dependent on the configuration of the coating itself. A range of biomaterials have been used as porous coatings for implants; polymeric, ceramic and metallic coatings have been used with varying success depending on their compatibility.

The choice of using polymeric materials began as early as the 1970's. The rationale behind using these materials was the low elastic modulus that could be compatible with bone. Spector et al. [140] used porous high-density polyethylene as implants in canine femurs to investigate the possibility of bone ingrowth. Good bone ingrowth at the end of 4 weeks was obtained, but for unloaded conditions. Biodegradable porous polymers based on polyurethane have also been used to fill in bone defects [141]. The use of polymeric materials as porous coatings for loaded conditions in human joints would not be feasible as its ability to withstand mechanical forces at the implant site would be limited. Excessive micromotion at the interface can also be problematic with the use of porous polymeric materials.

Porous ceramics have enjoyed success, primarily as fillers for bone defects. Foams of calcium phosphate, calcium titanate, calcium zirconate, and aluminium oxide have been investigated earlier in animal studies [139]. However, their role as porous coatings on loaded implants has been limited due to their inherent brittleness. Ceramics used in implants can be categorised as bioinert and bioactive. Bioinert ceramics like alumina and zirconia are currently used as articulating surfaces. Other ceramics based on calcium phosphate like bioactive glass and hydroxyapatite can be used as bioactive surface coatings on the implant substrate or on existing porous surfaces to promote osteoconduction. The osteoconductive nature of these bioactive ceramics promotes bone formation on the surface and in the process encouraging bone ingrowth into the pores of the coating. The role of these coatings will be explained in later sections.

The poor overall mechanical properties of ceramics and polymeric materials have restricted their use as porous coatings, and instead brought into prominence the use of metals as porous coatings [142]. Metallic coatings have good fracture and fatigue resistance. The initial rejection of metal for use as a porous surface was based on possible corrosion due to the large surface area and the high modulus that could cause remodelling of bone. However, improvements in fabrication techniques have reduced this problem and metals are currently the preferred biomaterial for porous surfaces on loaded implants. The metallic porous coatings used in implants for joint arthroplasty usually consist of a solid substrate of relatively high modulus on which the porous coating is applied. The modulus of the substrate is much higher when compared to the porous coating. The substrate provides the mechanical properties required by an implant (based on its location in the body). The coating is applied to the solid substrate by different techniques depending on the type of coating. An overview of the fabrication processes used currently in industry is explained in section 2.5.2.

Typical porous coatings used in hip and knee replacements are cobalt chrome or titanium alloy spherical beads that could range from a single layer to multiple layers of beads. Some of the implants using beads as porous coatings are the Porous coated anatomic (PCA) and the Anatomic Medullary locking (AML) prostheses (Co Cr beads), and the Microloc knee prosthesis (Ti beads). Other porous surfaces used are fibre mesh coatings mostly limited to titanium as the material (Harris/ Galante hip and knee). The titanium fibre mesh is applied on a titanium substrate. Cobalt Chrome alloys are generally not used as fibre mesh coatings. Grit blasted and plasma sprayed porous surfaces are also currently used in uncemented implants to promote bone ingrowth. They rely on their irregular surface for bone attachment rather than their limited porosity. Some of these surfaces are shown in figure 2.28.

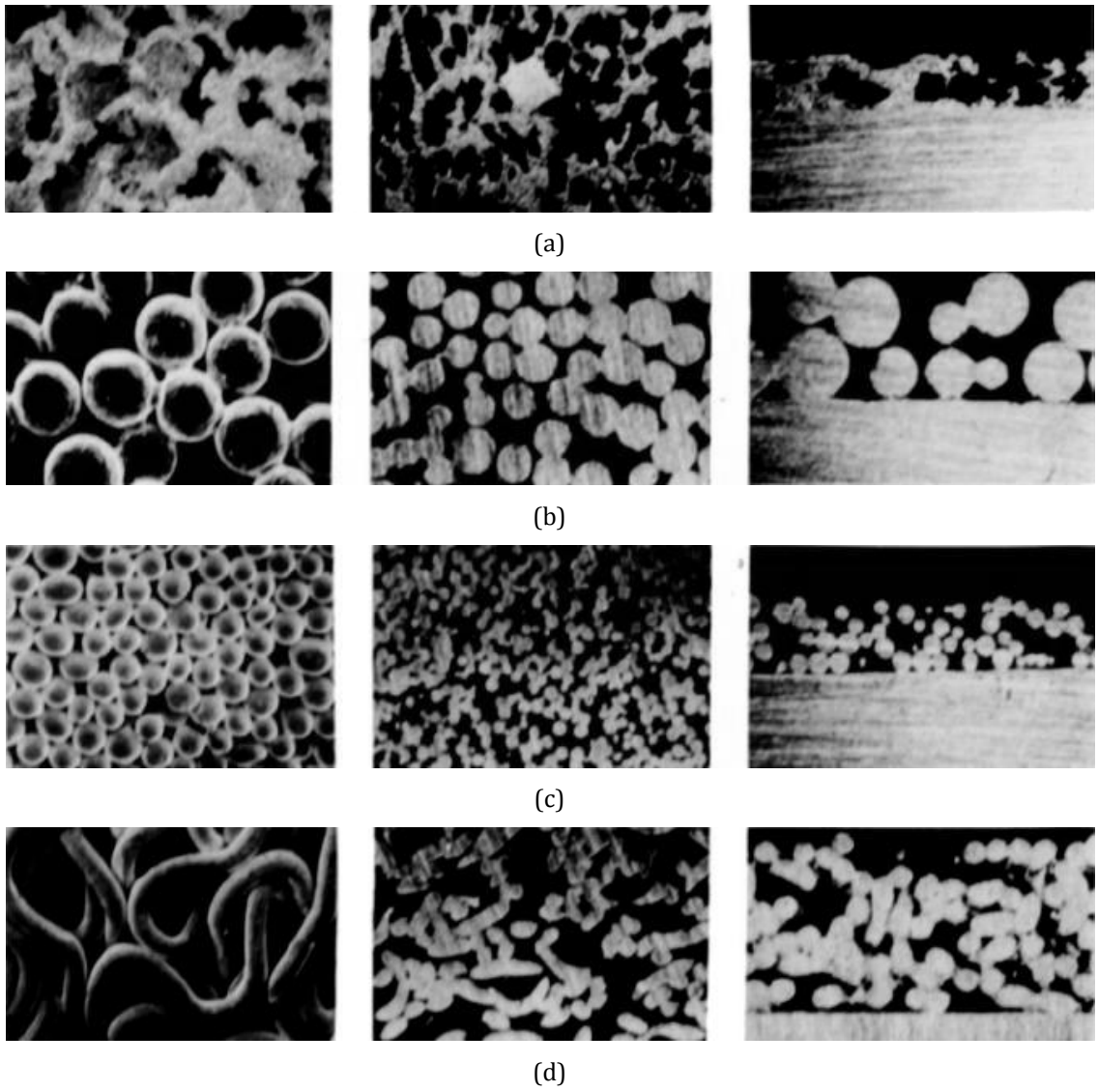

Figure 2.28: Different porous surfaces commonly used for bone ingrowth. (a) Plasma sprayed surfaces, (b) sintered beaded surfaces (large spheres), (c) sintered beaded (Small spheres), (d) diffusion bonded fibre metal surface. Figures left to right show cross sections through the porous surfaces [143].

Porous implants can be categorised as being (a) fully or partly porous coated substrates (b) fully porous materials or (c) porous metal segment joined to a solid metallic part. Fully porous materials are often used as bone grafts to fill in defects. There are two main categories of porous metals based on the connectivity of pores. They are open cell and closed cell porosities. In open celled porous materials, individual pores are interconnected to provide a complex network into which tissues and blood vessels can grow. This also means that there exists a continuous layer of tissue from the originating tissue into the implant, which could provide better fixation. In closed cell porous materials, each pore is surrounded and enclosed by a thin wall or membrane of metal, with no interlinking with other pores. This results in a closed structure and is usually a result of a random foaming process during manufacturing [142].

2.5.2 FABRICATION TECHNIQUES FOR POROUS METALS

Porous coatings are usually applied to the substrate metal by one of three techniques, sintering, diffusion bonding and plasma spraying. All of these processes are distinct and result in surfaces that are unique in their mechanical properties. These fabrication processes also differ in their complexities. Sintering is the simplest of the techniques and involves compacting, binding and sintering metal powders [142]. The process is based on extremely high temperatures that bonds particles to each other with minimum change of shape. A binder is used to provide adhesion between the particle and the substrate initially. The strength of the bond produced depends on the temperature, total time and impurities present. Powders and beads of Co-Cr, Ti, Ti alloys and NiTi have been used in this process. The porosity obtained by sintering is usually limited to around 30-50%. The potential problem of sintering is that the process results in the loss of fatigue strength of the substrate metal, especially with titanium [142].

Diffusion bonding has been used to counter some of the problems faced by sintering. Titanium fibre mesh porous surfaces are usually fabricated by this technique. The fibres with the required porosity are arranged on the substrate and then subjected to pressure and high temperature to attain the bonding [12]. The temperature is much lower than that used in sintering. Porosity can be controlled by arrangement of the fibres initially before bonding.

However, the most versatile of the aforementioned fabrication techniques is plasma spraying. The technique can be used to obtain graded distribution of pores for both metallic and non-metallic coatings like HA [12]. In this process, it's the powder used to create the porous surface that is heated and not the substrate hence maintaining the fatigue characteristics. An electric arc is generated between two electrodes that ionises, pressurises and raises the temperature of the gas present forming a plasma jet. The powder is released into this gas stream and impacted on the substrate through a nozzle. The porosity of the surface can be controlled by adjusting the spraying parameters [142].

2.5.3 COATING PARAMETERS FOR EFFECTIVE INGROWTH

2.5.3.1 PORE SIZE AND POROSITY

Pore size and porosity are important determinants of how much bone ingrowth can be achieved at the porous surface. The pore size should not be too small as to hinder the growth of new bone and blood vessels and not too large as to weaken the interface. Extremely large or small pore size could result in the formation of fibrous tissue. The minimum pore size for bone ingrowth for loaded implants has been considered to be around 100μm, although studies have shown bone ingrowth with pore sizes much lower [144-146]. The current standard remains the use of pore sizes ranging from 100-600μm to allow osteoid and vascular formation in the porous layer for optimum bone ingrowth. Canine studies have also indicated that the percentage of bone ingrowth does not differ much between pore sizes of 200 and 450μm [143]. Larger pore sizes have also been attributed to better strength of fixation as compared to those smaller than 100μm, but within the 100-600μm range, the strength has been found to not vary much [147].

Particle interconnectivity is another factor essential for the strength of the porous coating. It corresponds to the size of attachment between the particles of the coating. As reported by Haddad et al. [139], high and low interconnectivity could be detrimental to the strength of the tissue and ingrowth of bone. A high level of interconnectivity could result in smaller pore sizes, hence affecting ingrowth. Similarly, low interconnectivity could mean larger voids between particles and hence decreased structural strength of the coating itself. In addition, if large numbers of particles are present in the porous coating, a better frictional interface between the bone and the implant can be obtained due to more particle to bone contact. Hence, a compromise is essential to provide an optimum porous surface for bone ingrowth and yet maintain structural strength.

Porosity is often expressed as volume fraction porosity, which is the percentage of available gaps or voids within the coating. It is a function of the pore size, particle interconnectivity and particle size of the coating. A volume fraction porosity of 40% or higher is considered ideal with evidence of good bone ingrowth in these cases [148]. Higher percentages of bone ingrowth have also been obtained in porous surfaces with porosity greater than 60% as compared to lower porosities [149,150] confirming the need for good porosity within the porous surface. Good internal porosity is also essential for anastomosis of blood vessels and for ingrown tissue interconnectivity, ideally resulting in a continuous band from the tissue surrounding the implant into the porous surface. Formation of de novo bone (new bone) within the porous surface, devoid of connection with surrounding bone tissue would result in a mechanically weak interface. Figure 2.29 shows an example of two different porosities for sintered porous Ti implants

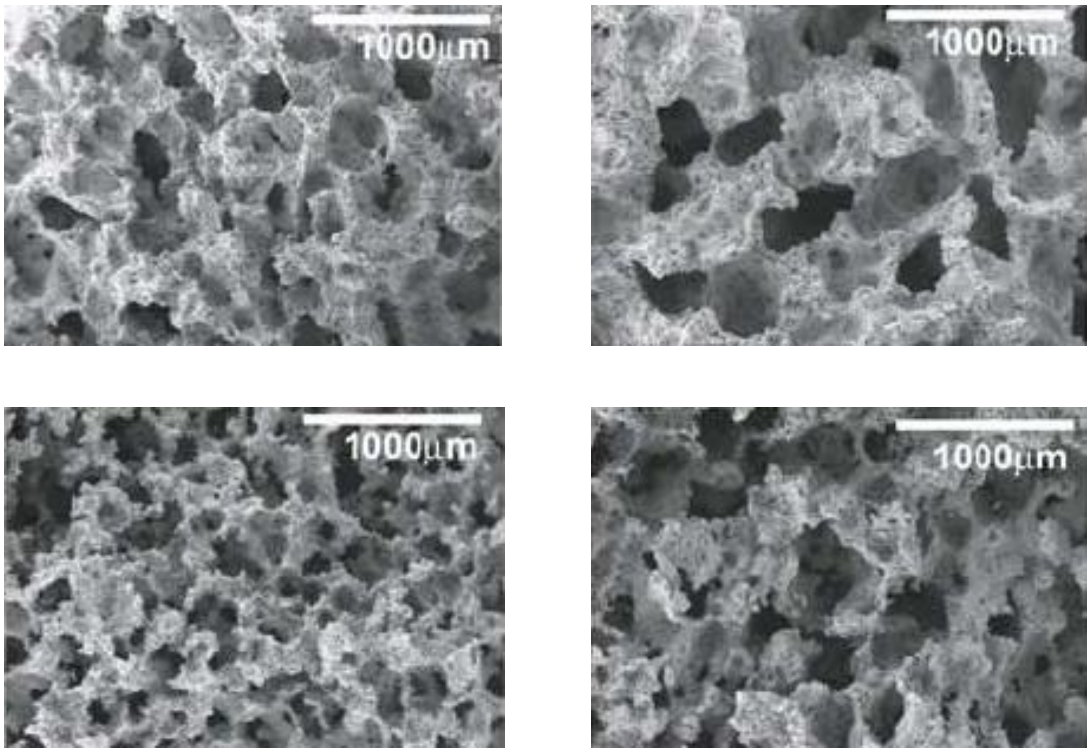

Figure 2.29: SEM view of sintered porous Ti implants with different porosities [150].

Controlling porosity is also essential, as high porosity could be detrimental. There has been evidence of totally porous implants having a weaker interface than porous coated implants due to improper anastomosis of blood vessels at the deeper levels of the implant, which could have an adverse effect on bone ingrowth. The mechanical strength has also been found to be compromised in these implants [151]. When considering coatings such as HA on porous surfaces, it should be noted that the porosity and pore size should be increased accordingly to prevent obstruction of the pores.

2.5.3.2 COATING EFFECTS

The influence of the type of metallic porous coating on bone ingrowth, ranging from single/multiple layers of sintered beads of Co Cr or titanium to fibremesh, grit blasted and plasma sprayed surfaces has been investigated [14,143,152-154]. Different surface textures might influence ingrowth in different ways. For example, plasma sprayed and grit blasted surfaces might provide a rough mechanical interlock, but their texture might not be as conducive to bone formation as other porous surfaces. The key to successful ingrowth of bone is to find an ideal porous surface with the right surface texture and pore characteristics. A study conducted by Friedman et al. [153] investigated the effects of four different porous coatings on strength of fixation and bone ingrowth. The coatings used were single layered Co-Cr beads, three layered Co-Cr beads, arc deposited titanium, plasma sprayed Co-Cr and grit blasted titanium. The results showed that at the end of six weeks, the single layered Co-Cr porous surface had maximum bone apposition, but there was no

significant difference between the single layered, three layered Co-Cr and arc deposited titanium at the end of twelve weeks. Mechanical strength was highest for the single layered Co-Cr beads, but was not significantly different from three layered and arc deposited surfaces. Bone apposition to the grit blasted and plasma sprayed surfaces was patchy and low and the mechanical interface weaker than the other surfaces (figure 2.30). Other studies have indicated better bone ingrowth in terms of volume and depth for titanium fibre mesh than beaded Co-Cr coatings [143,154] with the beaded coating showing good bone ingrowth initially but replaced by fibre mesh coatings for longer durations [14]. This has been attributed to the more open structure provided by the mesh.

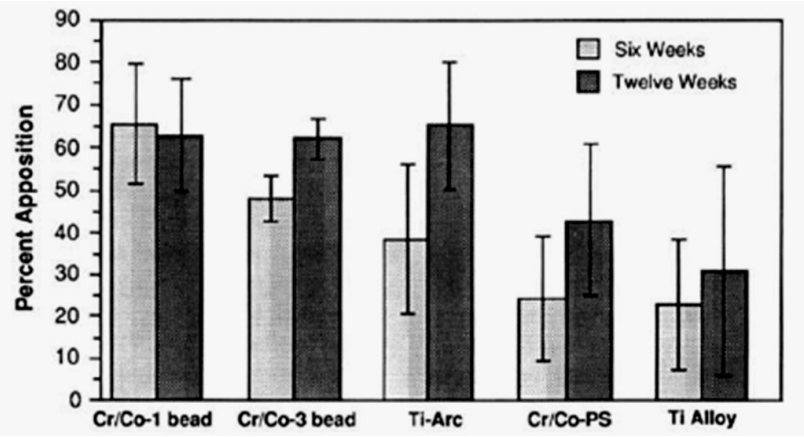

Figure 2.30: Bone apposition on five different porous surfaces as investigated by [153]. At the end of six weeks, single layered Co-Cr bead porous surface showed highest percentage of bone apposition. However, at the end of twelve weeks, barring plasma sprayed and grit blasted surfaces, there was no significant difference in bone apposition between the surfaces.

A similar result has also been found in a study by Simmons et al. [155], where the difference in percentage of bone ingrowth into titanium beaded and plasma sprayed titanium surface was not statistically significant at the end of sixteen days, but initial four to eight day ingrowth percentage for the beaded coating exceeded that of the plasma sprayed surface. This could suggest that initial healing and bone apposition of sintered beaded porous coating is much better than other surfaces. Moreover, the bone found ingrown on the sintered beaded surface was not localised and was adjoined to the host bone surrounding it, providing a stronger interface (figure 2.31).

A finite element analysis was also carried out by Simmons et al. [156] to investigate the initial rapid ingrowth into the beaded coating. The results showed that the beaded porous coating provided an interface zone with stiffer effective properties and larger strain protected regions as compared to the plasma sprayed coating. The distortional and volumetric strains in the tissue surrounding the beaded coating were lower. Low values of these strains have been cited to be favourable for bone formation during tissue differentiation [23] which will be discussed in detail in section 3.3. The beaded porous coating was also considered to have an advantage of a larger area in which the

tissue in between the spaces was strain protected, hence lowering the strains in the regions and influencing rapid bone ingrowth.

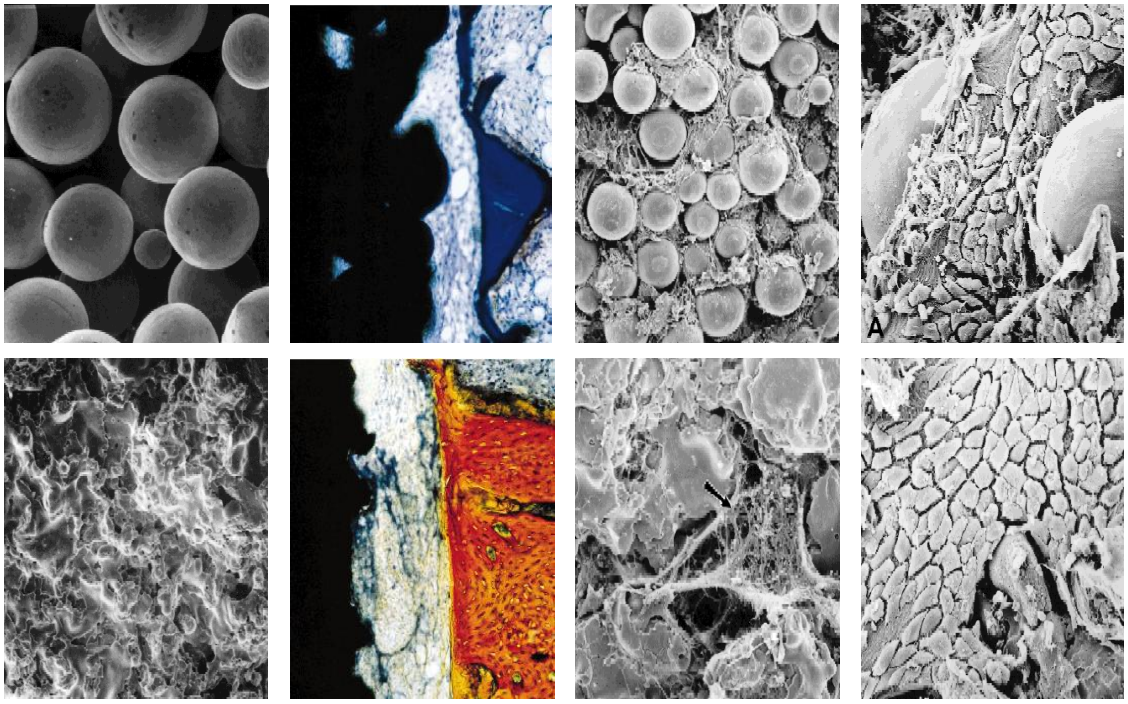

(1) (2) (3) (4)

Figure 2.31: Scanning electron micrographs of the titanium alloy-sintered porous-structured surface (top) and the Ti plasma spray-coated surface (bottom). Left to right shows histological sections demonstrating a (1) Well-defined interface zone adjacent to both the porous-surfaced and plasma-sprayed implants after 4 days of healing (2). More extensive coverage and interdigitation of the healing tissue matrix with the porous surface than plasma-sprayed surface 4 days post implantation (3). Some areas of the plasma-sprayed surface were devoid of tissue 16 days after implantation (4) showing extensive coverage and interdigitation of the porous and plasma-sprayed surfaces with mineralized tissue and dense matrix [155].

Comparing the same type of coating for both Co Cr and titanium alloys, more ingrowth has been found in titanium alloys [157], perhaps due to its better biocompatibility with bone. This could be due to the lower modulus of titanium, compared to that of Co Cr, which leads to better stress transfer to the surrounding bone resulting in better ingrowth of bone tissue. In addition, this could also be attributed to the higher affinity of bone to form on the oxide of titanium compared to those of other metals [158]. However, it has to be noted that both materials are still several times stiffer than bone and it cannot be confirmed that this is the reason for the difference. Therefore, based on literature, it can be declared that material and morphology of the coating does not significantly affect bone ingrowth long term, although initial bone ingrowth seems to favour the beaded porous coating. A preference of coating cannot be concluded unless the surface has been shown to be significantly different from other coatings long term.

2.5.3.3 INITIAL FIT AND PROXIMITY TO BONE

The degree of apposition of joint replacement prostheses to bone is primarily dependent on the implant geometry. Preparing the bone bed for insertion of the implant strictly according to its geometry is often difficult during surgery. Nevertheless, the closeness or fit with the host bone can often determine if bone ingrowth occurs at the porous surface or not. Close apposition with bone is often an indicator of good fixation and increases stability at the interface. Large gaps existing at the interface could easily lead to implant loosening on repeated loading [159-161].

Early canine studies have highlighted the importance of a good initial fit with close apposition to host bone. Camron et al. [159] studied interface gaps of 0-1.5 mm to determine the effects of large gaps on rate of bone ingrowth at 2, 3, 4, 6, 8, and 12 weeks. Bone ingrowth was evident at the end of the third week for the smallest gap and maximum strength at the interface at the end of the 4th week. The 1.5mm gap was also filled with bone at this period, although the quality was determined to be inferior to the smaller gap cases. A similar study by Sandborn et al. [160] has confirmed the result. Gaps of similar sizes were evaluated to investigate the quantity and quality of ingrowth at the cortical and cancellous regions. It was reported that for gaps ranging from 0-0.5 mm, the rate of mature bone formation was high when compared to the 2mm gap, which was observed to be considerably low. The 2mm gap case showed structurally weak bone formed at the porous surface. However, it cannot be assumed that small gaps would ensure ingrowth, as even a lower limit of 0.5mm has been found to show fibrous tissue formation as shown in figure 2.32 [143].

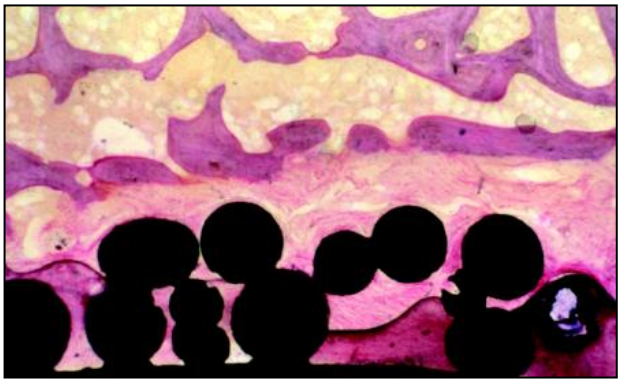

Figure 2.32: The gaps between the porous coating and the host bone predominantly filled with dense fibrous tissue. The bone adjacent to the fibrous layer was oriented tangential to the implant and showed signs of trabecular hypertrophy [143,162].

These studies clearly showed that although gaps could be filled by bone tissue at the end of 4-6 weeks, large gaps were often composed of qualitatively weaker bone than smaller gaps, which could decrease the interface shear strength. Even the slightest of gaps could compromise the integrity of the interface. The influence of gaps has also been simulated in a finite element model by

Spears et al. [161]. This showed patterns of bone ingrowth in regions that are fixed in close proximity of bone and no ingrowth in large gap regions. This can be explained by the difference in local stress and strain distributions in regions that do not have bone apposition. These regions would be subjected to poor stress distributions and would eventually resorb further compromising the fixation stability of the implant. The difference in ingrowth rates can also be explained biologically, related to the proliferation of bone forming cells at the site. During bone healing after insertion of the implant, pluripotent cells migrate and proliferate from the surrounding endosteal and bone marrow regions into the interface (see section 2.6.5). These cells are responsible for bone formation through a complex process of differentiation and maturation depending on the mechanical conditions existing at the site. Large interface gaps could effectively reduce the number of cells migrating across to the porous surface, which could adversely affect bone formation on the surface. Additionally, the high stresses formed at the site due to improper contact, could lead the cells to differentiate to fibroblasts or cartilaginous cells and not bone [162].

2.5.3.4 INTERFACIAL STABILITY

Stability at the implant bone interface is critical to the success of a porous coated implant. It is directly related to the amount of micromotion between the implant and bone, which in turn determines the type of tissue formed at the interface. Stability however, is dependent on implant design variables like geometry, cross section, coating etc and surgical tools used for rasping, drilling sawing etc. Interfacial stability can be categorized as primary or secondary stability; the former, immediate stability provided by the rough mechanical interlock of the implant and the latter, slower process by bone ingrowth. The use of additional components for fixation, like screws and pegs also enhance the stability at the site. Finite element studies have shown that a good frictional contact and use of screws and pegs prevent relative micro-movements at the interface [163,164]. The influence of initial press fit on the stability has also been shown in silico to affect the levels of micromotion at the interface [21]. Press fit conditions of 0.02mm, (implying the cavity is under-reamed 0.02 compared to the size of the implant) with high friction coefficient values were found to be inadequate with high micromotion at the interface. Press fit values of 0.2mm were ideal, with even relatively small friction coefficients preventing micromotion at the interface.

Femoral stem designs have also been shown to make a significant difference in stability and micromotion with curved stems preventing more micromotion than straight stemmed [165]. The role of micromotion has been well covered in the literature [7,166-168] in determining the type of tissue formed at the interface, and has been cited as the most important factor for bone ingrowth to be successful. An example of bone and fibrous tissue formation for sintered beaded coating from a microscale study on micromotion is shown in figure 2.33. Micromotion can be defined as any relative movement between the implant and the surrounding bone. Micromotions due to axial, tensile and torque are most common considering the loading regime at the hip.

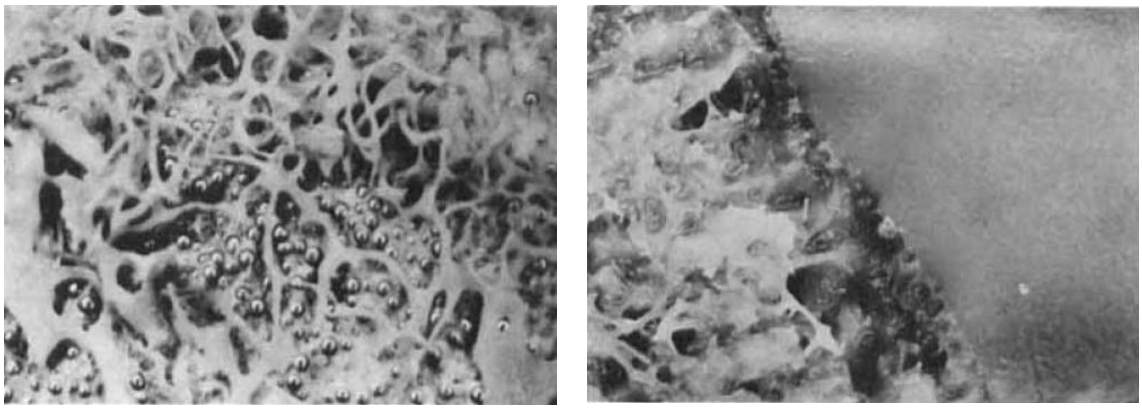

Figure 2.33: SEM view of trabecular bone formation (left) and fibrous tissue formation (right) for sintered beaded coating [169].

Torque has been shown to cause more micromotion than axial loads [166]. It is a consensus among the reviewed literature that high amounts of micromotion at the implant bone interface results in the formation of weak fibrous tissue that weakens the interface and hence cause loosening of the implant. Low levels of micromotion are said to promote the formation of bone at the interface and in the porous coating. The levels of micromotion that cause these opposite effects have been studied in animals extensively and also in a few clinical studies [7,143,167,170-172].

In one of the earliest canine studies [173], it was found that micromotions of 150μm resulted in the formation of fibrous tissue and micromotions of 28μm or lower resulted in the formation of bone tissue. However, it was also noted that the fibrous tissue formed had high collagen content and was not weak mechanically and provided stable fixation at the end of a one-year testing period. The upper limit of 150μm was further confirmed by Jasty et al. [7], when in canine experiments, repeated micromotion at this level resulted in the formation of a combination of fibrous tissue and bone (figure 2.34). However, the bone formed was not in continuity with the surrounding bone, but new bone that had arisen between pores of the coating. This could have been due to the invasion and maturation of osteoblastic cells during the initial healing process. The interface was found to be mechanically weak. For lower micromotion levels of up to 40μm (ideally 20μm), a stable interface with the surrounding bone extending inside the porous coating was observed. Normal patterns of bone growth have been observed in implants subjected to 20μm micromotion with fibrocartilage formation around the 20-40μm range and fibrous tissue formations in micromotions exceeding 150μm [143]. The results corroborate well with a human femoral retrieval study in which evidence of good bone ingrowth was observed in only those stems that displayed less than 40μm micromotion when tested *in-vitro*[167]. However, there have been exceptions. For example, an animal study where large micromotions (≈60μm) were evident, still result in the formation of bone and not fibrous tissue [168].

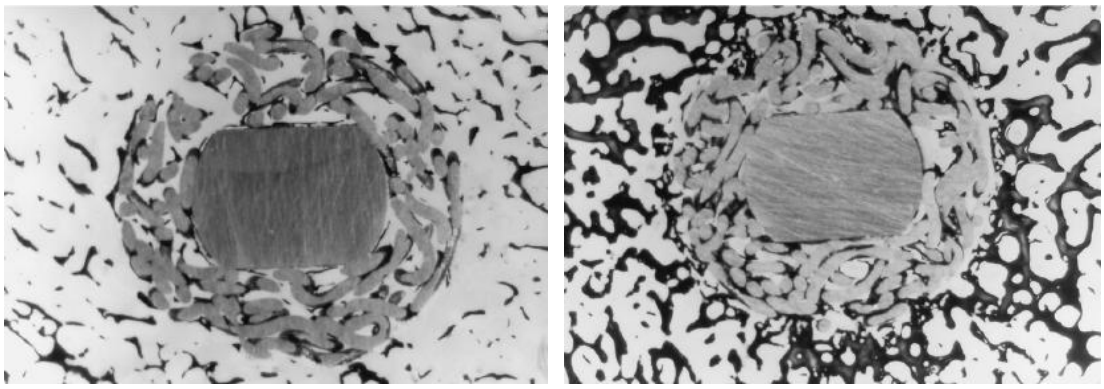

Figure 2.34: Bone formation in fibre mesh coatings at 20μm (left) and fibrous tissue/*de novo* bone formation at 150μm (right) micromotion [7].

The extent of porous coating has also been shown to influence micromotion and hence bone ingrowth. Retrieval studies have shown that extensively coated implants show more ingrowth not only due to the availability of the surface over the whole length of the stem for ingrowth but also due to the additional frictional interlock the implant can achieve with the host bone [174]. However, concerns remain of the stress shielding effects of using such extensively coated stems.

Although there have been numerous animal and retrieval studies to show the influence of micromotion on the stability of the interface, there have been few studies done *in silico.* Studies have dealt indirectly with the deleterious effects of soft tissue formation at the interface and how it weakens the interface and causes loosening [175,176]. Other studies have dealt with possible patterns of bone ingrowth and fibrous tissue based on micromotion [161,177]. The study by Spears et al. [161] on an acetabular cup model has shown that micromotion at the interface is dependent on the loading activity at the site. It was found for example, that for the slowest mode of gait, the maximum micromotion (100μm) occurred at toe-off but for faster modes of gait, it occurred at heel strike. This is possibly due to the higher loads during heel strike coupled with faster gait. Stair climbing was shown to affect micromotion the most. In addition, peripheral regions of the cup showed the least amount of micromotion as compared to the polar region. Conclusions cannot be drawn from such a model however, without clinical evidence.

Simulations detailing bone ingrowth into porous surfaces have been few, with the only extensive work by Andreykiv et al. [161] who simulated the ingrowth process on a glenoid component based on the amount of micromotion at the interface and also the influence of pegs at reducing micromotions. Cell migration and tissue differentiation at the interface was based on an existing algorithm [8]. It was found that maximum micromotion and lowest amounts of bone ingrowth at the end of 16 weeks occurred with the design devoid of pegs, which relied entirely on the press fit frictional interface. The pegs provided additional support and stability and limited the amount of

micromotion hence promoting more ingrowth (figure 2.35). The influence of reducing the stiffness of the porous coating also showed increased micromotion with formation of fibrous tissue and cartilage in addition to bone.

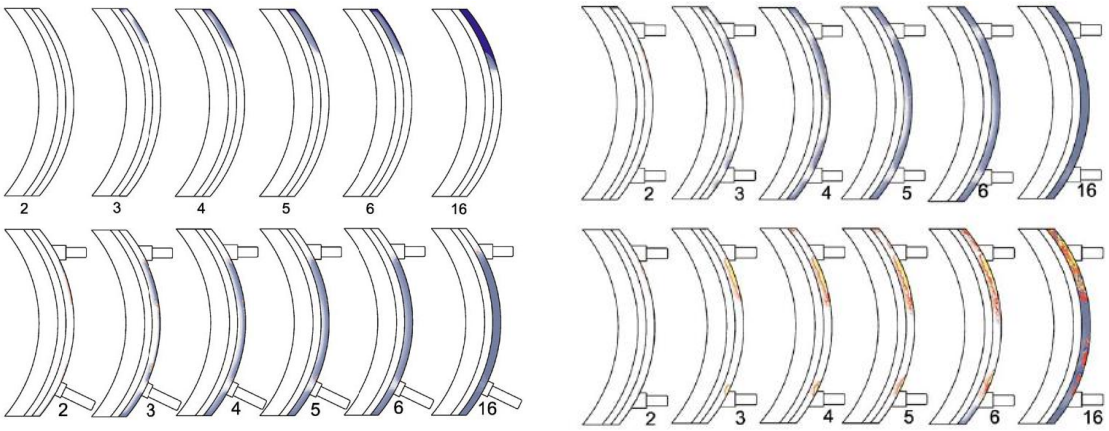

Figure 2.35: Bone ingrowth in four different designs for a glenoid component. More bone ingrowth was observed in the components with additional stability provided by the pegs [25].

A similar work using the same algorithm [178] for a sintered beaded coating for no particular prosthesis, has indicated formation of fibrocartilagenous tissue at the uppermost layer of the porous surface for intermediate levels of micromotion (>20μm) as compared to complete ingrowth at 5μm micromotion.

The influence of micromotion can be described as a relative process, if initial micromotion is reduced; bone starts to grow into the porous regions improving the stability of the interface, which in turn reduces further motion at the interface. The strength of fixation almost always increases over time unless there is poor stability to begin with, hence achieving good primary stability should be considered the top priority for a porous coated implant to succeed.

2.5.3.5 CLINICAL STUDIES RELATING TO POROUS COATED PROSTHESES

The performance of a porous coated prosthesis, as for any other, can be evaluated using either scores based on performance and pain, or by retrieval studies. Periodic radiographs can be an indicator of fixation and quality of bone surrounding the prosthesis, but quantifying the amount of ingrown tissue can only be done on retrieval or revision. To this end, a number of early implanted porous coated implants have been retrieved and studied. The largest clinical data set of sintered beads porous coated implants has been investigated by Engh et al. [174] consisting of 3,314 AML implants, partially and extensively coated and implanted in young patients (50-60 years). The results obtained were excellent with over 95% survivorship at 15 years. It was noted that among implants achieving bone ingrowth, there was no incidence of loosening. There was very low

occurrence of severe remodelling with the use of these implants. The authors also reiterated the importance of initial stability and filling of the bone bed accurately during surgery. Other studies have also shown over 95% success rates with the sintered beaded coating (S-ROM and PCA) showing well ingrown surfaces [179,180].

Porous coated prostheses mostly display excellent short-term stability and ingrowth, but there have also been problems associated with lysis, migration and resorption around the implant in the long term. Little et al.[66] reported 37% lysis and 21% migration in a series of 133 PCA components after 11 years, although the short-term follow up at 4 years showed good ingrowth and stability. The problems were attributed to wear particles from the articulating surface causing formation of fibrous tissue rather than failure of osseointegration. The influence of stability and low micromotion has also been clearly elucidated by a clinical study on retrieved tibial tray implants, with noticeable ingrown bone tissue around the pegs and fibrous tissue formation at the peripheries of the fibre mesh coating [135], which could be explained by the lack of movement around the pegs.

From the aforementioned clinical studies, it can be summarised that provided the initial fixation is stable and micromotion is prevented at the interface, bone ingrowth will occur and ensure long-term stability in the absence of other problems such as wear-particle induced osteolysis. Failed implants often display poor osseointegration, reflecting the drawback of poor fixation rather than failure after bone ingrowth.

2.5.3.6 MECHANICAL PROBLEMS OF POROUS COATINGS

The integrity of porous coatings plays an integral role in determining bone ingrowth into the surface, with sub standard coatings resulting in corrosion and particulate formation at the interface. The problems of porous coatings are mainly mechanical with few instances of the biological problems associated with mechanical failure. One of the major problems associated with metallic porous coating is the process of deposition of the coating on the substrate metal that weakens the substrate.

There have been reports of the fatigue life of the substrate metal decreasing during sintering due to the high temperatures involved, especially with titanium alloy with yield strength reducing from 625MPa to 200MPa [136]. The size of the particles used during the process also influenced the fatigue strength after sintering with smaller particles corresponding to smaller changes in fatigue strength. In addition, crack initiation was found to occur at the interface between the coating and substrate metal. This could be caused due to high stress concentrations due to irregular geometries at the bonding sites of the substrate metal and particles from the coating. These localised stress concentrations are referred to as the ‘notch effect’. This could lead to debonding of the particles

from the substrate and release of metallic debris that might cause adverse tissue reactions. In sintered beaded coatings, bead separation can also occur as shown in figure 2.36.

Figure 2.36: Debris from sintered beaded coatings [181].

Fragments of plasma sprayed particles have been found in the trabeculae surrounding the implant [135]. Corrosion is a possible cause for fractures in porous coatings and should be considered due to the large surface area involved. Corrosion behaviour for three different porous coatings with different porosities manufactured by sintering has been investigated by Becker et al.[182] and it was found that smaller pore sizes increased corrosion levels due to increased concentration gradients. It was also found that titanium alloys displayed the least corrosive behaviour when compared to stainless steel and cobalt chrome. The study also concluded that though cobalt chrome alloys had higher hardness, titanium alloys could combine high tensile strength and tolerance for plastic deformation and should be favoured during fabrication of porous surfaces.

2.5.3.7 ENHANCING BONE INGROWTH INTO POROUS SURFACES: OSTEOCONDUCTIVE COATINGS AND SYSTEMIC FACTORS

Osteoconductive surfaces not only allow bone ingrowth and migration, but also provide a scaffold for bone cells to attach and proliferate. Osteoconductive surfaces are normally composed of calcium phosphate or bioactive glass compounds. The most commonly used calcium phosphate coatings are hydroxyapatite [$Ca_{10}(PO_4)_6(OH)_2$] and tricalcium phosphate [$Ca_3(PO_4)_2$]. Bioactive glass is comprised mainly of SiO_2, Na2O and CaO and a small percentage of P_20_5.The application of these coatings is normally through pulsed laser deposition process and can be done either on the substrate metal or on an overlying porous coating. These coatings do not drastically reduce the porosity of the coatings as shown in figure 2.37.

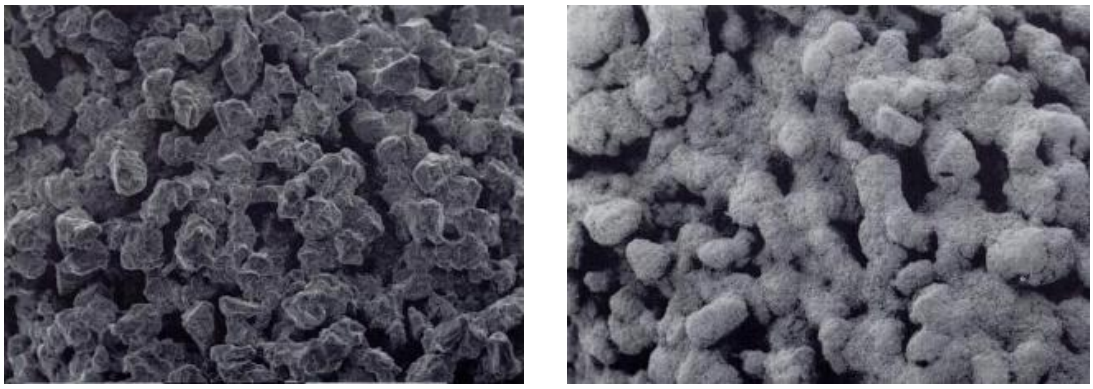

Figure 2.37: SEM view of a titanium plasma sprayed surface (left) and coated with HA (right). The HA coating has not compromised the overall porosity of the surface [183].

Thin calcium phosphate coatings have been applied to porous titanium implants and have been found to induce more bone ingrowth when compared to uncoated porous implants [184]. Similar results have also been obtained by Karlsson et al. [185] where rapid bone formation was observed on the surfaces of a coated titanium implant when compared to the uncoated version. Long term ingrowth issues have been raised [186] with grooved HA coated titanium implants showing higher ingrowth when compared to beaded coated titanium at four weeks, but lesser ingrowth overall at the end of twelve weeks. The study indicated that the coating only played an important role in the initial ingrowth of bone tissue and its effects long term remained to be explored. Mechanical stability of HA on porous coated surfaces has also been found to be higher than those on grit blasted surfaces with less delamination, indicating long term fixation stability with more HA retention [187].

There are no strong effects of HA pore size on ingrowth [188], although a pore size of 300μm has been proposed to be optimal. A highly porous sponge shaped HA block was also shown to be rapidly invaded by bone tissue, although its mechanical strength was compromised. The influence of micromotion and stability on HA coated implant have also been studied [189], with HA coated stems subjected to 500μm micromotions developing a stronger fibrocartilagenous tissue with high collagen content around them and uncoated stems developing weak fibrous tissue at the interface. HA has also been shown to convert fibrocartilagenous tissue formed initially due to high micromotion into bone in the long term (figure 2.38) [183]. This is believed to be a result of endochondral ossification of the fibrocartilagenous tissue that develops initially due to poor stability. Clinical studies of HA coated titanium stems have mostly shown signs of excellent osteogenic response and osseointegration long term [190], but others have shown no significant advantage using HA [191] when compared to uncoated titanium stems, perhaps due to the short follow up time. This again would be a contradiction, due to the widely regarded opinion of the HA coating encouraging rapid bone ingrowth. HA has also been reported to fill interfacial gaps as large as 2 mm that are formed during surgery due to improper preparation of the bone bed [192].

A major concern with the use of osteoconductive coatings is that they possess inadequate shear strength and poor bonding with the substrate metal/porous surface, which could result in release of debris and third party wear generation at the articulating surfaces. These wear particles could further hinder the stability of the fixation by affecting the interface [193]. However, the consensus from all the aforementioned studies is that HA does enhance the rate of bone ingrowth, and can be used in combinations with existing porous coatings to maximise its potential. The top three cementless hip implants used, according to the national joint register of England and Wales are HA coated [75].

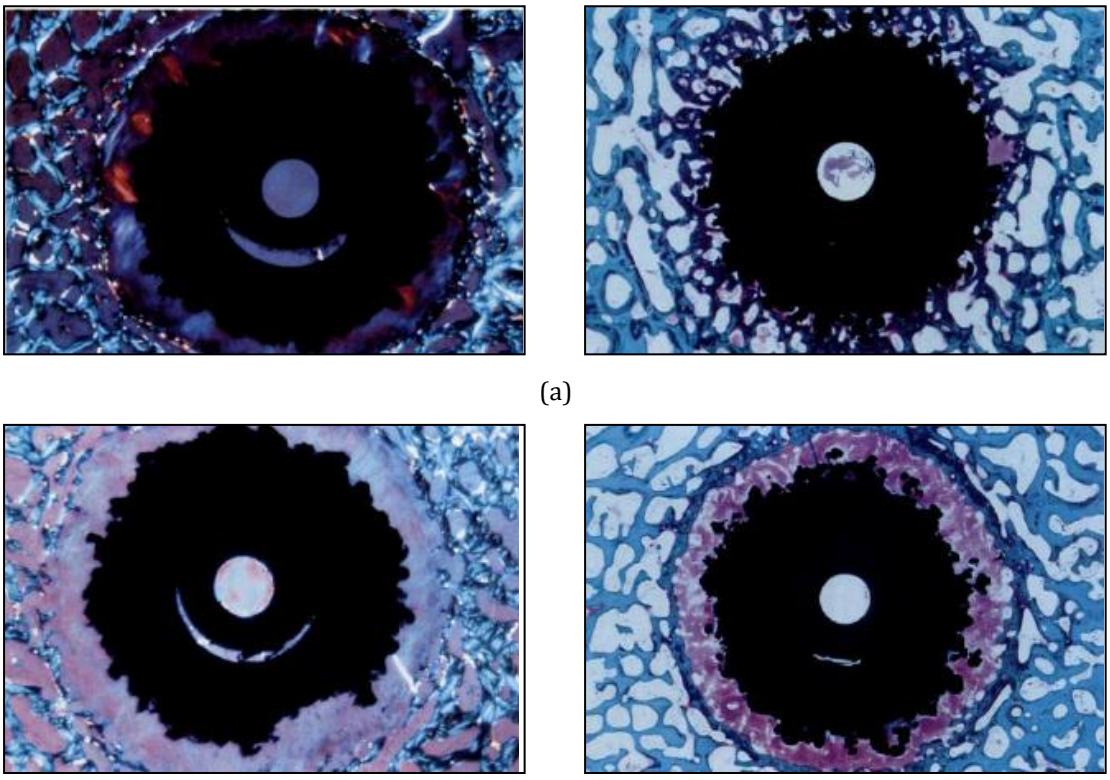

(a)

(b)

Figure 2.38: (a) HA coated Ti implant subjected to 150μm micromotion at the end of 4 weeks (left) and 12 weeks (right). (b) Titanium plasma sprayed implant at the end of 4 weeks (left) and 12 weeks (right). While Ti coated implant was surrounded by collagen fibres randomly oriented, HA coated shows more organised collagen fibres. At the end of 12 weeks, bone formation in the HA coated was clearly visible, but fibrous tissue was still visible for plain Ti implant [183].

Systemic factors can also affect ingrowth rates. Hormones and growth factors have been known to either enhance or inhibit bone formation at the implant site [138]. Transforming growth factor β (TGF β) which is known to play an important role in fracture repair has been used successfully to enhance the ingrowth process in animal studies [194]. However, studies have also shown that if quantities exceed the required dosage, the amount of ingrown tissue is significantly lesser. TGF β has been reported to increase matrix synthesis, chemotaxis, recruitment and proliferation of

osteoprogenitor cells and have been successful in filling gaps and defects in bone [195]. New porous surfaces for better bone ingrowth are constantly being developed and tested [59, 60]. New designs have involved the development of surfaces that are closer to the structure and modulus of bone for an ideal interface incorporating better stress transfer and ingrowth of bone.

Concerning bone ingrowth, the mechanisms pertaining to it are complex involving mechanical and biological factors alike. However, the sequence of events that take place around prostheses, post implantation is comparable to the process of bone fracture healing. The mechanism of bone fracture healing is well understood in literature and can be used a template to understand the process of ingrowth. A summary of the events that occur in fracture healing is provided in the next section that also elucidates the similarities between the two processes.

2.6 FRACTURE HEALING

2.6.1 INTRODUCTION

Bone is unique in the fact that it heals without a scar, and the properties of the original tissue are restored, depending on the location and function in the body. However, the processes involved are complicated and involve a cascade of events that could continue for several years after the initial fracture. The processes can be compared to those that take place at the growth plate during development, albeit, on a temporal rather than spatial scale. Fracture healing involves a sequence of cellular responses under the influence of different signalling pathways that can be biological or mechanical [26,196-201].

Fracture healing can occur through two pathways, primary or secondary fracture healing. Primary fracture healing occurs in rare cases when there is rigid internal fixation and excellent anatomical position [26]. In this case, there is no formation of an external callus or cartilage at the region. The cortex tries to re-establish itself by regeneration of the haversian systems in the region. The osteoclasts and osteoblasts resorb and form new bone across the fracture site. New osteons replace the old, and blood supply is established. The whole process takes around 5-6 weeks. Secondary fracture healing is the most common, considering the trauma and difficulty in achieving the conditions required for primary fracture healing. It involves three basic stages:

- Reactive stage
- Reparative stage
- Regenerative stage

2.6.2 REACTIVE STAGE

The reactive stage occurs from the time of injury, through the stage of induction to the stage of inflammation usually lasting up to a week. Following fracture, cells in the surrounding area begin signalling to need for new bone formation at the fracture site (induction), which involves recruitment and differentiation of bone forming cells. There are two theories used to explain the presence of bone forming cells, one theory reports that periosteal, endosteal and osteocytic cells undergo modulation to form osteoblasts. The other theory states that cells like fibroblasts, undifferentiated stem cells, muscle cells etc differentiate to form osteoblasts. A parallel process of inflammation also takes place at the fracture site at the same time of induction of these cells as soon as the fracture occurs. A haematoma is formed at the site due to the disruption of local blood supply. The site becomes acidic and a state of hypoxia exists. The bones at the ends of the fracture become necrotic and there is gross disruption of the osteons. Platelets release cytokines that recruit different cells at the site, osteoclasts are activated and polymorphs, mast cells and histiocytes appear at the site to clear the debris and dead tissue. Vascular supply begins to re-establish at the site with proliferation of fibroblasts to form a loose granular tissue with inter-dispersed cells.

2.6.3 REPARATIVE STAGE

The reparative stage is the main healing stage of the fracture healing process and at the end of this stage, the union is complete. It consists of a soft callus and a hard callus stage [202]. In the soft callus stage, an internal and external callus is formed and helps stabilize the site. The external collar shaped callus is formed by the osteoblastic activity at the periosteum and reaches maximum thickness around the actual fracture site slowly reducing in thickness in surrounding areas. In proximal regions of the callus, osteoblasts deposit new bone directly, but towards the fracture site, cartilaginous cells become visible, reaffirming the presence of progenitor cells that differentiate to either of the cells depending on the conditions at the site. Vascular supply increases and the proliferation of cells at a rapid rate cause a state of relative hypoxia. This condition is considered ideal for osteoblastic activity. However, it has also been shown that the presence of hypoxia for extended durations can also cause significant delays in fracture healing [197]. New bone deposition continues to take place in certain locations and these steps result in the formation of a soft callus that is harder than the initial granular tissue formed and helps prevent motion of the fragments. The process takes around three-four weeks.

The hard callus stage converts the internal and external callus to bone, through either intramembranous bone deposition in regions of high stability or endochondral ossification. There is increased vascularity and cellularity and the state of hypoxia continues. The acidic environment becomes neutral and old bone resorption through osteoclastic activity is quickly followed by new bone being laid down until the whole of the callus hardens. The hard callus stage lasts until the fragments are united with firm bone, at which stage the fracture is said to be clinically healed. The hard callus stage could last anywhere between six to twelve weeks.

2.6.4 REMODELLING STAGE

The new bone formed continues to harden and is converted entirely to lamellar bone. The process results in the restoration of functionality of the bone to the stage before fracture. The processes do not differ much from the normal osteoblastic and osteoclastic activities at any other bone site. Osteoclasts are continually at work to resorb and remodel the external callus. Ultimately, this would result in the disappearance of the callus. The internal callus is also resorbed at the same time to reconstitute the medullary canal. Vascular supply and oxygen supply return to normalcy. The bone becomes functionally and structurally compliant and regains its original shape. The process of remodelling starts at the end of the hard callus stage and can last for many years.

2.6.5 FRACTURE HEALING AND BONE INGROWTH

As mentioned before, the series of events during bone ingrowth are very similar to the events in fracture healing. Based on literature, the similarities can be explained as follows [5,122]. The events pertain to bone healing and deposition around the implant. During preparation of the bone bed for implantation, the bone trauma can be compared to the actual fracturing of bone. Haemorrhaging results followed by platelet adhesion, activation and degranulation. Cytokines and growth factors are also released during the process, which causes osteogenic cells to migrate towards the implant surface. The cells migrate through a complex network of fibrin matrix and proteins to the implant surface. In contrast to purely fracture healing events, the implant surface characteristics also play a big role in the interactions at the interface. Platelet response and protein adhesion are sensitive to the surface characteristics with higher adhesion to textured rather than smooth surfaces [203].

The other events following activation and recruitment remain the same, with macrophages, neutrophils and monocytes involved in phagocytosis of debris around the implant site and an acidic, low oxygen gradient present. The granulation tissue formed is similar to that of fracture healing, with cascaded cellular activity and vascularisation enhancing cell migration and proliferation. Fibroblasts synthesise the matrix under cytokine activity that forms the scaffold for the proliferating cells and blood vessels. The granulation stage is followed by a stage similar to the reparative stage of fracture healing, with the onset of bone formation. Woven bone is formed by osteoblasts, by mineralization of the collagenous matrix over the interfacial matrix formed earlier. The collagen fibres are randomly arranged and are of low mineral density. The stage lasts until about 6 weeks following implantation. Woven bone is then replaced by lamellar bone where collagen fibres are arranged in parallel layers adjacent to the implant, this gives the implant a rigid fixation.

Remodelling then takes over after approximately 12 weeks and continues through the implantation time depending on the mechanical conditions at the site. Bone formation at the implant site occurs

through two main mechanisms that act together; distance osteogenesis and contact osteogenesis. Distance osteogenesis takes place when damage at the implant site triggers a reparative reaction to remove the necrotic bone and replace it with newly formed bone. Contact osteogenesis occurs at the surface of the implant and relies on the migration of differentiating cells through the matrix. These concurrent activities are critical to the formation of bone on the implant surface.

2.7 MECHANOBIOLOGY

2.7.1 INTRODUCTION

Mechanobiology can be defined as the study of the effects of mechanical or physical conditions on regulating biological processes [204]. The role of mechanical influences in regulating tissue differentiation and healing in bones are well-documented [8,9,23,204-206]. The concept of mechanobiology, though not in exact terms arose as early as the 1800's with Roux introducing the theory of functional adaptation [207] . According to Roux's theory, the formation of different types of connective tissue is influenced by the mechanical environment. Compression was proposed as the stimulus for bone and tension for formation of connective tissue with a combination of the two stimuli with relative displacement for cartilage.

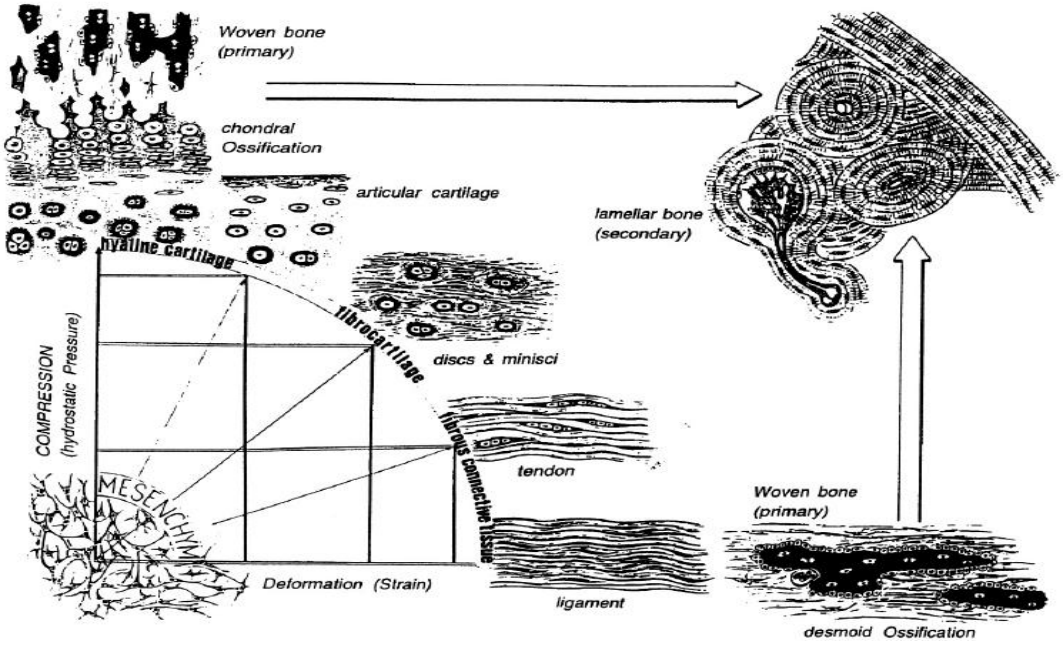

Figure 2.39: Pauwels's mechanobiology concept for differentiation of musculoskeletal connective tissue [208].

In 1960, Pauwels suggested that invariants of the stress and strain tensors guided the differentiation process in the fracture callus, with distortional strain a stimulus for fibrous tissue and hydrostatic pressure and compression as a stimulus for cartilage formation. Bone was

postulated to form after stabilization of the mechanical environment by the soft tissues and with low magnitudes of strain and hydrostatic stress. The schematic is shown in figure 2.39. Perren then followed on the concept in 1979, with his hypothesis of tissue differentiation based on tissue disruption and interfragmentary strain (figure 2.40). The hypothesis stated that if stresses exceeded the tissue strength or tissue elongation resulted in tissue damage, the tissue would change its phenotype such that tissue failure would not occur. The hypothesis focused on strain rather than stress as the mechanical stimulation because strain described the actual physical phenomenon of tissue elongation. The application of this concept was mainly to describe primary and secondary fracture healing.

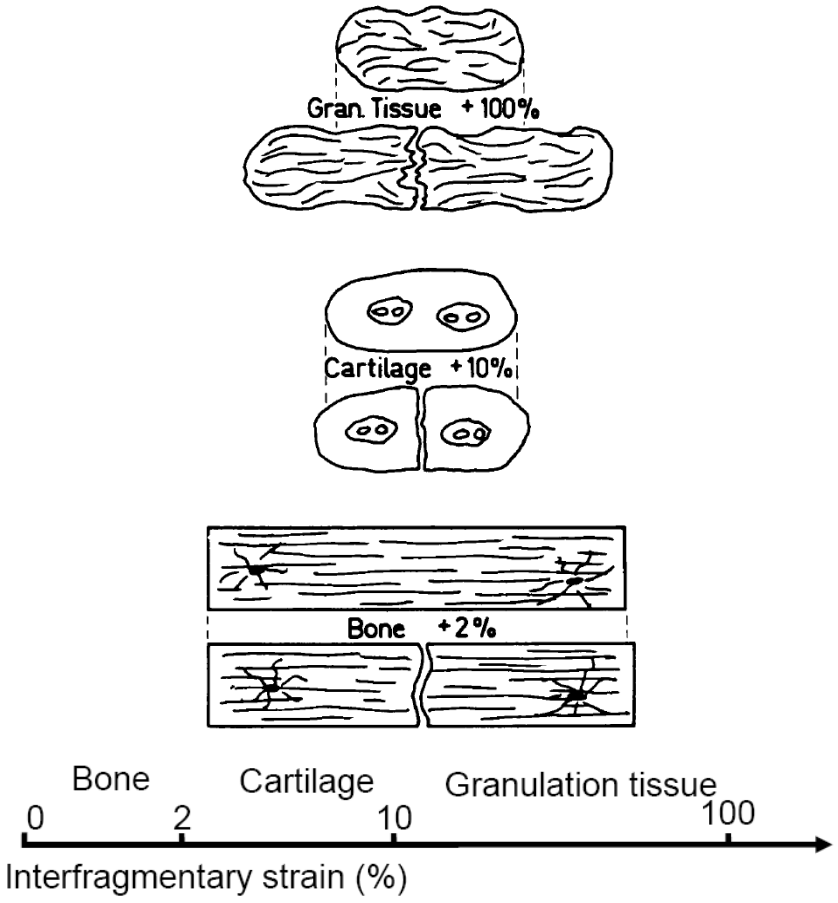

Figure 2.40: Perren's strain tolerance of the repair tissues [199].

The concept of mechanobiology can be addressed on four main levels; the molecular, cellular, tissue and organ levels. With specific application to skeletal mechanobiology, at the organ level, the mechanical signals can be characterized by the loading history (force, displacement, deformation, stiffness etc). At the tissue level, where it is treated as a continuous material, the mechanical stimulus is quantified as stress and strain and its variants (pressure, distortion, strain energy etc). At the cellular level, signals like cell pressure, inter cell interactions, nutrient supply, temperature etc can be identified. Factors that affect the matrix production at the cellular level like oxygen

tension and electric potentials are also quantified at the level. The bottom most molecular level is perhaps the most important for the study of mechanical signalling. Changes in cell activity are often the cause for the molecular signals. Cytoskeleton changes, integrins, growth factors, cytokines, ion activities are some of the signals [204]. The four levels and some of the possible mechanical signals are summarized below in table 2.2

ORGAN	*TISSUE*	*CELLULAR*	*MOLECULAR*
Force	Stress/Strain	Cell pressure	Cytoskeleton changes
Displacement	Hydrostatic stress/strain	Cell shape changes	Stretch activated ions
Stiffness	Shear stress/strain	Cell-matrix interaction	Integrins
Failure load	Strain energy density	Oxygen/nutrient supply	Growth factors
Loading rate	Fatigue damage	Electric potentials	Cytokines
Loading history	Stress and strain history	Temperature	Receptors

Table 2.2: Mechanobiology at four different levels [204].

Carter et al [204] cited an excellent example to show the relationship between the levels associated with mechanobiology. Considering fracture instability, they noted that this could lead to delayed fracture healing. At the tissue level, the instability is associated with increased stress and strain in the differentiating tissue and different forces lead to different spatial distributions of stress and strain in the tissues. The effect at the cellular level, local tissue stress and strain may cause changes in cell pressure or shape. At the molecular level, cell shape changes could disrupt the actin cytoskeleton which could cause different protein synthesis and on the organ level, cause delayed healing.

2.7.2 HYPOTHESES AND ALGORITHMS FOR TISSUE DIFFERENTIATION

Algorithms for mechano-regulation of tissue differentiation have been developed based on the concepts described above. The algorithms have been mostly developed for simulating the process

of fracture repair in the long bones; this is especially true for the tibia but can also be extended to simulate the process of tissue differentiation around an implant. The mechanisms of formation of bone or a fibrous tissue or a combination of both on and around an implant can be explained based on these algorithms. Some of the algorithms incorporating mechanical factors in simulating fracture healing are discussed.

2.7.2.1 CARTER AND ASSOCIATES

Carter and associates [23,204,209] developed their hypothesis based on how mechanical loading history contributed to skeletal development, but later extended to studying fracture healing of the tibia. The hypothesis developed was semi-quantitative, based on intermittent and cyclic stresses at the fracture callus, along with vascularity and loading history governing the formation of different tissues at the callus. The salient points of the hypothesis as applied to an early callus were:

1. A fracture elicits an osteogenic stimulus
2. Bone forms if there are minimal cyclic stresses or strains with good blood supply
3. High magnitude stresses will encourage tissue proliferation with a larger callus
4. High shear and/or tensile hydrostatic stresses encourage fibrous tissue formation
5. High compressive hydrostatic stresses encourage chondrogenesis
6. If cartilage or fibrocartilage forms, cyclic shear will promote and compressive hydrostatic stresses inhibit endochondral ossification

It was also hypothesized that the loading history was important in governing tissue differentiation and that fracture healing followed skeletal morphogenesis; cyclic compressive hydrostatic stresses inhibit or prevent ossification and cyclic shear stresses encourage tissue proliferation and ossification. Based on the hypothesis shown in figure 2.41, the tendency of ossification based on dilatational and octahedral stresses were represented by an index called the osteogenic index 'I'.

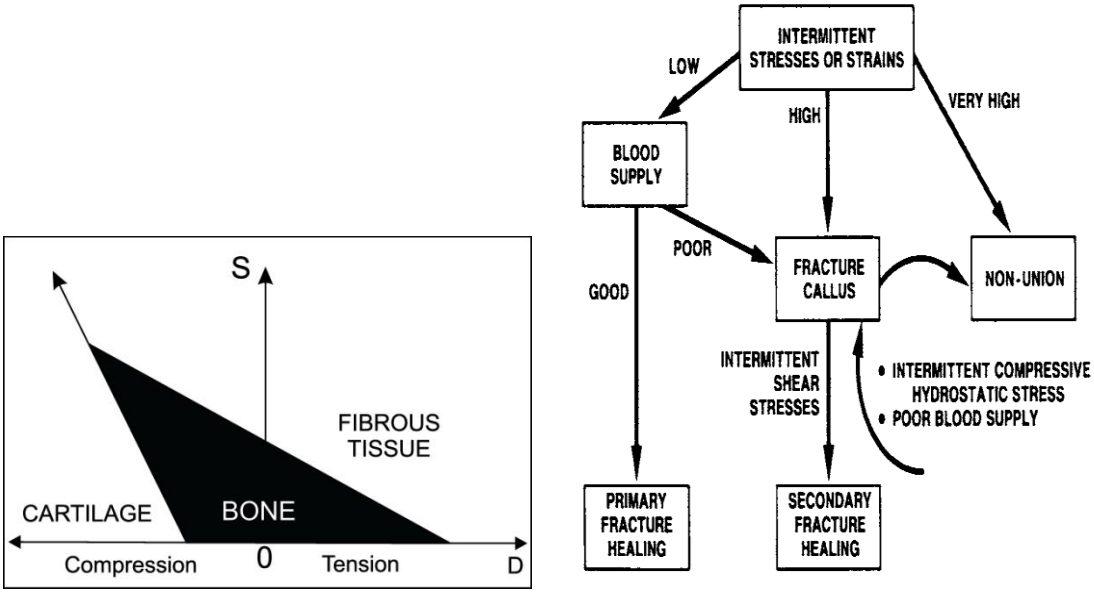

Figure 2.41: The hypothesis of Carter et al. for formation of different tissues (left) and the stages involved under the hypothesis. 'S' in the vertical axis represents cyclic octahedral shear stresses with dilatational stresses represented in the horizontal axis [23].

High index values would represent regions that had the highest chance of ossification with low index values representing regions of weaker tissue. The hypothesis was tested on finite element models of a fracture callus and the influence of different loads on the index and location in the callus was noted. The hypothesis has also been modified and applied in other studies by other authors. For example, to study tissue differentiation at bone-cement interfaces [206], oblique fractures [210] and corroboration and verification with other hypotheses [211,212].

2.7.2.2 CLAES AND HEIGELE, AND OTHER SINGLE PHASE HYPOTHESIS

Modelling fracture healing through finite element methods have also been carried out by other groups like Claes and Heigele [205], who have concentrated on the influence of mechanical stimuli on the fracture site regulating tissue differentiation, similar to the hypothesis of Carter et al. but by incorporating strain as well as stress as the guiding parameters. Their hypothesis was that new bone formation in fracture healing primarily occurred along existing bone and calcified tissue and that the type of bone formation depended on the hydrostatic pressure and strain magnitudes brought about by loading. Like Carter, two-dimensional models of a fracture callus were constructed, but different stages of healing were modelled by changing the type of tissues formed in the callus at each individual stage. Using specified loading conditions, the different stages were then studied for stress and strain regions and ossification paths were formulated. The hypothesis based on the findings is shown in figure 2.42.

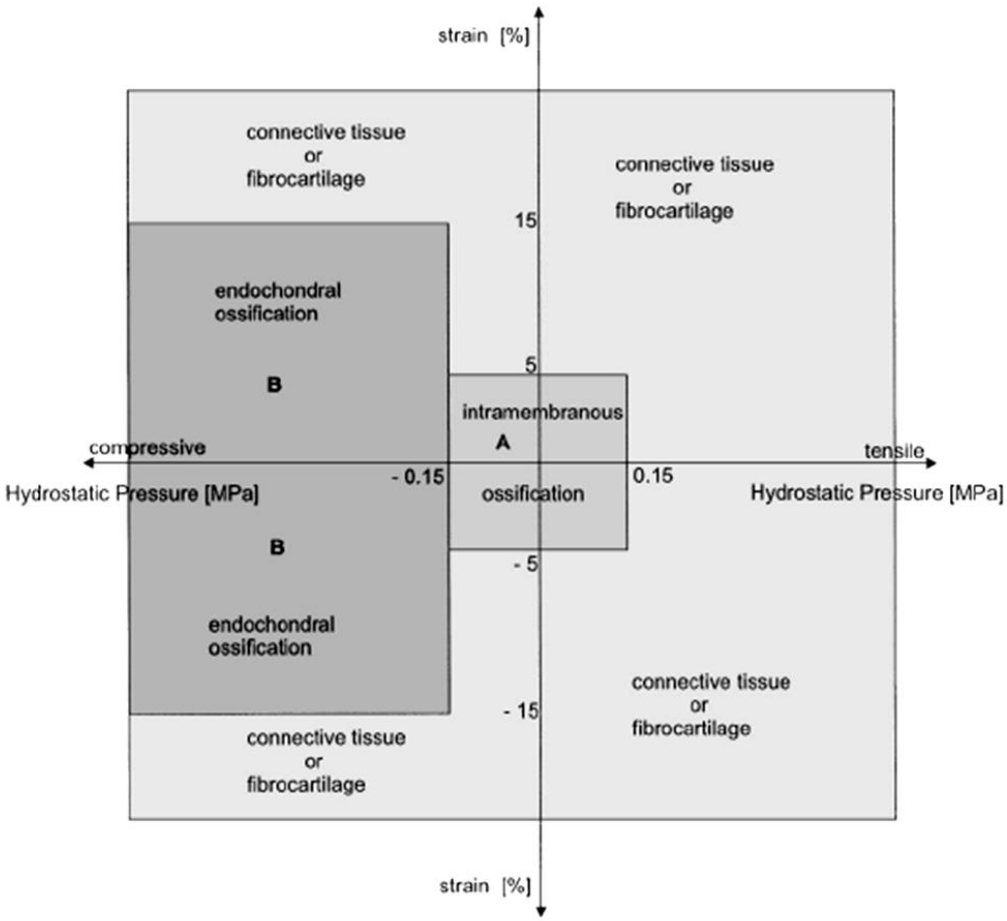

Figure 2.42: The hypothesis of Claes and Heigele for formation of different tissues formulated based on stress and strain [205].

To summarise, it was found that intramembranous ossification occurred only at low strains and low hydrostatic pressures. A compressive hydrostatic pressure of about 0.15 MPa and 5% surface strain was hypothesized to be the critical value that guided the cell differentiation either to an osteoblast or a chondrocyte, or that directed the tissue differentiation either to an intramembranous or an endochondral ossification.

A similar study was also carried out by Gardner et al.[213], who studied 4 different time points during healing, based on radiographic analysis, and comments made on the stress concentrations and inter-fragmentary forces (based on inter-fragmentary displacements) and their effects on tissue damage and healing. The same author, in a later study [211] has also reported the influence of individual stimuli taken from Carter's work, namely octahedral and dilatational stresses on the ossification of a fracture callus. It was reported that high shear stresses did indeed correspond to regions of fibrous tissue, but this was not the case for high tensile dilatational stresses. In addition, the osteogenic index was did not fully correspond to regions of ossification in their finite element models.

Fracture healing studies with a significant cellular component added to the mechanical stimuli in finite element models have also been popular. Garcia-Aznar et al. [214] and Gomez-Benito [215] have carried out extensive studies on the fracture callus by including cell diffusion, proliferation, maturation and death, influenced by the local mechanical stimulus and investigating parameters like fracture gap, length, callus geometry and fracture stiffness on the healing patterns.

2.7.2.3 PRENDERGAST AND ASSOCIATES

Moving away from modelling bone as a linear elastic material, Prendergast et al. [8] developed a new hypothesis based on experimental results on implant healing. This hypothesis is based on the premise of bone being a poroelastic, biphasic material, consisting of fluid and solid constituents. It was hypothesised that the mechanical environment changed in a sufficiently systematic way that biophysical stimuli could simulate the replacement of one cell population by another. The previous studies aforementioned relied on modelling the regenerating tissue as elastic, which worked well for large loads and deformations. However, considering there were significant amounts of fluid in the tissues, and cells responded to cell deformation and fluid flows, it was considered more accurate to model the tissue as poroelastic mixtures of solid and liquid constituents at the cellular level. The premise of the hypothesis was that the biomechanical stress acting on the cells would be higher if the fluid flow was high, therefore deformation and fluid flow should be considered together to define the mechanical stimulus on the cell. The hypothesis is shown in figure 2.43.

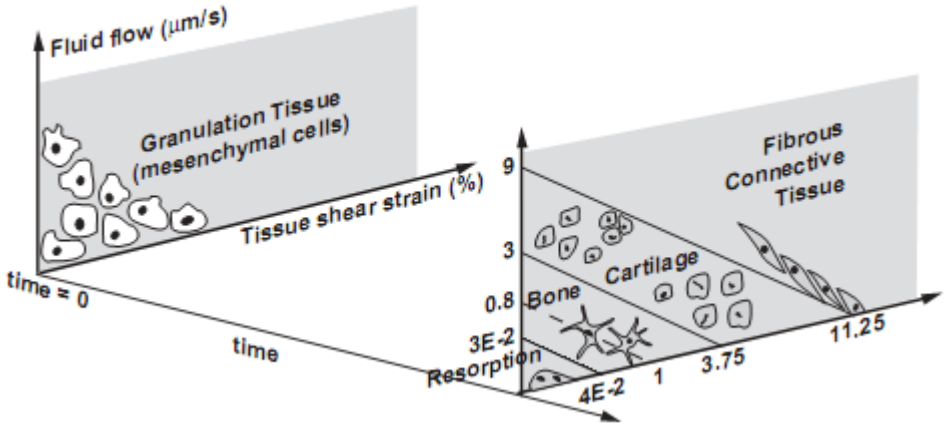

Figure 2.43: The hypothesis for tissue differentiation and resorption based on strain and fluid flow [8].

Deformation was represented by octahedral shear strain and the fluid component by fluid velocity. The stimulus for differentiation was given by the stimulus 'S' defined as

$$S = \frac{\gamma}{a} + \frac{v}{b}$$

Equation 3

Where γ = octahedral shear strain; V = fluid velocity; a, b = empirical constants

Bone was simulated to form if S < 1; fibrocartilagenous tissue if S > 1 and S < 3 and fibrous tissue if S > 3. The hypothesis has been successfully employed extensively to simulate fracture healing [20,22,164,216-218]and also tissue differentiation around implants [164,219] by incorporating the hypothesis in a iterative algorithm. One of the earliest applications of the hypothesis in an algorithm to simulate fracture healing in its entirety rather than model different healing stages as done by predecessors was by Lacroix et al. [220]. Cell migration was included through a diffusion equation, and the biophysical stimulus calculated was used to update material properties of the tissues for the next iteration. Different parameters like the effect of loading, gap size, external fixators have also been studied by the author using the same hypothesis [217,218]. The hypothesis has also found use in the simulation of repair of osteochondral defects [221,222]. Concerning simulating tissue differentiation around implants, the hypothesis has been used in two-dimensional studies for studying different glenoid component designs [164] and a porous coating [219] but has not been employed for simulating tissue differentiation around a hip or knee implant in three-dimensional models.

2.7.2.4 COMPARATIVE STUDIES OF DIFFERENT HYPOTHESES

Comparative studies investigating different hypotheses and their efficacy in simulating fracture healing have been carried out by a few authors [22,212,223]. Isaksson et al. [22,212] compared the hypotheses of Carter et al., Claes and Heigele and Prendergast et al. using models of a standard long bone fracture. The qualitative hypothesis of Carter was modified by incorporating values for the stress components by employing a parametric study and comparing it to realistic fracture healing, to make it quantitative. The author noted that all of the hypotheses when used in the same algorithm could simulate fracture healing successfully, but with different levels of accuracy. The hypothesis regulated by the mechanical constituents like stress and strain (Carter et al., Claes and Heigele) were found to not adequately represent healing when the fracture was subjected to high torsional loads. Only the hypothesis of Prendergast et al could simulate this successfully and also simulate resorption of the callus due to the presence of the resorptive component in their hypothesis. In addition, Isaksson et al., also studied the effects of individual stimuli like deviatoric strain, fluid velocity, and pore pressure and commented that none of the volumetric components were able to predict healing accurately. However, deviatoric strain could be used still be used as a

standalone factor to regulate tissue differentiation, reinforced by the results that closely matched the results obtained by Prendergast et al.

Epari et al. [223] compared the hypotheses of Perren, Claes and Heigele and Prendergast et al in a non iterative fracture model to study the differences in mechanical conditions produced by intrafragmentary shear and torsion to those produced by axial forces. In addition, individual stimuli in each of the hypothesis were also studied for their role in the initial mechanical environment in a callus. The author reported that using only deformation, fibrous tissue would result in the immediate fracture gap, surrounded by cartilage. This was consistent for all three hypotheses and for axial, shear or torsional forces. Pressure and fluid flow individually simulated the formation of only bone for shear and torsion, grossly overestimating the results. Deformation with pressure or fluid flow was consistent across the hypothesis using these parameters by simulating large presence of cartilage in the callus with fibrous tissue formation in the fracture gap between the bone. Overall, the initial tissue formation was dominated by the deformation stimulus more than the deviatoric components, which agrees well with the findings of Isaksson et al.

An important question to consider would be the choice of hypothesis to simulate tissue differentiation around implants. Considering the deformation stimulus is a significant factor in regulating the type of tissue formed at the interface, it would be imperative that this stimulus be included in any hypothesis to simulate tissue differentiation in particular as well. This would not pose a problem as all of the hypotheses reviewed have this stimulus as a contributing factor. The use of biological factors like the role of cells and systemic factors remain a concern. With fracture healing, which has been widely researched, simulating cellular factors would be justified by comparisons to clinical and other studies. Although the rates of cellular proliferation, maturation and apoptosis cannot be determined to accuracy, good estimates have been determined by these studies. However, with tissue differentiation and osseointegration, this would not be pertinent due to the lack of specific literature regarding cellular activity at the implant site. In this scenario, it was found apt to exclude any cellular activity to the hypothesis.

As aforementioned, the basic premise of all hypotheses considered remain the same, and have been shown to not differ significantly from each other barring few loading scenarios and the level of complexity modelled. It was found apt that the governing hypothesis to be used be simple, well established and easy to implement and at the same time allowing modifications to be made easily. It was therefore decided to employ the hypothesis of Carter as a template, with further modifications done to convert the otherwise qualitative hypothesis to a quantitative one. A more detailed explanation on the hypothesis and modifications done is presented in following chapter.

CHAPTER 3

GENERAL METHODOLOGY

This section explains the formulation of two different methods and their respective algorithms based on the original hypothesis.

3.1 INTRODUCTION

As explained in the preceding chapter, with regards to fracture healing, all of the hypotheses could simulate fracture healing successfully. The underlying premise involved in each of the hypotheses is the same, with high degrees of distortional stress or strain hindering osseointegration and promoting the formation of fibrous tissue. High levels of deviatoric stress and strain would promote cartilage formation if compressive, and fibrous tissue if tensile. Low deviatoric and dilatational components would be essential to encourage bone formation. The complexities associated with the hypotheses put forth have been varied, with both, monophasic and biphasic modelling used to simulate the process. If extending the concept to tissue differentiation around implants, the requirement would be slightly different to those applicable to fracture healing.

Fracture healing has been well studied in animal and human models with cellular activities closely monitored and replicated *in silico*. The same does not apply to tissue formation around implants, especially in humans as the source of progenitor cells would be limited to the rich bone marrow and no sources outside of this region. In contrast, for fracture healing, the source of cells that invade the callus is varied. Other than the marrow, the surrounding musculature, blood and the periosteum are important sources for these cells. In the absence of literature on cell activity at the implant site, which includes recruitment, proliferation and death, it was decided to exclude cellular phenomenon from the models. In addition, a purely monophasic model was considered to be adequate for the simulations. It has been shown that the predictive nature of these hypotheses are not compromised by assuming tissues to be linear elastic as opposed to poroelastic, encompassing solid and liquid phases [1]. Considering these factors, the hypothesis chosen to simulate tissue differentiation in the current model was based on the hypothesis proposed by Carter et al. to explain fracture healing. The algorithm was originally semi quantitative, with no actual formation of different tissues and used to describe regions where bone formation was most likely based on stress components. The algorithm was modified to include a quantitative module that could determine specific tissue type formed. The original hypothesis with the modified algorithm developed is explained in the following sections.

3.2 THE ORIGINAL HYPOTHESIS

According to the model proposed by Carter, intermittent and cyclic stresses, along with vascularity, governed tissue differentiation. Bone was considered to form if minimal cyclic stresses or strains, deviatoric or dilatational, existed at the region along with good blood supply. High shear and/or tensile hydrostatic stresses encouraged fibrous tissue formation with high compressive hydrostatic stresses encouraging chondrogenesis. Once cartilage or fibrocartilage formed, cyclic shear would then promote endochondral ossification with compressive hydrostatic stresses inhibiting the process. Under poor vascularity, only fibrous tissue would form, and mechanical signals would have no significance. In addition to these basic rules, the entire process also depended on the loading

history at the location. The loading activities over a period of time was decomposed into histograms of load histories that consisted of '*i*' discrete loading conditions (*i*= 1, 2, 3, ..., *c*) that were associated with n_i cycles of load applications per day. The tendency for ossification was expressed as the osteogenic index 'I', dependent on the peak cyclic deviatoric (S) and dilatational (D) stresses defined as,

$$S = \frac{1}{3}\sqrt{\left[\sigma_1 - \sigma_2 \right]^2 + \left[\sigma_2 - \sigma_3 \right]^2 + \left[\sigma_3 - \sigma_1 \right]^2}$$

Equation 4

$$D = \frac{1}{3}\left(\sigma_1 + \sigma_2 + \sigma_3 \right)$$

Equation 5

Using the stress states (S, D) and decomposing the loading history at the location over time, the osteogenic index I was then defined as,

$$I = \sum_{i=1}^{c} n_i \left(S_i + K D_i \right)$$

Equation 6

The osteogenic index 'I' represented the tendency of ossification over a particular region. A high index would mean the region was conducive to bone formation and a low value denoted the tendency to form fibrous tissue. The emphasis, according to Carter et al., was not on the rate of formation of 'I', but on the distribution of and the regions where 'I' was high. The value of 'K' was determined by investigating different values and choosing the value that closely matched with clinical results.

3.3 MODIFICATIONS TO THE HYPOTHESIS

The hypothesis of Carter et al. by itself was qualitative, with no actual formation of bone or any other tissue simulated in the original work. The ossification index 'I' represented regions of the callus which had high or low tendency to form bone. Since the regions of bone, cartilage or fibrous tissue were not delineated to specific values, a new method would have to be developed to simulate

the formation of different tissues using the osteogenic index. Moreover, to simulate tissue differentiation at the interface over time, including the change of one tissue type to another, an iterative procedure would be necessary, which was also absent. These important changes were incorporated into two modified algorithms. Each of the modified algorithms is explained below with reference to the finite element models that will be explained in the individual chapters.

3.3.1 METHOD 1

In this method, used as a precursor to a more descriptive method explained later, the main assumption was that the three main tissue types, bone, fibrous tissue and cartilage had an equal opportunity to form in each iteration. This was carried out to delineate the hypothesis into three separate regions representing bone, cartilage or fibrous tissue for iterative implementation in the form of an algorithm. Due to specific values for dilatational and deviatoric stress components being absent in the original hypothesis, the delineation of the regions in this way was found to be reasonable. In the finite element models in which the algorithm was implemented, as will be shown in the following chapters, the focus was on simulating tissue differentiation in a thin layer of granulation tissue surrounding the implant or in the pores of the porous coating. This was a direct analogy of the transformation of granulation tissue found in the gaps during fracture healing. The granulation tissue would differentiate into one of three tissue types depending on the osteogenic index 'I', defined by the stress components. It was assumed that there was excellent blood supply at the site, hence enabling bone formation. The specific steps involved in the algorithm can be further explained as follows:

Step 1: Import model and define region of interest **(granulation tissue)**

Step 2: Define array of elements corresponding to granulation tissue **[1, 2,..., e_n]**

Step 3: Apply Loading case **L (*i=1, 2, 3,..., c*)** for specific number of cycles ***'n'*** as per equation 6

Step 4: For each **L ( )**, calculate and record values of stress components for each element in the array defined; Deviatoric **S [1, 2,..., e_n]** and Dilatational **D [1, 2,..., e_n]**

Step 5: Calculate Osteogenic Index **'I'** for every element in the array using corresponding deviatoric and dilatational values as per equation 6

Step 6: Sort values of **I** obtained in ascending order and divide values into 3 regions, **[I_{low}], [I_{med}]** and **[I_{high}]** such that number of elements in each group is the same.

Step 7: Temporarily assign material property, Young's modulus **E** of bone, cartilage and fibrous tissue to the elements of the three delineated regions $\mathbf{E\ [I_{low}] \leftarrow E_{fibrous}}$; $\mathbf{E\ [I_{med}] \leftarrow E_{cartilage}}$; $\mathbf{E\ [I_{high}] \leftarrow E_{bone}}$

Step 8: Check conformation to other rules set forth in the hypothesis based on $\mathbf{S\ [1, 2,..., e_n]}$ and $\mathbf{D\ [1,2,..., e_n]}$

1. **FOR any e in $[I_{low}]$,**

   IF D [e] = compressive

   Change E [e] $\leftarrow E_{cartilage}$

2. **Monitor e in $[I_{med}]$ for S, D status**

   IF e in $[I_{med}]$ = compressive D

   Keep E [e] = $E_{cartilage}$

   ELSE IF e in $[I_{med}]$ = cyclic S

   Change E [e] $\leftarrow E_{bone}$

3. **FOR any e in $[I_{med}]$,**

   IF D [e] =low tensile

   Change E [e] $\leftarrow E_{bone}$

4. **FOR any e in $[I_{high}]$,**

   IF S [e], D[e] = high

   Change E [e] $\leftarrow E_{fibrous}$

Step 9: After assigning permanent material properties **E** for all tissues based on step 8, iterate over next loading cycle with existing boundary constraints till tissue stabilisation

The steps aforementioned summarise the implementation of the modification of the hypothesis carried out in some of the case studies presented in the thesis. The basic premise was to delineate the values of the index obtained for the elements in the granulation tissue defined, governed by the local stress states such that there was an equal chance for all three tissue types to form. Based on the original hypothesis where high values of 'I' corresponded to regions of bone formation and low values representing fibrous tissue, the three regions were assigned the material properties of bone, cartilage or fibrous tissue. In addition, additional constraints, as reflected in step 8, were put forth:

- No element experiencing compressive dilatational stress would be categorised as fibrous tissue
- Elements with high shear were to be classified as fibrous tissue

- No element experiencing tensile dilatational stress would be categorised as cartilage tissue
- If cartilage tissue formed, a log was kept on the stress state of the element; with low cyclic shear forming bone and repeated compressive dilatational stresses maintain the tissue as cartilage.
- Bone was not allowed to form if either of the deviatoric or dilatational values was extremely high

The rules were set out so as to avoid any discrepancy with the hypothesis and to avoid index values in the proximity of the delineations being categorised into the wrong tissue type. These rules would also ensure that the hypothesis holds good at every iteration. Therefore, based on the values of the index obtained and the additional checks carried out across all the elements in the granulation tissue, the elements were assigned the final material properties of either of the three tissue types. With the updated material properties, the next iteration was carried out and the process repeated for the remainder of the iterations proceeding to tissue stabilisation. Although the delineation scheme would be an approximation and values that lay in between would have to be demarcated into one of the three tissue types, the idea was to provide a gross region of bone, cartilage or fibrous tissue, concentrating on the regions that were more conducive to bone formation than others. Demarcation into the three regions would ensure index values that lay well within the boundaries would not present problems into being categorised into a specific tissue type and the additional rules employed ensuring values near the boundaries would also be categorised accurately.

The rationale behind this particular method would still follow the essential conditions of bone, cartilage or fibrous tissue formation as chartered out by Carter's hypothesis. This modification enabled a quantified tissue differentiation in the otherwise qualitative algorithm. As part of the iterative solution to monitor tissue change through every cycle, the values of the index were constantly updated through every iteration for the designated number of loading cases and the number of cycles that were input, and material properties were updated accordingly to the three defined tissue types. For example, the iterative procedure was carried on until a defined number of iterations were completed or there was less than a 5% change in tissue type between two successive iterations in the elements of the tissue layer. The number of set iterations was always kept high to avoid premature termination of the simulation in case the number of cycles were completed and there was still more than 5% tissue change at every iteration. Thus almost always, the iterations stopped at the less than 5% tissue change criterion rather than the completion of the maximum number of iterations.

3.3.2 METHOD 2

Method 1 provided a rough delineation scheme, assigning the index values obtained to one of the three tissue types. Although the method was effective in simulating gross tissue formation, the lack

of intermediate tissue types formed could be a limitation. Given the range of tissue types that granulation tissue could transform to, a new method was devised to not only reflect the range of values obtained for the index in every iteration, but also try and accommodate more tissue types in the simulations. In this method, a better technique was devised to map the osteogenic index obtained in each of the iterations to different tissues. The steps involved in this method were the same as method 1 until step 5, after which a mapping scheme was implemented to assign material properties to the indices.

Step 6: Create an array of known Young's modulus, obtained from literature ranging from fibrous tissue to mature bone. For example, **E [fibrous,.. fibrocartilage,...,cartilage,..., immature bone,..., mature bone]**

Step 7: Assign material properties of bone and fibrous tissue to the elements of the highest and lowest index respectively. $\mathbf{E\,[I_{low}] \leftarrow E_{fibrous}}$ **and** $\mathbf{E\,[I_{highest}] \leftarrow E_{mature\ bone}}$

Step 8: Use boundaries obtained from the previous method to assign values for intermediate tissues such as $\mathbf{E_{cartilage}}$ and $\mathbf{E_{immature\ bone}}$

Step 9: Use linear interpolation functions between reference values to obtain material properties corresponding to other indices; i.e. to find young's modulus of a tissue $\mathbf{E_{tissue}}$, Interpolate between corresponding index value $\mathbf{I_{tissue}}$, and closest known index and material properties. For example, if known material properties are $\mathbf{E_1}$ and $\mathbf{E_2}$ with corresponding index values $\mathbf{I_1}$ and $\mathbf{I_2}$, $\mathbf{E_{tissue}}$ can be calculated by

–

Step 10: With aforementioned steps carried out till all of the update Young's modulus has been assigned for all of the elements in the granulation tissue layer $\mathbf{E\,[1, 2,..., e_n]}$

Step 11: Map index values stored to corresponding material properties calculated, for example

$$\mathbf{\left[E\,[I_{low}],\ldots,\ E\,[I_{x1}]\ldots,\ E\,[I_{x2}]\ldots,\ E\,[I_{x3}]\ldots,\ E\,[I_{highest}]\right] \leftarrow \left[E_{fibrous},\ \ldots,\ E_{fibrocartilage},\ \ldots,\ E_{cartilage},\ \ldots,\ E_{immature\ bone},\ \ldots,\ E_{mature\ bone}\right]}$$

Step 12: Update material properties and iterate over next loading cycle with existing boundary constraints till tissue stabilisation

The aforementioned steps summarise the implementation of a mapping scheme to quantify the hypothesis and presented in some of the case studies undertaken in the thesis. The values obtained for the index from every element was sorted in increasing order and mapped on to the elastic moduli of commonly referenced tissue types in literature, ranging from the lowest, fibrous tissue to

cartilage, immature and fully mature bone, which was assigned the highest possible osteogenic index. The values for the tissues that lay in between were assigned by interpolating between the values assigned for these tissue types. By arranging the elastic moduli in equal segments depending on the number of osteogenic index values obtained, each of the index values could be mapped on to corresponding elastic moduli. Keeping elastic modulii values of known tissue types as reference points would enable properties to be assigned for other tissues that lay in between. In addition, the values were assigned such that under no condition was a low index 'I' mapped on to a stronger tissue type like immature or mature bone. The maximum elastic modulus assigned for the highest index was that of mature bone, 20GPa. The lowest possible modulus for the lowest index was that of fibrous tissue, starting at 2MPa. Due to the mapping scheme involved, a range of elastic modulii were assigned to each of the tissues, with any elastic modulii over 6000MPa assigned to mature bone, between 1000 and 6000MPa as immature bone, cartilage tissue between 10 and 1000MPa and fibrous tissue from 2 to a maximum of 10MPa.

This modification would allow a range of tissues to be mapped to the osteogenic index obtained in every loading cycle. It would also enable the properties to be updated iteratively so as to progressively monitor the type of tissues formed in every iteration. This was continued the same way as described in the method 1, till there was less than 5% tissue change between two successive iterations, relating to tissue stabilisation and equilibrium if attained. In addition, an upper limit on the number of iterations was also set so as to prevent premature end to the iterations before the less than 5% tissue change criteria was met.

Both methods described have been employed in chapter 4 to show the subtle differences that exist between the two methodologies. Method 2 gives a more realistic distribution of tissues through the iterations, rather than limiting to only three types that method 1 provides. However, it has to be noted that both methods provide comparable results, and differ only in their complexities and the amount of detail in the type of tissues formed. Each of the case studies presented as chapters henceforth provide more detailed information on the steps involved in implementing the methods. The case studies presented differ in their modelling complexities and applications, and exhibit the accuracy of the methods when corroborated with literature.

CHAPTER 4

TISSUE DIFFERENTIATION IN SHORT STEMMED UNCEMENTED IMPLANTS AND THE INFLUENCE OF DESIGN FEATURES

The research carried out in this chapter has been presented in parts, or completely in the following conference papers and journals:

- *Puthumanapully P.K., New A.M., Browne M. (2009**) "Osseointegration of a short stemmed femoral prosthesis as predicted by a mechanoregulatory algorithm"** Proceedings of the 55th annual meeting of the Orthopaedic Research Society.*

- *Puthumanapully P.K., New A.M., Browne M. (2009) **"Do size and shape matter? Osseointegration in a short stemmed femoral prosthesis as predicted by a mechanoregulatory algorithm"** Proceedings of the 22nd annual congress of the International Society for Technology in Arthroplasty (ISTA).*

- *Puthumanapully P.K., New A.M., Browne M. (2010) **"Design influences of a short-stemmed and long-stemmed uncemented implant on tissue differentiation at the interface: A computational study based on a mechanoregulatory hypothesis"** Proceedings of the 9th international symposium of computer methods in biomechanics and biomedical engineering (CMBBE).*

- *Puthumanapully P.K., Browne M. (2009) **"Tissue differentiation around a short stemmed metaphyseal loading implant employing a modified mechanoregulatory algorithm- a finite element study"** Journal of Orthopaedic Research (In Press).*

4.1 INTRODUCTION

Uncemented implants have traditionally been larger and bulkier than their cemented counterparts due to the fit and fill principle they employ to achieve a stable initial fit with the surrounding bone. Classic designs have included a long, well rounded stem that engages the endosteum of the proximal diaphysis, with the surface coating on the implant providing a strong frictional interlock. The proximal part of the implant, and its role for providing stable fixation was often overlooked due to the emphasis on the reproducible, distal fixation of the implant. While this rationale was not totally without evidence and results [167,225], there have been a number of problems that have been reported due to the inherent bulkiness of uncemented implants or the principle of diaphyseal fixation for long term stability. The occurrence of thigh pain after surgery has been reported, with the tight diaphyseal fit, hypertrophy of surrounding bone and impingement of the implant tip on the bone cited as possible causes [87,134]. Implant revision presents another problem, with a risk of fracture and difficulty in the removal of the implant. In addition, the large amount of bone removed for implantation remains a worry for future revision. However, the most important concern is the problem of stress shielding [226,227]. Distal fixation, compounded by poor proximal fixation and the presence of a stiff stem reduces bone strain in the proximal femur, channeling loads to the diaphysis of the femur. This results in bone remodelling and gradual atrophy of bone in the proximal femur through time, which could result in gross instability of the implant, causing and aggravating existing symptoms like pain, further loosening, dislocation, limited ROM to name a few. Torsional stability has also been an issue, with distal fixation alone found to be inadequate in preventing torsional motion of the implant within the canal [228].

Given these potential shortcomings, recent designs have focused on engaging the proximal femur, especially the metaphyseal region, more effectively, avoiding the detrimental effects of stress shielding and limiting torsion. It has been shown that a proximally fixed femoral implant can reduce the incidence of stress shielding [229]. Moreover, it has also been found that once adequate proximal fixation was achieved, the distal stem was no longer necessary for stability [230]. Older long stemmed implants, in an effort to engage the proximal femur have also restricted the use of the porous coating to only the proximal regions as opposed to being fully coated, but does not eliminate the long stem, which can still result in diaphyseal load transfer and a return of associated problems. The new school of thought is to eliminate this by either using the stem for only alignment purposes or completely removing or shortening the stem to avoid any diaphyseal contact. Newer designs have been manufactured based on this design philosophy and have been the focus of intense research in the last 10-15 years. For example, the IPS (Depuy International, Leeds, UK) is a stemmed metaphyseal loading uncemented implant that uses the stem only as a guiding and alignment tool and not to provide any distal fixation. An offshoot of this design rationale has been the development of conservative (bone preserving) metaphyseal loading implants, which preserves bone stock by the avoidance (stemless) or reduction of stem length (short-stemmed) and loads the metaphysis of the proximal femur. They aim to replicate near anatomic loading of the medial cortex

with little or no contact with the diaphysis. In addition, they also engage the large cancellous bone bed in the proximal femur, with its high vascularity that could assist in more rapid osseointegration of the implant.

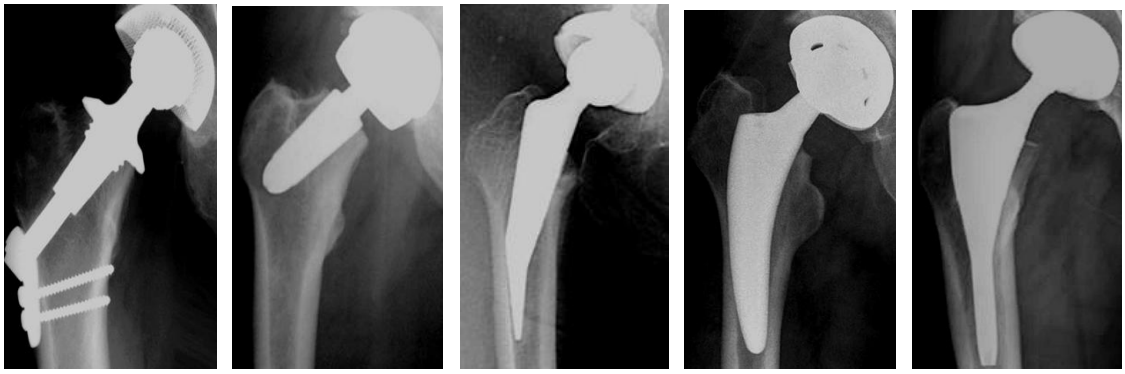

(a) (b) (c) (d) (e)

Figure 4.1: Radiographs showing some of the popular conservative implants (a) thrust plate prosthesis (b) Silent hip (c) Mayo hip (d) Fitmore hip (e) IPS.

Bone conservative implants have a three-fold purpose as listed by d'Imporzano et al [231], namely

1. Availability of bone for possible revisions
2. Proximal load to prevent stress shielding and thigh pain
3. Restoration of the native hip joint biomechanics

These implants would be ideal for the young patient, where bone quality is good and the cancellous bed in the proximal femur providing adequate fixation strength when implanted. They also provide the option of using a standard long stem implant if a revision is needed due to the bone stock preserved. Some of these conservative implants (figure 4.1) include the fully neck preserving Thrust Plate Prosthesis (Centerpulse, Winterthur, Switzerland) and the Silent Hip (DePuy, Warsaw, USA). Variants like the lower neck cut, distal support prostheses like the Mayo conservative hip (Zimmer, Warsaw, USA), the ESKA femoral neck endoprosthesis (ESKA implants, Lubeck, Germany), the Metha (Bbraun, Melsungen, Germany), Fitmore hip (Zimmer, Switzerland) and Nanos (Plus orthopaedics, Aarau, Switzerland) prostheses and the purely metaphyseal loading prostheses like the IPS and the Proxima (DePuy; Leeds, UK).

Conservative stems are only now being used clinically after years of research and is a relatively unknown commodity in terms of functional performance and longevity as it would require a minimum of 10-15 years to truly gauge the implant. Considering there have been no large scale retrieval studies conducted for these implants and the lack of substantive clinical data, computational methods can be applied to give an indicator of the prospective performance of such implants. However, at present, this is limited, especially in the predictive modeling of tissue differentiation and ingrowth around these implants. The type of tissue formed in response to the implant at the interface could determine the longevity and performance of the implant itself.

Clearly, implant design is a contributing factor to this and needs to be investigated. For the focus of the current study, one of the more popular short stemmed implant, the Proxima is considered.

4.1.1 THE PROXIMA IMPLANT

The Proxima, aptly named due to its novel stemless design to load the proximal femur, is a conservative, metaphyseal loading implant that has a prominent lateral flare designed to conform to the lateral aspect of the proximal femur. Although the implant has a medial flare, it is less pronounced and is not the distinguishing feature of the implant. Manufactured from titanium alloy, it is anatomically shaped with an anteverted neck and a 12/14 taper [130]. The design is a combination of two design philosophies originating from the lateral flare of the IPS, and the custom made Santori short stem [232].

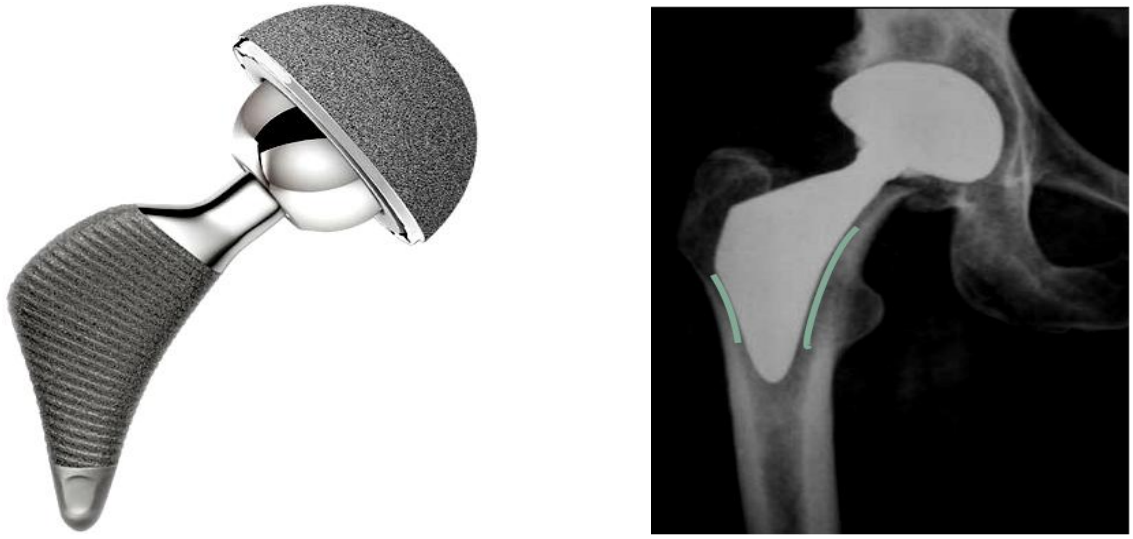

Figure 4.2: The Proxima (left) and the metaphyseal seating of the implant as seen in a radiograph (right). Note the lines depicting positioning of the lateral and medial flares on the proximal femur.

The Proxima, as aforementioned, is designed to have a very pronounced lateral flare and a very high femoral neck cut, producing a wedging effect between the proximal medial femur and lateral metaphysis that prevents distal migration and subsidence of the implant [132]. Rotational and axial stability is provided primarily by the anatomic shape and correct sizing of the implant. The implant is porous coated and has two versions; a standard porocoat, sintered beaded coating and a ridged "ZTT" surface. Both versions incorporate a thin layer of hydroxyapatite for encouraging bone ingrowth. The Proxima and a radiograph depicting the seating of the implant is shown in figure 4.2.

4.2 AIM

To study the behavior of the conservative implant Proxima, and its design features on tissue differentiation and bone ingrowth around the implant using the modified mechanoregulatory algorithm. This is carried out in two sections. The first section deals with general tissue differentiation around the implant. The second section focuses on a specific design feature, that of the influence of the prominent lateral flare, carried out by comparing it to a flare-less model.

4.3 METHODOLOGY

The technique used to simulate tissue differentiation around the implant was to combine finite element models of the implant and surrounding bone with the methodology described in Chapter 3 employing simplified loading and boundary conditions. For this study, both versions of the modified hypothesis and algorithm were employed for comparison. The individual steps involved are described below.

4.3.1 GEOMETRIC AND FINITE ELEMENT MODELS

Macroscale modelling of the tissue differentiation around the implant was carried out in several steps. The first step involved creating geometries and components to be used in the study. The main components of the study; geometries of the femur, the implant and the tissue layer at the interface were either obtained from existing files or from constructed from CT scans.

4.3.1.1 THE PROXIMA IMPLANT

The geometry and solid model of the implant was obtained from DePuy (DePuy International, Leeds, UK). The implant was then scaled for size to fit the femur used in the study using solid body operations in Rhinoceros (Robert McNeel & associates, Seattle, UK). The solid model of the implant is shown in figure 4.3.

An important point to note was that the coating, neither the porocoat nor the ZTT surface was modelled on the implant. The focus of the study was to determine tissue differentiation around the implant as a whole rather than specifically the coating itself. In addition, the computational expense required to include the coating would be very high and the level of detail beyond what was aimed to be simulated.

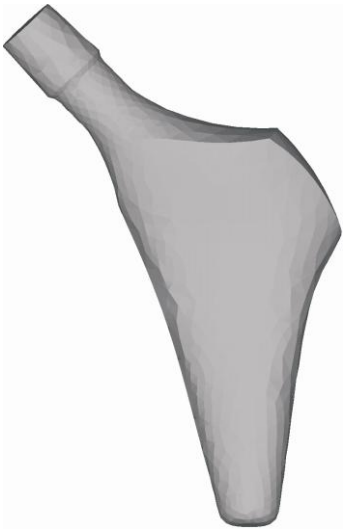

Figure 4.3: The model of the proxima used in the study.

4.3.1.2 FEMUR

The geometry of the femur was obtained from computer tomography (CT) scans of a 43 year old male with an estimated height of 1.73m and weight of 75kg based on a BMI of 28. The length of the femur was measured at 463mm, and the scan resolution was 0.781mm with a slice thickness of 2mm. Segmentation and reconstruction of the scans were done in Amira (Visage Imaging, Berlin, Germany) to produce the final solid model of the femur. Considering the size of the implant in question, it was decided to only include the proximal part of the femur for computational ease. The femur was cut at a distance of 60mm from the tip of the implant for this study after implantation. A schematic of the construction of the solid model of the femur from CT scans is shown in figure 4.4.

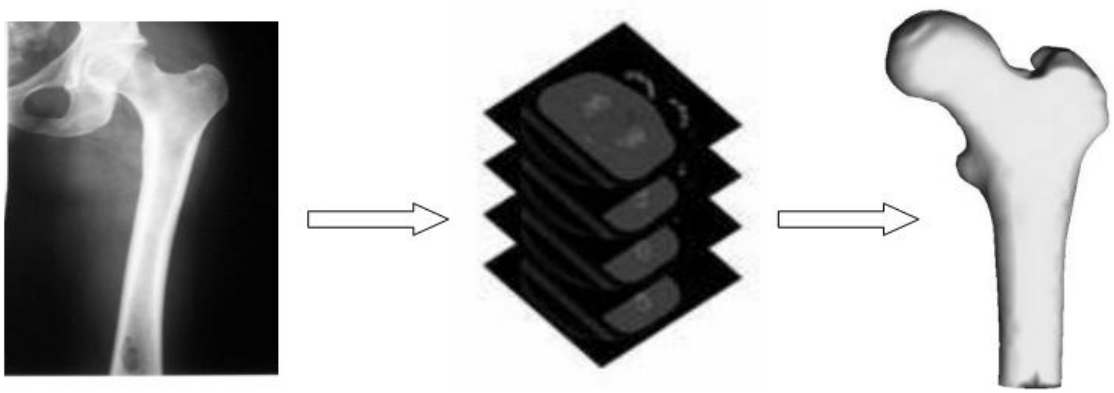

Figure 4.4: A schematic of the steps involved in producing the solid model of the femur used in the study. CT scans of the femur were segmented and reconstructed using the software to form the final solid model.

4.3.1.3 TISSUE LAYER

Implantation of the prosthesis and the corresponding osteotomy was performed in the software Rhinoceros(Robert McNeel & associates, Seattle, USA). The osteotomy plane and seating of the implant in the created implant bed was kept as close as possible to actual surgical procedures. It was not possible to follow the roundabout technique for implantation of the process [233], but the final positioning of the Proxima along with the high neck cut and the wedge on the lateral and medial flare replicated the final operative condition. Because the implant geometry was oversized, it was scaled to be of optimum fit in the femur and compared to radiographs to ensure size and positioning were accurate. The implant occupied a major portion of the proximal epiphysis and metaphyseal regions.

An additional healing tissue, i.e. granulation tissue layer, was also created around the implant. This granulation tissue over time, depending on the mechanical conditions at the implant site then differentiates to form a host of tissues. The chain of events that occurs in fracture healing explained in chapter 2 can be used for comparison. It has been found that immediately after surgery; the necrotic bone surrounding the implant begins to resorb and is replaced by granulation tissue resulting in minimal direct-bone implant contact. Most of the stability is provided by this healing tissue and its interaction with the implant surface [155]. In the absence of any direct contact between implant and bone, and to simulate tissue differentiation around the implant, it was decided to subject this healing tissue to tissue differentiation, a process that would normally occur in addition to changes in the surrounding bone. Other authors like Keaveny et al [234] have previously used a no tension, frictional interface with emphasis on micromotion to simulate various interface conditions and their implications on the long term biomechanical effects of ingrowth but have not provided an iterative, changing interface to simulate interface behaviour. With predictive modelling at the interface, the evolution of different tissues as regions around the implant get weaker or stronger can be shown.

The thickness of the layer surrounding the implant was made on an assumption of the thickness of what would otherwise be a 3 layer porous coating of 250 micron diameter beads that the Proxima normally employs and would be filled with granulation tissue. Even though the beads haven't been modelled in this case, this was considered to be a reasonable assumption as a start point. In addition, other studies have used a maximum thickness of 1mm for simulating fibrous tissue layer surrounding the implant [177,235]. Granulation tissue is comparable to fibrous tissue used in these studies and a 750 micron thick layer was also a conservative assumption based on this.

The construction of the tissue layer was carried out by uniformly exploding the geometry of the implant that was in contact with the proximal bone by 0.750mm in all directions. The implant geometry was then subtracted from the newly created tissue block to produce a 0.750mm uniform

hollow layer into which the implant could be fit without the formation of any gaps. This additional layer was then subtracted from the original implant gap in the bone to accommodate the new dimensions, resulting in three separate components, namely, the osteotomised bone, the tissue layer and the implant (figure 4.5). The whole assembly consisting of the bone, tissue layer and the implant was then exported for meshing.

(a) (b) (c) (d)

Figure 4.5: Solid models of the components used in the study (a) osteotomised bone (b) tissue layer (c) tissue layer enveloping the implant and (d) the complete assembly.

4.3.2 FINITE ELEMENT MESH

The next step in the process after obtaining the solid models was to mesh the components. This was carried out in Ansys ICEM (Ansys Inc, Canonsburg, PA, USA). All parts of the assembly were then checked for faults in geometry and subsequently repaired and meshed together. Element size to be used was determined by exploring different mesh configurations, and the resultant effect on the osteogenic index obtained after a single iteration of implementing the modified algorithm. The decision to use the osteogenic index as opposed to the more conventionally used stress and strain values for the mesh convergence study was based on the emphasis being solely on the tissue differentiation in the layer. In addition, due to the nature of granulation tissue as a compliant surface, stress or strain values by themselves would not be an appropriate parameter to consider.

A number of combinations of different mesh sizes and densities were investigated and a visual inspection of the regions of high and low osteogenic index were noted and compared across the

models along with the computational time needed to finish the ten iterations. Ten iterations, with each iteration corresponding to 100 cycles of normal walking and stair climbing would allow a good portion of a specific tissue type to form and be easily compared across the models. The different element sizes investigated for convergence and index distribution in the tissue layer are shown in table 4.1.

Max, Min - element size	***Total number of elements***
2, 0.2	1,332,177
2, 0.5	286,288
3, 0.2	1,058,645
3, 0.5	273,080
4, 0.2	960,571
4, 0.5	55,522

Table 4.1: Different mesh densities investigated for mesh convergence.

It was found that there were no significant differences in the patterns of index obtained in the tissue layer for all of the configurations tested (see appendix B) However, computing times for the finer meshes were high, and in the event of near similar patterns across the models, it was decided to use the 4, 0.5 configuration for the remainder of the analysis.

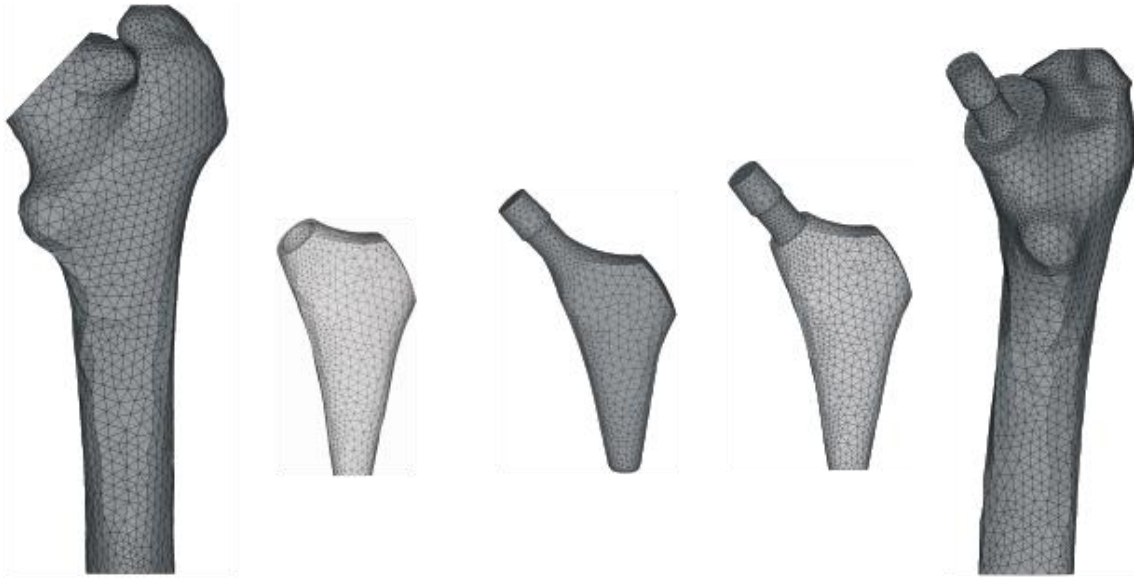

(a) (b) (c) (d) (e)

Figure 4.6: Finite element models of (a) bone (b) tissue layer (c) implant (d) tissue layer enveloping the implant and (e) complete assembly.

Volume meshes were then generated for each of the parts and were in the degenerate form of 4-node tetrahedral elements. The model consisted of 55,522 elements and 10,872 nodes. The meshed components are shown in figure 4.6.

4.3.3 MATERIAL PROPERTIES

The material property assigned to bone is an important parameter in the current study. Considering an interface tissue is modelled between the implant and bone, the local stiffness of the bone would influence the way the tissue responds to mechanical stimuli and hence regulate tissue differentiation. Hence it was important that a standard set stiffness not be used for the whole of bone and element specific properties be assigned instead. Therefore, the material properties of bone were applied using BONEMAT [19], developed at the University of Bologna, Italy. BONEMAT relates a 3D finite element mesh to the bone radiographic density (Hounsfield units, HU) available from the corresponding CT data set. The BONEMAT routine then assigns an elastic modulus to each element based on the apparent bone density on the corresponding element location on the CT data set using a nonlinear relationship [236]. In this fashion, every element in the bone mesh was assigned a material property number and values for density and elastic modulus. A standard Poisson's ratio of 0.3 was set for all the bone elements. The elastic moduli assigned to bone after the procedure is shown in figure 4.7, along with the seating of the implant.

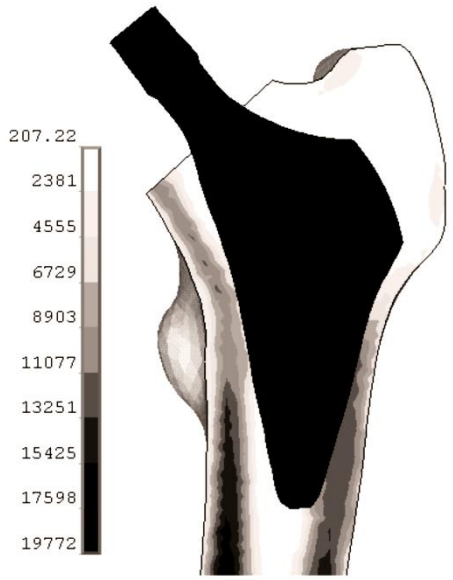

Figure 4.7: Elastic moduli (MPa) assigned to bone after implementing the BONEMAT routine. Note that the implant is shown for reference and its material property is not represented.

The Proxima implant is manufactured from Ti alloy, so an elastic modulus of 110GPa and Poisson's ratio of 0.3 was assumed. The granulation tissue surrounding the implant was also assumed to be linear, elastic and isotropic. Granulation and other tissues surrounding the implant were assumed

to be linear, elastic and isotropic in keeping with the literature [216-218]. It should be noted that since the current study employs both of the modified hypothesis and algorithm, one employing set values and the other mapping a range of values, the material properties used were adjusted accordingly. For example, employing method 1 would imply using set elastic moduli values for bone, cartilage and fibrous tissue. As long as the elastic moduli differed significantly from each other, it would not affect the result of the simulation due to only three types of tissues formed and the clear demarcation of each type. However, for method 2, a range of tissue types would have to be mapped and the list of material properties used for this is shown in table 4.2.

PROPERTY ***TISSUE***	***ELASTIC MODULUS***	***POISSON'S RATIO***
Femur	CT derived element specific	0.3
Granulation tissue	1	0.17
Fibrous tissue	>2 to ~10	0.17
Cartilage	>10 to ~1000	0.17
Immature bone	>1000 to ~6000	0.3
Mature bone	> ~6000	0.3

Table 4.2: Material properties assigned to different tissues based on values obtained from literature [216-218].

4.3.4 BOUNDARY CONDITIONS AND LOADING

The boundary conditions assigned were simplified, with the distal part of the proximal femur fully constrained in all directions. At the interface, the granulation tissue layer was assumed to be fully bonded to the implant and the bone. Granulation tissue was assumed to be a compliant and conforming layer formed in the space, adhering to surfaces well [219]. Experimental work that has simulated fibrous tissue using a 1mm layer of silicone [235] was used as the underlying concept for representing granulation tissue in this way. Further, in computational studies pertaining to fracture healing, granulation tissue formed in the callus space and that later transformed to other tissue types, had similar assumptions [20,218].

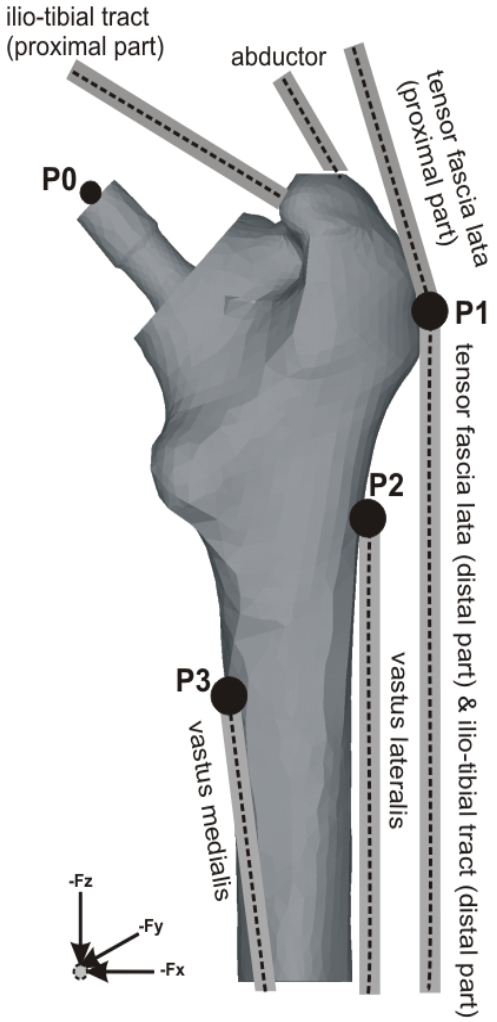

Normal walking - Maximum contact force				
Force [%BW]	**X**	**Y**	**Z**	**Acts at point**
hip contact	-54.0	-32.8	-229.2	P0
abductor	58.0	4.3	86.5	P1
tensor fascia lata (proximal part)	7.2	11.6	13.2	P1
tensor fascia lata (distal part)	-0.5	-0.7	-19.0	P1
vastus lateralis	-0.9	18.5	-92.9	P2

Stair climbing - Maximum torsional moment				
Force [%BW]	**X**	**Y**	**Z**	**Acts at point**
hip contact	-59.3	-60.6	-236.3	P0
abductor	70.1	28.8	84.9	P1
ilio-tibial tract (proximal part)	10.5	-3.0	12.8	P1
ilio-tibial tract (distal part)	-0.5	-0.8	-16.8	P1
tensor fascia lata (proximal part)	3.1	4.9	2.9	P1
tensor fascia lata (distal part)	-0.2	-0.3	-6.5	P1
vastus lateralis	-2.2	22.4	-135.1	P2
vastus medialis	-8.8	39.6	-267.1	P3

Figure 4.8: The muscles, along with their attachment points and their corresponding forces used in the study [18].

Loading and direction vectors of the muscle forces in the femur were based on the data reported by Bergmann et al [18]. Both normal walking loads and stair climbing loads were considered for an individual weighing 75 kilograms. Only the maximum contact force in each of these two load cases was used. The list of muscles and their corresponding forces are shown in figure 4.8. Due to the use of only the proximal femur in the simulation, none of the muscles attaching beyond the mid-distal femur were included. The forces were applied by selecting a group of nodes within a 3mm diameter patch around each specific attachment point and dividing the force equally among this set of nodes.

4.3.5 IMPLEMENTATION

As aforementioned, the emphasis of this study was to predict the change in the tissue layer between the implant and bone. The elements of the tissue layer were initially assigned granulation tissue properties and depending on the mechanical stimuli, i.e. the osteogenic index calculated for the individual elements, they were modified to represent the specific tissue type depending on the

method used. Using method 1 would eventually form one of the three tissue types for every element and method 2 would provide a more smooth distribution, with intermediate tissue values represented as well. Stair climbing and normal walking were considered as two separate load cases and assumed to occur in equal proportion per iteration at an average of 100 steps a day. This was carried out primarily until what was defined as tissue stabilization; when there was less than 5% change between two successive iterations for elements in the model. An additional safety constraint on the number of iterations was also set, albeit very high, that assumed tissue stabilization would always occur through tissue convergence. A flowchart of the steps involved is shown in figure 4.9.

With regards to the hypothesis, the value of 'K' to be used in the simulation needed to be determined. In the original study by Carter, this was carried out by a parametric study of different K values and comparisons to clinical data to determine which value of K would be the closest representation. A similar approach was taken in the current study with a parametric study of K values, ranging from 0 to 3 in intervals of 0.5 for a single load case of normal walking run until tissue stabilisation. While in the original hypothesis, a comparison could be made to actual fracture healing studies; it would be extremely difficult in the current study due to the absence of large scale follow up studies on the implant. Therefore, the value of K was based on tissue convergence and a comparison to another metaphyseal fixing porous coated implant (The IPS). The IPS design, which is a conservative implant with a stem for purely alignment purposes, also incorporates a lateral flare, although not as pronounced as the Proxima. The Proxima was an offshoot of this design philosophy. The IPS has been used longer than the Proxima and is more clinically well documented in comparison. By comparing the results obtained for different K values for the Proxima and the IPS, it would be possible to decide on a value to use for the remainder of the simulations. A comparative view of both implants is shown in appendix C.

Whilst the determination of K through this comparison may not be entirely accurate, it was found to be a reasonable condition in the absence of relevant literature to determine the value of K. Moreover, it has been shown previously that the deviatoric components are more influential in regulating tissue differentiation at the interface when compared to the dilatational components [22]. Since K is the constant value that applies to the dilatational component, small changes in the value of K would not be the most contributing factor to the tissue differentiation around the implant. The results are mostly presented visually, due to the emphasis on determining the regions of bone formation around the implant.

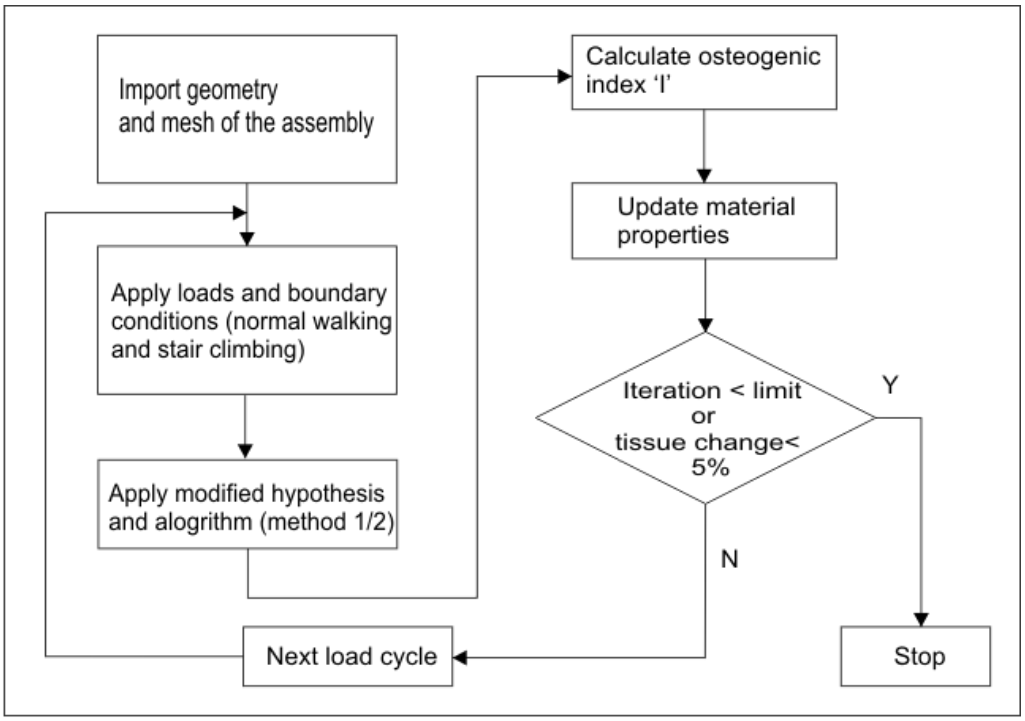

Figure 4.9: Flowchart describing the steps involved in the process of simulating tissue change in the interfacial layer.

4.4 RESULTS

4.4.1 SELECTION OF K VALUE

Selected results, for values of K=1, 2 and 3 based on method 1 are presented in figure 4.10. It was found reasonable that method 1 be used for obtaining the gross formation of tissues rather than the detailed description provided by method 2. Method 1 is also quicker to implement than method 2. However, both methods have been implemented for the remainder of the simulations as presented in the later sections. The results obtained for some of the K values were in contrast to others. The tissues formed for K=1 were sporadic and inconsistent with no defined pattern in the formation of any one type of tissue. This was also observed for values of 0.5 and 1.5. Patterns obtained for values of K=2 till K=3 were more comparable. However, in the case of K=3, the results were inconsistent with patches of tissue formed in the proximal regions of the implant which was found to be not consistent with patterns found in radiographic data obtained for the IPS [237].

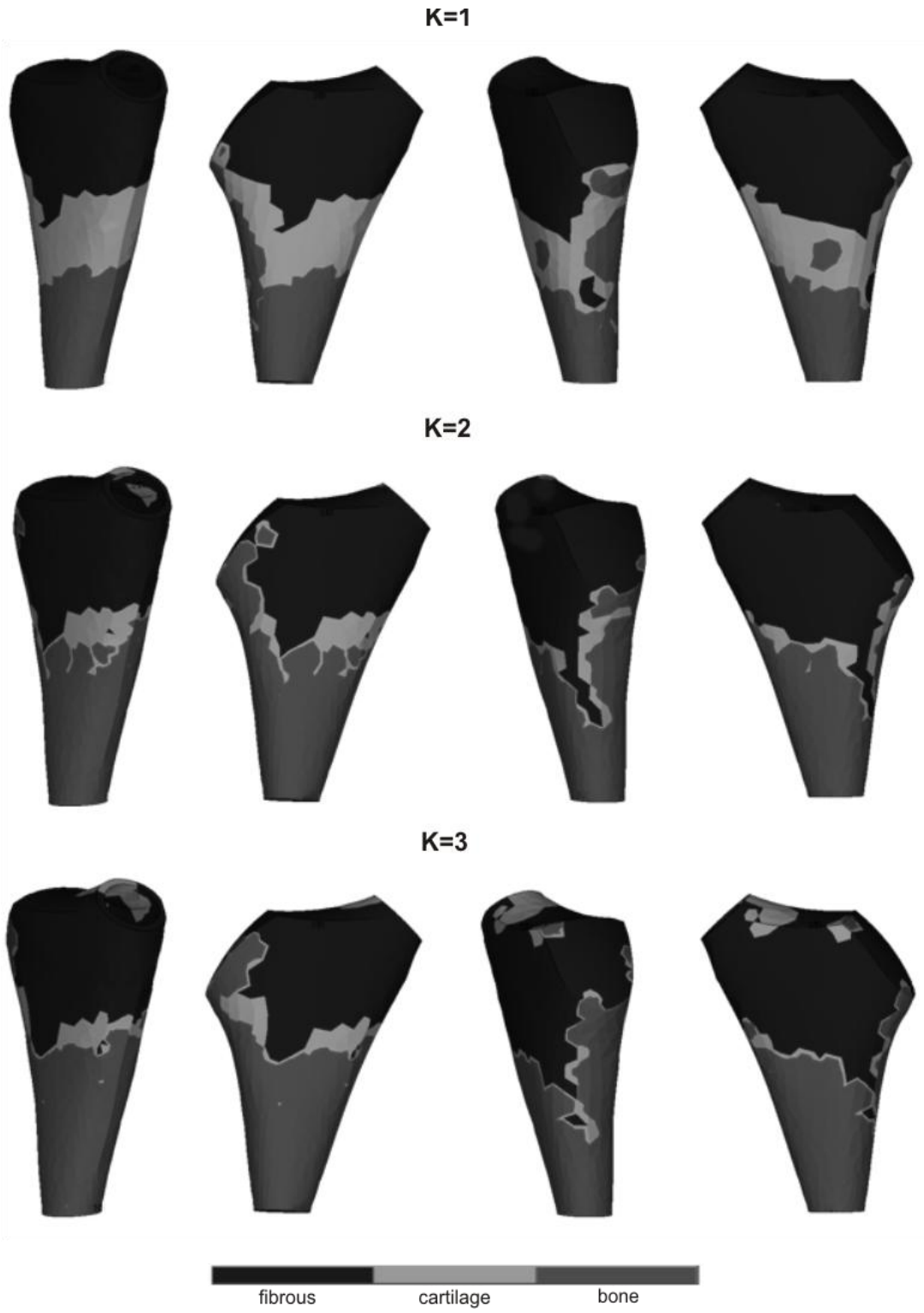

Figure 4.10: Tissue formation for different K values at stabilisation for a single load case of normal walking.

With respect to the transformation of granulation tissue, all K values produced a very similar trend. At the start and the initial few cycles, the majority of the tissue type formed was fibrous, with limited amounts of bone and cartilage formation. However, as the iterations progressed, there was

a distinct increase in the amount of bone formed. The value of K=2 was chosen for the remainder of the analyses as it provided the most stable solution for tissue convergence and when compared to the IPS, a realistic distribution of the different tissue types around the implant. A comparative figure of the chosen K value against the osseointegration found in the IPS from literature [237-239] is shown in appendix C. This was found to be a reasonable assumption considering the lack of clinical data relating to the implant and its behaviour long term. It is worth noting that the value of K used matched the value chosen in the original hypothesis by Carter et al. in the finite element analysis simulating fracture healing.

4.4.2 RESULTS OBTAINED FOR METHOD 1 AND METHOD 2

At the start of the iterations, all of the tissue is granulation tissue, (see Chapter 3). Granulation tissue then differentiates as the iterations progress. In method 1, considering the tissue type changed between fibrous, cartilage and bone and no other tissues in between, the majority of the tissue type formed was fibrous, extending around the implant and enveloping it completely. There was no bone formation during the initial stages and very little presence of cartilage tissue (~10%).

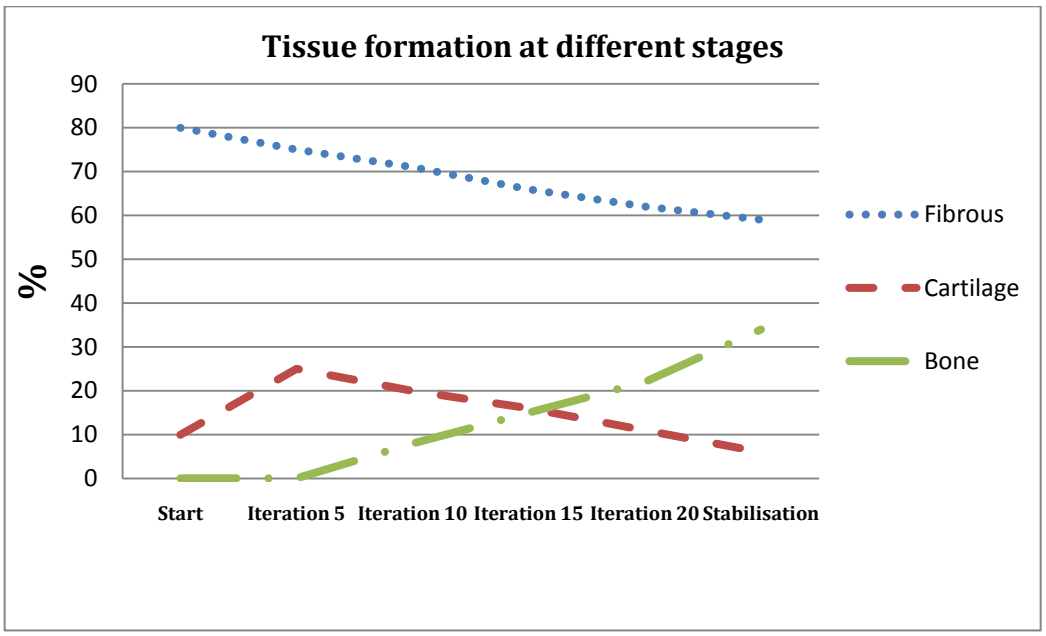

Figure 4.11: The change in tissue type through the iterations using method 1.

Cartilage tissue increases in the next few iterations to a maximum of 25% volume of occupied tissue. Bone formation does not start until past the 5th iteration, around the distal regions of the implant and occupies around 8% of the tissue layer. As the iterations progress, the regions of cartilage tissue are gradually replaced by bone, reducing to around 20% (figure 4.11).

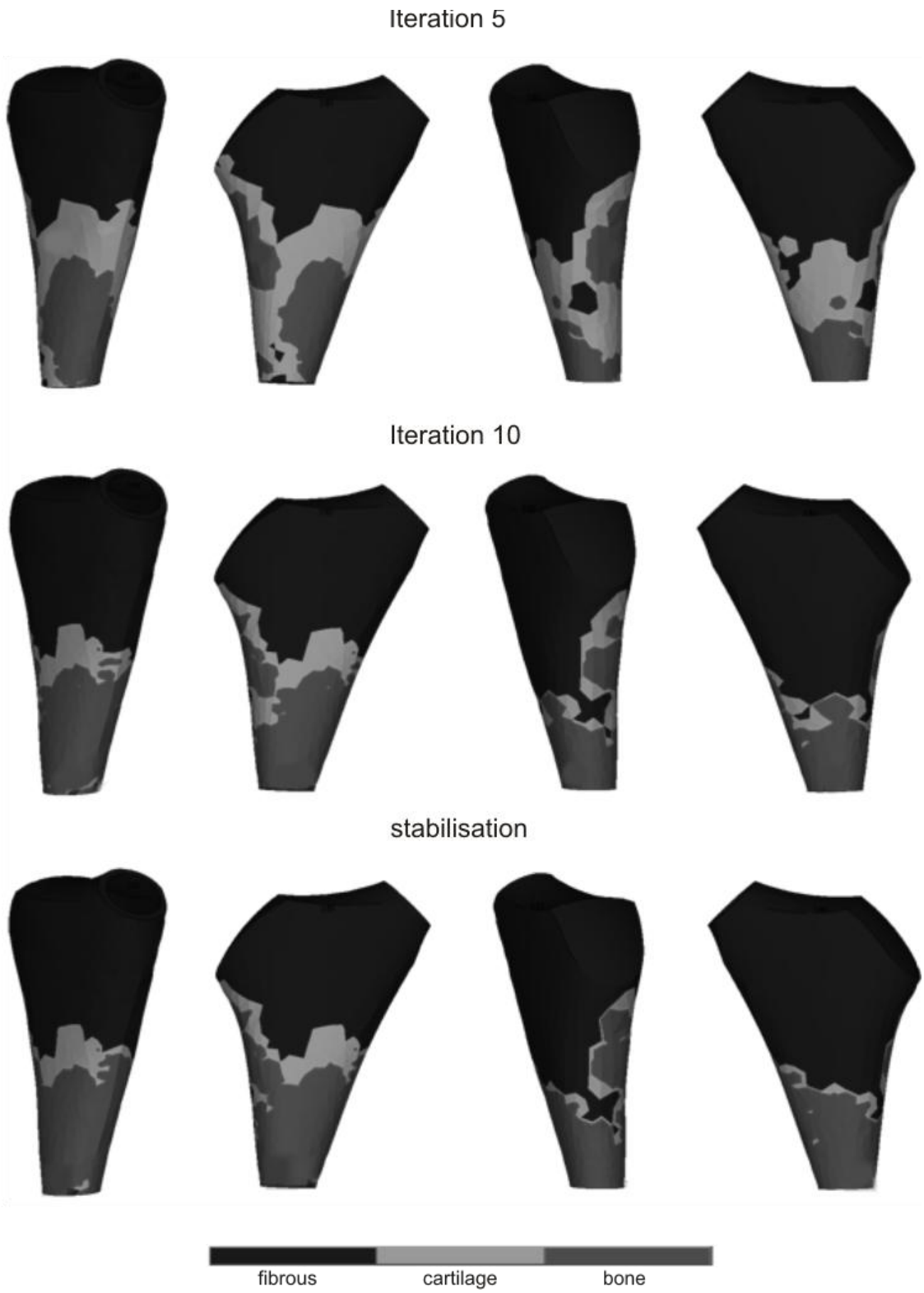

Figure 4.12: Tissue differentiation using method 1 through different stages in the iterations showing four different views of the interface tissue for each stage.

The fibrous tissue occupying the proximal regions does not vary much, with the majority of the change seen in the decrease in cartilage and a corresponding increase in bone tissue through the iterations, until stabilization. However, this is mainly due to the change in the mid regions of the tissue layer, where fibrous tissue is more inclined to change to cartilage and eventually, bone.

Figure 4.12 shows tissue change through the iterations, progressing to stabilisation. Bone formation is seen in the distal regions of the implant, mostly below the lateral flare. Cartilage continues to decrease and occupies very little of the interface at stabilisation (8%).

The data presented in figure 4.12 shows the actual change in tissue type as tissue differentiation proceeds. The percentage of bone tissue increases steadily after the 5th iteration to occupy over 30% of the interface at stabilisation. Bone occupies the distal anterior, posterior, lateral and medial regions of the layer. The amount of fibrous tissue decreases through the iterations, but not as rapidly as cartilage tissue. There is a 20% drop in the amount of fibrous tissue at the end of the iterations, but the tissue still occupies most of the proximal regions of the implant, presenting a weak interface proximally. However, the presence of bone and the small percentage of cartilage in the distal regions of the implant could provide stability to the implant.

The results obtained by implementing method 2 (figure 4.13) do not differ significantly from the results of method 1 barring better description of tissue formation at the interface. During the initial stages, only fibrous tissue formation is dominant occupying the whole of the tissue space, with cartilage appearing around iteration 5 in the distal regions of the implant. Tissues start to become more stable around iteration 10 with signs of bone formation, replacing the original regions of cartilage formation. Immature bone formation is present in the distal-anterior regions of the implant and the anteromedial regions. Cartilage tissue further occupies the surrounding areas of the newly formed bone, paving a route for mature bone formation over existing immature bone. This process continues with immature bone replacing cartilage tissue and mature bone replacing immature bone as the surrounding tissues become more stabilised.

At complete tissue stabilisation, immature and mature bone occupies most of the distal regions of the implant in the anterior, posterior, medial and lateral aspects. Bone formation is found more in the posterior aspects of the implant compared to the anterior regions. Cartilage tissue is limited at tissue stabilisation, having been replaced by bone formation. Cartilage occupies the mid regions of the implant, serving as a boundary between the fibrous tissue formed proximally, and bone distally. Fibrous tissue formation is consistent in the proximal regions of the implant through the iterations without change. As shown in method 1, most of the decrease in fibrous tissue is accounted for in the regions under the lateral flare.

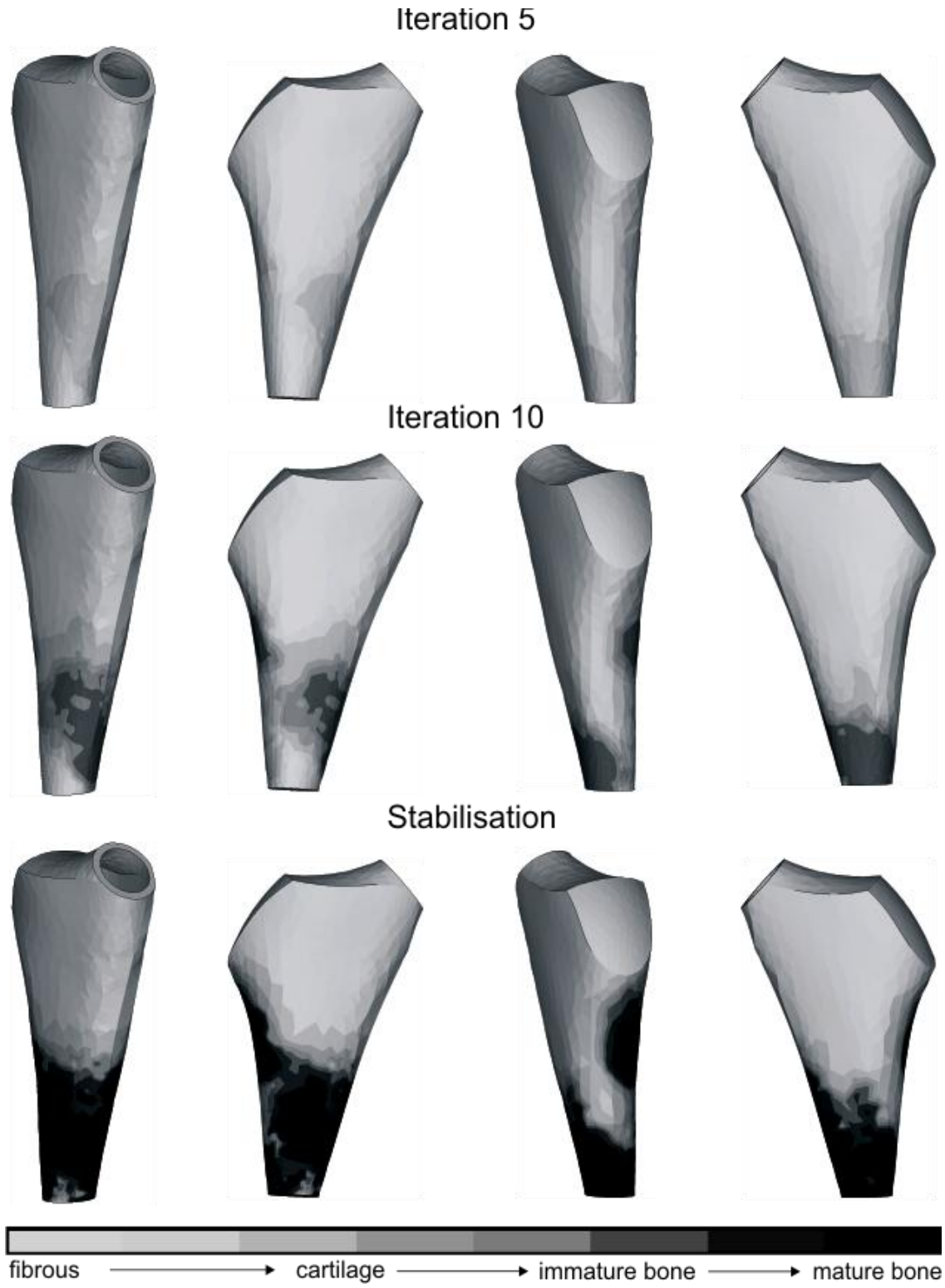

Figure 4.13: Tissue differentiation using method 2 through different stages in the iterations showing four different views of the interface tissue for each stage.

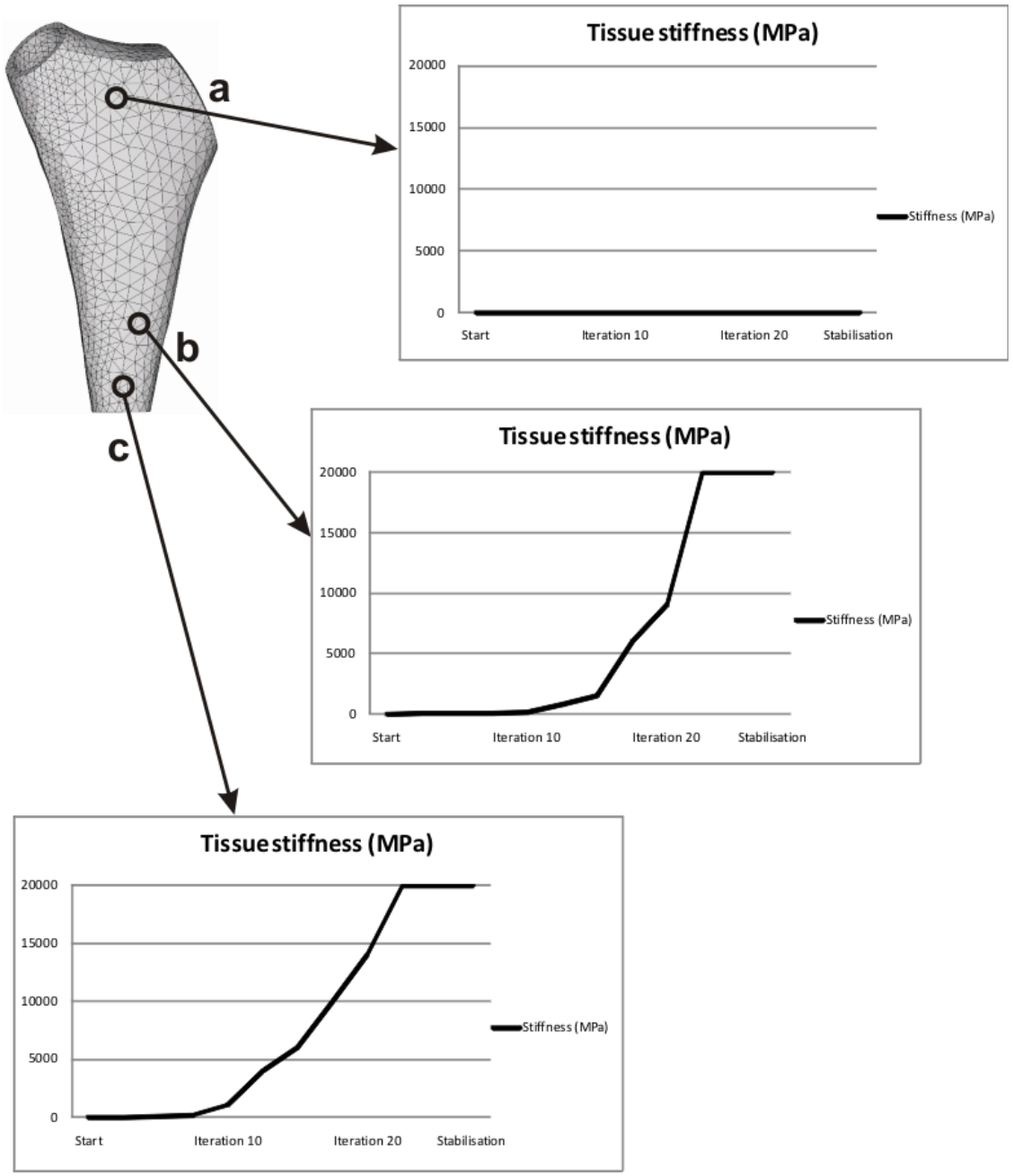

Figure 4.14: The change in tissue stiffness from the start to stabilisation for three specific locations a, b and c in the tissue layer.

Tissue stiffness changes at varied rates at different locations in the tissue layer. At some locations, in the tissue layer, there is not much change in tissue type and only small stiffness changes within a specific tissue. For example in figure 4.14, which shows the change in tissue stiffness at 3 specific locations in the anterior regions around the implant, there is no cartilage or bone formation through the course of the iterations until stabilization in the superior region of the tissue marked 'a'. The location remains fibrous, with stiffness changes well within the elastic moduli boundaries defined for fibrous tissue.

At location b, a smoother transition is seen, with cartilage formation towards the 10th iteration, followed by immature bone that gradually stiffens to form mature bone as the iterations progress. The stiffness increases until the maximum stiffness of 20GPa is achieved and is maintained till stabilization, where less than 5% tissue change between successive iterations occurs. A more rapid formation of immature bone is seen in location c, where fibrous tissue is present only for the first few iterations, followed by rapid formation of cartilage tissue and immature bone. The stiffness increases steadily and mature bone formation occurs around the 14th iteration, compared to the 19th iteration in location b. Although the iterations don't represent an actual temporal scale of tissue formation, the number of iterations taken to reach each stage is important, and the distal regions clearly stabilise quicker than the mid-proximal regions of the tissue layer. This could have implications on the stability of the implant.

4.5 DISCUSSION

In the current study, tissue differentiation around the novel and existing short stemmed implant, (the Proxima) is predicted and discussed. The general trend observed using the two methods is a large region of fibrous tissue proximally, with bone in the distal regions of the implant. This agrees well with the only documented large scale study conducted on the behaviour of the implant [131,132]. In a clinical follow up after 5 years on average, endosteal spot welds were common, with bone bridging in the distal regions of the implant in the majority of the implants. This agrees very well with the results obtained in the current study, with most of the bone formation in the same region.

The regions of tissue formation an also be classified on the basis of Gruen zones. Gruen zones have often been used to describe bone remodelling changes around an implant [97], this can be extended to describe tissue differentiation as well . Modified Gruen zones have been adapted for the implant in the absence of a stem [130]; Gruen zones 3 and 5 which would represent the lateral and medial sides of an implant normally, have been excluded. The zones 1,2,4,6 and 7 are used to describe the regions around the implant as shown in figure 4.15. If the results obtained using both methods are categorized through these Gruen zones, the majority of the regions of bone formation are zones 2 and 6 with a halo pedestal formation around the tip of the implant. Most of the implants in the clinical follow up have had bone formation on both sides but have also included cases where only the lateral side has ingrowth. This again agrees well with the current study where more bone formation is predicted in the lateral side of the implant rather than the medial side.

The clinical study also presented evidence of bone ingrowth under the lateral flare in around 20% of the cases and this was also observed in the current study. The original hypothesis predicted fibrous tissue formation around the tensile regions of the implant; the presence of bone on the lateral side can be explained by the compressive forces provided by the muscles acting at that

location balancing out the tensile forces. The inclusion of this factor is important as it has been shown that Koch's model [240] of regions of tensile and compressive stresses acting on the femur are not accurate due to the non inclusion of muscle forces in the original model [241]. The large fibrous tissue presence (~60%) in regions above the lateral flare was anticipated due to the muscle attachment points promoting high stresses in the region. This was also evident from the radiographs obtained in the Proxima study, where in the few cases of loosening, the proximal regions of the implant near the greater trochanter were the main failure regions. Although this was primarily related to stress shielding and bone wasting in the region, the presence of a weak interface due to the development of fibrous tissue at the interface in these regions cannot be ruled out; indeed, Carter, in his study, had hypothesized that even a few cycles of high stresses in the region would result in the formation of fibrous tissue [23].

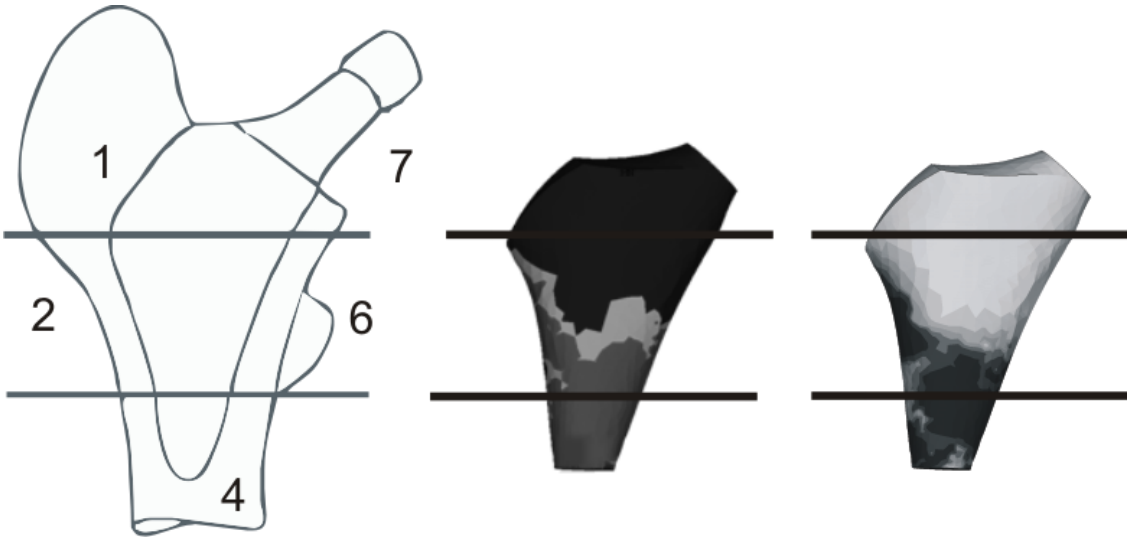

Figure 4.15: Adapted Gruen zones for the Proxima (left) and the corresponding regions as applied to the results obtained in the study.

Another point to note was the presence of cartilage tissue which is later replaced by bone. This would be logical as healing would proceed in the direction of the stronger tissues as shown previously [20,22,212]. Bone gradually replaces cartilage as the major tissue type distally, further strengthening the interface under the lateral flare. The stiffness of the surrounding bone influencing tissue differentiation is also important. On careful observation it can be seen that the regions of bone formation correspond directly to the regions where the surrounding bone is stiffer. Fibrous tissue formation occurs where the surrounding bone is less stiff compared to regions where there is bone formation, in this case, the proximal regions. Dual energy X-ray absorptiometry (DEXA), which measures bone mineral density (BMD) has also been used to study the Proxima [233,242]. The findings of the study showed that in zones 2 and 4 the BMD values were superior to even that of the healthy contralateral femur. It is notable that these are the regions where bone and

cartilage tissue has been predicted to form in the current model. In addition, bone bridging or pedestal formation was reported; a finding supported by the current study.

4.5.1 INFLUENCE OF THE LATERAL FLARE

The influence of the lateral flare in the design would appear to be important given the significant bone formation below this region. The lateral flare has been well documented to provide more proximal loading due to the seating of the flare on the lateral cortex of the femur; this feature also provides good stability to the implant and reduces the incidence of migration and subsidence [237,239,242]. This is clearly shown by the formation of the stronger tissues in and around the region (figure 4.16). Even during early iterations, the presence of stronger tissues such as bone and cartilage is evident, due to the better circumferential stress transfer to the surrounding bone through the region. The proximal region of the implant, although lying on the cancellous bed, is influenced by the strong abductor forces and the hip contact force acting on the head of the implant, which gives rise to high compressive and tensile stresses, accounting for the presence of fibrous tissue here.

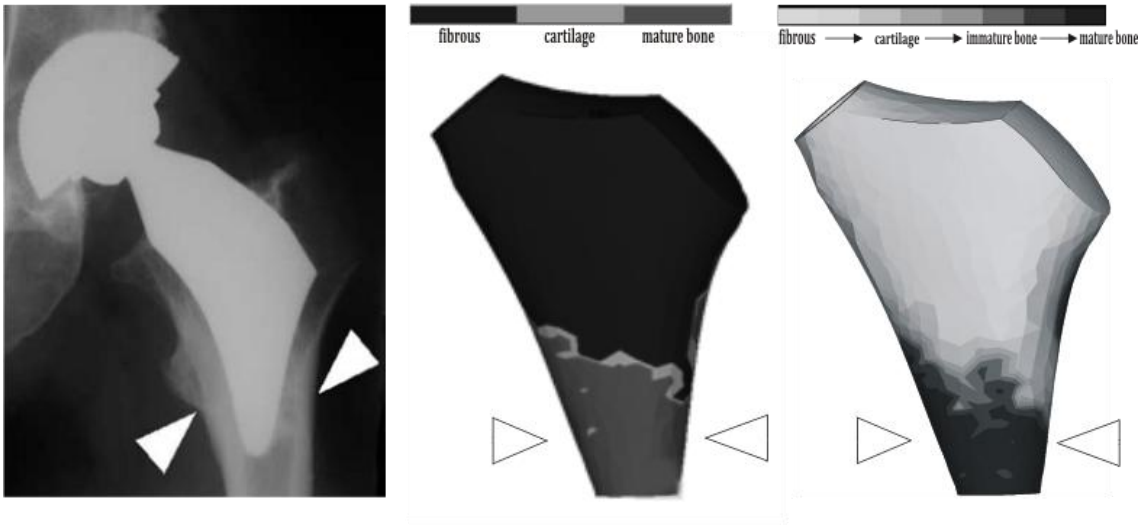

Figure 4.16: Radiographic evidence of osseointegration in the distal regions of the implant, under the lateral flare from the study by Santori et al. (left) [132] compared to the results using method 1 (centre) and method 2 (right). Note the regions of bone formation are identical.

Primary stability is an important factor for cementless implants, especially for short stemmed implants. Due to the absence of a stem and distal fixation, subsidence and migration remain a concern. The Proxima, resting in the metaphysis in the cancellous bed requires good quality bone in the region to avoid the aforementioned problems. Micromotion, which also governs tissue differentiation, but has not been investigated in the study, is also heavily dependent on the positioning and quality of the bony bed. In a cadaveric study by Westphal et al. [243], it has been

found although the overall cyclic motion of the Proxima is lower than other long stemmed implants considered in the study, it is essential that good quality bone and the correct sizing of the implant be used depending on the size of the femur it is implanted in. In this study, sizing and seating of the implant was carried out to the best ability based on the instructions provided for the implant. The seating of the implant was in the cancellous bed that had stiffer properties just under the calcar regions of the femur, explaining the formation of bone in the region.

Although the prediction of ingrowth around the Proxima was consistent with clinical data, the study as its limitations. Primarily, the role of biological factors is not modelled in the study due to the lack of literature on local cellular activity. In addition, the number of muscles included was based on simplified data and only peak forces for normal walking and stair climbing were included. An accurate model for simulating the post operative healing period would have to include different points in the gait cycle for each of these activities in addition to more muscle forces. It would also be highly beneficial to add a temporal, time dependent aspect to the algorithm and simulations. Moreover, the influence of micromotion is not studied due to an interfacial tissue layer being modelled. Micromotion as a tool to regulate or determine tissue differentiation at the interface would be pertinent if there was a direct contact model between the implant and the surrounding bone, which is not the scenario being modelled in the study. Due to the presence of the compliant tissue layer between the implant and bone, micromotion values obtained would not be an accurate representation of the behaviour of the implant with the surrounding bone.

Notwithstanding the above issues, the present model has predicted bone formation mainly in the regions under the lateral flare. The corroboration with clinical data available on the implant is encouraging and suggests that the proposed model could form a suitable basis for more advanced models. The proximal part of the implant was largely covered with fibrous tissue throughout the process and at tissue stabilization. Bone formation was restricted to the distal regions under the flare and would suggest that this particular design aspect plays a large role in regulating bone formation in the region. To investigate if this is indeed the case, additional studies on a similar design without the lateral flare would be necessary. A comparative study of the Proxima with and without the flare is presented in the next section, (section 4.6). Since bone formation was rapid, and seen even during the initial stages, this could mean that the implant is stabilized early by the formation of bone and cartilage at the distal and mid regions around the implant. Although proximal regions of the implant appear not be osseointegrated, the distal fixation obtained could still provide enough stability to the implant and prevent implant migration and subsidence.

4.6 INFLUENCE OF THE LATERAL FLARE ON TISSUE DIFFERENTIATION

4.6.1 INTRODUCTION

Conventional uncemented implants have typically relied on long stemmed, diaphysis engaging designs that have had a number of concerns associated with their use. For example, thigh pain [134], subsidence, aseptic loosening [244] and insufficient proximal loading, leading to proximal bone atrophy due to stress shielding that can have adverse effects on the long term stability of the implant [74]. Recent uncemented implant designs have attempted to address these issues; one such design improvement has been the inclusion of the lateral flare that seeks to load the proximal femur better than conventional uncemented implants The traditional Koch model of the mechanics of the hip loading associated tensile forces on the superior neck and proximal lateral three quarters of the femoral shaft, and compressive forces on the distal lateral and entire medial femoral surfaces [240]. The inclusion of a lateral flare that rests on the metaphyseal region of the femur has developed from an updated biomechanical model developed by Fetto et al. [241] that also includes soft tissue influences on femoral loading. The inclusion of the ilio-tibial band and the gluteus medius-vastus lateralis complex as dynamic tension bands along the lateral aspect of the lower limb subjects the lateral femur to compressive rather than tensile forces during unilateral stance. If this is indeed the case, the femoral component would have to be designed to load the lateral side of the femur in addition to the medial side in the metaphyseal regions.

The incorporation of a lateral flare feature designed to load the lateral cortex, below the greater trochanter of the metaphysis, could assist transmission of loads to the proximal femur by plugging the region, providing more stability and minimising distal stress transfer [245]. The presence of the lateral flare on the implant has also been shown to produce strains close to anatomic strains in the femur [246]. Some of the more recently developed implants that have used the lateral flare and have shown promising short term results in terms of stability with minimal migration and subsidence have been the Proxima, IPS, Revelation, and FMS anatomic stems [237,238,247].

Although the short term results obtained from implants with this specific design feature suggest that stability and proximal loading is indeed better than implants without the flare, there have not been any computational studies investigating if the presence of the lateral flare alters tissue differentiation at the interface and if there is any benefit of incorporating the flare specifically for osseointegration. In the absence of any long term clinical data for these implants, computational methods can be employed to predict the biomechanical response to this implant. In the current study, the short stemmed Proxima implant, described in the previous chapter, is considered. The implant has been investigated for changes in tissue differentiation if the prominent lateral flare that it employs for stability and proximal femur loading is absent.

4.6.2 AIM

The study aims to investigate the influence of the lateral flare feature on tissue differentiation around the short stemmed Proxima implant. To achieve this, the tissue response to the flared implant is compared to that of the same implant with a conventional straight lateral aspect.

4.6.3 METHODOLOGY

The steps involved in simulating tissue differentiation for the non flared Proxima was similar to those described for the conventional one, explained in detail in section 4.3. The most significant difference in the model creation process for the non flared Proxima was the removal of the lateral flare. This was carried out through solid model operations in Rhinoceros (Robert McNeel & associates, Seattle, USA), using a plane perpendicular to the lateral flare; splitting and removing the flare at the shoulder level of the implant. This resulted in a shape that conventional uncemented implants employ, with a straight lateral side as shown in figure 4.17.

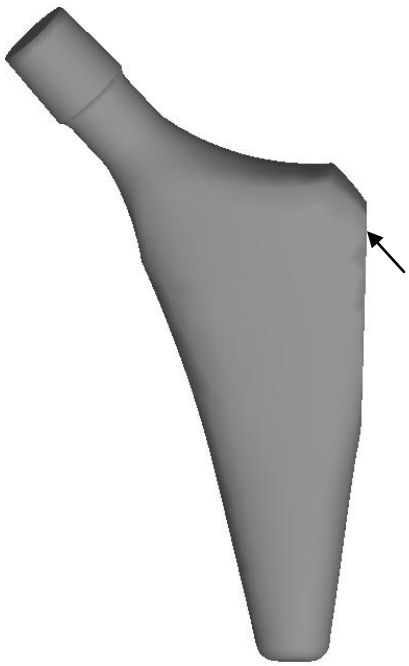

Figure 4.17: The Proxima implant without the lateral flare. Note the straight lateral aspect of the implant (arrowed).

After the non-flared Proxima was created, it was then implanted into the femur in the same or as close a position as the flared Proxima. This was carried out by maintaining the placement of the medial flare in both models. Other operations pertaining to implantation, for example, the femoral neck cut used and implant sizing were also kept the same as the flared Proxima. A tissue layer of thickness 0.750mm surrounding the implant was created through solid body operations similar to the previous study. The proximal femur used for the flared Proxima was used in the current study as well.

After the models were created, they were then meshed in Ansys ICEM (Ansys Inc, Canonsburg, PA, USA). Considering the only difference in the models was the absence of the lateral flare and to maintain similarity to the mesh used for the flared model, a mesh convergence study was not conducted. The models were meshed using the final element sizes used for the flared Proxima study, i.e. maximum and minimum values of 4 and 0.5 respectively. The finite element mesh of the implant with the surrounding tissue layer is shown in figure 4.18.

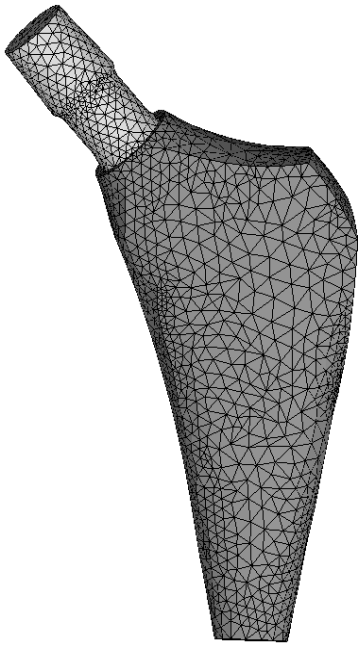

Figure 4.18: The finite element mesh of the implant and the surrounding tissue layer.

The finite element meshes were then exported to Ansys (Ansys Inc, Canonsburg, PA, USA) for implementation of the modified algorithm explained in chapter 3. However, for the current study, only method 2 was employed as it provided more detailed tissue formation around the implant. The value of K, loading and boundary conditions remained the same as that described in the previous chapter and the algorithm was carried out using the same termination criteria defined for the original study. Material properties assigned to the individual components were kept the same with CT derived material properties used for the proximal femur. Tissue differentiation through the iterations was monitored until stabilisation and the results obtained were compared to those obtained for the flared Proxima.

4.6.4 RESULTS

In the absence of a flare, there was more fibrous tissue and less bone formation through all of the iterations around the implant. Bone formation was very slow as the iterations progressed and was sparse around the implant. Even at the start of the iterations, tissue conversion to cartilage and bone was limited compared to the flared model. Figure 4.19 shows the early tissue formation for both models (5 iterations). Although bone formation had not commenced in either case, it is clear that the formation of cartilage is more prominent and visible in the flared Proxima. The tissue accounted for around 25% as opposed to only 10% formation for the non flared Proxima. For the non flared Proxima, the location of the cartilage tissue formed was restricted to the distal postero-medial side.

In sharp contrast, for the flared Proxima, cartilage tissue formation was also seen in the distal posterior and antero-medial and lateral sides of the tissue layer. The regions corresponding to the flare and immediately under the flare were still mostly populated with fibrous tissue in both cases. Fibrous tissue occupied more of the tissue space when the flare was absent, (around 90%) when compared to the flared Proxima, which had only 75% of the tissue space occupied by fibrous tissue.

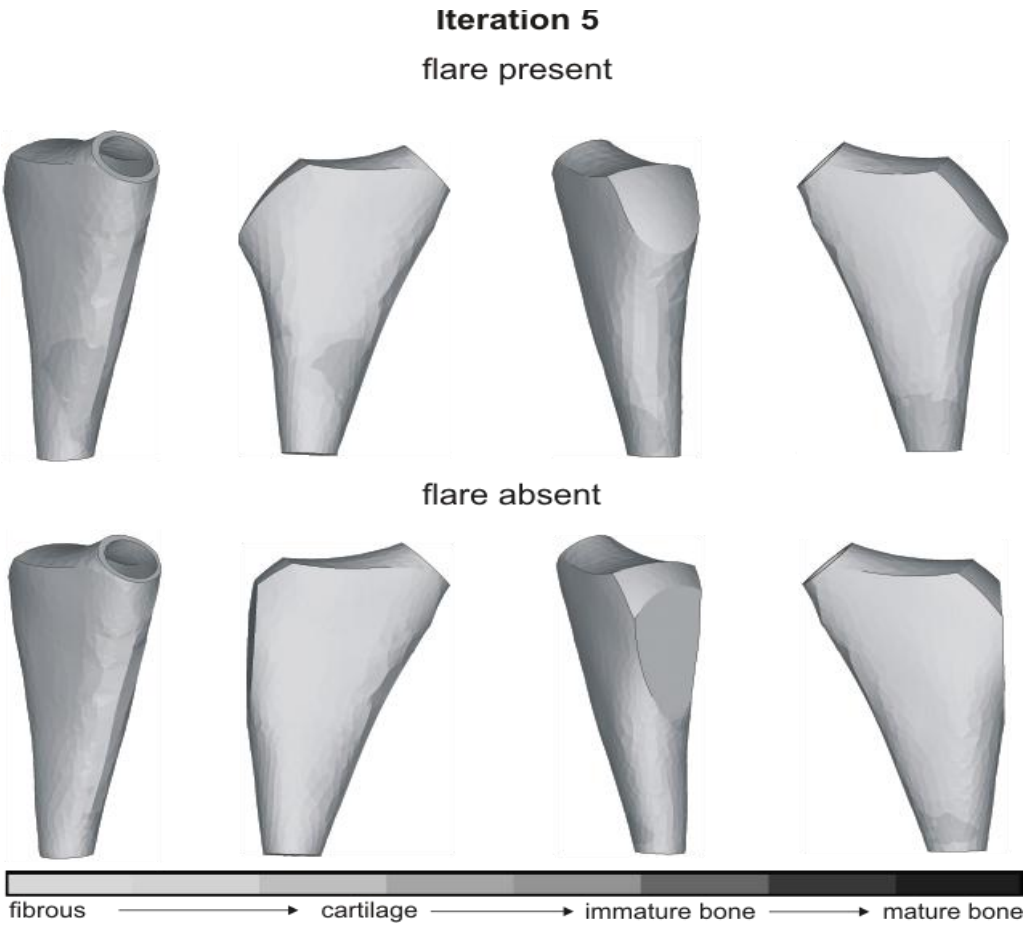

Figure 4.19: Comparison of the tissues formed after 5 iterations for both models.

As tissue differentiation proceeded, more cartilage and immature bone formation was seen for both models. After 10 iterations, as seen in figure 4.20, cartilage formation was prominent in the distal

regions of the implant. However, immature bone formation was very limited and was not as pronounced when compared to the flared Proxima. The flared Proxima also showed immature bone and early stages of mature bone formation in regions directly under the flare which was absent for the non flared Proxima. The distal aspects of the flared Proxima were found to be already stabilized through the formation of immature bone whereas cartilage tissue occupied the same regions for the non flared Proxima. A common observation for both models was that fibrous tissue began to recede and reduce in percentage, but was more pronounced for the flared Proxima. Cartilage tissue was also slowly replaced by immature bone tissue at this stage and observed in both models.

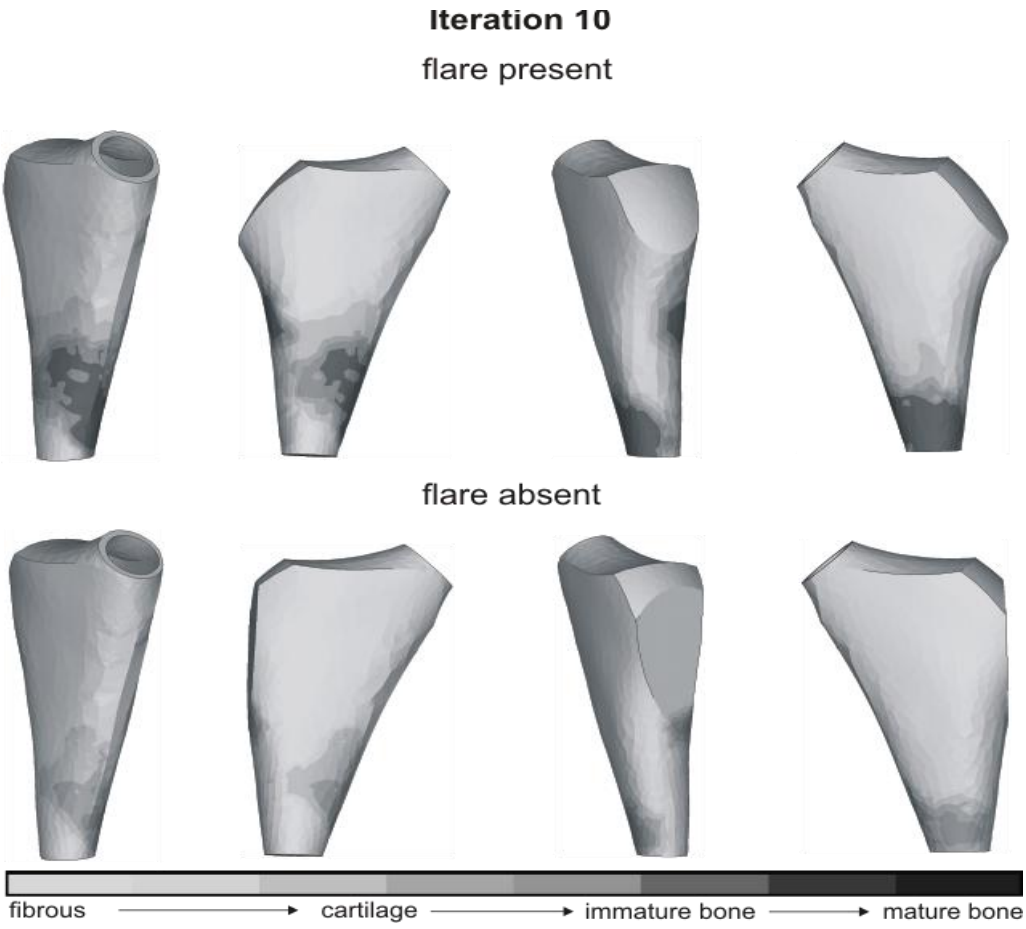

Figure 4.20: Comparison of the tissues formed after 10 iterations for both models.

The most notable difference in tissue formation was found at tissue stabilization. Although there was mature bone formation even without the lateral flare present, it was significantly less than the flared Proxima. Figure 4.21 shows both the models at stabilization. The model predicted around 10% more mature bone formation with the flare present, which could influence the stability of the implant. Regarding specific regions of immature and mature bone formation, the postero-medial and posterior aspect around the implant had more bone formation compared to the anterior side. However, overall bone formation was less than that observed for the flared Proxima. The difference between the two models was most notable in regions directly under where the flare would be

located, with very little bone formation. This was in sharp contrast to the results obtained for the flared Proxima. Cartilage was almost entirely replaced by bone at stabilisation for both models and there was also a corresponding decrease in fibrous tissue overall to stabilize at 59% and 70% for the flared and non flared models respectively.

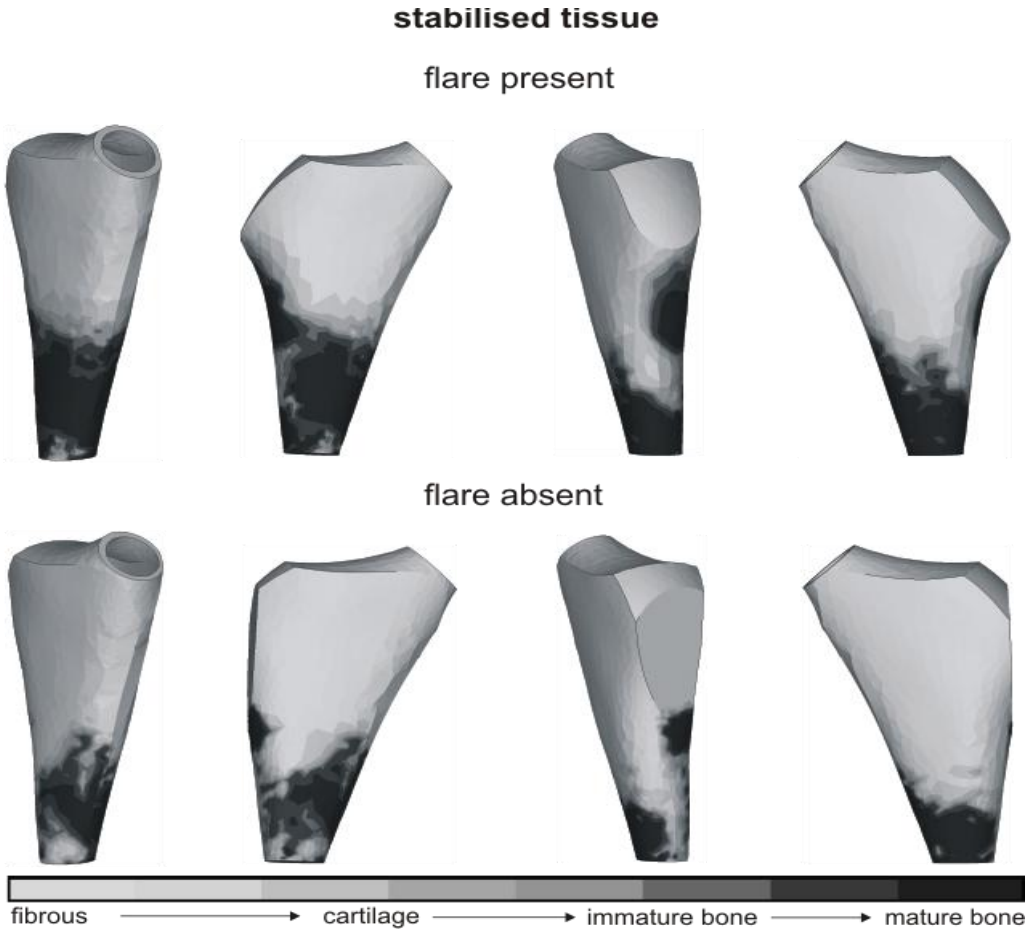

Figure 4.21: Comparison of the tissues formed at stabilisation for both models.

The overall percentage decrease and increase of the three main tissue types, fibrous tissue, cartilage and mature bone, obtained by combining values of the mapped regions (for example, immature and mature bone was combined for an overall bone percentage), formed at various stages is shown in figure 4.22 for each of the models. There was a decrease in fibrous and cartilage tissue formation with a corresponding increase in immature and mature bone formation observed for both models.

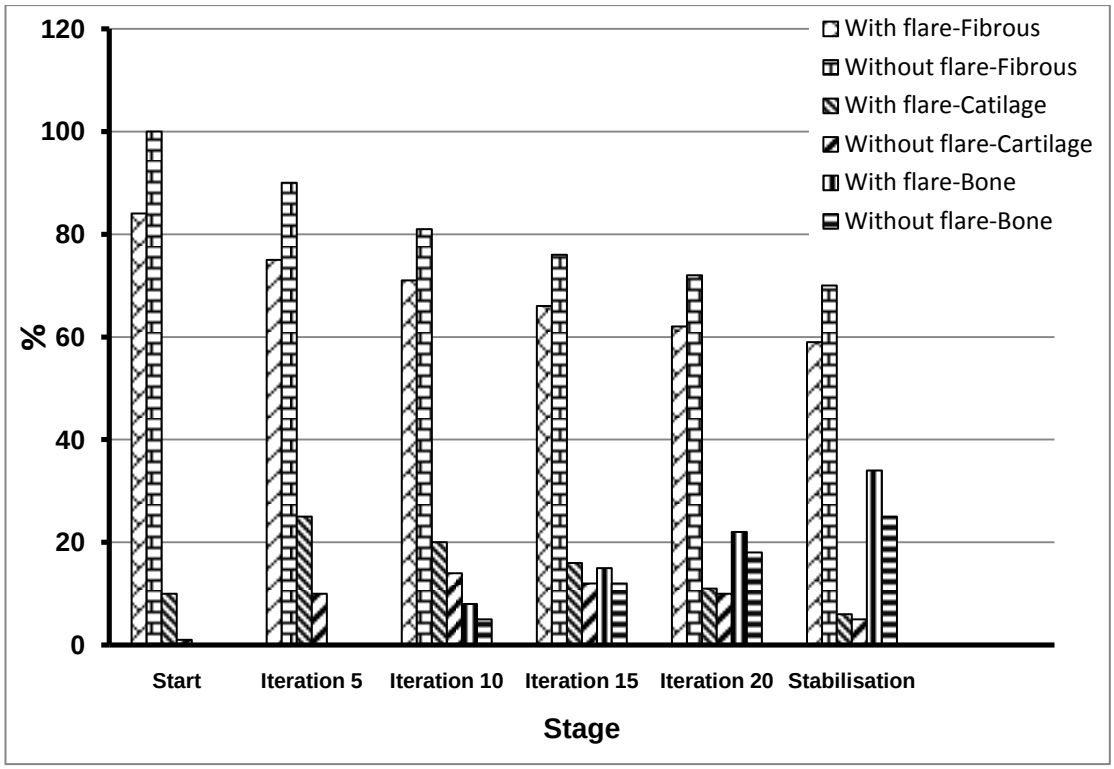

Figure 4.22: The percentage of the three main tissue types formed, fibrous, cartilage and bone at various stages proceeding to stabilisation.

The influence of the lateral flare in regulating the formation of stronger tissues can be exemplified further by investigating the change in tissue stiffness with and without the flare. Although formation of different tissues is not consistent across the implant, with sporadic and often patchy formation of bone tissue, Figure 4.23 shows the change in tissue stiffness in three specific locations located on or directly under the flare for both models. Location a, on the lateral flare is shown to slowly ossify as iterations progress; in contrast, without the flare this region is covered with fibrous tissue throughout. There is a steady change in tissue type which is absent with no flare present.

At location b, situated directly under the flare, there is steady progress towards mature bone formation for both models. However, there is a delay in the onset of stronger tissues, for example, cartilage and bone formation for the model without the flare. With the flare present, the increase in tissue stiffness is more rapid, and stabilisation through bone formation occurs faster. At location c, which is at the distal end of the implant, a similar trend is observed. There is a gradual transition through intermediate tissue types leading to the stiffness corresponding to mature bone. Although bone tissue stiffness is reached at stabilisation in both cases, there is a marked increase in tissue stiffness with the flare present, with stiffness increasing quicker through the iterations. Peak value of mature bone is also achieved faster in this case, just past the 20th iteration which is quicker than the model without the flare.

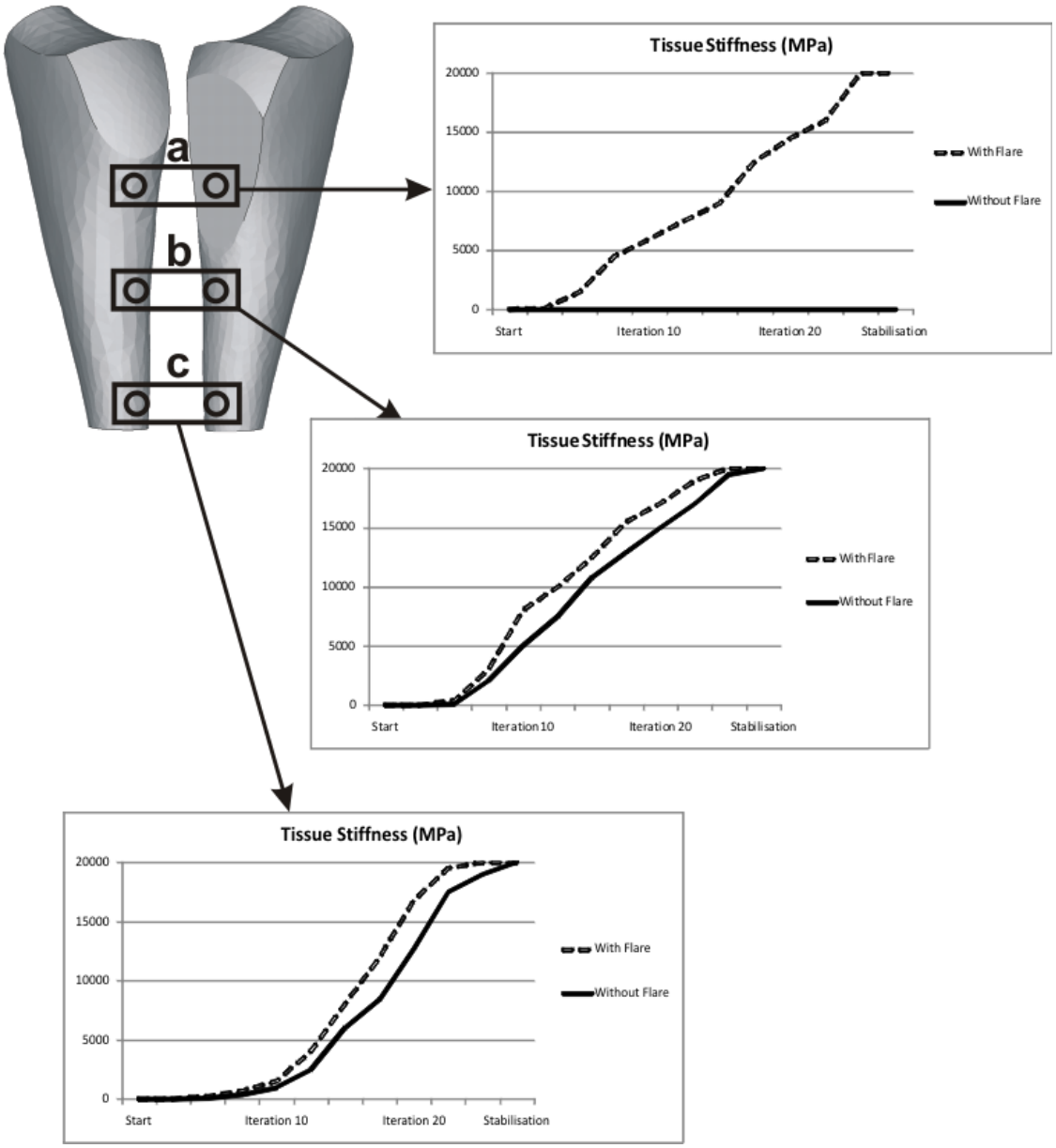

Figure 4.23: The change in tissue stiffness across three specific locations a, b, c located on or under the flare for both models.

4.6.5 DISCUSSION

The inclusion of the prominent lateral flare in uncemented hip implants has been a recent and novel design improvement to load the proximal femur by use of the large medial lateral taper on the infero-lateral part of the greater trochanter. The shape also provides to provide a good "rest fit" that minimises axial and torsional instability [237]. Retrieval and clinical studies on the flared Proxima have been limited and to the author's knowledge, there have not been any studies that have assessed the implications of incorporating the flare in the Proxima design. The current study

has aimed to distinguish tissue formation around the implant with and without the prominent lateral flare through the use of the algorithm described previously.

The predicted results have shown that there is indeed a marked difference in bone formation around the implant when the flare is present, especially in regions directly under the flare. This is perhaps due to the shielding effect the lateral flare provides, limiting regions under it from high stresses that in turn lead to more stable tissue formation. This has also been previously shown in literature, for short stemmed and conventional lateral flared implants, where there is endosteal bone formation in the aforementioned regions [132,248]. The flared shape helps transfer the load to the lateral and medial regions around the greater trochanter and this has been also been shown in literature, with an increase in bone mineral density in regions beneath the flare [249], all of which correlate well with the results of the current study.

Although there have not been any experimental or clinical studies carried out comparing the Proxima with and without the flare, other studies with lateral flared implants have shown that the flare also minimizes stress and strain on the proximal femur when compared to non flared implants and the strain distribution also matches that of an intact femur closely [246]. Considering the algorithm used relies mainly on stress components, this agrees well with the predicted tissue formation for both models, with bone formation for the flared Proxima exceeding that of the non flared Proxima. Another parameter that can also be used to justify the results in favour of inclusion of the flare is micromotion. Although not explicitly simulated in the current study, literature has shown that incorporating the flare minimises micromotion, migration and subsidence [248]. The predicted results correlate very well this, with the flared Proxima demonstrating more bone formation and less fibrous tissue covering the implant when compared to the non flared Proxima.

The results also show that it is not just the grosser formation of stronger tissues that reinforces the importance of the lateral flare, but also the rate of formation of these tissues. The flared Proxima has been shown to predict faster formation of bone around the implant, which could help strengthen the interface very early and provide more stability early on. The flare may be a contentious choice to employ along with a diaphyseal fillings stem in a long stemmed implant but it's applicability for a short stemmed implants could be vital; employing the dual role of loading the proximal femur and maintaining axial and torsional stability at the same time. In the absence of biological factors and considering mechanical stimuli alone, the predicted results of the study suggests that the use of a prominent lateral flare in addition to the medial flare that normal implant designs incorporate improves bone formation and minimizes fibrous tissue formation around the implant.

To summarize, short stemmed uncemented implants for hip replacement are a recent and novel development recommended for young patients requiring hip arthroplasty. The preservation of bone stock and the less invasive surgery required for implantation is an attractive option for surgeons and patients alike. Considering the growing interest in these implants, the unknowns

associated with osseointegration, stress shielding and associated long term behaviour, along with timescales and the expense involved with clinical trials, it would be useful to predict implant behaviour through computational models. Notwithstanding the limitations with such an approach, such models could provide a useful basis for further design iterations.

CHAPTER 5

EFFECT OF THE POROUS COATING GEOMETRY ON TISSUE DIFFERENTIATION IN A CONVENTIONAL LONG STEMMED IMPLANT

The research carried out in this chapter has been presented in part in the following conference papers:

- *Puthumanapully P.K., Browne M. (2009)* ***"Predicting bone ingrowth and tissue differentiation around a long stemmed porous coated hip implant using fracture healing principles"*** *Proceedings of the 22nd Annual Congress of International Society for Technology in Arthroplasty (ISTA)*

- *Puthumanapully P.K., New A.M., Browne M. (2010)* ***"Design influences of a short-stemmed and long-stemmed uncemented implant on tissue differentiation at the interface: A computational study based on a mechanoregulatory hypothesis"*** *Proceedings of the 9th international symposium of computer methods in biomechanics and biomedical engineering (CMBBE).*

5.1 INTRODUCTION

Uncemented implants have come into prominence from the 1970's with many designs used to substitute cemented implants due to associated problems of using bone cement such as osteolysis, described in detail in chapter 2. These implants employ porous coated surfaces to encourage bone ingrowth, securing and providing biological fixation. The design of these implants has been varied, with changes in stem shape, size and extent of coating employed. One of the most clinically successful implants developed during the late 1970's, and one which continues to enjoy excellent survivorship even today, is the anatomic medullary locking prosthesis, also known as the AML [250]. The AML, first introduced in 1977, is commercially manufactured by DePuy Orthopaedics (Warsaw, Indiana, US). It was developed by Charles Engh Sr based on the Moore implant and the first of its kind to offer biological fixation [251]. The implant is forged and made from Co-Cr alloy. The AML employs a design rationale of diaphyseal fixation by "fitting and filling" the diaphysis. One of the implant's main strength has been its simple, easily reproducible design. The AML has a straight lateral side, with the medial side contoured to the calcar regions for a good proximal fit. The proximal regions of the implant have an almost rectangular cross section that becomes rounded at the diaphysis for a tight distal fit. In addition, the easy union of the cylindrical parallel sided femoral diaphysis with the implant through the use of cylindrical reamers also ensures excellent canal fill, leading to good initial stability. This core design of the implant has remained the same for the last three decades[174] with only minor modifications such as head size, offset, taper, modular heads and use of the collar. The AML has also been marketed under other names such as the Prodigy and Solution stems which incorporate changes in implant anteversion or stem length respectively. These changes have been justified by the excellent clinical success and the need to cater to a wider patient population. In a recent follow up of 223 total hip replacements with the AML, only 2% loosening was observed at 20 years[252]. The implant has also recorded survivorships of up to 99% at 14 years [250] with comparable survivorship data obtained for shorter follow up periods [253,254] as well.

The implant has been studied extensively with regular follow up periods to offer a panoptic view on the functioning of the implant in terms of the influence of various design factors, longevity and problems associated with its use. One design parameter that has been investigated is the extent of the sintered beaded coating that the implant employs for biological fixation. In its current form, the implant can be categorised as being extensively or fully porous coated and uses a bullet shaped non coated distal end to avoid impingement with the endosteum (see figure 5.1). However, this has not always been the case and the porous coating used has been applied in varying extents over the implant surface through the years, accompanied by minor shape and design changes in stem diameter [174,251,255]. Some of the different versions of the AML with varied porous coated areas are shown in figure 5.2.

Figure 5.1: The AML implant with its extensive porous coated surface, in deployment since the late 1990's.

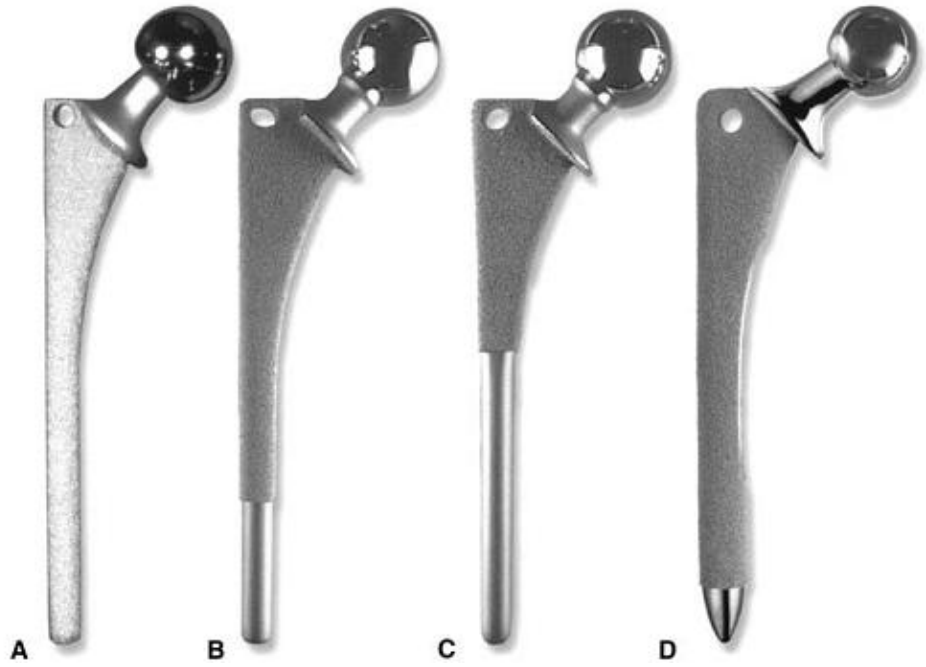

Figure 5.2: Porous coatings on the AML, (A) fully coated (B) 4/5 coated (C) 1/3 coated (D) fully coated AML marketed as Prodigy stem incorporating implant anteversion [174].

The implant was fully coated when it was first introduced but problems associated with proximal stress shielding led to modifications on the extent of porous coating. It was believed that the

inherent bulkiness, along with the full porous coating could compromise stress transfer to the proximal regions of the implant [75]. To eliminate this problem, the proximally 1/3 coated AML was introduced in the 1980's. The implant saw a sudden rise in popularity in 1985 before its eventual decline in the 1990's, primarily used in younger patients with good bone stock [174]. The results obtained from the aforementioned comparative study graded on survivorship, stress shielding, pain and overall satisfaction indicated that both versions performed well clinically. The outcomes for both versions of the implant were comparable with only a slight advantage for the fully coated stems with longer survivorship and reduced loosening. A further study has looked at the mean density of bone ingrowth for the proximal coated and fully coated implant; results were comparable [167] with slightly better ingrowth observed around the fully coated implant. The reason behind the decline of the proximally coated version could be that the stability obtained by bone ingrowth over the shaft of the stem surmounted the possible instability that could result from stress shielding proximally. In view of comparable results, the fully coated version was preferred. Retrieval and cadaveric studies of the AML has demonstrated this, with very low levels of micromotion recorded for fully coated implants [10].

The current version of the AML has undergone a small change in stem design compared to the older versions with the use of a more rounded stem and a larger diameter distal end. The current version is also fully coated with only the distal tip free of the coating. There have been no AML designs currently that have been coated just proximally or to any other length along the stem. One of the key concerns with the performance of the AML, as described in a study by Charles Engh [253], has been bone ingrowth along the stem and to identify and quantify regions of bone ingrowth along with their distribution. The current study aims to determine if the fully coated AML is best for osseointegration or if reducing the porous coating to the proximal regions can give comparable, if not better results.

5.2 AIM

To investigate the effect of the extent of porous coating on tissue differentiation around the traditional and clinically successful long stemmed implant, the AML. This is carried out by comparing and contrasting three different porous coated versions of the implant; the fully coated, 3/4 coated, and the proximal 1/3 coated. By considering these different lengths and their effect on tissue differentiation and bone ingrowth around the coating, the rationale for the current coating length can be justified and/or a better coating length can be determined.

5.3 METHODOLOGY

The technique used to simulate tissue differentiation around the AML for all three models was identical to that used for the short stemmed implant study in chapter 4. Finite element models of the implant and surrounding bone were combined with the mechanoregulatory algorithm described in detail in chapter 3. For this study, only method 2 of the algorithm was employed for

comparison, due to its ability to predict more detailed tissue formation. The individual steps involved are described below.

5.3.1 GEOMETRIC AND FINITE ELEMENT MODELS

Macroscale modelling of the tissue differentiation around the three implant models was carried out in several steps. The first step involved creating geometries and components to be used in the study. The main components: geometries of the femur, the implants and the tissue layer at the interface were either obtained from existing files or reconstructed from CT scans.

5.3.1.1 THE AML IMPLANT

The geometry and solid model of the implant was obtained from DePuy (DePuy International, Leeds, UK) and scaled for size to fit the femur used in the study. The solid model of the AML is shown in figure 5.3.

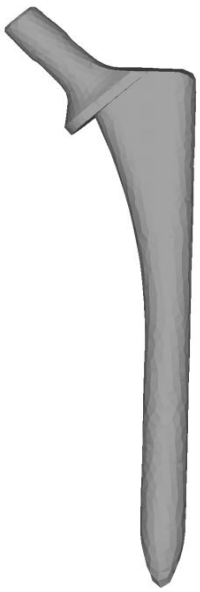

Figure 5.3: Solid model of the AML used in the study.

The sintered beaded porous coating was not modeled explicitly, due to the large computational expense it would warrant. Moreover, the focus of the study was to simulate tissue differentiation around specific lengths around the implant, where the porous coating would normally be present. This would not require the coating to be modelled separately and simulations can be carried out by modeling a tissue layer in those specific areas. Details of the tissue layer and its construction for the three models are described in the following sections.

5.3.1.2 TISSUE LAYER

The construction of the three models was carried out as follows. The first step was to identify regions where the tissue layer would be present. For the fully coated AML, the region below the collar and just above the bullet shaped distal tip was considered. For the 1/3 and 3/4 coated models, the length of the implant from the shoulder to just above the tip was determined; the two lengths were marked and considered for the tissue layer placement. The construction of the tissue layer was carried out by uniformly exploding the geometry of the implant by a value of 0.750mm in all directions. The original implant geometry was then subtracted from the newly created tissue block to produce a 0.750mm uniform hollow layer into which the implant could be fit without the formation of any gaps. The layer was then split at the 1/3 and 3/4 levels, and the unwanted regions deleted to leave the tissue layer surrounding the implant for all three models. The solid models of the three AML versions are shown in figure 5.4.

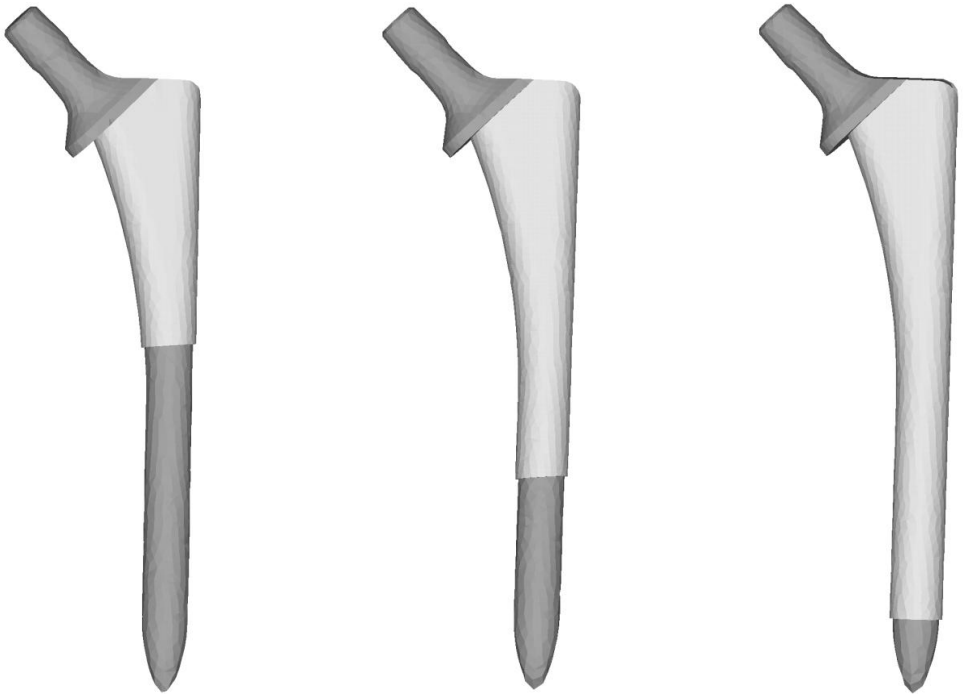

Figure 5.4: Solid models of the three AML models used in the study. Proximal 1/3 coated (left), 3/4 coated (centre) and extensively coated (right).

The thickness of the layer surrounding the implants was made on an assumption of the thickness of what would otherwise be a 3 layer porous coating of 250 micron diameter beads (Porocoat®, DePuy) that the AML normally employs and would be filled with granulation tissue. Even though the beads haven't been modelled in this case, this was considered to be a reasonable assumption as a start point. In addition, other studies have used a maximum thickness of 1mm for simulating the fibrous tissue layer surrounding the implant [177,235]. Granulation tissue is comparable to fibrous

tissue used in these studies and a 750 micron thick layer was also a conservative assumption based on this. Granulation tissue has been described in detail under the methodology section in chapter 3.

5.3.1.3 FEMUR

The femur geometry used for the study was the same as that used in chapter 4. However, with the implant size considerably larger than the Proxima, the length of the proximal femur was deemed to be insufficient. To this end, a parametric study was carried out to determine at what length the femur needed to be sectioned so as to not adversely affect bone strains. This was carried out through a single load of 1000 N applied to the implant, with boundary constraints on sectional cuts made on the femur every 20mm from the level of the tip of the implant. The femur length chosen (figure 5.5) was the minimum length from the set that produced the most consistent strains in the femur. The final length chosen was 120mm from the level of the tip of the implant as the maximum strains in the femur beyond this length varied less than 5% (see appendix D). Neither method 1 nor method 2 was employed for a comparative study on the change in the tissue layer as this step was carried out to solely determine the length of the femur to be employed for the long stemmed implant.

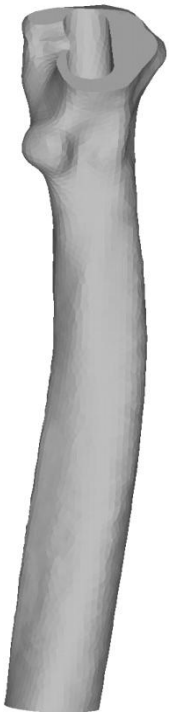

Figure 5.5: The proximal femur used in the study showing the osteotomy cut.

Implantation of all three models and the corresponding osteotomy on the femur was performed in the software Rhinoceros (Robert McNeel & associates, Seattle, USA). The osteotomy plane and seating of the implant in the created implant bed was kept as close as possible to actual surgical

procedures. The collar of the AML rested on the cut surface of the bone with contact established between the two surfaces as seen in figure 5.6. The implant models were oversized on construction and had to be scaled down to be of optimum fit in the femur; they were then compared to radiographs to ensure size and positioning were accurate. The final positioning of the implant was that of the stem filling the diaphysis in case of the fully coated implant, with smaller gaps present for the 1/3 and 3/4 coated models between the distal regions of the implant and the diaphyseal endosteum. There was excellent proximal contact for all three models, evidenced by the close fit conforming to the implant geometries in the endosteum of the femur.

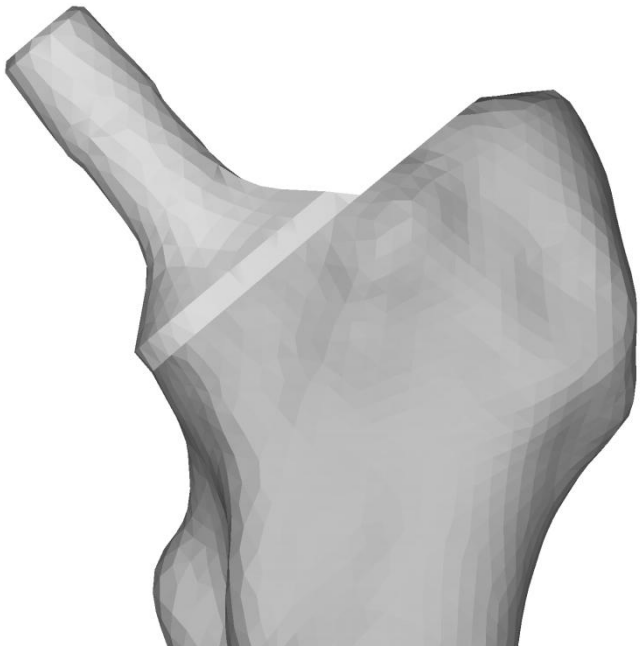

Figure 5.6: The collar of the AML for all three models rested on the cut surface of the bone as per surgical instructions. The surfaces were in contact with each other.

5.3.2 FINITE ELEMENT MESH

All of the constructed components were exported to Ansys ICEM CFD for meshing. They were checked for faults in geometry and subsequently repaired and meshed together. Mesh convergence studies were carried out in an identical way to those carried out in chapter 4, based on using the osteogenic index rather than stress or strain values for convergence checks. Element size to be used was determined by exploring different mesh configurations, and the resultant effect on the osteogenic index obtained after a single iteration of implementing the modified algorithm.

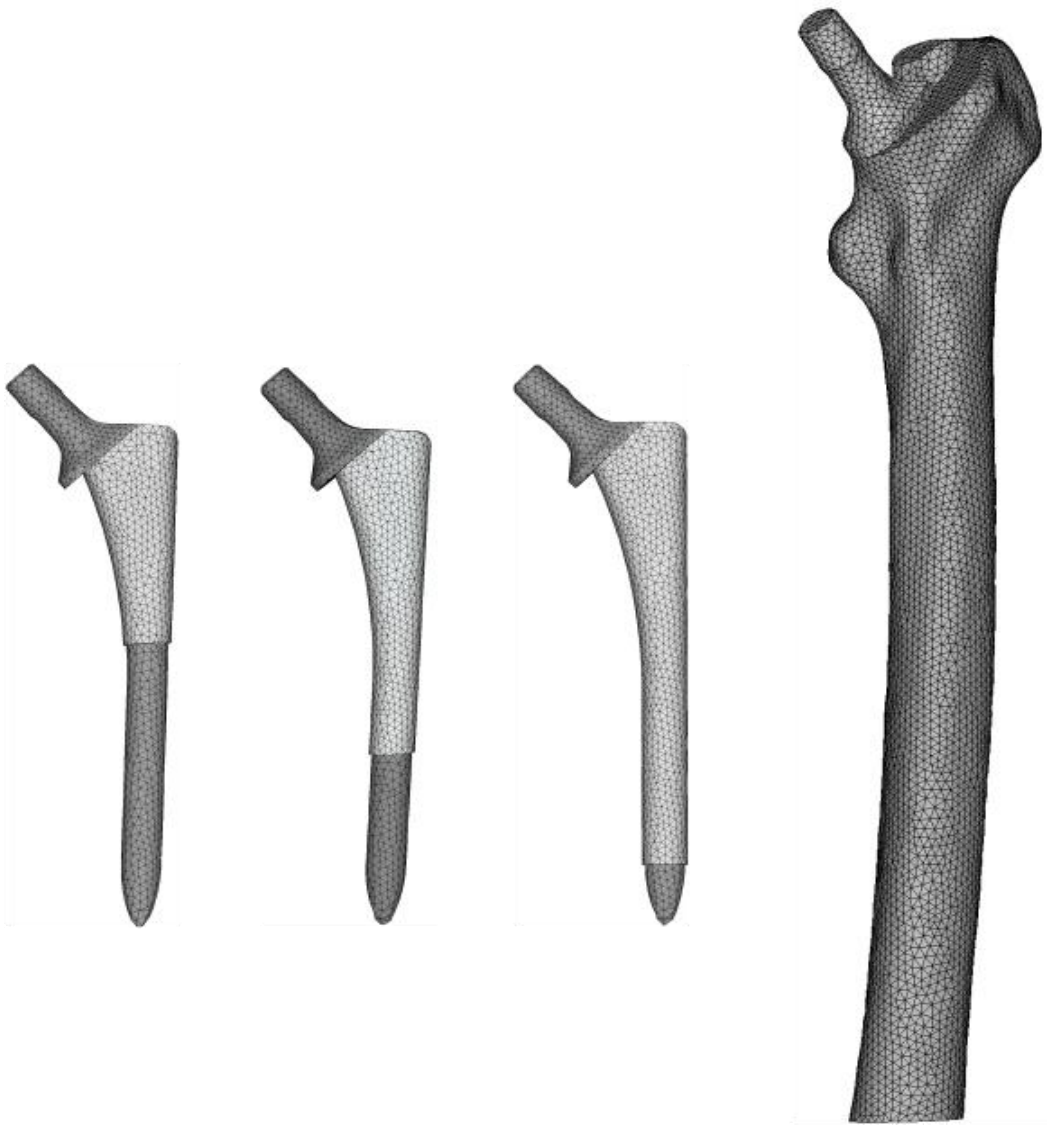

Figure 5.7: The finite element meshes of the three AML models and the implanted femur.

Different element sizes and mesh densities were investigated and a visual inspection of the regions of high and low osteogenic index was compared across the models, along with the respective computational times needed for the completion of ten iterations for the fully coated AML. The different combinations investigated with maximum and minimum sizes respectively were (1,0.5), (1,1), (2,0.5), (2,1), (2,2), (3,0.5), (3,1) and (4,0.5). The tissue patterns obtained for all aforementioned combinations, barring the 4, 0.5 were comparable but with differing computational times (see appendix E). Therefore it was decided to use the element size with a maximum and minimum size of 3mm and 0.5mm for the remainder of the simulations as it was the least computationally expensive, could accommodate the tissue thickness of 0.750mm and produced tissue differentiations patterns comparable to all other combinations used. Figure 5.7 shows the finite element meshes of the different components used in the study.

5.3.3 MATERIAL PROPERTIES

The material properties assigned to bone was element specific and the steps involved identical to those described in chapter 4. BONEMAT, described previously, was applied to map material properties from CT data to the individual elements based on the radiographic density. A standard Poisson's ratio of 0.3 was set for all the bone elements. A section of the femur showing the implant positioning in the stem and the elastic moduli assigned to the femur (in MPa) is shown in figure 5.8. As seen in the figure, the denser cortical bone surrounds the distal aspects of the implant with cancellous bone surrounding the proximal regions of the implants.

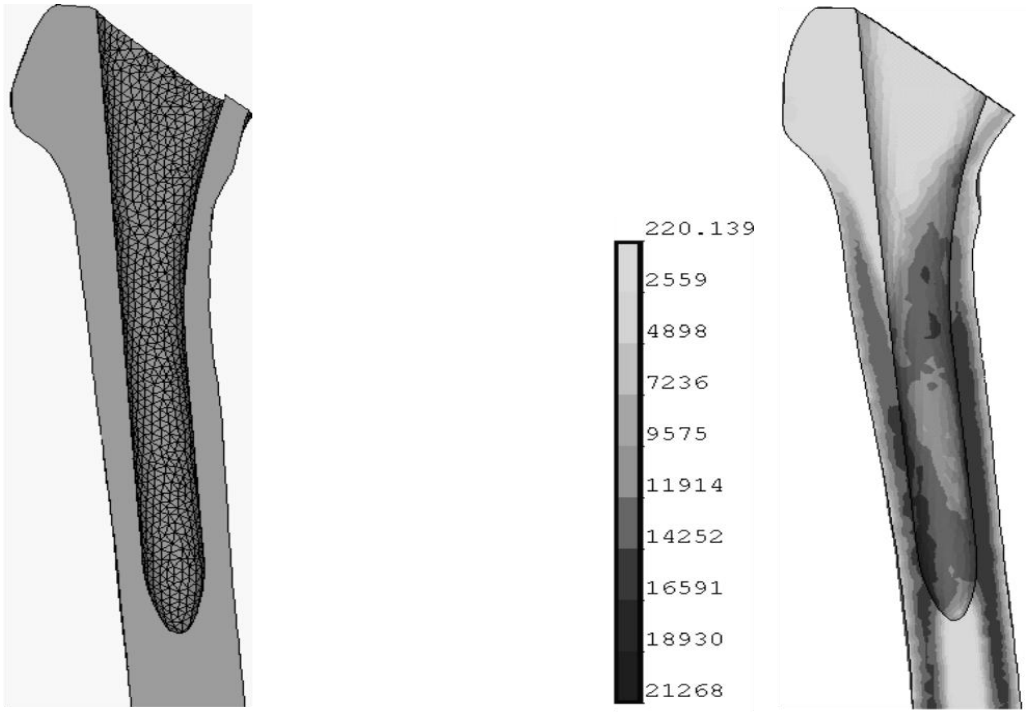

Figure 5.8: Sectional view showing the positioning of the AML in the femur (left) and the elastic modulus assigned to the femur (right). Modulus scale shown in MPa.

The AML implant is forged from Co-Cr alloy, so an elastic modulus of 220GPa and a Poisson's ration of 0.3 was assumed. The granulation tissue surrounding the implant was also assumed to be linear, elastic and isotropic. Granulation and other tissues surrounding the implant were assumed to be linear, elastic and isotropic in keeping with the literature [216-218] and as described in previous chapters.

5.3.4 BOUNDARY CONDITIONS AND LOADING

The muscle attachment and loading locations were similar to those employed for the Proxima study and described in detail in chapter 4. The distal part of the sectioned proximal femur was fully constrained in all directions. At the interface, the granulation tissue layer was assumed to be fully bonded to the implant and the bone. Loading and direction vectors of the muscle forces in the femur were based on the data reported by Bergmann et al [18]. Both normal walking loads and stair climbing loads were considered for an individual weighing 75 kilograms. Only the maximum contact force was applied as shown in figure 5.9 for both of the two load cases was used. Due to the use of the sectioned femur, rather than the entire femur in the simulation, none of the muscles attaching beyond the mid-distal femur were included. The forces were applied by selecting a group of nodes within a 3mm diameter patch around each specific attachment point and dividing the force equally among this set of nodes.

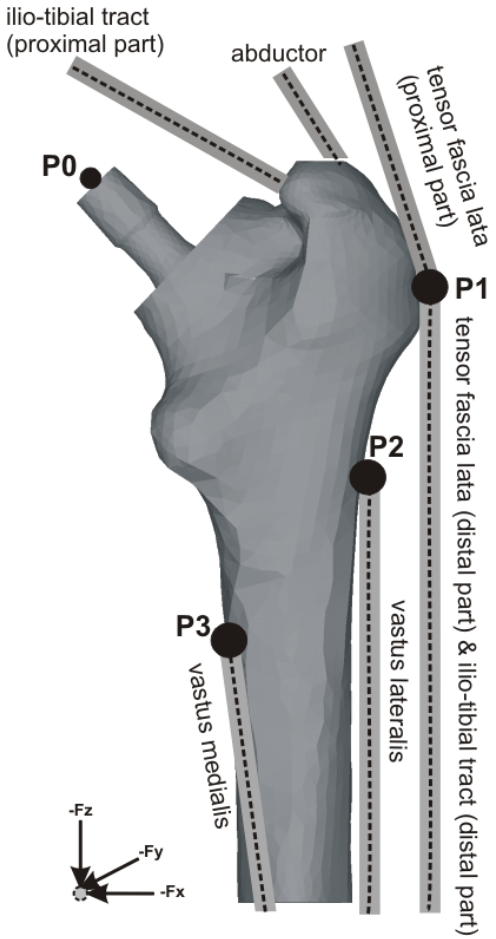

Normal walking - Maximum contact force				
Force [%BW]	**X**	**Y**	**Z**	**Acts at point**
hip contact	-54.0	-32.8	-229.2	P0
abductor	58.0	4.3	86.5	P1
tensor fascia lata (proximal part)	7.2	11.6	13.2	P1
tensor fascia lata (distal part)	-0.5	-0.7	-19.0	P1
vastus lateralis	-0.9	18.5	-92.9	P2

Stair climbing - Maximum torsional moment				
Force [%BW]	**X**	**Y**	**Z**	**Acts at point**
hip contact	-59.3	-60.6	-236.3	P0
abductor	70.1	28.8	84.9	P1
ilio-tibial tract (proximal part)	10.5	-3.0	12.8	P1
ilio-tibial tract (distal part)	-0.5	-0.8	-16.8	P1
tensor fascia lata (proximal part)	3.1	4.9	2.9	P1
tensor fascia lata (distal part)	-0.2	-0.3	-6.5	P1
vastus lateralis	-2.2	22.4	-135.1	P2
vastus medialis	-8.8	39.6	-267.1	P3

Figure 5.9: The muscles, along with their attachment points and their corresponding forces used in the study [18].

5.3.5 IMPLEMENTATION

For the overall implementation of the study, method 2 of the modified algorithm was employed. However, the value of 'K' to be used for the simulations needed to be determined. This was carried out through a parametric study for different K values (1, 1.5, 2, 2.5 and 3) and comparing it to clinical results reported in literature. A single load case of normal walking was run until tissue stabilization. Unlike the previous case for the Proxima implant in chapter 4, where literature on the implant was limited and a comparison to a similarly designed implant (the IPS) had to be carried out, the clinical history of the AML is well documented as described in the aforementioned introduction section. By comparing the results obtained for different K values with radiographic evidence found in literature, the value of K to be used for the remainder of the analyses could be found. Moreover, this would follow the original study by Carter et al., of comparison to clinical studies for the determination of K.

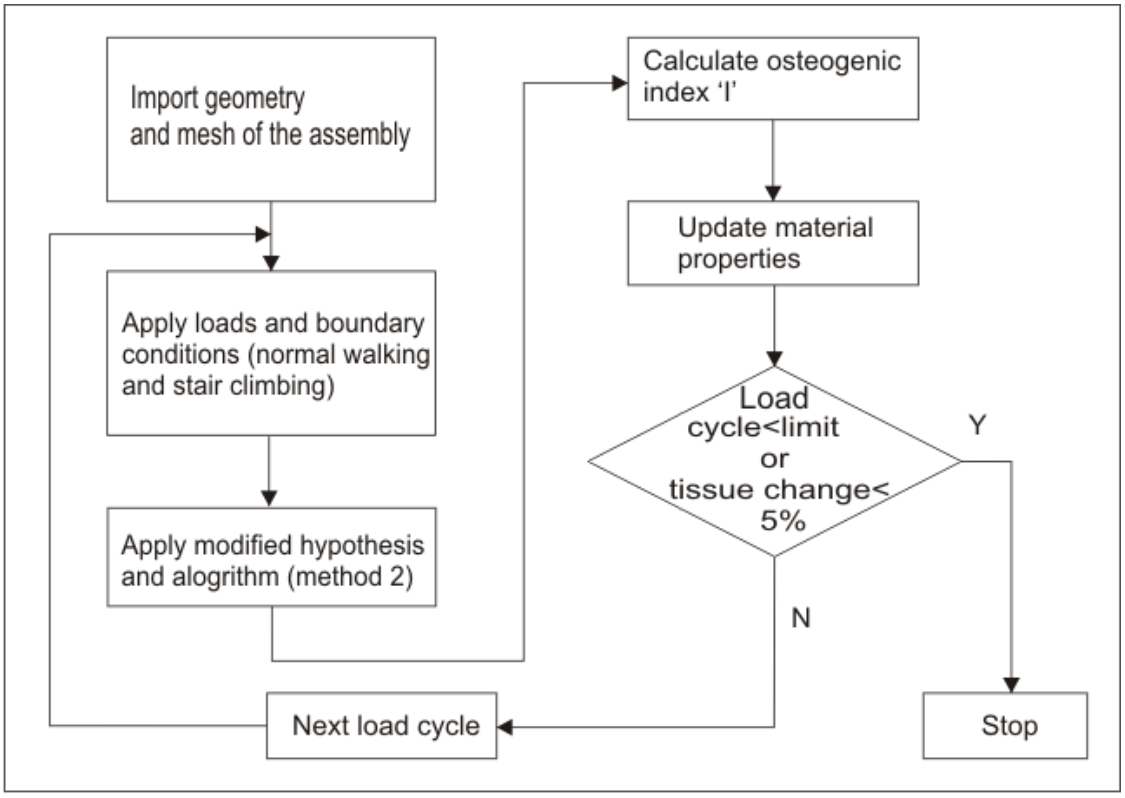

Figure 5.10: Flowchart describing the steps involved in the process of simulating tissue change in the interfacial layer.

However, even though it was decided to use method 2 for the study, method 1 was computationally faster of the two methods and gave gross formation of tissue around the implant. For the simple task of comparing the results to literature, this was found to be sufficient without the need for detailed tissue formation. Therefore method 1 was used to determine K, with method 2 employed for the actual study comparing the three different versions of the implant. Literature available on the more widely used fully coated implant was used for comparison for different values of K. The

flowchart of the steps involved in the process is shown in figure 5.10. The steps are the same as those implemented for the Proxima.

5.4 RESULTS

5.4.1 SELECTION OF K VALUE

The results obtained for values, K=1, 2 and 3 are shown in figure 5.11 .

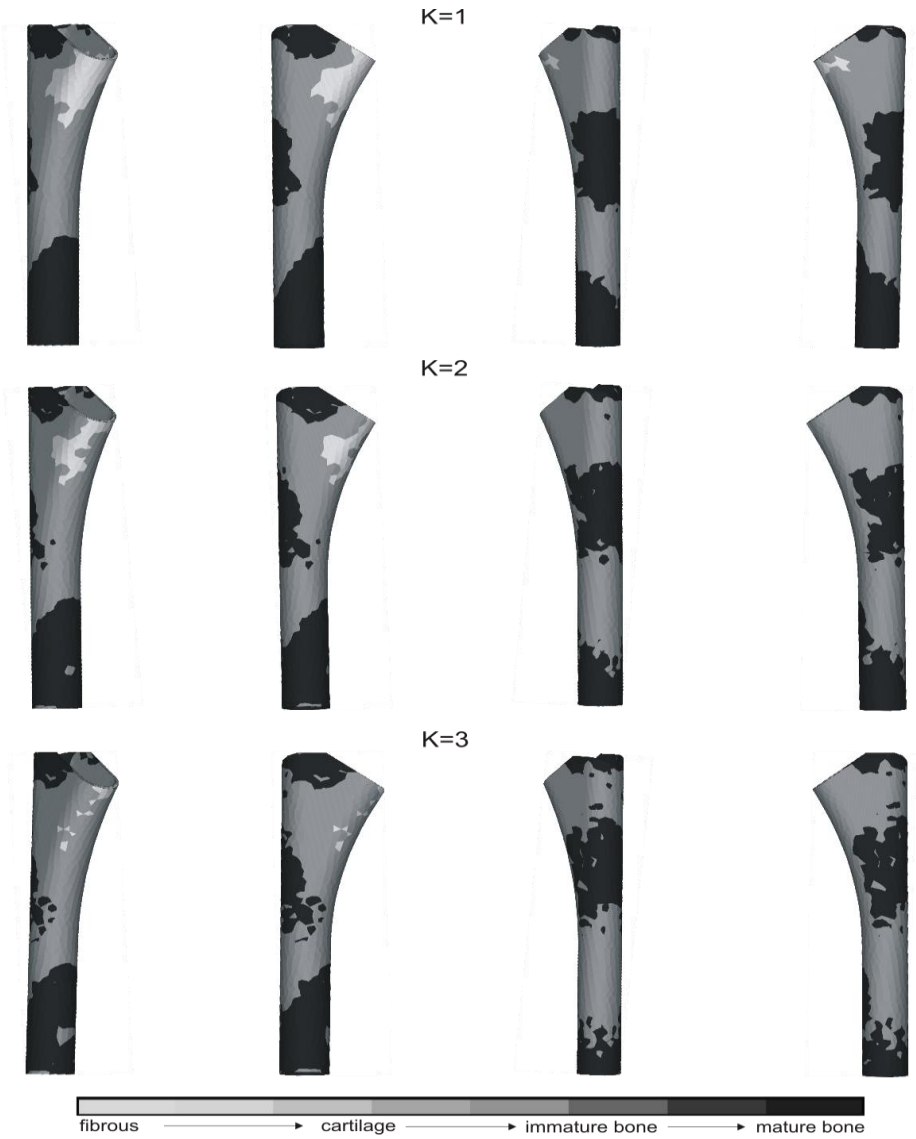

Figure 5.11: Tissue formation for different K values at stabilisation for a single load case of normal walking.

As seen in the figure, the formation of the individual tissue types was comparable in each case. There weren't any large deviations in the location and amount of tissues formed across the different K values, even for bone formation. This was found to be consistent with literature on the AML [10,167,172,174,225,251], with the formation of stronger tissues reported along the length of

the stem of the implant with fibrous tissue formation in the proximal regions. When tissue formation is compared across the models, it was found that K=1 gave the smoothest distribution of tissue around the implant with a maximum deviation of only ±6% for any particular tissue type formed across all values of K simulated. Considering the comparable distribution of tissues across all K values and their closeness to results seen in clinical and retrieval studies, the value of K=1 was chosen for the remainder of the simulations.

5.4.2 RESULTS FROM IMPLEMENTING METHOD 2

Tissue differentiation was successfully simulated around all three AML implants. The tissues formed at specific stages, from start to stabilisation for the three AML implants considered are shown in figures 5.12 - 5.17. The anterior, antero-lateral, posterior and postero-medial views are detailed. As expected, at the start of the iterations, the majority of tissue formed is fibrous (>90%) across all the models. This is seen extensively in the medial regions of the implant, occupying the proximal to mid-distal areas around the implant. The cartilage tissue formed in the case of the 1/3 and 3/4 coated implants is mainly located surrounding the distal aspects of the implant. Fibrous tissue percentage around the implants slowly decreases as the iterations progress and at iteration 5, cartilage tissue formation is more emphasised. This is observed predominantly for the 1/3 coated implant, with more cartilage formation compared to the 3/4 and the fully coated implants. In addition, there is no bone formation for any of the models at this stage. The various tissues formed, along with their locations are shown in figure 5.12 and figure 5.13.

As the iterations progress, the tissue begins to increase in stiffness. Although there is no mature bone formation at this stage, there is immature bone formation across the three models. This is clearly seen around iteration 10, where immature bone is evidenced for all three of the implants but in varying quantities. The 1/3 coated AML shows the most bone formation at this stage with over 30% of occupied space around the implant consisting of immature bone, in similar amounts to fibrous and cartilage tissue. There is little immature bone formation for the 3/4 and extensively coated implants with only 10% of bone tissue in the case of the latter. Cartilage and fibrous tissue formation is prominent, accounting for over 40% each of the tissue formed for the implant. The location of the immature bone formation is restricted to the distal aspects in all of the implants, gradually replacing cartilage tissue. However, the antero-lateral and lateral sides also show increased stiffness, indicating the trend to ossify as the iterations progress towards stabilisation as seen in figure 5.14 and figure 5.15.

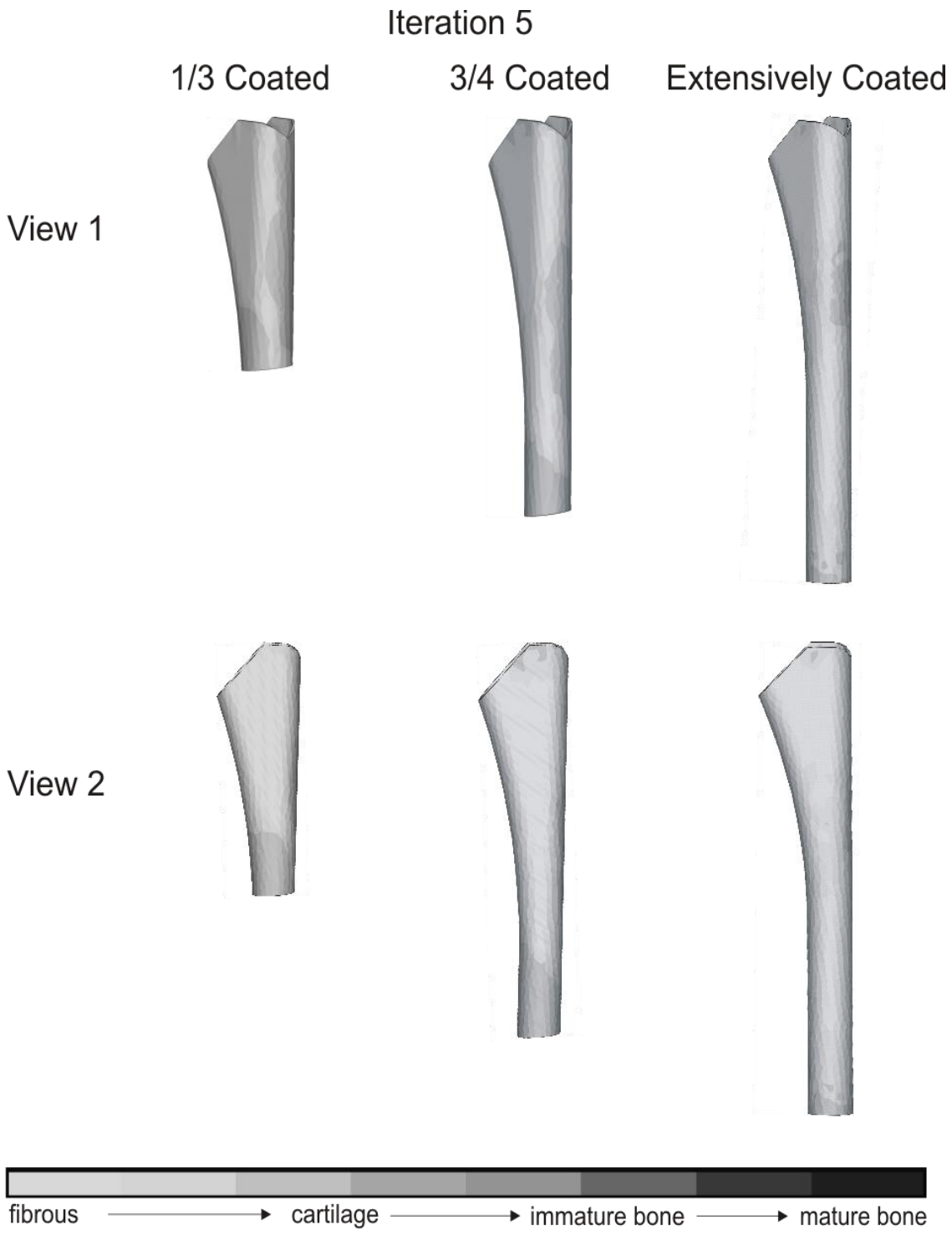

Figure 5.12: The antero-lateral (top) and anterior (bottom) views of the tissue surrounding the implant for the three AML models at iteration 5.

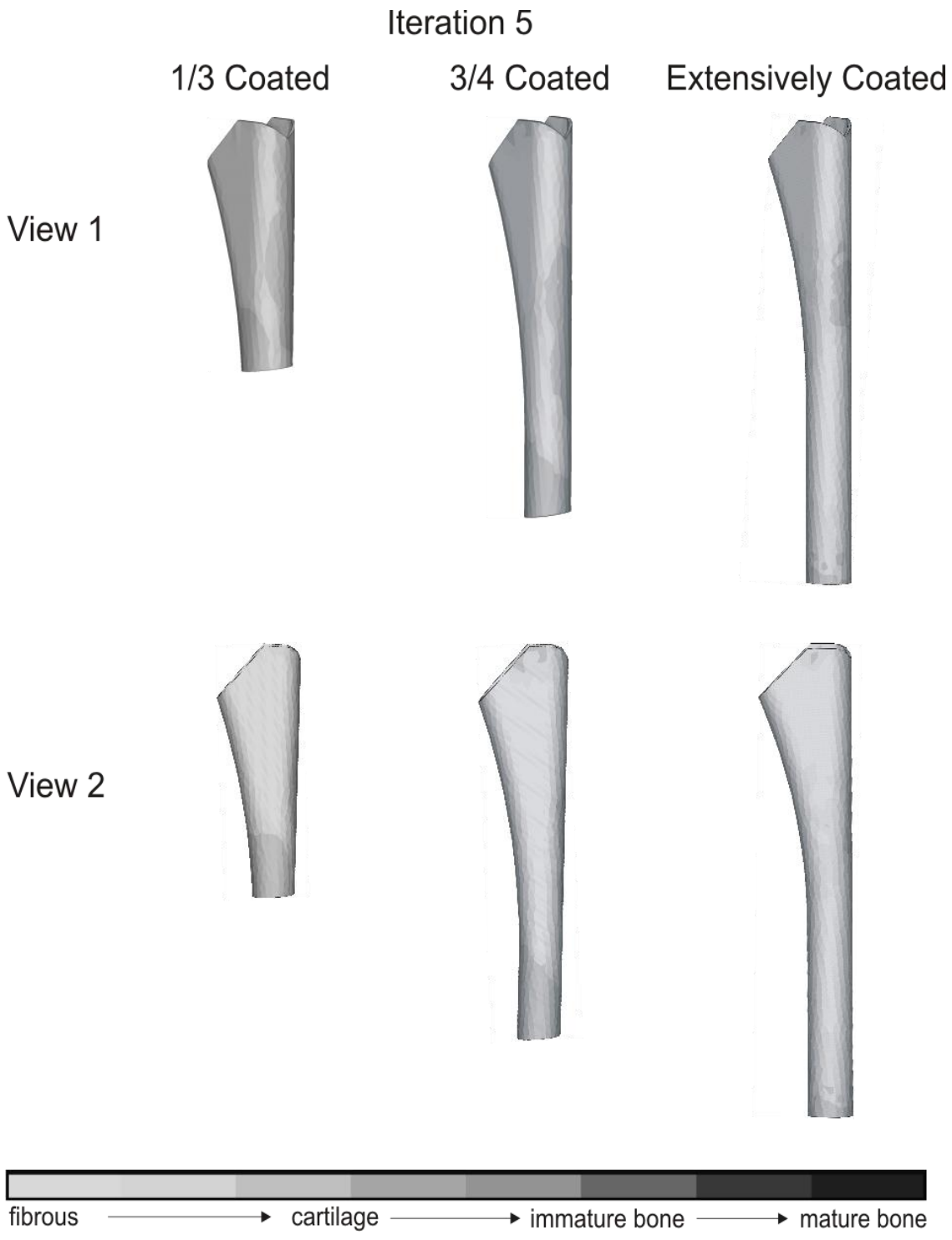

Figure 5.13: The postero-medial (top) and posterior (bottom) views of the tissue surrounding the implant for the three AML models at iteration 5.

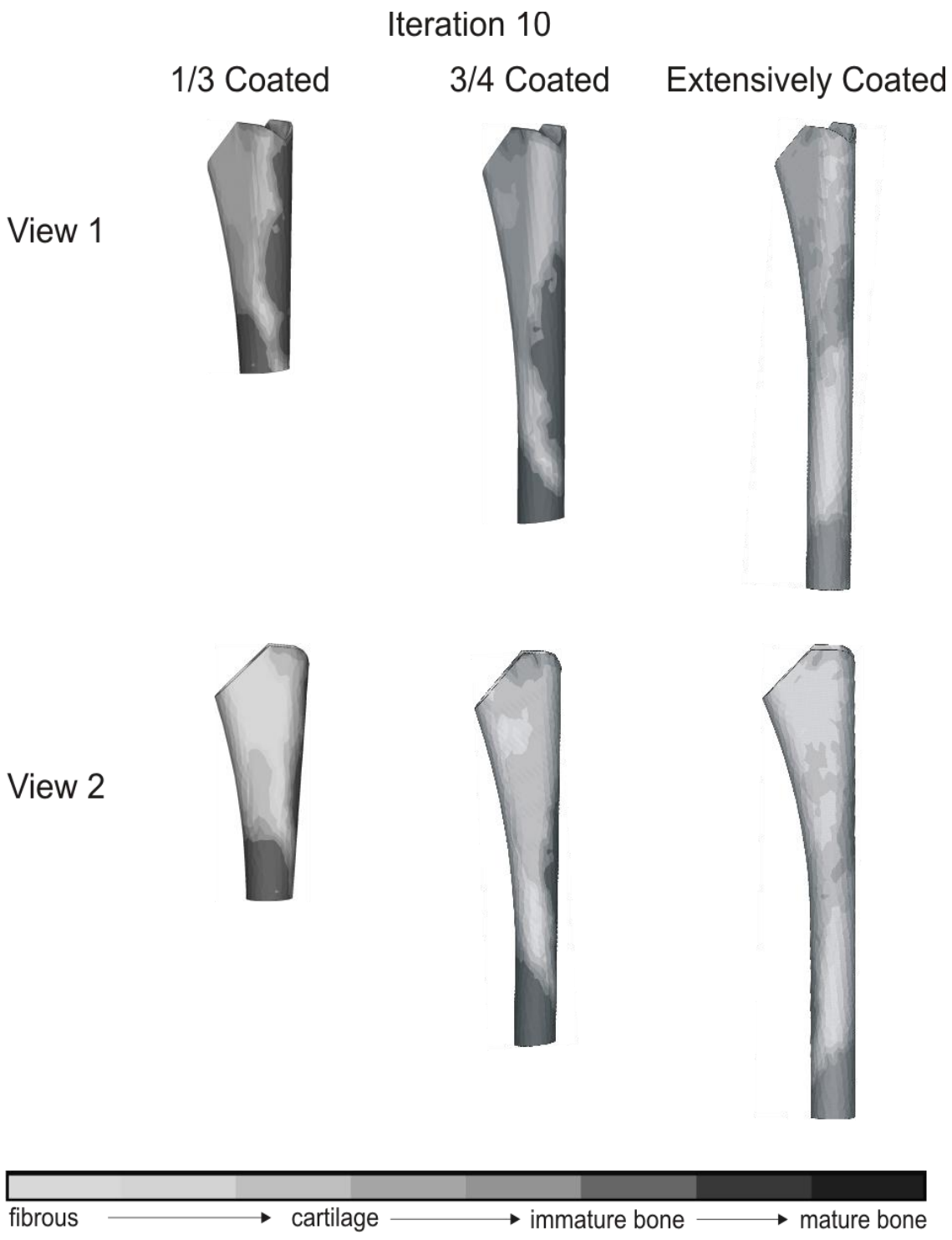

Figure 5.14: The antero-lateral (top) and anterior (bottom) views of the tissue surrounding the implant for the three AML models at iteration 10.

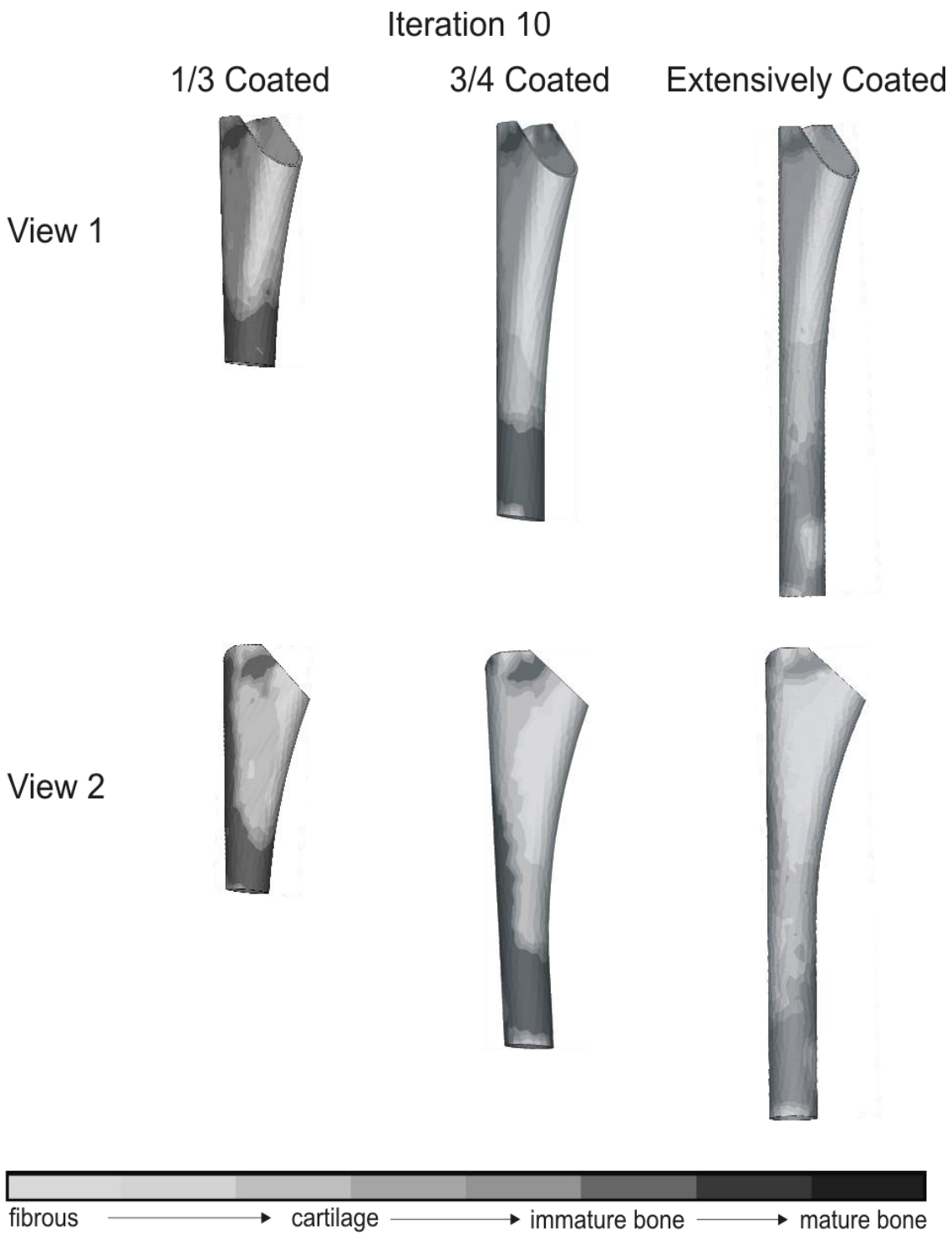

Figure 5.15: The postero-medial (top) and posterior (bottom) views of the tissue surrounding the implant for the three AML models at iteration 10.

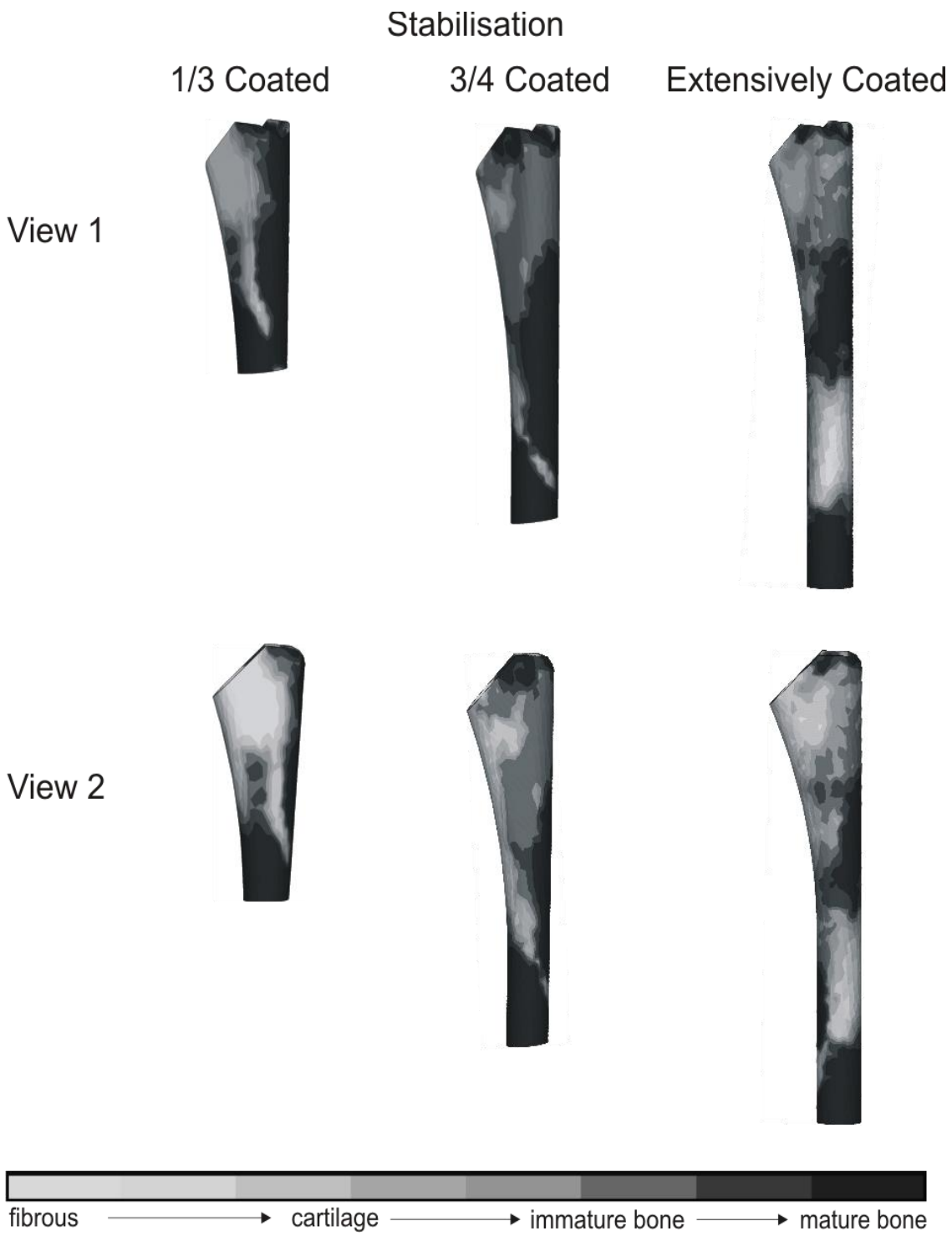

Figure 5.16: The antero-lateral (top) and anterior (bottom) views of the tissue surrounding the implant for the three AML models at stabilisation.

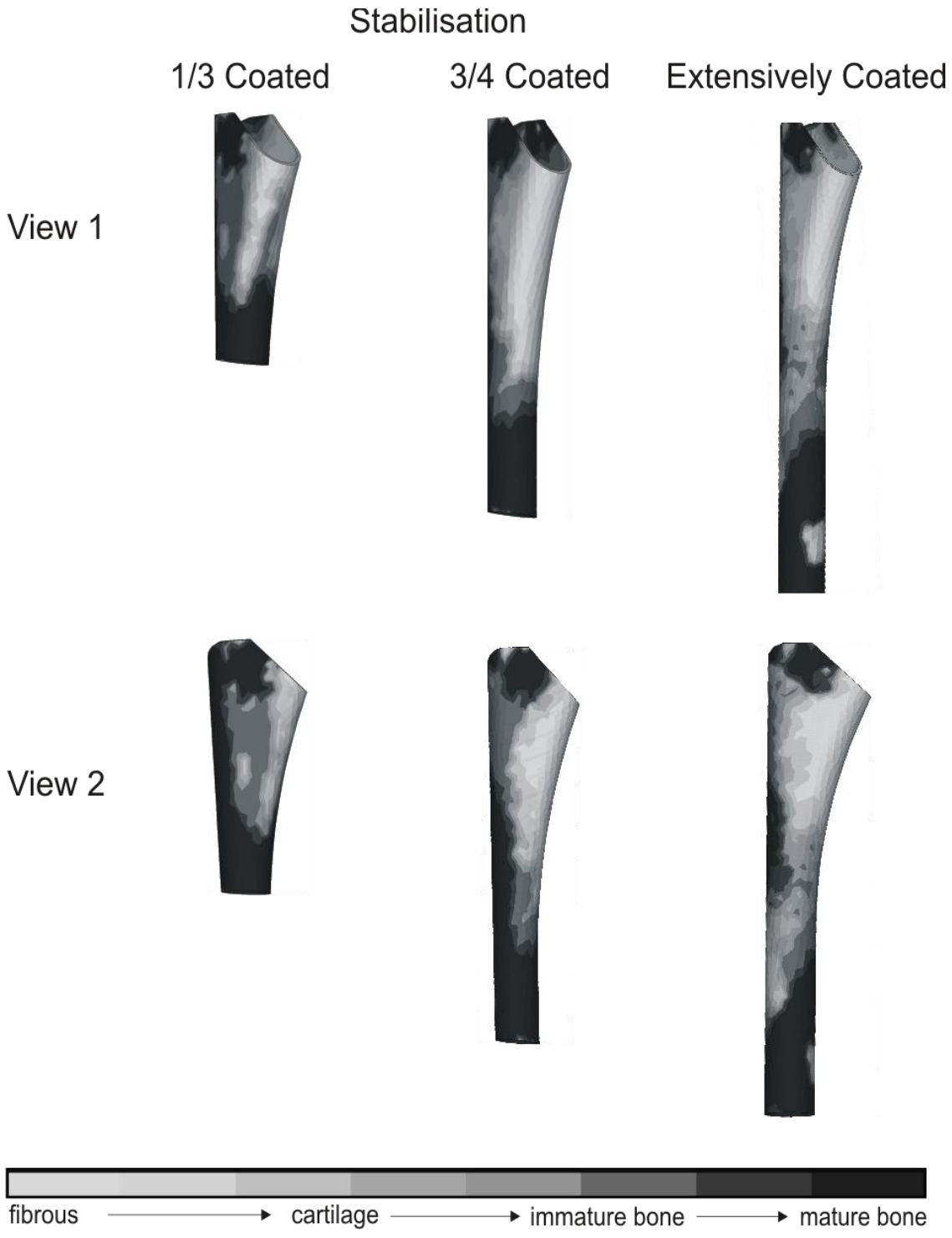

Figure 5.17: The postero-medial (top) and posterior (bottom) views of the tissue surrounding the implant for the three AML models at stabilisation.

The increase in tissue stiffness as the iterations progress is evidenced in the formation of stiffer cartilage tissue and mature bone. There is a marked improvement in the percentage increase of

mature bone formation for all the implants, especially for the extensively coated implant. Mature bone replaces immature bone through the stages. The amount of mature bone formed for the implant is comparable to the other two implants around the half way stage, even though it had considerably lower percentage of immature bone formation in the earlier stages. There is also decreased fibrous tissue formed for all three implants, most notably for the 1/3 coated implant with only 26% of the tissue surrounding the implant. In addition, the regions of fibrous tissue formation are mostly in the proximal medial regions of the implants. Most of the lateral and the distal regions (including the distal medial) sides showed increased bone formation overall, due to cartilage tissue being replaced by immature bone, which is later replaced by mature bone.

At stabilisation, the majority of the tissue type surrounding the implants was a combination of mature bone and immature bone, forming in excess of 60% in all cases. However, the most bone formation was seen for the 1/3 coated implant, occupying 72% of the tissue space as opposed to 68% and 63% for the 3/4 and extensively coated implants respectively. Fibrous tissue was found to occupy very little of the tissue space, with the rest of the surrounding tissue consisting mainly of the harder cartilage tissue. The tissues formed for the three implants at stabilisation are shown in figure 5.16 and figure 5.17. The overall tissue formation across the three models at different stages of the iterations proceeding to stabilisation is shown in figure 5.18. The increase in overall bone formation, along with the corresponding decrease in cartilage and fibrous tissue is clearly demonstrated.

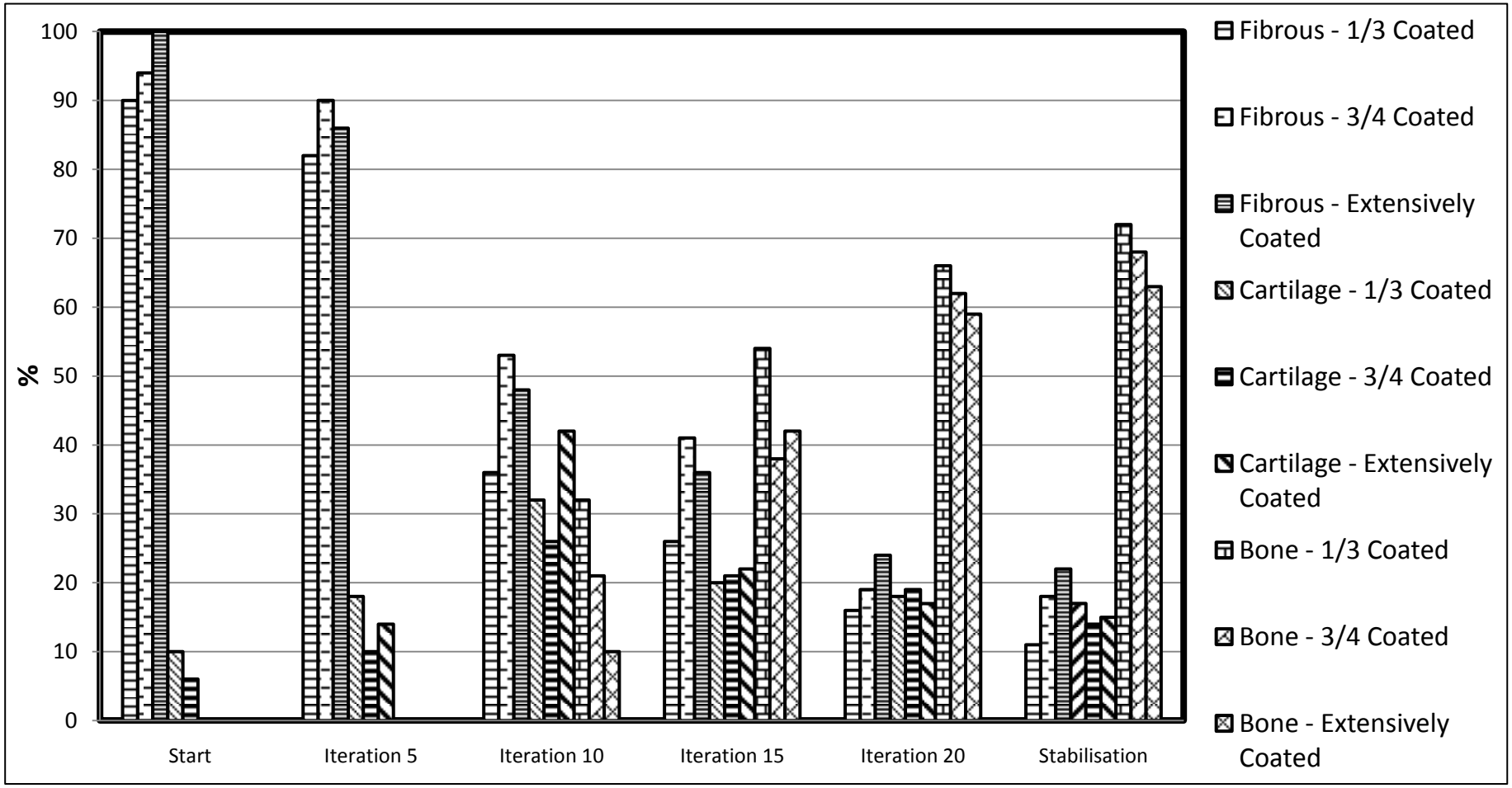

Figure 5.18: The percentage of the three main tissue types formed, fibrous, cartilage and bone at various stages proceeding to stabilisation for the three models of the AML considered.

5.5 DISCUSSION

In the current study, tissue differentiation around three different versions of the AML has been predicted and analysed. The general trend observed across all of the models is the high percentage of bone formation (>60%) seen at stabilisation, with very limited fibrous tissue formation. Due to the more extensive literature available on the extensively coated AML, tissue formation around it can be commented on first. The location of the bone formed for the extensively coated implant, primarily around the distal regions of the stem, corresponds well with retrieval and radiographic data from literature [174,225,250,254]. Figure 5.19 shows a comparative view of distal bone formation in the extensively coated implant as seen in literature and the result obtained in the current study. These distal regions of bone formation shown in the figure are known as endosteal "spot welds" and usually represent regions through which stress transfer to the diaphysis takes place. In addition, it has also been found that the lowest bone mineral density occurs on the medial side, in the most proximal 1cm of the implant, followed by regions directly under it [256]. These regions correspond to the regions occupied by fibrous tissue in the current study.

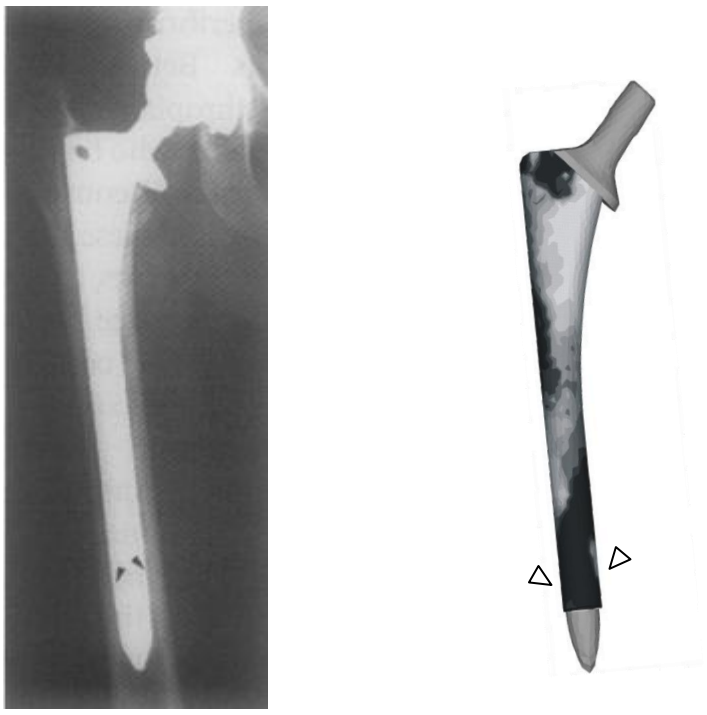

Figure 5.19: Bone ingrowth locations around the extensively coated implant as seen in literature (left) [225] and the current study (right).

In further support of the results, also including the 1/3 coated AML, the tissues formed at stabilisation also compares well with those obtained from a finite element study by Folgado et al. [257]. In the Folgado study, the effect of the extent of porous coating on a Co-Cr cylindrical stem based on a novel displacement model was carried out. Bone ingrowth patterns matched those

found in the current study as seen in figure 5.20. Ingrowth locations, in the proximal medial and lateral rounded corners, were consistent with the current study and of that found in literature [258]. In addition, ingrowth percentage reported in the Folgado study was over 60%, as observed in the current study. In another study comparing regions of BMD around proximally and fully coated implants, it was shown that the most decrease in BMD was noticed in the proximal 1cm of the medial femoral cortex for extensively coated implants [256], which agrees well with the regions of fibrous tissue formation obtained in the current study. Overall, the results obtained in the current study show the same trends of bone formation for extensively and proximally coated AML implants as seen in literature.

Figure 5.20: The comparative bone ingrowth patterns for the 1/3 coated and fully/extensively coated AML from the Folgado et al [257] (shown on the left of the current results in either case) and the current study. Darker regions represent bone formation.

The advent of proximally coated AML implants, as noted in the introduction, was due to the higher incidence of stress shielding associated with the extensively coated version [172]. However, clinical results obtained have only shown a limited advantage in preventing stress shielding with their use, with studies showing no significant difference between the two models [174,225]. Moreover, for a different implant, it has also been shown that the proximal coating did not protect against bone loss proximally or distally in the femur [259], with videodensitometric analysis showing less decrease in bone density for the extensively coated when compared to the proximally coated implant. It has been the general consensus in the literature that the amount of ingrowth that can be achieved in extensively coated AML implants far surpasses the disadvantages of stress shielding associated with them [167]. In the current study, the rate of bone ingrowth for the proximally 1/3 coated

implant is excellent, with rapid stabilisation of tissue through the formation of mature and immature bone. 3/4 and extensively coated implants also show good bone formation, but stabilisation (inferred from immature and mature bone formation at every stage of the iteration) is far less when compared to the 1/3 coated implant. However, whether early stabilisation can be the rationale for preferential use of the 1/3 coated implant, especially when the bone formation at stabilisation is comparable across the three implants remains debatable.

Not restricted to the AML implant alone, similar results have been obtained in other studies. Al Hertani et al.[260] investigated different hydroxyapatite coated beaded coatings extents on bone ingrowth in a canine hip study and found that the fully coated stems had greater percent bone apposition, more connectivity, less micromotion and comparable proximal fixation compared to the just proximally coated implant. The location of bone formation, in the lateral quadrant as opposed to the medial side also matches well with the results obtained from the simulation. One of the major factors listed in favour of using extensively coated implants in literature is the large surface area available for bone ingrowth. If ingrowth can be achieved over the length of the stem, good stability can be achieved compared to other coating lengths. Based on the results from the current study, no significant advantage can be shown in terms of the amount of bone tissue formed considering available space. There is less bone formation compared to the 1/3 and 3/4 coated implants. However, it has to be acknowledged that the data presented is only in terms of available space around each of the implants and does not compare the total amount of bone tissue formed across the three models. In this regard, the extensively coated implant does have more bone formation due to the larger surface area available for tissue differentiation. This is in keeping with the rationale of using extensively coated implants.

The case for the use of extensively coated implant has often been the additional stability provided by the diaphysis and this has been clearly demonstrated in finite element studies, where the 1/3 coated implant has less stability compared to the extensively coated implant [257]. In addition, micromotion has been found to be more in areas that are not porous coated, with the extent of micromotion between the implant and bone near the uncoated tip of the implants found to be inversely related to the amount of porous coating on the implant [253]. This has been shown in another study, with the maximum tip motion of the proximally coated AML implant as high as 210 microns, with extensively coated implants only displaying 40 microns [10]. Subsidence of proximally coated AML implants has also been an issue [261], which is avoided with the extensively coated implants due to the tight diaphyseal fit.

There are other limitations associated with the use of the proximally 1/3 coated AML. Firstly, their use has been advocated to patients with good proximal bone stock, which would mean they would be restricted to mostly young patients. In the absence of good initial stability, a problem exacerbated by poor proximal bones stock, proximally coated implants are at a higher risk of failure than extensively coated implants due to the lack of diaphyseal fixation [262]. In contrast, the

extensively coated AML has been, and continues to be used for patients in all age groups. Another important factor is that 1/3 coated AML implants can rarely be used for revision surgery due to the lack of bone proximally to support the implant. It is imperative in this case to achieve a diaphyseal fit and the extensively coated implant is the logical choice. The confidence of achieving a stable long term fixation through the use of just a proximal coating does not match that of the extensively coated AML, which is assured of a good diaphyseal scratch fit even if ingrowth fails to occur. On a similar note, attaining a congruent fit is also easier with the extensively coated implant in comparison [128]. Proximally coated implants also need to be circumferentially coated to seal the diaphysis from wear debris; inadequate proximal fixation and poor stability could exacerbate this problem and lead to osteolysis [263]. Another important factor that needs to be addressed is stem design. There is an increasing trend to manufacture more proximally coated uncemented implants in view of reducing distal stress shielding. This however, cannot be a rationale used for all uncemented implants as some stem designs may not have a significant difference as the aforementioned studies have shown. However, there have been other studies that show the advantage of enhancing stem designs for proximal coatings, but have often sacrificed overall stability for proximal fixation [264]. Whether this trade off is justified and if the positives of obtaining proximal fixation surpasses bone ingrowth over the entire surface of the stem can only be ascertained through long term follow ups of these current designs.

There are limitations associated with the study, primarily concerning the absence of biological factors modelled. It would be useful to include cellular influences that also contribute to the type of tissues formed at the interface. The source of these cells would be the marrow and the endosteum. The issue of determining the value of K is not a major concern in the current study, due to the extensive literature review available on the implant. Although the tissue differentiation patterns obtained are comparable to those found in literature, it would be extremely useful to include bone remodelling along with the tissue differentiation to present a more realistic comparison to clinical studies. This would also allow further investigation into the differences in stress shielding when each of the different implant versions is used.

To conclude, all three versions of the AML show excellent and consistent bone ingrowth. Although the 1/3 and 3/4 coated implants show slightly more bone formation with regards to available space for tissue formation, the overall quantity of bone formed is more for the fully coated implant due to the larger surface available around the implant. In addition, for the 1/3 coated implant, the added advantage of early stabilisation and the disputable reduced stress shielding (based on literature), is a weak justification for its preference over the other two implants. Based on the results obtained in this computational study, where it has been shown that there is little difference, if any, with regards to bone formation, it would appear that the fully coated implant is the most attractive option as it also has the advantage of better initial stability, ease of repeatable implantation and more surface area for ingrowth.

CHAPTER 6

MICROSCALE STUDY OF TISSUE DIFFERENTIATION IN THE PORE SPACE OF A BEADED POROUS COATING AND THE INFLUENCE OF DESIGN FEATURES

The research carried out in this chapter has been presented in part in the following conference and journal:

- *Puthumanapully P.K., New A.M., Browne M. (2009)* ***"Simulating bone ingrowth in porous coated implants"*** *Exploring the biological/biomechanics interface. Arup campus, Blythe valley park, Solihull, UK.*

- *Puthumanapully P.K., New A.M., Browne M. (2008)* ***"Do multi-layer beads on porous coated implants influence bone ingrowth? A finite element study"*** *Journal of Biomechanics. Vol 41 (1) S290. 2008.*

6.1 INTRODUCTION

Bone ingrowth is key to the long term stability of porous coated uncemented implants. One of the primary mechanical factors that influences bone ingrowth is micromotion. Micromotion has been described as the tangential displacement of the femoral implant relative to the bone during one loading cycle [265]; the irreversible displacement that occurs due to micromotion after repeated loading is described as migration. Micromotion is a small, three-dimensional and complex motion at the interface [67]. Micromotion can result due to poor initial press fit and stability [21] and further contribute detrimentally to the more important long term secondary stability of cementless implants by hindering the formation of osseointegration at the interface. The role of micromotion in determining the type of tissues formed at the interface has been studied extensively by a number of authors through animal or retrieval studies [6,7,10,143,168,173,266,267].

Large micromotions over a long period are hypothesised to encourage the formation of fibrous tissue at the interface as opposed to bone. Although the exact values of micromotion that lead to this are unknown and may vary on an individual basis, reports have suggested conservative values of even >30-40 microns micromotion at the interface resulting in fibrous tissue. 150-200 microns is normally considered the value beyond which fibrous tissue formation will form [7,10,143,173,177]. Fibrous tissue has extremely poor mechanical properties compared to bone [9] and can result in loosening of the implant, especially when subjected to large shearing forces as reported by Hori and Lewis [268]. Micromotion has also been studied computationally by a few authors through the use of finite element models employing two main methods; a) by relating regions of high micromotion to fibrous tissue formation through comparisons to radiographs or b) simulating evolution of tissue based on a mechanoregulatory algorithm [163,178,269,270].

Fibrous tissue has been shown to proliferate within porous structures once it has formed and the formation increases with time [271]. Therefore it is imperative that this be prevented in order to maintain long term stability of the implant. The formation of bone rather than fibrous tissue needs to be encouraged, and ideally for porous coated implants this would extend from the existing bone surface to the pores. Although various porous surfaces have been and are being developed, layers of beads arranged on the surface of the implant has been a popular choice to date and will therefore be the subject of this investigation.

Beaded layers have been used as coatings to provide anchorage, initially through a scratch-fit frictional interface with the surrounding bone and then, presenting the opportunity for long term biological fixation through osseointegration. They have been the coating of choice on the clinically proven AML and PCA implants and have historically been a constant feature in cementless stems. The aforementioned implants use “Porocoat®”, the proprietary porous coating from DePuy orthopaedics. Currently, the Porocoat coating consists of commercially pure titanium sintered beads on a titanium alloy substrate (figure 6.1). The beads are spherical, but sometimes lose shape

during sintering. The coating employs a bead size of 200-250 microns, applied in layers with pore size ranging from 200-300 microns. The uncemented implants of the late 70s and 80's used cobalt chrome beads but have currently been replaced by titanium due to their lower elastic modulus.

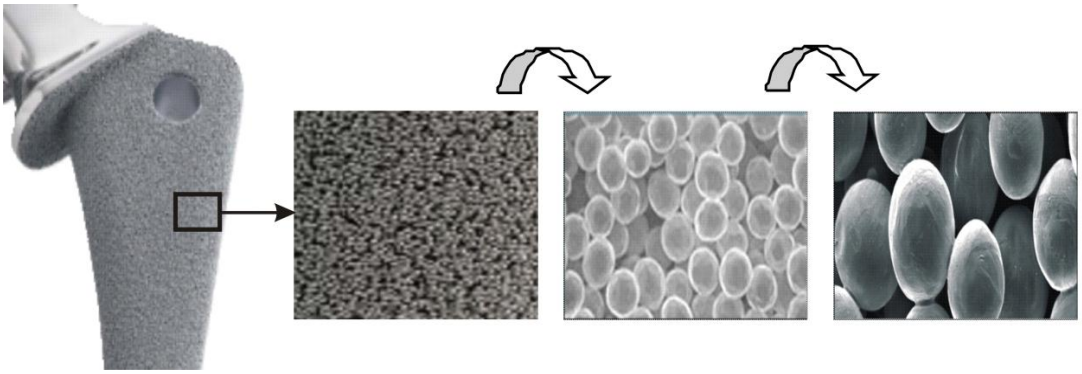

Figure 6.1: The beaded porous coating "Porocoat" employed for bone ingrowth.

The porous coating also employs a porosity gradient; the beads are arranged in such a way that the porosity is higher on the outer edge in contact with the bone and lower near the substrate. This is to ensure that the top layer encourages rapid penetration of bone and the substrate layer of beads increases the bond strength. The depth of the coating is normally three layers, and can sometimes extend to four layers. The structured and layered beads form an interconnecting pore network for bone ingrowth to take place. This interconnection also allows the porous surface to be stable and provides higher resistance to shear and tensile stresses. They have often been preferred over grit blasted and plasma sprayed surfaces due to the larger interconnecting pore space available, which is ideal for bone formation and provides more regions protected from high strains at the interface [155].

To the author's knowledge, computer simulation of the evolution of tissues at the bead-bone interface on a microscale level has only been conducted by one author [219] and the influence of different layers and micromotion combined has not been undertaken as yet. The idea behind the current study is that by observing the influence of structure and micromotion on the type of tissues formed at the interface, design modifications could be made that could enhance more bone formation at the interface and reduce the incidence of fibrous tissue at the interface.

6.2 AIM

To develop a 2D microscale model of the interface between the bone and coating and to study the evolution of tissues at the interface and pore space for a standard three layer beaded coating under different levels of micromotion.

6.3 METHODOLOGY

The technique used in the study was similar to those described in the previous chapters. Two-dimensional FE models of the porous coating were combined with the modified mechanoregulatory algorithm described in detail in chapter 3 with relevant boundary and loading conditions. In contrast to previous studies, only method 1, describing overall tissue formation was employed as a finer detailed model within the pores was not required. Moreover, the study focused on gross tissue formation and the information provided by method 1 was considered to be adequate.

6.3.1 THE "POROCOAT®" BEADED COATING

Samples of the Porocoat porous coating were obtained from DePuy International (DePuy, Leeds, UK) in two different bead configurations, (i) A three layered and (ii) a two layered configuration of titanium beads on a titanium alloy substrate, in small blocks of 10mm X 10mm each. Each of the samples was viewed and photographed under a standard microscope to help understand the structure. On average, the bead size was 250 microns, as shown in figure 6.2.

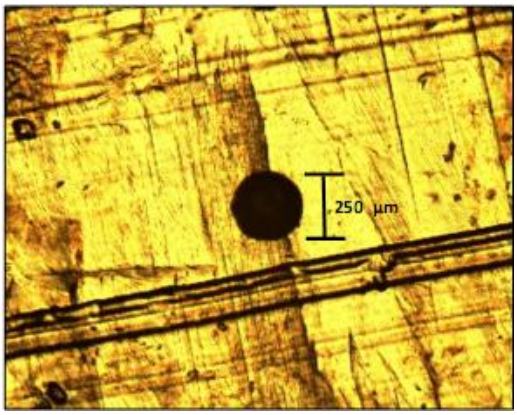

Figure 6.2: A single bead from the Porocoat porous coating on a titanium substrate viewed from above.

6.3.2 GEOMETRIC AND FINITE ELEMENT MODELS

A two-dimensional finite element model was created in Ansys (Ansys Inc, Canonsburg, PA, USA), based on the Porocoat samples and a previous model developed by Liu et al.[219]. The model represented a plane cut through a body centered cubic unit cell of the coating in contact with the bone, with bead sizes of approximately 200 microns in diameter. The original geometry was first developed in Solidworks (Dassault Systèmes SolidWorks Corp. Massachusetts, USA) and exported to Ansys in the form of an IGES file. The two-dimensional structure measured 1.00mm x 0.975mm and contained areas defined for bone, the beads, the granulation tissue and the substrate. For comparative purposes with the study by Liu et al., the size of the beads was reduced to 200 micron,

at the lower end of the specification of the beads in the commercially produced coating. The minimum distance between the individual beads in a layer was approximately 60 microns. The substrate was assumed to be 100 microns thick. [178]. The bonding of the bottom layer of beads was modelled by flattening the geometry of the beads near the substrate as shown in figure 6.3.

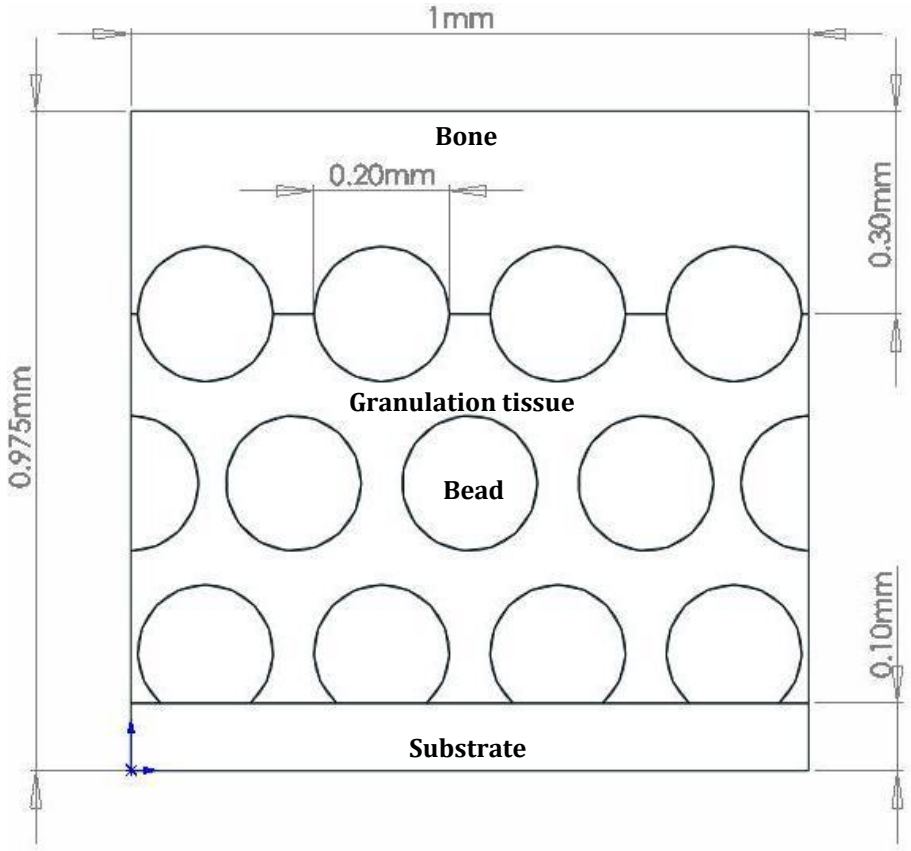

Figure 6.3: The two-dimensional geometric model of a standard 3 layer beaded coating developed for the study.

The top layer of bone was modelled to be 0.3mm away from the interface and 0.2mm away from the beads in the top layer. The areas were then meshed using second order plane strain elements, and had 8 nodes each with 2 degrees of freedom, translations along the x and y axes at each node. This element was chosen due to it being well suited to mesh curved boundaries. A uniform element size of 0.01mm was defined the structure was meshed. The number of elements for each region of the model is given in table 6.1. The resulting finite element mesh is shown in figure 6.4. The total number of elements and nodes in the model were 10776 and 33246 respectively.

REGION	***ELEMENTS***

Bone	2239
Granulation tissue	2458
Beads	4983
Substrate	1096
TOTAL	**10776**

Table 6.1: Number of elements in each region of the finite element model.

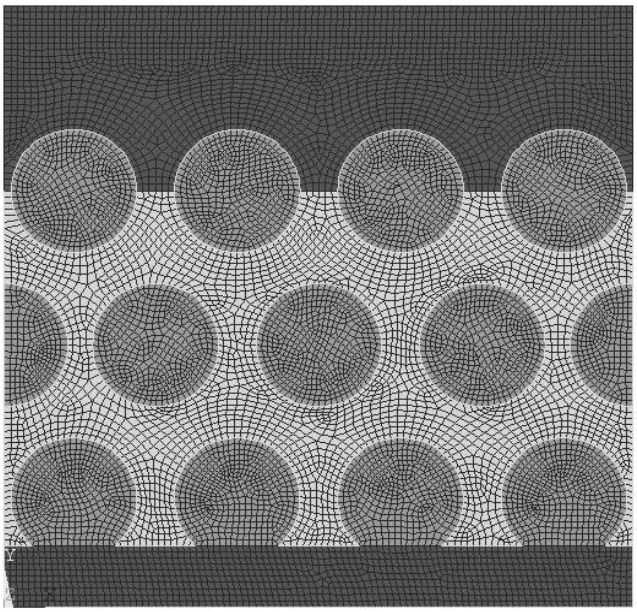

Figure 6.4: The finite element model used in the study showing bone occupying the top layer, the titanium beads with granulation tissue surrounding the beads and the substrate.

6.3.3 BOUNDARY CONDITIONS, LOADING AND MATERIAL PROPERTIES

The whole structure was assumed to be part of an infinitely long scaffold in situ. Nodal displacements on the lateral faces were constrained in the horizontal direction to simulate this assumption. The bottom substrate was fixed and fully constrained in all directions. All the beads were assumed to be rigid and fixed. Frictionless sliding contact was assumed between the granulation tissue, the fixed beads and the bottom substrate. The rationale was that although adhesion of the tissue to the beads would occur, the resulting forces would be small in relation to the contact forces. This was also in keeping with the aforementioned study [219] where a frictionless case was shown to be a reasonable initial choice.

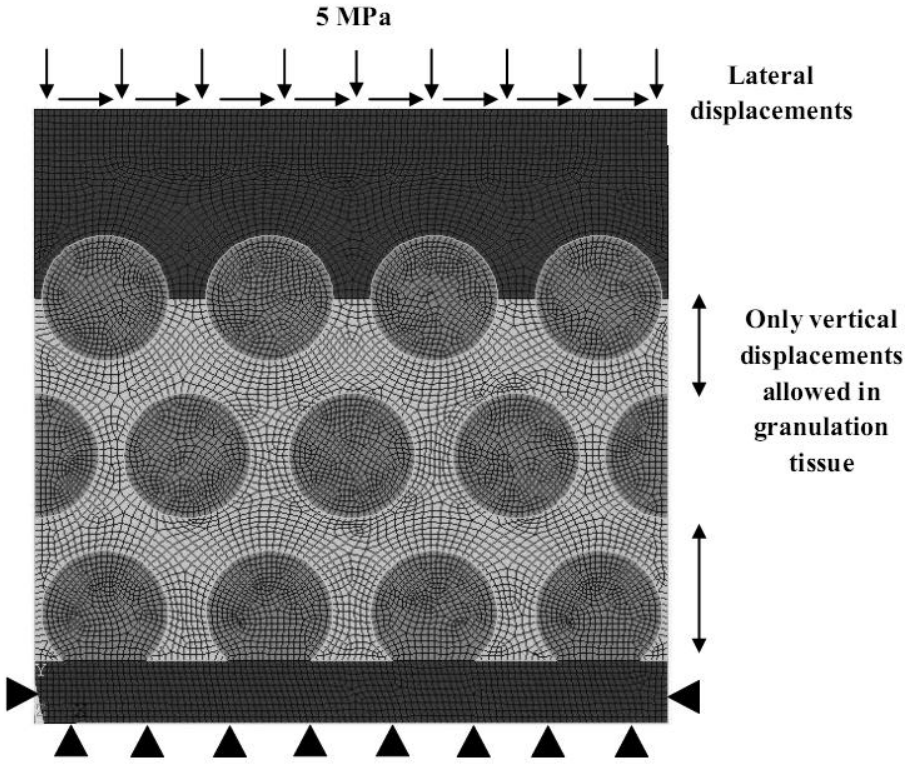

Figure 6.5: The boundary conditions applied to the model. The bottom substrate was constrained in all directions. A compressive pressure of 5 MPa and micromotion in the form of lateral displacements were applied to the top surface of the bone. Nodal displacements on the lateral faces of only the granulation tissue were applied to simulate an infinitely long scaffold.

The press fit condition was represented by applying a compressive stress of 5MPa, corresponding to the maximum load predicted along the length of a press fit porous coated implant [234]. To simulate the effects of micromotion at the bone implant interface, a lateral displacement of 1, 10, 20 and 100 microns was applied to the upper surface of the bone. There were three loading cases used in the study. The first loading case was a set number of cycles of the compressive load used for the press fit condition. This was then followed by a combination of the compressive force and micromotion in one direction on the top surface of bone. The next loading case included the compressive force and micromotion applied in the opposite direction. These loading cycles were then set to run for a set number of iterations. The finite element model with the loading and boundary conditions is shown in figure 6.5.

Material properties were assigned based on values obtained in literature and tabulated previously in chapter 4. All the materials were modelled as linear, elastic and isotropic. The bone layer assumed was cancellous, modelled with an elastic modulus of 500 MPa and Poisson's ratio of 0.3. The titanium substrate was modelled with an elastic modulus of 110 GPa and Poisson's ratio of 0.3. The porous coating, also made of titanium was assumed to be 50% as dense as the parent material

and given an elastic modulus of 55 GPa and Poisson's ratio 0.3. This was in keeping with the study by Ramamurti et al [21]., where the beads were modelled in a similar way. Granulation tissue was assigned an elastic modulus of 1MPa with a Poisson's ratio of 0.17.

The emphasis of the study was not on the surrounding bone, beads or substrate and was focussed entirely on the transformation of the initial granulation tissues in the pores into any of the three primary tissues; bone, cartilage or fibrous tissue. The region of interest is shown in figure 6.6.

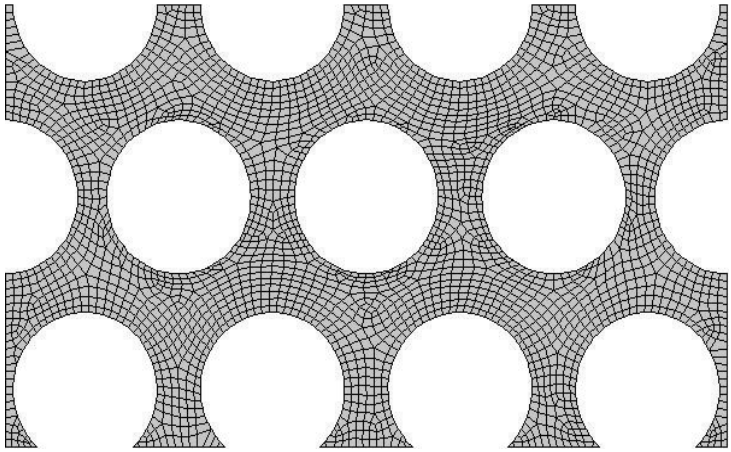

Figure 6.6: The granulation tissue surrounding the beads that undergoes differentiation.

The hypothesis and the associated developed algorithm was implemented in method 1 as described in chapter 3 until the defined number of iterations or there was less than 5% change in tissue type between two successive iterations. The number of iterations was always kept high (~30 iterations) to avoid premature termination of the simulation in case the number of cycles was completed and there was still more than 5% tissue change at every iteration. In almost all cases, the iterations stopped at the latter criteria rather than the completion of the iterations.

In keeping with the methodology used in the previous chapters, the value of K to be used in the simulations needed to be determined. K, the weighting factor for the dilatational component of the osteogenic index was investigated for values of K=0, 0.5, 1, 2, 3 etc for a micromotion value of 20 microns**.** This value represents an intermediate level of micromotion, which has been shown in literature to show formation of all three tissue types, good bone formation along with fibrous tissue and cartilage [7]. By comparing the results obtained to the description of the tissues found in literature, the value of K to be used for the remainder of the simulations can be determined. In addition, the results obtained by Liu et al [219] for 20 microns micromotion in a similar model but employing a different hypothesis and modification was also used to check which value of K matched closest.

6.4 RESULTS

6.4.1 SELECTION OF K VALUE

The results obtained were first used to choose an ideal value of K, after which that value would be used for the remainder of the studies on the influence of micromotion. The first set of results is shown in figure 6.7 across four K values considered; K=0.5, 1, 2, 3 and for a micromotion value of 20 microns. Only the change in granulation tissue is shown, without any additional geometry, the surrounding bone, beads and substrate present. The results presented for choosing K are the plots obtained after tissue stabilization.

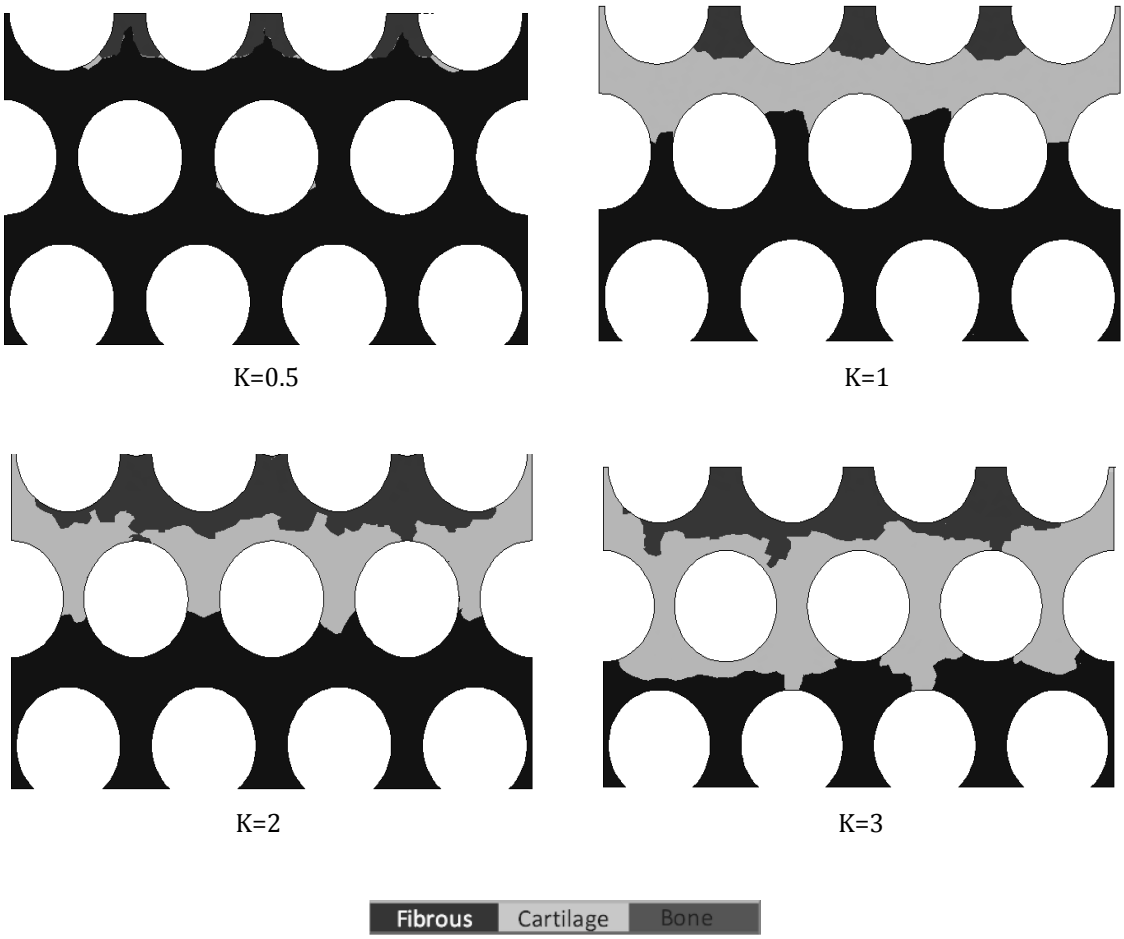

Figure 6.7: The transformed granulation tissue for different K values for 20 microns micromotion.

The plots obtained for different K values were compared to the description of tissues in literature [7,143] and the finite element study of Liu et al. K=0.5 and 1 showed excessive formation of fibrous tissue in the pore space which is not to be expected for a relatively low micromotion level of 20 microns. Bone and cartilage formation were very limited and did not represent a feasible scenario.

K=2 and K=3 were very similar in their distribution of bone tissue but different in the cartilage and fibrous tissue percentage. However, the description of K=2 was the closest to observations in literature; with bone formation in the top layer of beads and interconnectivity around the beads with significant fibrous tissue formation near the substrate. Moreover, the location and percentage of bone tissue formed also closely matched the results obtained by Liu et al at stabilisation. Based on these comparisons, this value was selected for the remainder of the study.

6.4.2 INFLUENCE OF MICROMOTION

With the K value decided, the simulations were run with the algorithm to investigate the influence of micromotion on tissue differentiation in the pores. Micromotion ranging from 1 micron to 100 microns was investigated and tissue differentiation plots were obtained. The specific values of micromotion used were 1μm, 10μm, 20μm and 100 μm. The low value of 1 micron would represent the ideal scenario where the implant is well fixed and there is minimal or no micromotion, and 100 would represent the extreme case. Plots were obtained of the initial stages of tissue formation and the final stabilised stage.

The two stages reported here distinguish between the percentage of tissues formed in the initial stages of the iterations and at tissue stabilisation that normally occurs around iteration 20±5 in most cases. Iterations 5 and ~20 were chosen as they presented the best possible time frame for each case to illustrate the disparity in the type of tissue formed.

MICROMOTION = 1 MICRONS

Iteration 5 **Stabilisation**

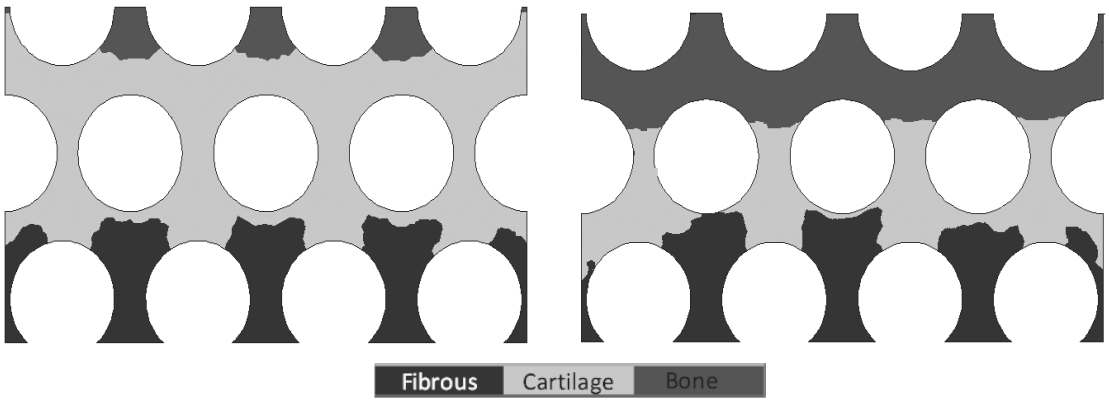

MICROMOTION = 10 MICRONS

Iteration 5 **Stabilisation**

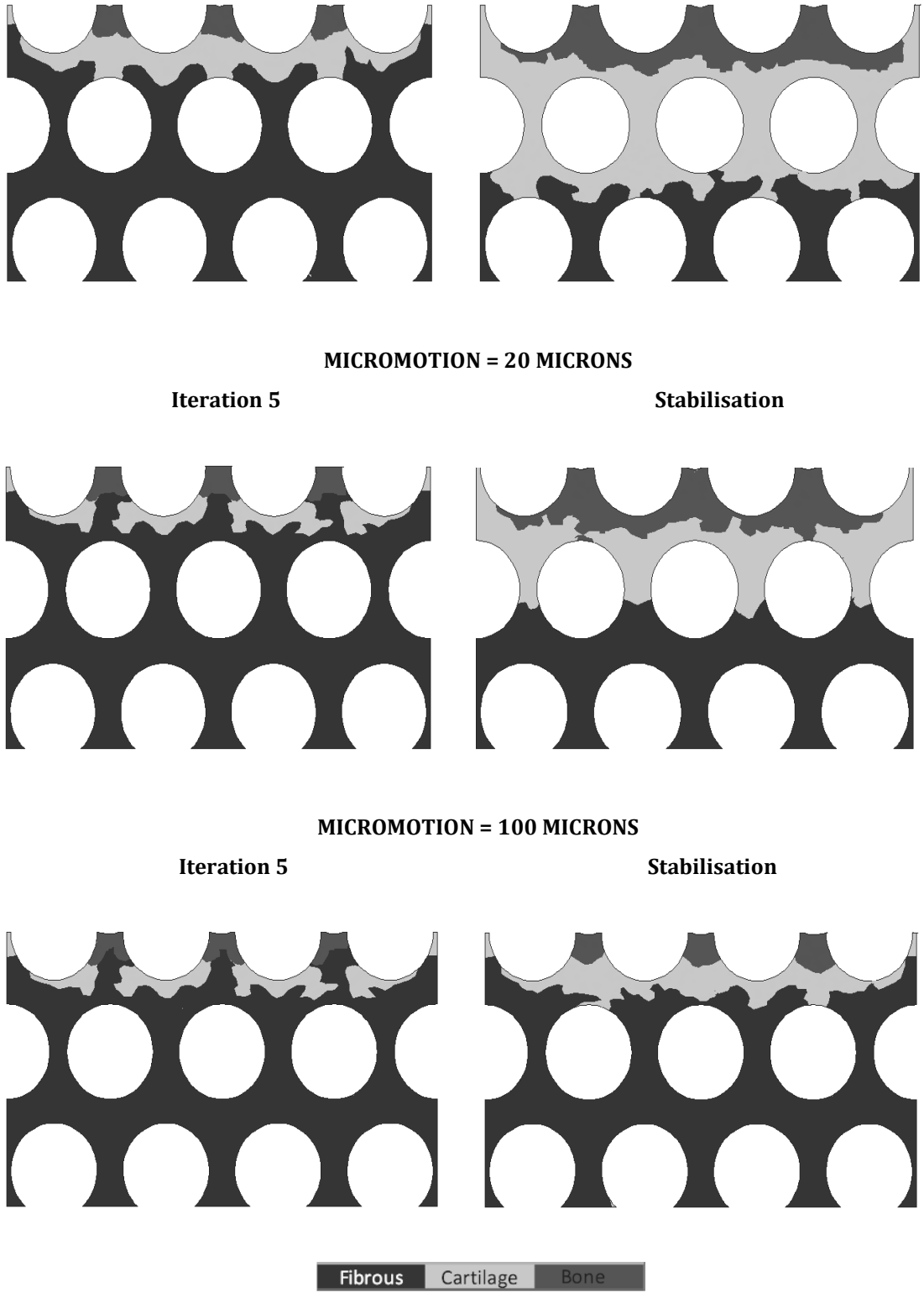

Figure 6.8: Tissue formation in the pore space for different levels of micromotion during initial stages of tissue differentiation (left) and at stabilisation of tissue (right).

The results clearly show the change in tissue type from granulation tissue into bone, cartilage or fibrous tissue (figure 6.8). There is considerable change in tissue type across iterations as well as different levels of micromotion. A high level of micromotion, representative here of poor initial

fixation and simulated by a micromotion of 100 microns, clearly shows a large percentage of fibrous tissue at the end of the iterations. Even during the early stages, the level of fibrous tissue is far greater than any of the other tissue types formed, accounting for nearly 85% of the tissue formed in the pore space.

Considering lower levels of micromotion, in the case of 1 micron micromotion, which represents an extremely well fixed implant, the results are quite different. Even during the initial stages, though bone formation is very low and restricted to the interface regions, there is a large presence of cartilage tissue (~65%). Towards the end of the iterations however, there was a large amount of bone formation, increasing to nearly 35% of the pore space. In addition, there was also very good interconnectivity of bone around the beads of the top layer and extending to the mid layer of beads. It should however be noted that it would be extremely difficult to limit micromotion to this level and this represents a best case scenario. For intermediate levels of micromotion of 10 and 20 microns, which represent micromotion comparable to conditions *in vivo,* and can be thought to be achieved through reaming and proper placement of the prosthesis, the results suggest that bone formation is far less, with the proportion of cartilage tissue increasing and then subsiding, with increasing amount of fibrous tissue formation. The percentage of tissues formed for the different levels of micromotion is shown in figure 6.9.

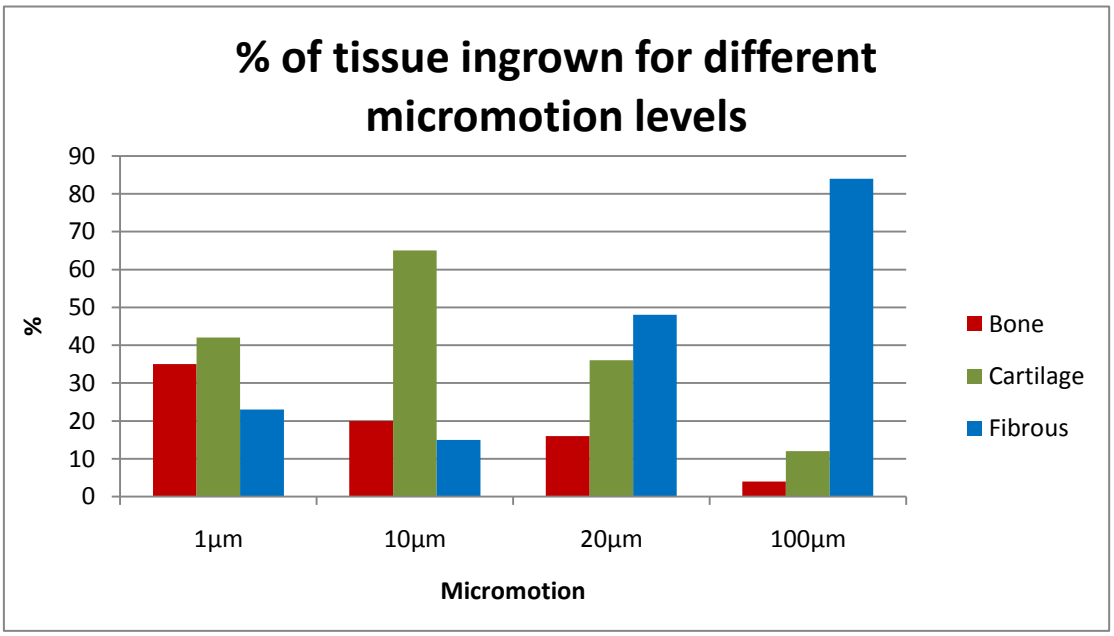

Figure 6.9: The percentage of each tissue type formed for different levels of micromotion.

In the case of 10 microns micromotion, fibrous tissue is prominent during the initial stages, similar to the case of 100 microns but then bone percentage gradually increases to occupy regions in the top layer of beads with added interconnectivity during the final stages. There is also a large amount of cartilage tissue present which could help stabilize the prosthesis. Fibrous tissue at tissue stabilisation is restricted to regions around the substrate and occupies less area (15%) compared

to bone (20%) and cartilage (65%). A similar trend is observed in the 20 micron case, with poor bone ingrowth during the initial stages, but resulting in around 16% of the pore space being filled towards the final stages. However, the amount of cartilage tissue eventually formed is vastly reduced with fibrous tissue the prominent tissue type, accounting for nearly 49% of the pore space. Cartilage occupies a relatively small region as compared to the 10 micron case, restricted to mid regions of the structure and filling up around 35% of the pore space.

6.5 DISCUSSION

Micromotion is a key parameter that determines the type of tissues formed at the interface, especially for uncemented implants. This purely mechanical parameter has been shown to regulate osteoblastic and osteoclastic activity at the interface [272,273] and therefore influence long term stability of the implant. The premise of large micromotions promoting the formation of fibrous tissue rather than bone has been well cited in literature [9,151,163,177,271,274,275]. The aim of the study was to simulate tissue differentiation, particularly ingrowth of bone at the interface of a typical beaded coating for different levels of micromotion. The results obtained in the study agree well with literature, with increasing levels of micromotion disposed to form fibrous tissue rather than bone.

With the largest micromotion case of 100 microns, bone and cartilage formation was very restricted, and occupied only the regions near the interface with no interconnectivity around the beads. Although representing bone ingrowth, the interface would still be assumed to be weak due to the presence of a large amount of fibrous tissue. A parallel can be drawn to the study by Jasty et al.[7], where bone formation was found even in the case of 150μm micromotion, but was noted to have no continuity to the surrounding bone or with bone formed in other pore spaces. Additionally, most of the pore space was found to be filled with dense fibrous tissue, from the substrate to the top layer of the coating. The results are more in agreement with the cited study for lower levels of micromotion. Micromotion values of 0 and 20μm resulted in good bone ingrowth with interconnectivity between bone in the pores and with the surrounding bone. However, it also has to be acknowledged that the coating used in the Jasty et al study was a fibre mesh, so finer points on specific regions of ingrowth and fibrous tissue formation cannot be commented on.

The large percentage of bone and cartilage tissue formed in the lowest micromotion case would be ideal, as literature reports that bone occupying around 40% of the pore space would represent good bone ingrowth [138]. However, this is not often achieved clinically and even 10-20% of bone occupied tissue can provide a stable long term fixation. Jasty et al.[276], in another study noted that even with a low ingrowth of only 5.5%, but with interconnectivity in some regions, the fixation was stable and categorised as “good ingrowth”. The percentage of bone and cartilage formed in the current study for the 10 and 20 micron cases can be categorised as being in this “good ingrowth”

category. Although with an extremely low percentage of bone as compared to other tissues, it could still provide good fixation.

Liu et al [219] carried out bone ingrowth simulations into the pore space with a similar geometry. However, the tissues were modelled as being biphasic and hence employing the hypothesis of Prendergast et al [8] with remodelling modifications . It was found that for micromotion exceeding 20 microns, there was minimal bone formation but formation of soft tissue. At 5 and 10 microns micromotion, the results reflected the current study at micromotions of 1 and 10 microns. It was found in the study that at tissue stabilisation, there was interconnectivity of bone between the beads in certain regions, with no bone resorption at the interface. However, unlike the current study where there was fibrous and cartilage tissue formation in regions near the substrate, there was no tissue formation near the substrate. This was observed for all of the micromotion levels simulated. Bone was simulated to form near the interface and one level of beads down depending on how high and low the micromotions were respectively.

There are a number of limitations to the study. Firstly, the geometry used was simplified and represented an idealised representation of the interface between the porous coating and bone. The actual geometry is complex and random, with possible ingrowth with interconnectivity and tissue differentiation across the 3D structure between the beads presenting more complexity. The interaction of the tissue in a 3D environment with the interfacial bone and rigid beads would differ significantly compared to the present model. In addition, the loading conditions described with compressive fit and micromotion applied to the top layer of the bone is very basic with no temporal scale involved in the loading regime. The duration and frequency of the loading cycle is important and due to the lack of experiments relating specifically to the current study, this has not been possible. However, the study does present a unique and novel technique to determine if micromotion does relate to the tissues formed at the interface; for example, high micromotions hindering bone ingrowth has been clearly shown in the study. Another shortcoming is the presence of a non changing bone volume used in the study. The emphasis on tissue differentiation in the pore space in this simplified model did not warrant the changes in surrounding bone. The author acknowledges that tissue differentiation and bone changes often go together and modelling changes in the surrounding bone volume could be an important step in improving the model.

The algorithm could predict bone ingrowth and tissue differentiation in the pore space based on micromotion that matches well with literature. Although extremely good fixation of implants with micromotion levels of 1 micron is hard to accomplish surgically, the results obtained for the more attainable 10 and 20 microns cases in the current study also show encouraging results for further ingrowth. High micromotion of 100 microns simulated the formation of fibrous tissue occupying the majority of the pore space and going by the results obtained, would present a scenario where the implant is stabilised only by the initial frictional interlock with little or no contribution through bone ingrowth.

The beaded porous coating continues to be a popular coating for osseointegration of implants with bone. The coating provides good surface morphology for bone ingrowth as compared to roughened plasma sprayed surfaces [155], with a three dimensional morphology for interconnectivity between the tissues formed that contributes to the stability at the interface by limiting micromotion and migration. In addition, as shown by Simmons et al.[156], in a finite element study, the morphology of the coating also provides strain protected regions that could be beneficial for osseointegration. With specific aims of promoting osseointegration into the pores, the key is to limit micromotion at the interface through better initial fixation.

6.6 COMPARATIVE STUDY OF THE EFFECT OF MICROMOTION ON TISSUE DIFFERENTIATION FOR 2 LAYER AND 3 LAYER BEADED COATINGS

6.6.1 INTRODUCTION

The beaded porous coating, described in detail in the previous chapter, is one of the most popular porous coatings for long-term osseointegration of the implant. However, there are a number of factors specific to the coating that can influence the type of tissue formed at the interface. Some of these have been highlighted in Chapter 2. Pore size and porosity have been studied extensively [147,251,277] and different surfaces and materials for ingrowth have been investigated [152,169,278]. However, the depth of the coating, i.e. the number of layers used for the coating is one such factor that could also influence tissue differentiation at the interface and has not been investigated in much detail. Among the few studies conducted, there have been mixed reports on the importance of the depth of the coating. Cook et al.[151] reported no significant influence of the depth of coating or the number of layers on the formation of bone. However, Friedman et al.[153], in an animal study showed disparity in the initial osseointegration rates between different surfaces and layers of beaded coatings. Another study has highlighted the importance of having multiple layers, but entirely for the integrity of the coating [279]. Overall, there remains no clear verification on the influence of the number of layers in a coating on osseointegration or tissue differentiation at the interface.

The importance of micromotion in regulating tissue differentiation in the pore space has been highlighted in the previous chapter. Computational simulation of the effect of micromotion on tissue differentiation in the pore space for two different configurations of coating has not been previously reported. Given this lack information on what could be an important factor determining ingrowth at the interface, the current study therefore aims to simulate tissue differentiation in the pore space for two different coating configurations.

6.6.2 AIM

The aim of the study was to investigate the influence of pore geometry, specifically 2 and 3 layered beaded coatings on tissue differentiation in the pore space for different levels of micromotion.

6.6.3 METHODOLOGY

The rationale behind the choice of 2 and 3 layers was based on common configurations used for the beaded coatings and the requirement of multilayer coatings for improved tensile strength [279].

Moreover, interconnectivity of pore space is an important factor in determining interfacial strength if osseointegration occurs. A single layer of beads attached to the substrate would not satisfy these criteria and was hence excluded.

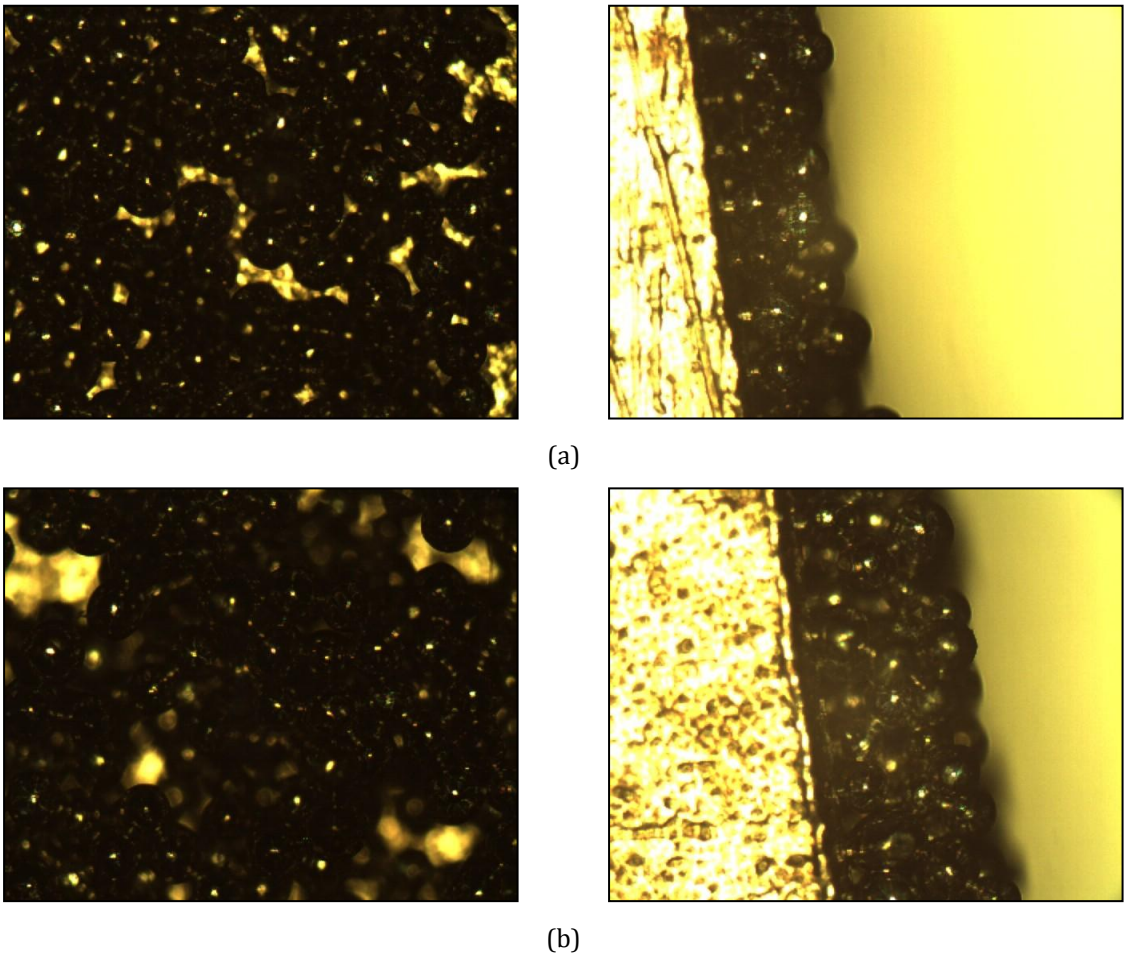

Figure 6.10: (a) two layered beaded coating with top (left) and sectional views (right) (b) three layered beaded coating with top (left) and sectional views (right).

The development of the 3 layered model was explained in the previous chapter. The two and three layered samples obtained were kept as reference for developing the finite element models. Top and sectional views of the coating are shown in figure 6.10. For the purpose of the current study, an additional finite element model was developed with a 2 layered beaded structure based on the 2 layered samples obtained (figure 6.10b) and the existing 3 layered model. In the finite element model, this was carried out by eliminating the topmost layer and using the middle layer as the top layer. The bone layer was interfaced with this layer as shown in figure 6.11. The dimensions of the structure were 1mm x 0.675mm, the titanium substrate was of the same thickness, measuring 100 microns. The beads measured 200 microns in diameter. The distance between the beads was approximately 60 microns and the bone-granulation tissue was 250 microns from the top surface of the bone. Most of the dimensions remained the same, except for the absence of the additional layer that was present in the previous study. The structure was then meshed using elements of the same

size used in the 3 layer study (mesh size of 10 microns). The resultant mesh had a total of 23145 nodes and 8422 elements, with 2493 elements in the granulation tissue under consideration.

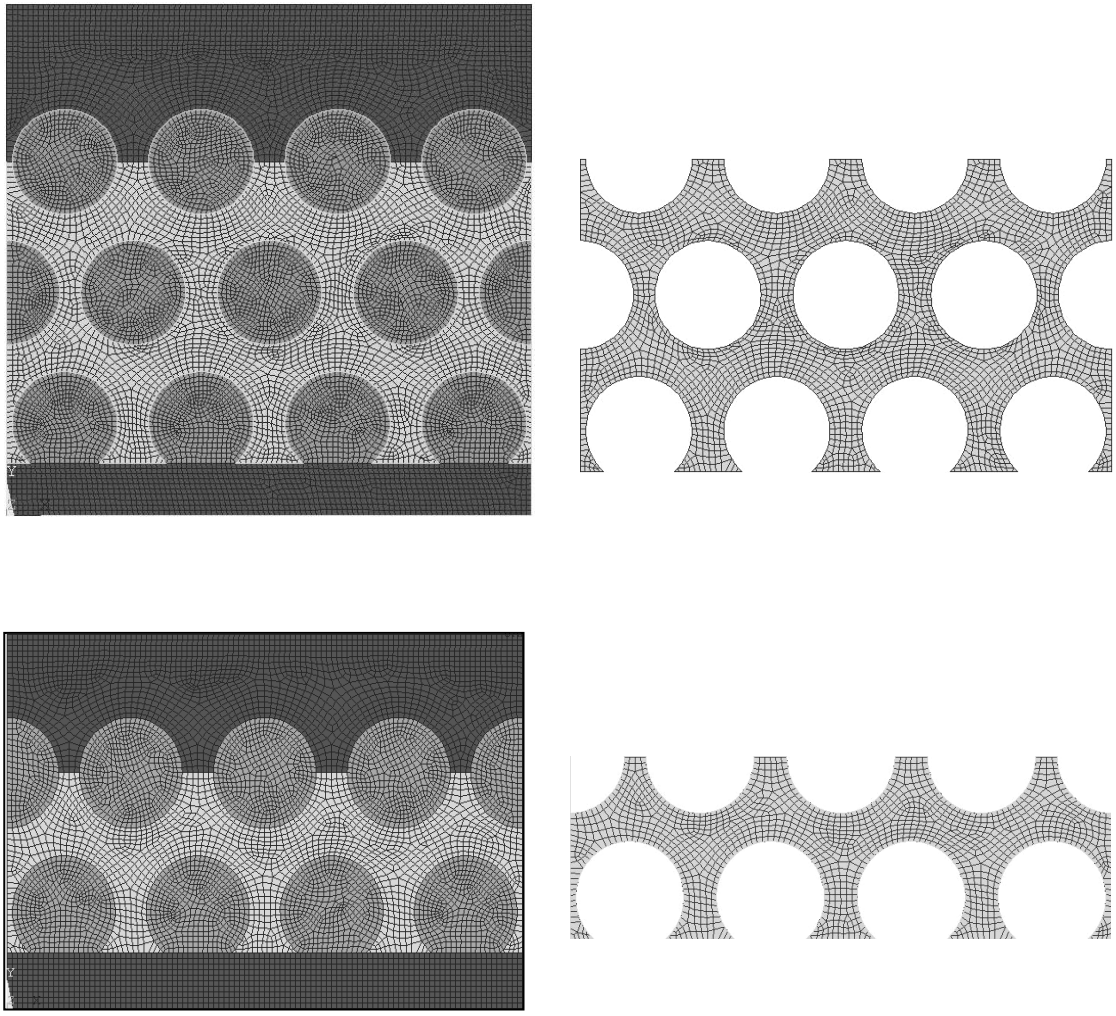

Figure 6.11: The finite element models used in the study (left) along with the area of interest (right). The three layer (top) and two layer (bottom) models are shown along with their pore space.

The boundary conditions used were similar to those used for the 3 layer study in the previous chapter; a compressive force was applied to the top surface of the bone, with micromotion applied as displacements at the same location. The lateral faces were simulated to be part of an infinitely long scaffold in situ. The substrate and beads were modelled to be rigid. These boundary conditions were the same applied to the three layer model; hence a direct comparison could be made on the tissue change in the pores. The same levels of micromotion were investigated, ranging from 1-100 microns. As reported in the last study, the emphasis was on the differentiation of the granulation tissue in the pore space. To maintain uniformity with the three layer model, the value of K used was

also kept the same based on the justification provided in the previous study and applied to the two layered model. This enabled a direct comparison between the two models.

6.6.4 RESULTS

The results are presented based on a visual and quantitative comparison of the type of tissue formed in both models with the same boundary conditions and loads. The percentage of the type of tissue formed in each case is reported. The results are shown with the plots of the differentiated tissue through three distinct stages at the start, the intermediate and the final iterations. The micromotion plots for each of the stages for the two models are shown in figures 6.12 - 6.15.

MICROMOTION = 1 MICRONS

Iteration 5

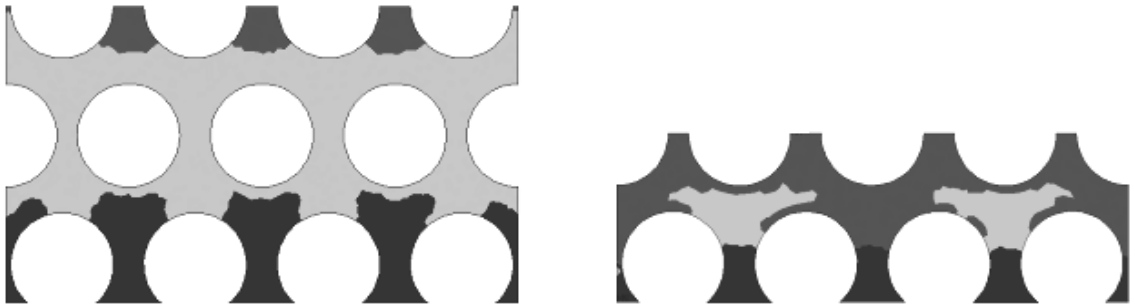

Iteration 10

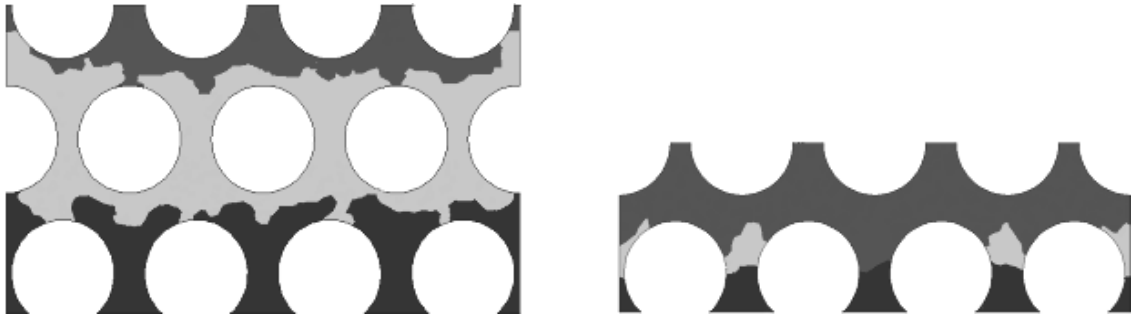

Stabilisation

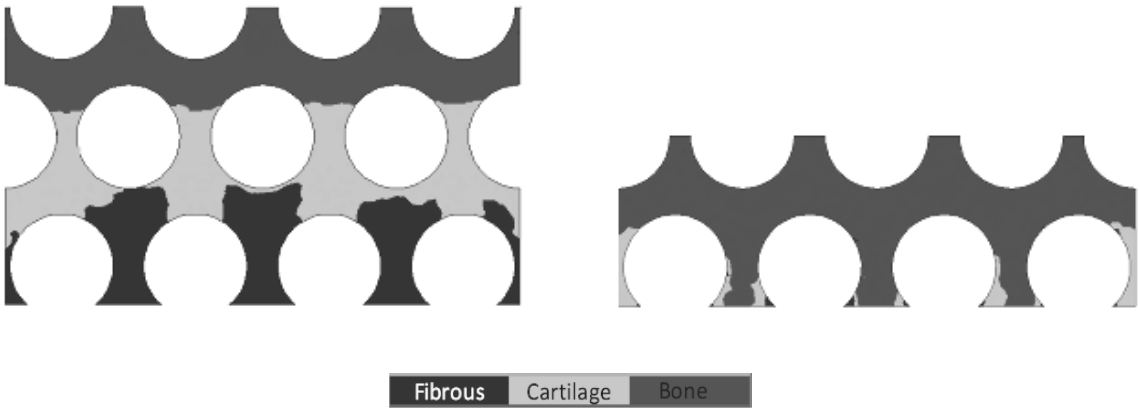

Figure 6.12: Tissue formation in the pore space for 1μ micromotion at the start (top), intermediate (middle) and at stabilisation of tissue (bottom).

MICROMOTION = 10 MICRONS

Iteration 5

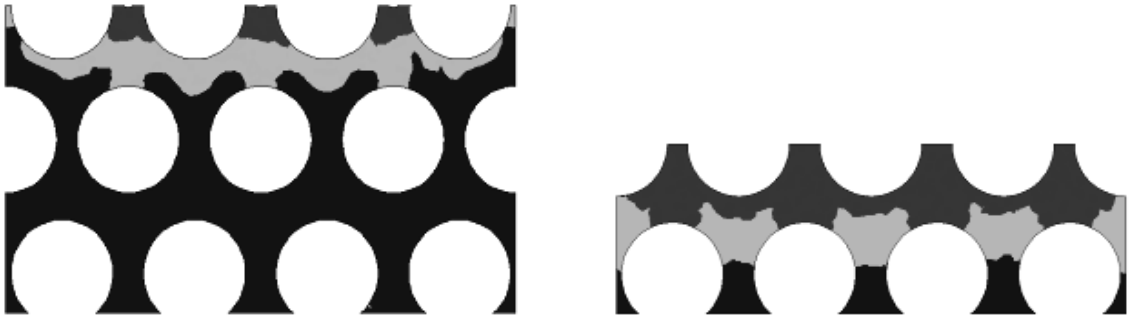

Iteration 10

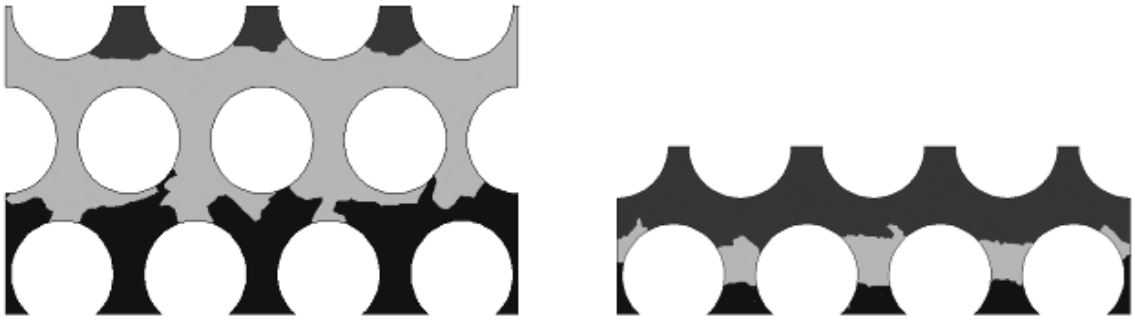

Stabilisation

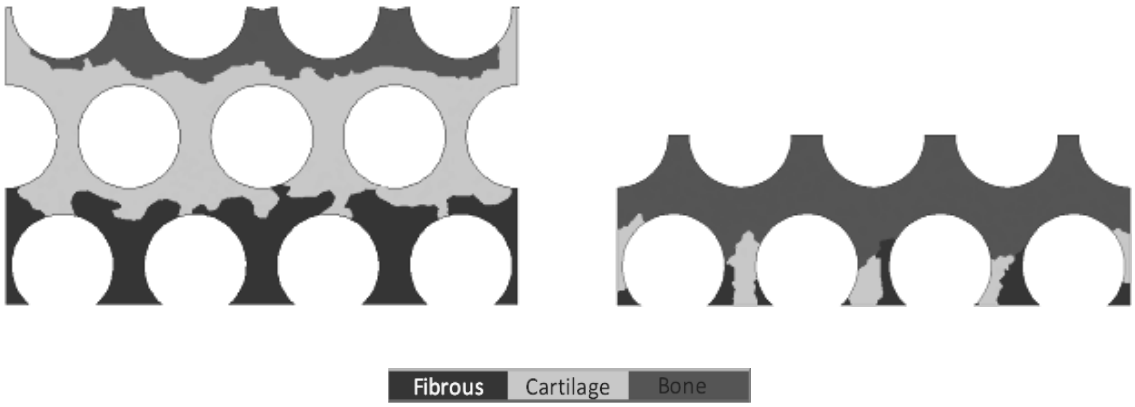

Figure 6.13: Tissue formation in the pore space for 10μ micromotion at the start (top), intermediate (middle) and at stabilisation of tissue (bottom).

MICROMOTION = 20 MICRONS

Iteration 5

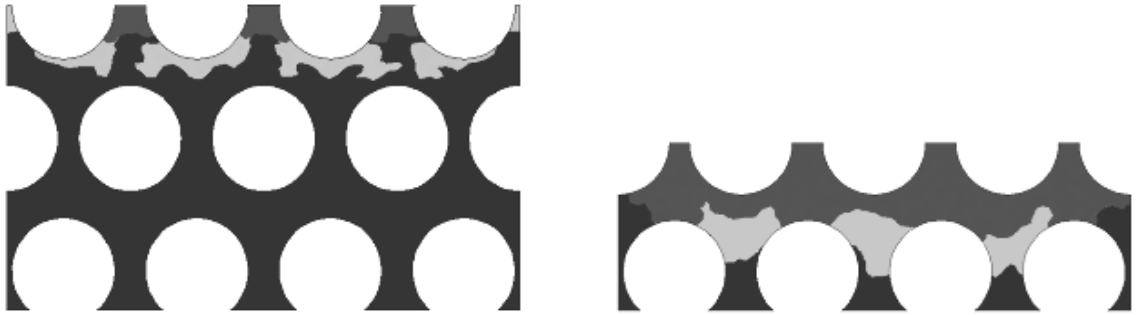

Iteration 10

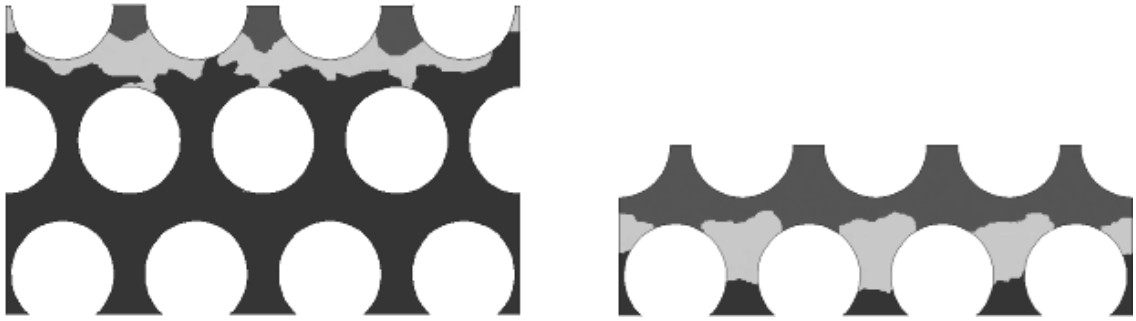

Stabilisation

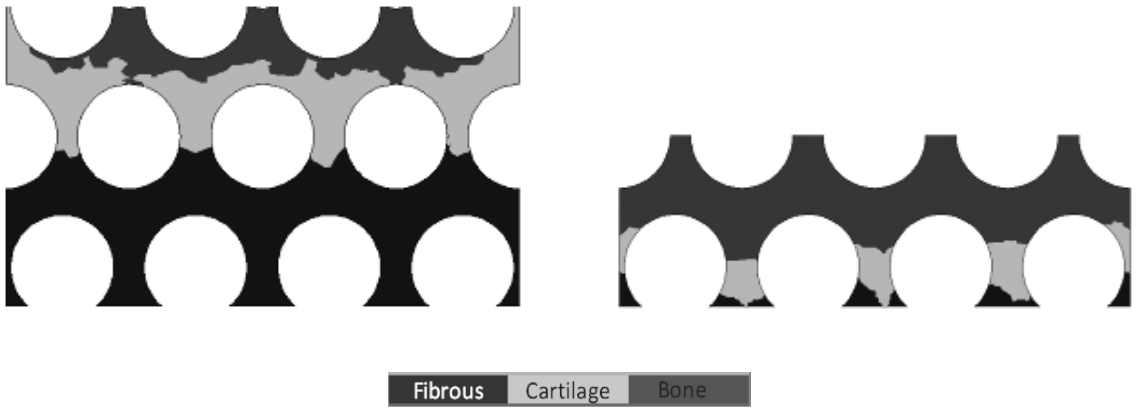

Figure 6.14: Tissue formation in the pore space for 20μ micromotion at the start (top), intermediate (middle) and at stabilisation of tissue (bottom).

MICROMOTION = 100 MICRONS

Iteration 5

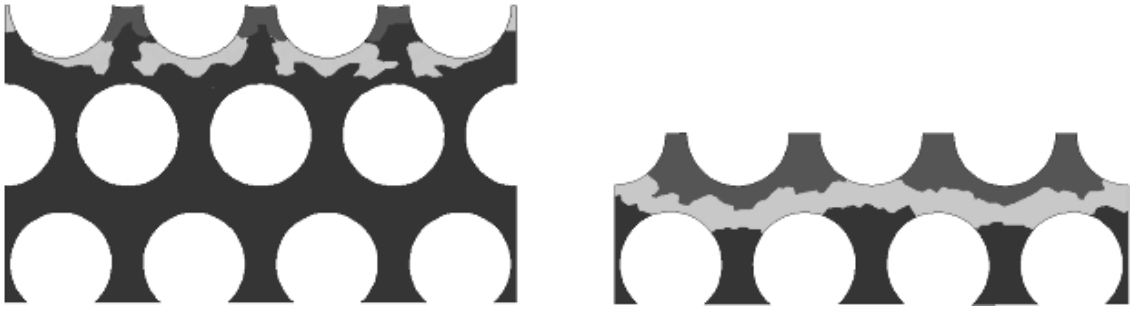

Iteration 10

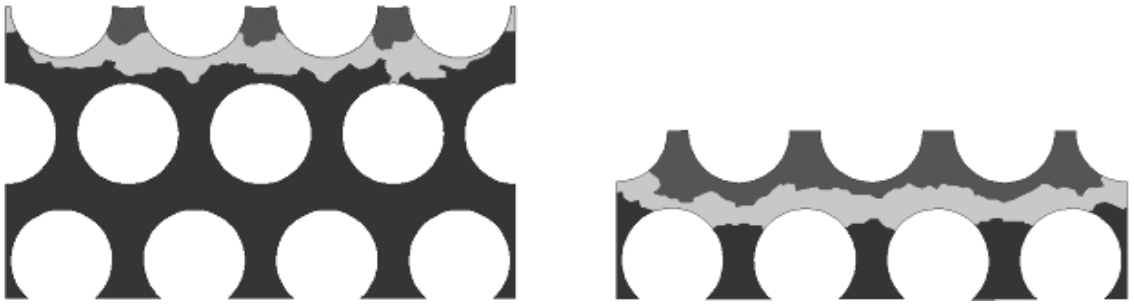

Stabilisation

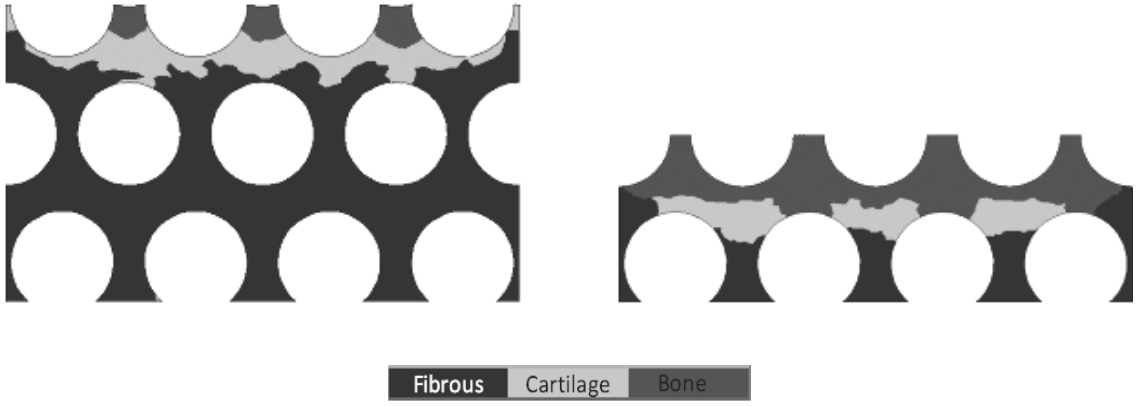

Figure 6.15: Tissue formation in the pore space for 100μ micromotion at the start (top), intermediate (middle) and at stabilisation of tissue (bottom).

The plots obtained for the tissue type formed in each case show that the two layered structure is more conducive to bone ingrowth when compared to the 3 layered structure. This is seen across all degrees of micromotion. In the case of the lowest level micromotion of 1 micron, there is very good bone ingrowth for both models. However, the 2 layered structure appears to be more stable, with excellent ingrowth even during the initial iterations, and additional interconnectivity of bone formed between the beads. During the last iterations, bone extends to the region near the substrate, with fibrous tissue accounting for only 1% of the formed tissue type. In the 3 layer case, during the initial stages, there is very little bone formation, restricted to the region between the top layer of beads. The major tissue types at this stage are fibrous and cartilage accounting for nearly 55% and 35% of the transformed tissue. However, during the final iterations, bone formation is substantial, increasing to about 35%, albeit, still well short of the 85% in the 2 layered coating. There is good interconnectivity of the bone formed at the top layer of the beads with a large formation of cartilage in the mid regions and a decrease in the formation of fibrous tissue.

For slightly higher levels of micromotion of 10 and 20 microns, still well under the values of micromotion that literature reports to be detrimental to ingrowth, the 2 layered model shows more ingrowth of bone, but considerably reduced to that formed in the 1 micron case. For 10 microns micromotion, bone occupies the top layer completely with interconnectivity between the beads during the initial iterations and increases as the iterations progress to occupy regions around the bottom layer of beads. The percentage increase in bone tissue is nearly 40% from the start to the finish of the iterations. For the three layered structure, the starting stages are similar to the 1 micron case, with respect to bone formation. Fibrous tissue occupies most of the differentiated tissue space at the start and is gradually occupied by fibrous tissue in the later stages. Bone formation is not substantial and at the end of the iterations, occupies only 20% of the tissue space, around the top layer of beads. Cartilage formation is prominent in the mid regions with fibrous tissue formation along the pore space near the substrate.

For an intermediate micromotion value of 20 microns, the amount of fibrous tissue formation increases in the 3 layered model and is the prominent tissue type formed for most iterations. This reduces towards the final iterations, but is still considerably large, occupying nearly 50% of the pore space. Bone tissue formed is similar to the 10 micron case through the iterations, occupying 16% of the pore space, restricted to in and around the pore space near the topmost layer of beads. The two layered model follows the 10 micron micromotion case as well, with steady bone ingrowth, but restricted to the top layer of beads and no formation near the substrate. Cartilage and fibrous tissue occupy the mid and bottom regions respectively. The total amount of bone formed occupied nearly 70% of the pore space with cartilage and fibrous tissue accounting for 20% and 10% respectively. A comparative graph showing the percentage of tissues formed for the models for different levels of micromotion is shown in figure 6.16.

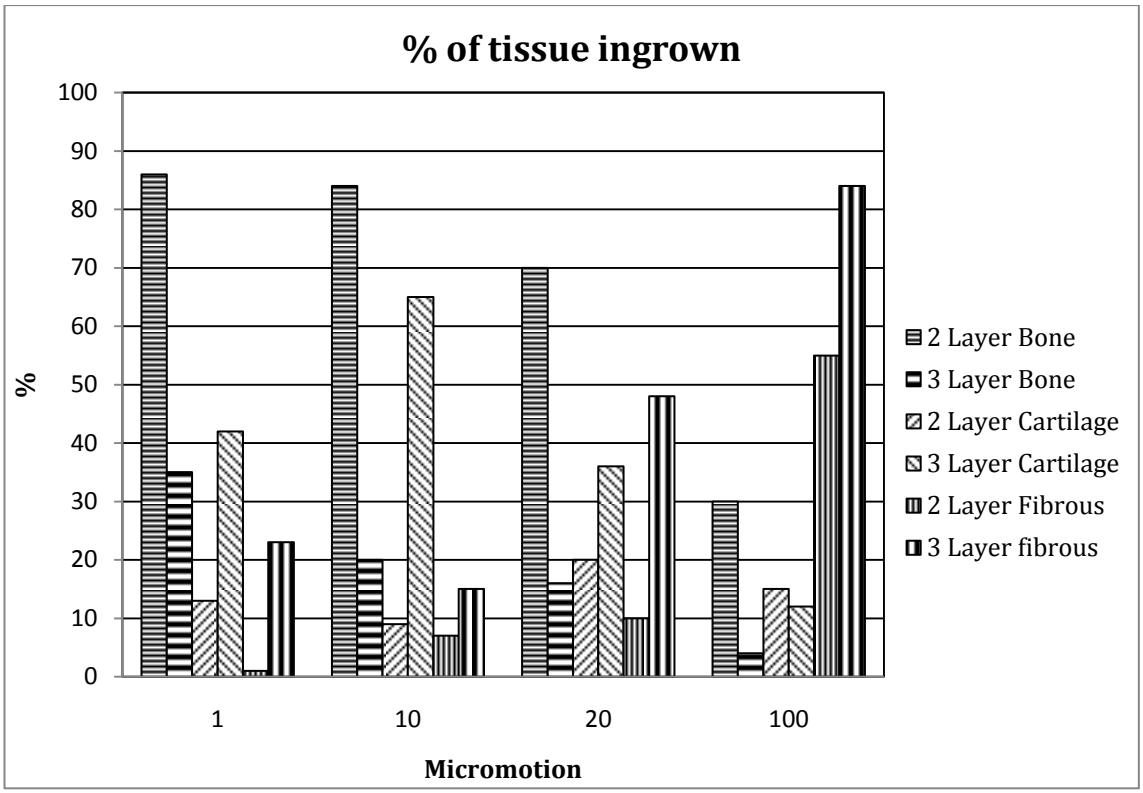

Figure 6.16: A combined graph of tissue type formed for the two and three layer models for different levels of micromotion.

For the highest micromotion case of 100 microns, bone formation in the pore space is limited for both models, particularly for the 3 layered structure. Considering the amount of bone formed throughout the iterations, there is less than a 3% change with a final resting value of well under 10 % tissue formed. The majority of the tissue is fibrous, filling up nearly 85% of the pore space. The situation is similar for the 2 layered structure with total bone formation of 30% at the end of the iterations, the lowest for all micromotion levels considered. Fibrous tissue is again prominent, filling up the pore space near the substrate and mid regions. 55% of the pore space is fibrous with around 15 % of cartilage tissue formed.

6.6.5 DISCUSSION

For large degrees of micromotion at the surface of the bone, the differentiation of granulation tissue to fibrous tissue was expected for both models. As seen in the previous chapter and extensively in literature, large micromotions have a detrimental influence on bone ingrowth and encourage fibrous tissue formation [6,7,143,266] . However, in the current study, the two layer models clearly display more bone ingrowth, particularly at lower micromotion values, even at high levels of micromotion.

In an animal study by Simmons et al. [155] comparing osseointegration in a 2 layer beaded coating on an implant to a plasma spray coated one, it was reported that the beaded coating showed more rapid and extensive osseointegration, with greater attachment strength and interfacial stiffness. Although plasma sprayed coatings have not been considered due to the complexity involved in modelling the coated surface, a similar outcome is observed in the current study. Bone formation is observed to be rapid, which can help reduce further micromotion at the interface and encourage more bone formation. For all micromotion values, there is rapid bone and cartilage formation that helps stabilise the interface and promote stronger tissue formation for the remainder of the iterations. This further helps reduce fibrous tissue formation, limiting it to mostly regions near the substrate. Figure 6.17 shows the regions of osseointegration for the beaded coating found in the Simmons et al. study.

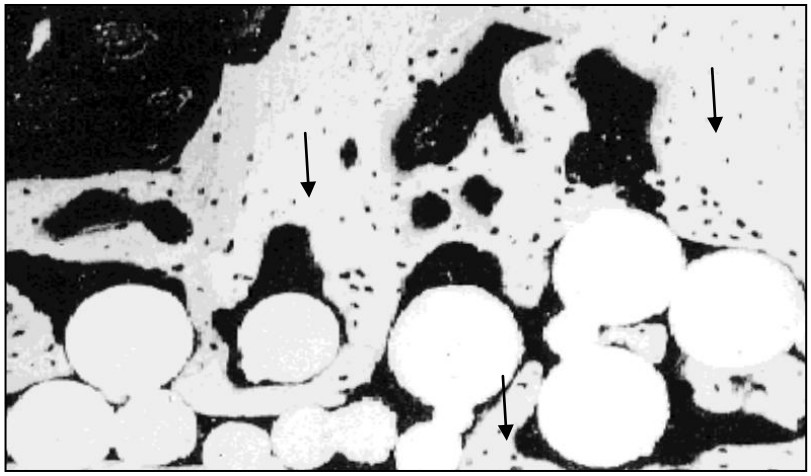

Figure 6.17: Back-scattered electron micrograph of the 2 layer beaded porous coated surface after 16 days post implantation. White regions (shown by the arrows) depict regions of osseointegration[155].

Mechanical integrity of the coating is extremely important in preventing delamination or wear of particles from the coating that may result in osteolysis. While having only a single layer may compromise on the tensile strength, too many layers can cause delamination of the beads in the top layers of the coating. Debris from beaded coatings due to repetitive loading has been cited earlier [280]. Pilliar et al [281] reported that this could be avoided if the porosity could be reduced, but a potential pitfall of this would be the diminished availability of space for tissues to form. Conversely, by employing many layers, other than mechanical integrity problems, the penetration depth for tissues being too large in coatings also remain a worry.

As noted in the previous chapter, computational simulations inevitably include simplifications and assumptions. In addition to the issues raised in the previous chapter, the results obtained in the study cannot be directly compared to literature due to the approximations made during the

formulation of the algorithm and the exclusion of biological effects so essential for bone ingrowth. Based on mechanical conditions alone, the results are promising; favouring the two layered beaded structure. However, according to a clinical study by Friedman et al [153], comparing different surface textures that included two different beaded configurations of one and three layers, along with plasma sprayed and arc deposited surfaces, it was found that for bone ingrowth, although the short term results favoured the single layer structure, the long term effects were similar in both configurations. The amount of ingrown bone was similar at the end of the 12 week test period with around 60% apposition to bone. The conclusion of the study was that at the end of the testing period of 12 weeks, there was no advantage of multiple layers of beads on bone ingrowth. If this result is applied to the *in silico* model, it can be hypothesised that the good bone ingrowth shown for the two layered structure can be attained by the three layer model as well, if the methodology used modelled temporal aspects of tissue differentiation.

There are limitations to the model that need to be considered. Firstly, the models are simplifications of the actual beaded coating geometries. Other than the simplification of the three dimensional geometry as a two dimensional one, the structure has been idealised for ease of simulation. In reality, the sintered beads would have a randomised scatter on the substrate and the periodic arrangement described in the study would occur less frequently due to the variations in the sintering process. The prediction of tissue formation for both the geometries needs to be corroborated by experimental data by incorporating mechanical and biological factors. Currently, the algorithm works based on mechanical stimuli but literature has shown that biological factors can be responsible for bone formation from within the porous coating, from on or near the substrate and extending towards the interface [122]. Simulating this would require extensive experimental or clinical data which is currently not available in literature.

To conclude, based on the results obtained in the simulation, it can be hypothesised that the two layer model has its advantages with rapid bone ingrowth for low and high levels of micromotion. This could lead to very early stabilization of the implant and minimize micromotion that could encourage more bone ingrowth. The two layer structure also presents a more stable structure mechanically to encounter shear forces at the interface. The three layered structure, although reported to have almost equal bone ingrowth long term [153], does not provide the implant the rapid initial bone ingrowth to stabilize the implant from further micromotion. The three layers also protect the tissue between the pores from mechanical effects that could be detrimental to bone formation as granulation tissue needs to be stimulated, albeit with low mechanical stimuli, for it to differentiate and encourage osteogenic cells to the site. This is particularly notable in regions near the substrate. The two layered structure provides the appropriate mechanical stimuli for the tissue in between the pores to differentiate into bone. Overall, based on short term results in this study, the two layered structure presents a distinct advantage over the three dimensional counterpart.

CHAPTER 7

DISCUSSION AND CONCLUSIONS

This chapter aims to summarise the work presented in the individual chapters with emphasis on the novelty and impact of the findings in a clinical setting. The chapter is presented in three main sections; **motivation**, addressing the importance and the need of the research presented; **novelty**, accentuating the findings of the case studies on implant design through the deployment of the novel algorithm and the **application** section, covering overall conclusions, implications of the research and its potential use as a preclinical testing tool for predicting implant behaviour.

7.1 MOTIVATION

The number of hip replacement surgeries is on the rise in many countries as evidenced in the national joint registries of various countries [2,50,59,137,282]. This may be expected, with the benefits of THA extended to the younger more active patient and the improved quality of life possible post implantation, including pain relief and a resumption of normal activities. However, the marked increase in the number of surgeries includes both primary and revision hip procedures. To exemplify the rise in revision surgeries, according to the national joint registry of England and Wales, there was an overall increase of around 1000 hip procedures reported in 2010 in comparison to 2009, with revision procedures alone accounting for 10% of this increase, a 1% increase in a one year period [2]. Although hip replacements have enjoyed good clinical performance with survivorship of over 95% at 10 years [2,50,59,137,282], the aforementioned example shows that primary hip replacements are by no means fail-safe and implant longevity remains a concern. With the average age of patients requiring primary hip surgeries decreasing every year, and considering the active life they lead and the resultant higher demands on the implant, the onus is on providing a long lasting, well functioning implant and reducing the need for a revision procedure.

Other than patient trauma, the socio-economic problems associated with primary and revision surgery are high, with the burden on manufacturers, hospitals and surgeons to provide the best suited implant and procedure at the risk of not compromising patient activity and comfort. The economic burden and the need to reduce revision rates is further justified with revision surgeries costing nearly twice as much as primary hip surgeries [283]. With regards to fixation, cemented stems have traditionally enjoyed a higher rate of use worldwide [59]. However, problems associated with cemented fixation such as osteolysis, necrosis and debonding have resulted in uncemented implants experiencing a strong rise in usage over the last few years, even more so than cemented implants in many countries [2,137,282]. This is not to say that uncemented implants have better longevity, but with improvements in implant design, comparable survivorship, and the age of patients requiring hip arthroplasties decreasing, the potential benefit of long term biological fixation offered by uncemented implants has proven popular. In addition, concerns over the costs associated with uncemented implant surgeries have also been alleviated as studies have shown that the overall cost is similar, if not less than that of cemented implant surgery [284,285]. Improvement of implant design, leading to better stability and osseointegration at the interface together with improved instrumentation and surgical techniques are vital to achieving a long lasting, well functioning implant. However, new designs would require extensive preclinical testing. Implants that are under evaluated can lead to early failures as seen in the early recall of 3M capital hip prosthesis and more recently, the ASR resurfacing system (MDA hazard HN9801 and MDA/2010/069 respectively). Comprehensive preclinical testing of these implants through a combination of computational and experimental tests can help minimise the occurrence of such incidents.

Preclinical testing can help avoid potential problems by exploring possible failure scenarios and proposing design changes that can improve the functional performance and longevity of the implant. Factors such as implant micromotion, migration and subsidence can be measured through the use of mechanical testing machines [6,100,286] but others, such as osseointegration cannot be explored as it is an adaptive process and would require a combination of biological and mechanical inputs that could prove to be extremely difficult to replicate *in vitro*. In addition, whereas new designs can be tested through mechanical testing, it can prove to be cumbersome, expensive and time consuming if design changes have to be incorporated based on the outcomes and fed back to the initial design stage in a repetitive process. In this case, computational evaluation through finite element models could prove beneficial due to its adaptability in incorporating new changes in a rapid manner. Parametric changes to loading and boundary conditions can be easily controlled and adjusted as per user requirement. While static models can be used to obtain specific outputs; dynamic inputs can also be incorporated in finite element models giving users complete control over the simulation.

Adaptive finite element models have been used extensively in the past to simulate different scenarios such as bone fracture healing [20,212,214-217,287-289] and bone remodelling around an implant [207,290-295]. Implant interface behaviour has also been simulated, albeit in a few computational studies [21,234,269]. These studies have mainly focussed on the consequences of the lack of bone ingrowth or excessive micromotion at the interface without actually modelling the processes adaptively over time. Studies specifically dealing with tissue differentiation at the interface have also been very limited. Of the few studies that have looked at this, the focus has either been on simulating experimental set ups with animal studies or simulating activity around implants in two dimensions [8,164,296].

The current work aimed to add to the limited number of computational studies that have attempted to simulate tissue differentiation around implants. In particular, the studies presented in this thesis aimed to investigate design factors that could prove beneficial to osseointegration. Previous studies have only investigated static models, with the results used to hypothesise what would take place at the interface. For example, micromotion plots at the interface showing regions of eventual osseointegration or fibrous tissue formation. These studies have not shown the evolution of tissues at the interface through an adaptive process. If a tool, in this case a predictive algorithm based on finite element modelling can be formulated and verified, it could be used to predict how an implant design could influence tissue differentiation around it, specifically osseointegration. This could prove beneficial for the prediction of long term interfacial behaviour of novel implants, which would normally not be possible to predict through conventional testing, and help eliminate weak or dubious implant designs or features, and emphasise the designs that can contribute to better osseointegration.

7.2 NOVELTY

The novelty of the work arises from the development of the new algorithm and its subsequent implementation to investigate design features of implants on tissue differentiation. This has been carried out by extending an existing mechanoregulatory hypothesis devised by Carter et al [23] for fracture healing, which was originally qualitative (described in detail in chapter 3), and modifying it to simulate actual tissue differentiation rather than predicting patterns of osteogenic index. Two methods have been formulated, in differing complexities, and implemented to study the behaviour of different implants and their specific design features. The main advantage of the algorithm is its simplicity and adaptability to study implant behaviour. Although other hypotheses and algorithms have been developed, the author is not aware of any similar study that has dealt with their application to studying implant design. The algorithm has been employed successfully for a number of case studies involving various implant designs and features to show progressive and iterative formation of tissues, proceeding until stabilisation. Demonstrating good corroboration with clinical studies as shown in the case studies, the algorithm has potential to be used as a qualitative indicator to predict implant interface behaviour and provide surgeons and implant manufacturers a tool to investigate various implant designs for ingrowth prior to implantation.

A recent advancement in the field of uncemented implants has been the development of short stemmed implants. These were developed in an attempt to minimise a number of long term problems that have been observed in conventional long stemmed implants such as proximal bone atrophy, thigh pain, extensive remodelling and stress shielding (see literature review section). There are a number of short stemmed implants in the market currently and tissue differentiation around one such implant, the Proxima has been simulated. The implant employs some specific design features such as the prominent lateral flare that has specifically added to provide stability and load the proximal femur adequately, preventing atrophy and loosening in the region due to stress shielding. Although the study presented in chapter 4 does not explicitly address this, the tissue differentiation patterns found around the implant justify the inclusion of the particular design aspect with bone formation around the region. The results obtained in the study have corroborated well with short term results seen in radiographs obtained from clinical studies. To evaluate the effect of the flare itself, a separate study detailing tissue formation without the flare was carried out and compared to the original implant. A difference in tissue differentiation patterns, particularly in the quantity, location and rate of bone and fibrous tissue formation was observed. The implant incorporating the lateral flare showed more bone formation around and under the lateral flare when compared to the non flared model. Thus, the study shows the importance of incorporating specific design features, in this case the lateral flare, to enhance osseointegration.

Long stemmed diaphyseal loading stems have been used successfully for the last three decades and a good example of such an implant is the anatomic medullary locking implant (AML). Literature on

the AML demonstrate excellent clinical results for both short and long term follow ups of the implant [252]. Currently, the AML is used in its extensively coated version with a design not dissimilar to when it was first introduced. The stem of the implant has increased in diameter compared to the original design. Concerning the extent of porous coating used, the implant has not always been fully coated and different coating lengths have been investigated with the intention of avoiding proximal stress shielding and achieving bone ingrowth. Clinical results have not demonstrated a preferable coating coverage for optimising bone ingrowth and avoiding problems associated with stress shielding [174,250,254]. The present work found that the fully coated implant induced bone formation along the entire length of the stem in contact with the diaphysis, corroborating well with clinical results. It was also found that the proximally coated version experienced a slightly higher percentage of bone ingrowth for its available surface area compared to the other coating geometries. However, the fully coated implant showed more overall bone formation due to the larger surface area available over the entire length of the stem, whilst exhibiting comparable results to the proximally 1/3 and 3/4 coated implants in terms of percentage bone ingrown. This could provide additional support for the prosthesis. As there was no advantage to the proximally coated implant over the extensively coated implant in terms of bone ingrowth, and the latter offering larger areas for osseointegration, it was shown that extensively coating long stemmed implants is justified as a favourable option.

The effect of micromotion has often been cited in literature of having a strong bearing on the type of tissues formed at the interface (as detailed in chapter 2) and this has been computationally explored in chapter 6 in the form of a microscale model of a popular type of porous coating. Tissue differentiation in a typically used three layered beaded coating was investigated for different levels of micromotion, which was structured based on a similar study by Liu et al.[297], but carried out with a different mechanoregulatory algorithm. Although the cited study was more complex as it incorporated a remodelling segment in addition to tissue differentiation, based on the results obtained without the addition of the segment, the results of the two studies were comparable. The addition of the remodelling segment in the cited study underestimated bone ingrowth within the pores but agreed with the general trend of higher micromotion levels decreasing bone formation. The observations of the current study also corresponded well with literature from clinical and animal studies with increasing levels of micromotion resulting in less bone and more fibrous tissue formation. The algorithm was then employed in a comparative study to investigate the difference, if any, of employing different levels of the beaded coating (by investigating the layered structure; three layered versus two layered) on tissue differentiation. Few studies have investigated this clinically, with animal studies often proving inconclusive in terms of highlighting a preferential type of coating [153]. However, the present results suggest a two layered coating offers better bone distribution with interconnectivity between the beads when compared to the typically used three layered structure. This was observed for all levels of micromotion simulated, particularly pronounced for lower micromotion values. Although more complex models would be required to build confidence for application in a clinical setting, the findings of the study suggest that the two

layered beaded coatings may perhaps be a better alternative. This could potentially have implications on future porous coatings designs on uncemented implants.

The aim of the project was twofold; firstly, to successfully simulate tissue differentiation around uncemented hip implants which included development of an algorithm based on an existing mechanoregulatory hypothesis. Secondly, to apply the algorithm for the assessment of various design features in uncemented implants that would be beneficial to osseointegration of the implant that could secure long term stable fixation. The application of the algorithm has included old and new implant designs with their associated features. Finer design features like the extent of the porous coating used and the design of the beaded coating itself have been investigated. This, to the author's knowledge, is the first time that such work has been undertaken to this detail. Related studies have focussed primarily on the development of suitable algorithms and not exploring the influences of design on osseointegration. Stability and micromotion studies for different implants have been implemented computationally [269], however long term effects in terms of regulating tissue differentiation at the interface through an iterative, adaptive model has not been carried out. The case studies presented have addressed this through the use of the novel algorithm developed.

7.3 APPLICATION

A thorough understanding of osseointegration and the computational tools required to simulate the process is provided in the literature review of this thesis. However, it is the methodology adopted in the current project that is of significance in the context of this thesis. The technique of combining finite element models with an underlying mechanoregulatory algorithm enables dynamic simulation of tissue differentiation. This is not just limited to the current work; the methodology can be modified to suit different adaptive processes related to skeletal morphology and adaptation.

A particularly important aspect of the research lies in its application to implant design and development. The microscale and macroscale models that have been used to simulate tissue differentiation in this thesis provide valuable information on design features that can be considered important for osseointegration and also comments on others that may have a less significant effect on the process. Literature has cited aseptic loosening of uncemented implants to be a direct result of the lack of osseointegration at the bone-implant interface [266] and various implant designs and surface coatings have been developed with a view to promoting osseointegration. If the inclusion of certain features encourages osseointegration of the implant, these can then be incorporated. Another advantage would be patient specific implant selection based on the type and quality of the femur. This would be particularly useful if there are abnormalities in the femur or pre-existing conditions that may compromise the longevity of the implant. However, it has to be acknowledged that altering implant design to suit long term stable fixation is one thing, and accounting for functional performance is another issue altogether. Design changes made to promote

osseointegration should not compromise other factors such as range of motion, wear, and positioning to name a few that could also lead to early failure of the implant.

The methodology developed and described in this thesis can be used in conjunction with other techniques (described below) to provide a holistic representation of interface healing and behaviour post implantation; however, as with any computational study, the findings must be assimilated within context of its limitations. One such limitation is the assignment of peak forces to represent normal walking and stair climbing loading. Musculo-skeletal models have been developed in conjunction with finite element models to study strain in the implanted femur at different points in the gait cycle [16]. Although computationally very expensive, if the current algorithm is combined with these models, a more accurate representation of tissue differentiation through time can be obtained. Another limitation of the work is that biological processes such as cellular influences, systemic factors and blood supply have not been simulated. All of these factors have been highlighted in literature (Chapter 2) as influencing osseointegration at the interface. However, the dearth of specific information and values for simulating these processes for implant healing has prevented their incorporation into the methodology. Unlike fracture healing which has been extensively reviewed through animal and clinical studies, if more information relating to these parameters are available in the future, they can then be combined with the developed algorithm to provide a more descriptive and comprehensive model. In addition, there is also the possibility of adapting the algorithm for probabilistic studies to investigate implant related and positioning factors that can influence tissue differentiation at the interface. Dopico-Gonzalez et al [298,299], for example, found that that implant design, positioning and femur characteristics affected strain and micromotion at the interface; the current study if combined with such techniques can help determine the ideal positioning and design to promote osseointegration at the interface. Thus, the algorithm can be easily adapted and added to other research approaches to enhance the performance and longevity of the implant. Even as a stand-alone component, the algorithm and the associated features can be used to get a qualitative idea of how an implant would behave, if preoperative CT scans of patients are available and correct implant sizing and position templating were carried out prior to implantation. Considering fixation alone, the long term predictive capabilities could help in decision making at the preoperative stage for a specific patient.

To summarize, the developed algorithm that has been described and implemented in the chapters presented in this thesis have successfully predicted tissue formation, especially osseointegration around implants. The predicted patterns have matched closely with those reported in literature in the case of well documented implants and identified key locations in others that have not been so well documented due to their recent advent and short implantation time. The algorithm has potential to be used as a preclinical testing tool to predict long term interface behaviour of novel implants. Moreover, design features that are beneficial to osseointegration at the interface have been identified and can be incorporated in other novel implants. In light of the limitations described above, the results obtained could be used to gauge qualitatively how certain implant

designs could influence the process positively or adversely. The author believes that the work presented contributes in a positive way to the betterment of implant design through prediction of long term interface behaviour. The author agrees that for any pre clinical testing tool to be successful and minimise long term failure of implants, there should ideally be complimentary tests that cover different possible scenarios. While prediction of implant behaviour through novel computational methods provides a good first step, laboratory testing and clinical testing will always be necessary to ensure other potential modes of failure are highlighted, and in turn inform further computational modelling efforts.

CHAPTER 8

FUTURE WORK

This chapter elaborates the improvements, additions and modifications that can be incorporated in the current work to improve its clinical relevance and applicability.

The previous chapter has briefly described some of the applications of the current work. In addition, the limitations of the work have also been elucidated in the individual chapters. Based on these, there are a number of improvements and additions that can be incorporated in the future. A few of these are addressed in more detail in this chapter.

Concerning the development of the algorithm from the mechanoregulatory hypothesis, the rationale for selection was the simplicity and the extensibility (shown by the quantitative development) of the hypothesis. However, issues remain on some aspects of the implementation, especially the value of K that has been chosen for the studies. In the original study by Carter, the value was chosen based on results obtained clinically for fracture healing. In the current work, K values have been chosen based on comparison to similar studies and/or short term radiographic evidence or information gathered from literature. While this may be reasonable for the work carried out in this thesis, a better technique for the determination of K needs to be devised if the algorithm is to be applicable widely. Another improvement that can be made is the inclusion of biological and systemic factors in the study. Studies by Lacroix and Prendergast et al.[217,220] have included cellular activity by considering cell sources from the surrounding environment such as the periosteum and the muscles. While this would be apt for fracture healing, implant healing presents a different scenario with the marrow providing the majority of cells. If more research into the contribution of bone marrow to cell differentiation around implants is carried out, cell specific factors can be included and the algorithm strengthened. On a similar note, the influence of blood, oxygen and nutrient supply if simulated, can also be highly beneficial. Some of these have already been investigated independently [289,300] for different applications. Therefore, the incorporation of biological process to the existing algorithm could be highly beneficial and critical to simulating implant healing successfully.

Increasing the complexity through the addition of new features is another future work area to be explored. As briefly mentioned in the applications section in the previous chapter, boundary and loading conditions used in the studies can be improved by incorporating more complexity. Rather than use peak forces on specific muscle groups during stair climbing and normal walking as has been carried out in the work, if the forces at different points in the gait cycle can be incorporated, along with the relevant boundary conditions, the results obtained would be more accurate and representative of what occurs in reality. Activities and their duration and frequency have been studies previously in literature [44] and if combined with the relevant loading information, can then be used to simulate implant healing on a temporal scale. This could have a positive outcome on the healing and rehabilitation regime a patient should be put through following an uncemented hip arthroplasty.

Another future work would be to develop a tool to assist the surgeon plan an uncemented hip arthroplasty in view of obtaining excellent initial stability and maximum osseointegration. Probability studies for implant positioning have shown that some positions may be better than

other to reduce bone strain and micromotion [299] and this information could be added to the work presented in this thesis to predict bone formation under various positions and hence determine which would be ideal long term for osseointegration.

Micromotion, which has only been briefly in the microscale scale study, also needs to be incorporated in the macroscale model. While the presence of an adaptive tissue layer presents a challenge, other modelling methodologies, such as those employed by Kadir et al [269] and Keaveny et al [234] can be employed to include micromotion as a parameter to regulate tissue differentiation, using values obtained from literature for determination of limits for tissue formation. In addition, another important addition that can be incorporated to the existing work is a remodelling component. As literature as shown, remodelling and tissue differentiation occurs simultaneously and if both these processes can be implemented together, the results obtained could be more accurate. This has only been carried out in a two dimensional model for a coating [219] and not in a full implant model. Similarly, the changes to the bone surrounding the implant has not been considered and adding remodelling to the simulated tissue in addition to the surrounding bone would be more accurate representation of conditions *in vivo*.

A final and vital area of further work would be experimental data to corroborate the results obtained in the work presented in this thesis. Retrieval studies and results from radiographs have been an integral part of corroborating the results obtained in the study. The complexities involved in simulating the work experimentally are difficult to overcome; but smaller, specific experiments that can contribute to the accuracy of the algorithm can be included. For example, mechanical stimulation of osteogenic cells on a porous coating can help understand the stimuli needed for cells to differentiate, proliferate and form bone. Overall, the work presented in this thesis is well rounded and aims to answer many research questions but as is the case with research in any field, it can always be improved and executed better.

CHAPTER 9

APPENDICES

Supplementary material referenced in various chapters in the main body of this thesis is presented in this chapter.

9.1 APPENDIX A: REFERENCES

[1] 2009. Swedish Hip Arthroplasty Register.

[2] 2010. National joint registry, England and Wales.

[3] 2008. Canadian Joint Register. Joint Register.

[4] 2008. Australian Joint register.

[5] Davies JE. 1996. In vitro modeling of the bone/implant interface. The Anatomical Record 245: 426-445.

[6] Burke DW, O'Connor D, Zalenski EB, Jasty M, Harris WH. 1991. Micromotion of cemented and uncemented femoral components. Journal of Bone and Joint Surgery Br 73B: 33-37.

[7] Jasty M, Bragdon CR, Burke D, O'Connor D, Lowenstein J, Harris WH. 1997. In vivo skeletal responses to porous-surfaced implants subjected to small induced motions. Journal of Bone and Joint Surgery Am 79: 707-714.

[8] Prendergast PJ, Huiskes R,Soballe K. 1997. Biophysical stimuli on cells during tissue differentiation at implant interfaces. Journal of Biomechanics 30: 539-548.

[9] Huiskes R, Van Driel WD, Prendergast PJ, Soballe K. 1997. A biomechanical regulatory model for periprosthetic fibrous-tissue differentiation. Journal of Materials Science: Materials in Medicine 8: 785-788.

[10] Engh CA, O'Connor D, Jasty M, McGovern TF, Bobyn JD, Harris WH. 1992. Quantification of implant micromotion,strain shielding, and bone resorption with porous-coated anatomic medullary locking femoral prostheses. Clinical Orthopaedics and Related Research 285: 13-29.

[11] Jasty M BC, Maloney WJ, Haire T, Harris WH. 1991. Ingrowth of bone in failed fixation of porous-coated femoral components. Journal of Bone and Joint Surgery Am 73: 1331-1337.

[12] Hamblem DL, Paul JP. 1988. The integrity of porous coatings for cementless implants. Journal of Bone and Joint Surgery Br 70B: 521-523.

[13] Jasty M, Bragdon CR, Haire T, Mulroy RD Jr, Harris WH. 1993. Comparison of bone ingrowth into cobalt chrome sphere and titanium fiber mesh porous coated cementless canince acetabular components. Journal of Biomedical Materials Research 27: 639-644.

[14] Turner TM, Sumner, Urban RM, Rivero DP, Galante JO. 1986. A comparative study of porous coatings in a weight-bearing total hip arthroplasty model. Journal of Bone and Joint Surgery Am 68: 1396-1409.

[15] Huiskes R, Van-Rietbergen B. 1995. Preclinical testing of total hip stems: The effects of coating placement. Clinical Orthopaedics and related research 319: 64-76.

[16] Manders C, Taylor M. 2010. How does the position of a hip replacement affect the femoral strain? Journal of Biomechanics 43: S47.

[17] Bergmann G, Graichen F, Rohlman A 1993. Hip joint loading during walking and running, measured in two patients. Journal of Biomechanics 26: 969-980.

[18] Bergmann G, Deuretzbacher G, Heller M, Graichen F, Rohlmann A, Strauss J, Duda GN. 2001. Hip contact forces and gait patterns from routine activities. Journal of Biomechanics 34: 859-871.

[19] Zannoni C, Mantovani R, Viceconti M. 1998. Material properties assignment to finite element models of bone structures : a new method. Medical Engineering & Physics 20: 735-740.

[20] Lacroix D. 2000. Simulation of tissue differentiation during fracture healing. PhD Thesis.

[21] Ramamurti BS, Orr TE, Bragdon CR, Lowenstein JD, Jasty M. 1997. Factors influencing stability at the interface between a porous surface and cancellous bone: A finite element analysis of a canine in vivo micromotion experiment. Journal of Biomedical Materials Research 36: 274-280.

[22] Isaksson H, Wilson W, Corrinus C, Donkelaar V, Huiskes R, Ito K. 2006. Comparison of biophysical stimuli for mechano-regulation of tissue differentiation during fracture healing. Journal of Biomechanics 39: 1507-1516.

[23] Carter DR, Blenman PR, Beaupre GS. 1988. Correlations between mechanical stress history and tissue differentiation in initial fracture healing. Journal of Orthopaedic Research 6: 736-748.

[24] Claes LE, Heigele CA, Neidlinger-Wilke C, Kaspar D, Seidl W, Margevicius, Augat P. 1998. Effects of mechanical factors on the fracture healing process. Clinical Orthopaedics and related research 355s: S132-S147.

[25] Martin RB, Sharkey N, Burr D. 1998. Skeletal tissue mechanics. Springer, US.

[26] Heppenstall B. 1980. Fracture treatment and healing. Saunders, Philadelphia.

[27] Tortora GJ, Grabowski SR. 2000. Principles of Anatomy and Physiology. John Wiley, New York.

[28] Whittle MW. 2007. Gait analysis: An Introduction. Butterworth Heinemann, Elsevier.

[29] Van Wynsberrghe D, Noback CR, Carola R. 1995. Human anatomy and physiology. McGraw Hill Inc.

[30] Nordin M, Frankel VH. 2001. Basic biomechanics of the musculoskeletal system. Lippincott Williams & Wilkins, Baltimore.

[31] Murray MP 1967. Gait as a total pattern of movement. American journal of physical medicine 46: 290-333.

[32] Farley CT, Ferris DP 1998. Biomechanics of walking and running: centre of mass movements to muscle action. Exercise and Sport Sciences Reviews 26: 253-285.

[33] Hansen AH, Childress DS, Meier MR. 2002. A simple method for determination of gait events. Journal of Biomechanics 35: 135-138.

[34] Takeda R TS, Natorigawa A, Todoh M, Yoshinari S. 2009. Gait posture estimation using wearable acceleration and gyrosensors. Journal of Biomechanics 42: 2486-2494.

[35] Morris JRW. 1973. Accelerometry – a technique for the measurement of human body movements. Journal of Biomechanics 6: 729-736

[36] Kleissen RFM, Buurke JH, Harlaar J, Zilvold G 1998. Electromyography in the biomechanical analysis of human movement and its clinical application. Gait and posture 8: 143-158.

[37] Miller CA, Verstraete MC. 1996. Determination of the step duration of gait initiation using a mechanical energy analysis. Journal of Biomechanics 29: 1195-1199.

[38] Capozzo A, Della Croce U, Leardini A, Chiari L 2005. Human movement analysis using stereophotogrammetry. Part 1: theoretical background. Gait and posture 21: 186-196.

[39] Davy DT, Kotzar GM, Brown RH, Heipele KG, Goldberg VM, Heipele KG, Berilla J, Burstein AH. 1988. Telemetric force measurements across the hip after total arthroplasty. Journal of Bone and Joint Surgery Am 70: 45-50.

[40] Kotzar GM, Davy DT, Goldberg VM, Heipele KG, Berilla J, Heipele KG, Brown RH, Burstein AH. 1991. Telemeterized in vivo hip joint force data : A report on two patients after total hip surgery. Journal of Orthopaedic research 9: 621-633.

[41] Rydell NW. 1966. Forces acting on the femoral head-prosthesis. Acta Orthopaedica Scandinavica 37: 1-132.

[42] Stansfield BW, Nicol AC, Paul JP, Kelly IG, Graichen F, Bergmann G. 2003. Direct comparison of calculated hip joint contact forces with those measured using instrumented implants. An evaluation of a three-dimensional mathematical model of the lower limb. Journal of Biomechanics 36: 929-936.

[43] Taylor SJG, Perry JS, Meswania JM, Donaldson N, Walker PS, Cannon SR. 1997. Telemetry of forces from proximal femoral replacements and relevance to fixation. Journal of Biomechanics 30: 225-234.

[44] Morlock M, Schneider E, Bluhm A, Vollmer M, Bergmann G, Muller V, Honl M. 2001. Duration and frequency of every day activities in total hip patients. Journal of Biomechanics 34: 873-881.

[45] Pedersen DR, Brand RA, Davy D. 1997. Pelvic muscle and acetabular contact forces during gait. Journal of Biomechanics 30: 959-965.

[46] Duda GN, Schneider E, Chao EYS. 1997. Internal forces and moments in the femur during walking. Journal of Biomechanics 30: 933-941.

[47] Speirs AD, Heller MO, Duda GN, Taylor WR. 2007. Physiologically based boundary conditions in finite element modelling. Journal of Biomechanics 40: 2318-2323.

[48] Brand RA, Crowninshield RD, Wittstock CE, Pederson DR, Clark CR, van Krieken FM 1982. A model of lower extremity muscular anatomy. Journal of Biomechanics 104: 304-310

[49] Brand RA, Pederson DR, Friederich JA 1986. The sensitivity of muscle force predictions to changes in physiologic cross-section area. Journal of Biomechanics 19: 589-596.

[50] 2008. New Zealand National joint registry.

[51] 2009. National joint registry, England and Wales.

[52] Crawford RW, Murray DW 1997. Total hip replacement: indications for surgery and risk factors for failure. Annals of the Rheumatic Diseases 56: 455-457.

[53] Arthritis care: www.arthritiscare.org.uk. 2004. Living with osteoarthritis. In.

[54] Royal college of Physicians. 2008. Osteoarthritis : National clinical guideline for care and management in adults. In: The national collaborating centre for chronic conditions.

[55] Arthritis care: www.arthritiscare.org.uk. 2004. Living with rheumatoid arthritis.

[56] Royal college of Physicians. 2008. Rheumatoid arthritis : National clinical guideline for care and management in adults. In: The national collaborating centre for chronic conditions.

[57] Lieberman JR, Berry DJ, Montv MA, Aaron RK, Callaghan JJ, Rayadhyaksha A, Urbanaik JR. 2002. Osteonecrosis of the hip: Management in the twenty-first century. Journal of Bone and Joint Surgery Am 84: 834-853.

[58] Mont MA, Jones LC, Einhorn TA, Hungerford DS, Reddi H. 1998. Osteonecrosis of the femoral head. Clinical Orthopaedics and related research 355S: S314-S335.

[59] 2008. Swedish Hip Arthroplasty Register.

[60] 2008. National Joint Registry, England and Wales. Joint Register.

[61] Verdonschot N, Huiskes R. 1997. The effects of cement-stem debonding in THA on the long-term failure probability of cement. Journal of Biomechanics 30: 795-802.

[62] Verdonschot N HR. 1997. The effects of cement-stem debonding in THA on the long-term failure probability of cement. Journal of Biomechanics 30: 795-802.

[63] Verdonschot N, Huiskes R. 1997. Cement debonding process of total hip arthroplasty stems. Clinical Orthopaedics and Related Research 336: 297-301.

[64] Lennon AB, Prendergast PJ. 2002. Residual stress due to curing can initiate damage in porous bone cement: experimental and theoretical evidence. Journal of Biomechanics 35: 311-321.

[65] Lennon AB PP. 2001. Evaluation of cement stresses in finite element analyses of cemented orthopaedic implants. Journal of Biomechanical Engineering 123: 623-628.

[66] Little BS, Wixson RL, Stulberg SD. 2006. Total hip arthroplasty with the porous-coated anatomic hip prosthesis. The Journal of Arthroplasty 21: 338-343.

[67] Huiskes R. 1993. Failed innovation in total hip replacement: Diagnosis and proposals for a cure. Acta Orthop Scand 64: 699-716.

[68] McCormack BAO, Prendergast PJ, Gallagher DG. 1996. An experimental study of damage accumulation in cemented hip prostheses. Clinical Biomechanics 11: 214-219.

[69] Murphy BP, Prendergast PJ. 2002. The relationship between stress, porosity, and nonlinear damage accumulation in acrylic bone cement. Journal of Biomedical Materials Research 59: 646-654.

[70] Schmalzried TP, Jasty M, Harris WH. 1992. Periprosthetic bone loss in total hip arthroplasty. Polyethylene wear debris and the concept of the effective joint space. Journal of Bone and Joint Surgery Am 74: 849-863.

[71] Yanming B, VanDeMotter R, Ragab AA, Goldberg VM, Anderson JM, Greenfield EM. 2001. Titanium Particles Stimulate Bone Resorption by Inducing Differentiation of Murine Osteoclasts. Journal of Bone and Joint surgery Am 83: 501-508.

[72] Jasty M, Floyd WE, Schiller AL, Goldring SR, Harris WH. 1986. Localized osteolysis in stable, non-septic total hip replacement. Journal of Bone and Joint Surgery Am 68: 912-919.

[73] Wolff J. 1986. The law of bone remodelling (translation of the German 1892 edition). Springer.

[74] Engh CA Jr., Young AM, Engh CA Sr., Hopper RH,. 2003. Clinical consequences of stress shielding after porous-coated total hip arthroplasty. Clinical Orthopaedics and Related Research 417: 157-163.

[75] Bugbee WD, Culpepper WJ, Engh CA Jr, Engh CA Sr. 1997. Long-term clinical consequences of stress-shielding after total hip arthroplasty without cement. Journal of Bone and Joint Surgery Am 79: 1007-1012.

[76] Surin VV, Sundholm K, Backman L. 1983. Infection after total hip replacement. Journal of Bone and Joint Surgery Br 65: 412-418.

[77] Downes EM. 1977. Late infection after total hip replacement. Journal of Bone and Joint Surgery Br 59: 42-44.

[78] Salvatti EA, Robinson RP, Zeno SM, Koslin BL, Brause BD, Wilson PD. 1982. Infection rates after 3175 total hip and total knee replacements performed with and without a horizontal unidirectional filtered air-flow system. Journal of Bone and Joint Surgery Am 64: 525-535.

[79] Fitzgerald Jr RH. 1995. Infected Total Hip Arthroplasty: Diagnosis and Treatment. Journal of the American Academy of Orthopedic Surgery 3: 249-262.

[80] Lewinnek GE, Lewis JL, Tarr R, Compere CL, Zimmerman JR. 1978. Dislocations after total hip-replacement arthroplasties. Journal of Bone and Joint Surgery Am 60: 217-220.

[81] Phillips CB, Barrett JA, Losina E, Mahomed NN, Lingard EA, Guadagnoli E, Baron JA, Harris WH, Poss R, Katz JN. 2003. Incidence rates of dislocation, pulmonary embolism, and deep infection during the first six months after elective total hip replacement. Journal of Bone and Joint Surgery Am 85: 20-26.

[82] Kotwal RS, Ganapathi M, John A, Maheson M, Jones SA. 2009. Outcome of treatment for dislocation after primary total hip replacement. Journal of Bone and Joint Surgery Br 91: 321-326.

[83] Beaule PE, Schmalzried TP, Udomkiat P, Amstutz HC. 2002. Jumbo femoral head for the treatment of recurrent dislocation following total hip replacement. Journal of Bone and Joint Surgery Am 84: 256-263.

[84] Fender D, Harper WM, Thompson JR, Gregg PJ. 1997. Mortality and fatal pulmonary embolism after primary total hip replacement. Journal of Bone and Joint Surgery Br 79: 896-899.

[85] McNally MA, Mollan RAB. 1993. Total hip replacement, lower limb blood flow and venous thrombogenesis. Journal of Bone and Joint Surgery Br 75: 640-644.

[86] Bras JM, Veraart BEEMJ. 1980. Pulmonary bone embolism after total hip replacement. Journal of Bone and Joint Surgery Br 62: 22-24.

[87] Campbell ACL, Rorabeck CH, Bourne RB, Chess D, Nott L. 1992. Thigh pain after cementless hip arthroplasty- Annoyance or ill omen. Journal of Bone and Joint Surgery Br 74: 63-66.

[88] Lindahl H, Garellick G, Regner H, Herberts P, Malchau. 2006. Three hundred and twenty-one periprosthetic femoral fractures. Journal of Bone and Joint Surgery Am 88: 1215-1222.

[89] Munson FT, Heron DF. 1941. Facial reconstruction with acrylic resin. American Journal of Surgery 3: 291-250.

[90] Haboush E. 1953. A new operation for arthroplasty of the hip based on biomechanics, photoelasticity, fast-setting dental acrylic, and other considerations. Bulletin Hospital for Joint Diseases 14: 242-277.

[91] Charnley J. 1970. Acrylic cement in orthopaedic surgery. Baltimore: Williams and Wilkins.

[92] Lee AJC. 2000. The time-dependent properties of polymethylmethacrylate bone cement: the interaction of shape of femoral stems, surface finish and bone cement. In: Learmonth ID editor, Interfaces in total hip arthroplasty: Springer-Verlag Ltd, pp. 11-19.

[93] Timperley AJ, Gie GA, Lee AJC, Ling RSM. 1993. The femoral component as a taper in cemented total hip arthroplasty. Journal of Bone and Joint Surgery Br 75: 1-33.

[94] Crawford R, Gie G, Ling R, Murray D. 2001. Femoral osteolysis and the incomplete cement mantle. Journal of Bone and Joint Surgery Br 83: 315.

[95] Rockborn P, Olsson SS. 1993. Loosening and bone resorption in Exeter Hip Arthroplasties: review at a minimum of five years. Journal of Bone and Joint Surgery Br 75: 865-868.

[96] Crawford RW, Evans M, Ling RSM, Murray DW. 1999. Fluid flow around model femoral components of differing surface finishes - In vitro investigations. Acta Orthopaedica Scandinavica 70: 589-595.

[97] Gruen TA, McNeice GM, Amstutz HC. 1979. "Modes of failure" of cemented stem-type femoral components: a radiographic analysis of loosening. Clinical Orthopaedics and Related Research 141: 17-27.

[98] Harrigan TP, Kareh JA, O'Connor DO, Burke DW, Harris WH. 1992. A finite element study of the initiation of failure of fixation in cemented femoral total hip components. Journal of Orthopaedic research 10: 134-144.

[99] Hung JP, Chen JH, Chiang HL, Wu JS. 2004. Computer simulation of fatigue behaviour of cemented hip peostheses: a physiological model. Computer Methods and Programs in Biomedicine 76: 103-113.

[100] Zhang HY, Brown L, Barrans S, Blunt L, Jiang XQ. 2009. Investigation of relative micromotion at the stem-cement interface in total hip replacement. Proceedings of the Institute of Mechanical Engineers: Part H 223: 955-964.

[101] Anthony PP, Gie GA, Howie CR, Ling RSM. 1990. Localised endosteal bone lysis in relation to the femoral components of cemented total hip arthroplasties. Journal of Bone and Joint Surgery Br 72B: 971-979.

[102] Maloney WJ, Jasty M, Rosenberg A, Harris WH. 1990. Bone lysis in well-fixed cemented femoral components. Journal of Bone and Joint Surgery Br 72B: 966-970.

[103] Haddad FS, Levell NJ, Dowd PM, Cobb AG, Bentley G. 1995. Cement hypersensitivity : A cause for aseptic loosening. Journal of Bone and Joint Surgery Br 77B: 329-330.

[104] Haddad FS, Cobb AG, Bentley G, Levell NJ, Dowd PM, . 1995. Hypersenstivity in aseptic loosening of total hip replacements. Journal of Bone and Joint Surgery Br 78: 546-549.

[105] Nuno N, Avanzolini G. 2002. Residual stresses at the stem–cement interface of an idealized cemented hip stem. Journal of Biomechanics 35: 849-852.

[106] Jasty M, Maloney WJ, Bragdon CR, O'Connor DO, Haire T, Harris WH. 1991. The initiation of failure in cemented femoral components of hip arthroplasties. Journal of Bone and Joint Surgery Br 73B: 551-558.

[107] Dunne NJ, Orr JF, Mushipe MT, Eveleigh RJ. 2003. The relationship between porosity and fatigue characteristics of bone cements. Biomaterials 24: 239-245.

[108] Dunne NJ OJ. 2001. Influence of mixing techniques on the physical properties of acrylic bone cement. Biomaterials 22: 1819-1826.

[109] Orr JF, Dunne NJ, Quinn JC. 2003. Shrinkage stresses in bone cement. Biomaterials 24: 2933-2940.

[110] Andersson GBJ, Freeman MAR, Swanson SAV. 1972. Loosening of the cemented acetabular cup in total hip replacement. Journal of Bone and Joint Surgery Br 54B: 590-599.

[111] Deramond H, Wright NT, Belkoff SM. 1999. Temperature elevation caused by bone cement polymerization during vertebroplasty. Bone 25: 17S-21S.

[112] Homsy CA, Anderson HS, Differante NM, King JW. 1972. Some physiological aspects of prosthesis stabilization with acrylic polymer. Clinical Orthopaedics and Related Research 83: 317-328.

[113] Charnley J, Follacci FM, Hammond BT, . 1968. The long-term reaction of bone to self-curing acrylic cement. Journal of Bone and Joint Surgery Br 50B: 822-829.

[114] Charnley J. 1970. The reaction of bone to self curing acrylic cement: A long-term histological study in man. Journal of Bone and Joint Surgery Br 52B: 340-353.

[115] Jefferiss CD, Lee AJC, Ling RSM, . 1975. Thermal aspects of self-curing polymethylmethacrylate. Journal of Bone and Joint Surgery Br 57B: 510-518.

[116] Stanczyk M, Van-Rietbergen B. 2004. Thermal analysis of bone cement polymerisation at the cement–bone interface. Journal of Biomechanics 37: 1803-1810.

[117] Linder L. 1977. Reaction of bone to the acute chemical trauma of bone cement. Journal of Bone and Joint Surgery Am 59: 82-87.

[118] Carter DR GE, Harris WH 1982. Strain controlled fatigue of acrylic bone cement. Journal of Biomedical Materials Research 16: 647-657.

[119] Topoleski LD, Ducheyne P, Cuckler JM 1990. A fractographic analysis of in vivo polymethylmethacrylate bone cement failure mechanisms. Journal of Biomedical Materials Research 24: 135-154.

[120] Bishop NE, Ferguson S, Tepic S. 1996. Porosity reduction in bone cement at the cement stem interface. Journal of Bone and Joint Surgery Br 78B: 349-356.

[121] Rice J, Prenderville T, Murray P, McCorkack B, Quinlan W. 1998. Femoral cementing techniques in total hip replacement. International Orthopaedics 22: 308-311.

[122] Davies JE. 2003. Understanding peri-implant endosseous healing. Journal of Dental Education 67: 932-949.

[123] Capello WN, D'Antonio JA, Manley MT, Feinberg JR. 1998. Hydroxyapatite in total hip arthroplasty. Clinical Orthopaedics and Related Research 355: 200-211.

[124] Engh CA BJ, Glassman AH. 1987. Porous-coated Hip replacement: The factors governing bone ingrowth, stress shielding, and clinical results. Journal of Bone and Joint Surgery Br 69: 45-55.

[125] Kim YH. 2002. Cementless total hip arthroplasty with a close proximal fit and short tapered distal stem (third-generation) prosthesis. The Journal of Arthroplasty 17: 841-850.

[126] Kim YH. 2008. The results of a proximally-coated cementless femoral component in total hip replacement. Journal of Bone and Joint Surgery Br 90: 299-305.

[127] Laine HJ. 2001. Anatomy of the proximal femoral medullary canal and fit and fill characteristics of cementless endoprosthetic stems. Dissertation.

[128] LaPorte DM MM, Hungerford DS. 1999. Proximally porous-coated ingrowth prostheses:limits of use. Orthopedics 22: 1154-1160.

[129] Niinimaki T, Junila J, Jalovaara P. 2001. A proximal fixed anatomic femoral stem reduces stress shielding. International Orthopaedics 25: 85-88.

[130] Renkawitz T, Santori FS, Grifka J, Valverde C, Morlock MM, Learmonth ID. 2008. A new short uncemented, proximally fixed anatomic femoral implant with a prominent lateral flare: design rationals and study design of an international clinical trial. BMC Musculoskeletal disorders 9.

[131] Santori FS, Manili M, Fredella N, Tonci Ottieri M, Santori N. 2006. Ultra-short stems with proximal load transfer: Clinical and radiographic results at five year follow-up. Hip International 16: S31-S39.

[132] Santori N, Lucidi M, Santori FS. 2006. Proximal load tranfer with a stemless uncemented femoral implant. Journal of Orthopaedics and Traumatology 7: 154-160.

[133] Sinha RK, Dungy DS, Yeon HB. 2004. Primary total hip arthroplasty with a proximally porous-coated femoral stem. Journal of Bone and Joint Surgery Am 86: 1254-1261.

[134] Bourne RB, Rorabeck CH, Ghazal ME, Lee MH. 1994. Pain in the thigh following total hip replacement with a porous-coated anatomic prosthesis for osteoarthrosis. A five-year follow-up study. Journal of Bone and Joint Surgery Am 76: 1464-1470.

[135] Sumner DR, Kienapfel H, Jacobs J, Turner TM, Urban RM, Galante JO. 1995. Bone Ingrowth and Wear Debris in Well-fixed Cementless Porous-coated Tibial Components Removed From Patients. The Journal of Arthroplasty 10: 157-167.

[136] Yue S, Pilliar RM, Weatherly GC. 1984. The fatigue strength of porous-coated Ti-6% Al-4% V implant alloy. Journal of Biomedical Materials Research 18: 1043-1058.

[137] 2008. Australian national joint replacement registry.

[138] Kienapfel H, Sprey C, Wilke A, Griss P. 1999. Implant fixation by bone ingrowth. The Journal of Arthroplasty 14: 355-368.

[139] Haddad RJ, Cook SD, Thomas KA. 1987. Biological fixation of porous-coated implants. Journal of Bone and Joint Surgery Am 69: 1459-1466.

[140] Spector M , Flemming W R, Kreutner A, Sauer B W. 1976. Bone growth into porous high-density polyethylene. Journal of Biomedical Materials Research 10: 595-603.

[141] Van Tienen TG, Heijkants RG, Buma P, de Groot JH, Pennings AJ, Veth RP. 2002. Tissue ingrowth and degradation of two biodegradable porous polymers with different porosities and pore sizes. Biomaterials 23: 1731-1738.

[142] Ryan G, Pandit A, Panagiotis D, Apatsidis P. 2006. Fabrication methods of porous metals for use in orthopaedic applications. Biomaterials 27: 2651-2670.

[143] Bragdon C, Jasty M, Greene M, Rubash H.E, Harris WH. 2004. Biologic fixation of total hip implants: Insights gained from a series of canine studies. Journal of Bone and Joint Surgery Am 86: 105-117.

[144] Welsh PR, Pilliar RM, Macnab I. 1971. Surgical implants: The role of surface porosity in fixation to bone and acrylic. Journal of Bone and Joint Surgery Am 53: 963-977.

[145] Martens M, Ducheyne P, De Meester P, Mulier JC. 1980. Skeletal Fixation of implants by bone ingrowth into surface pores. Archives of Orthopaedic and Traumatic Surgery 97: 111-116.

[146] Cameron HC. 1981. Essential considerations for microporous implants: Preliminary considerations. Journal of the Royal Society of Medicine 74: 887-891.

[147] Bobyn JD, Pilliar RM,Cameron HU,Weatherly GC. 1980. The Optimum Pore Size for the Fixation of Porous Surfaced Metal Implants by the Ingrowth of bone. Clinical Orthopaedics and related research 150: 263-270.

[148] Homsy CA, Cain TE, Kessler FB, Anderson MS, King JW. 1972. Porous implant systems for prosthesis stabilization. Clinical Orthopaedics and related research 89: 220-235.

[149] Kujala S, Ryhanen J, Danilov A, Tuukkanen J. 2003. Effect of porosity on the osteointegration and bone ingrowth of a weight-bearing nickel-titanium bone graft substitute. Biomaterials 24: 4691-4697.

[150] Otsuki B, Takemoto M, Fujibayashi S, Neo M, Kokubo T, Nakamura T. 2006. Pore throat size and connectivity determine bone and tissue ingrowth into porous implants: Three-dimensional micro-CT based structural analyses of porous bioactive titanium implants. Biomaterials 27: 5892-5900.

[151] Cook SD, Walsh KA, Haddad RJ. 1985. Interface Mechanics and Bone Growth into Porous Co-Cr-Mo Alloy Implants. Clinical Orthopaedics and related research 193: 271-280.

[152] Friedman RJ, Black J, Galante JO, Jacobs JJ, Skinner HB. 1993. Current concepts in orthopaedic biomaterials and implant fixation. Journal of Bone and Joint Surgery Am 75: 1086-1109.

[153] Friedman RJ, An YH, Ming J, Draughn RA, Bauer TW. 1996. Influence of biomaterial surface texture on bone ingrowth in the rabbit femur. Journal of Orthopaedic Research 14: 455-464.

[154] Sumner DR, Turner TM, Urban RM, Galante JO. 1992. Remodeling and ingrowth of bone at two years in a canine cementless total hip arthroplasty model. Journal of Bone and Joint Surgery Am 74: 239-250.

[155] Simmons CA, Nancy V, Pilliar RM. 1999. Osseointegration of sintered porous-surfaced and plasma spray–coated implants: An animal model study of early postimplantation healing response and mechanical stability. Journal of Biomedical materials research 47: 127-138.

[156] Simmons CA, Meguid SA, Pilliar RM 2001. Differences in osseointegration rate due to implant surface geometry can be explained by local tissue strains. Journal of Orthopaedic Research 19: 187-194.

[157] Jinno T, Goldberg VM, Davy D, Stevenson S. 1998. Osseointegration of surface-blasted implants made of titanium alloy and cobalt–chromium alloy in a rabbit intramedullary model. Journal of Biomedical Materials Research 42: 20-29.

[158] Branemark R, Branemark P-I, Rydevik B, Myers RR,. 2001. Osseointegration in skeletal reconstruction and rehabilitation: A review. Journal of Rehabilitation Research and Development 38: 175-181.

[159] Camron HU, Pilliar RM, Macnab I. 1976. The rate of bone ingrowth into porous metal. Journal of Biomedical Materials Research 10: 295-302.

[160] Sandborn PM, Cook SD, Spires WP, Kester MA. 1988. Tissue response to porous-coated implants lacking initial bone apposition. Journal of Arthroplasty 3: 337-346.

[161] Spears IR, Pfleiderer M, Schneider E, Hille E, Bergmann G, Morlock MM. 2000. Interfacial conditions between a press-fit acetabular cup and bone during daily activities: implications for achieving bone in-growth. Journal of Biomechanics 33: 1471-1477.

[162] Claes LE, Augat P, Suger G, Wilke HJ. 1997. Influence of size and stability of the osteotomy gap on the success of fracture healing. Journal of Orthopaedic Research 15: 577-584.

[163] Tissakht M, Eskandarl H, Ahmed AM. 1995. Micromotion analysis of the fixation of total knee tibial component. Computers and Structures 56: 365-375.

[164] Andreykiv A, Prendergast PJ, Van Keulena F, Swieszkowskic W, Rozing PM. 2005. Bone ingrowth simulation for a concept glenoid component design. Journal of Biomechanics 38: 1023-1033.

[165] Callaghan JJ, Fulghum CS, Glisson RR, Stranne SK. 1992. The effect of femoral stem geometry on interface motion in uncemented porous-coated total hip prostheses. Comparison of straight-stem and curved-stem designs. Journal of Bone and Joint Surgery Am 74: 839-848.

[166] Biegler FB, Reuben JD, Harrigan TP, Hou FJ, Akin JE. 1995. Effects of porous coating and loading conditions on total hip femoral stem stability. The Journal of Arthroplasty 10: 839-847.

[167] Engh CA, Hooten JP, Zettl-Schaffer KF, Ghaffarpour M, McGovern TF, Bobyn JD. 1995. Evaluation of bone ingrowth in proximally and extensively porous-coated anatomic medullary locking prostheses retrieved at autopsy. Journal of Bone and Joint Surgery Am 77: 903-910.

[168] Jasty M, Bragdon C R, Zalenski E, O'Connor D, Page A, Harris W H. 1997. Enhanced stability of uncemented canine femoral components by bone ingrowth into the porous coatings. The Journal of Arthroplasty 12: 106-113.

[169] Collier JP, Mayor MB, Chae JC, Surprenant VA, Suprenant HP, Dauphinais. 1988. Macroscopic and Microscopic Evidence of Prosthetic Fixation with Porous-Coated Materials. Clinical Orthopaedics and Related Research 235: 173-180.

[170] Biegler FB, Reuben JD, Harrigan TP, Hou FJ, Akin JE. 1995. Effect of porous coating and loading conditons on total hip femoral stem stability. The Journal of Arthroplasty 10: 839-847.

[171] Bragdon C, Burke D, Lowenstein JD, O'Connor DO, Ramamurti B, Jasty M, Harris WH. 1996. Differences in stiffness of the interface between a cementless porous implant and cancellous bone in vivo in dogs due to varying amounts of implant motion. The Journal of Arthroplasty 11: 945-951.

[172] Engh CA, Glassman AH, Suthers KE. 1990. The case for porous-coated hip implants: The femoral side. Clinical Orthopaedics and related research 261: 63-81.

[173] Pilliar RM, Lee JM, Maniatopoulos C. 1986. Observations on the effect of movement on bone ingrowth into porous-surfaced implants. Clinical Orthopaedics and Related Research 208: 108-113.

[174] Engh CA, Hopper RH. 2002. The Odyssey of Porous-Coated Fixation. The Journal of Arthroplasty 17: 102-107.

[175] Vicenconti M, Monti L, Muccini R, Bernakiewicz M, Toni A. 2001. Even a thin layer of soft tissue may compromise the primary stability of cementless hip stems. Clinical Biomechanics 16: 765-775.

[176] Rapperport DJ, Carter DR, Schurman DJ. 1987. Contact finite element stress analysis of porous ingrowth acetabular cup implantation, ingrowth, and loosening. Journal of Orthopaedic Research 5: 548-561.

[177] Buchler P, Pioletti DP, Rakotomanana LR. 2003. Biphasic constitutive laws for biological interface evolution. Biomechanics and Modeling in Mechanobiology 1: 239-249.

[178] Liu X, Niebur GL. Effects of micromotion on bone ingrowth predicted by a mechano-regulatory tissue differentiation algorithm.

[179] Walter WL WW, , Zicat B. 2006. Clinical and Radiographic Assessment of a Modular Cementless Ingrowth Femoral Stem System for Revision Hip Arthroplasty. The Journal of Arthroplasty 21: 172-178.

[180] Moskal JT, Jordan L, Brown TE. 2004. The porous-coated anatomic total hip prosthesis: 11-to 13 year results. The Journal of Arthroplasty 19: 837-844.

[181] Manley MT, Capello WN, D'Antonio JA, Edidin AA, Geesink RGT. 1998. Fixation of Acetabular Cups without Cement in Total Hip Arthroplasty. A Comparison of Three Different Implant Surfaces

at a Minimum Duration of Follow-up of Five Years. Journal of Bone and Joint Surgery Am 80: 1175-1185.

[182] Becker BS, Bolton JD. 1997. Corrosion behaviour and mechanical properties of functionally gradient materials developed for possible hard-tissue applications. Journal of Materials Science: Materials in Medicine 8: 793-797.

[183] Soballe K, Hansen ES, Brockstedt-Rasmussen H, Bunger C. 1993. Hydroxyapatite coating converts fibrous tissue to bone around loaded implants. Journal of Bone and Joint Surgery Br 75-B: 270-278.

[184] Yang C. 2002. Effect of calcium phosphate surface coating on bone ingrowth onto porous-surfaced titanium alloy implants in rabbit tibiae. Journal of Oral and Maxillofacial Surgery 60: 422-425.

[185] Karlsson KH, Ylanen H, Aro H. 2000. Porous bone implants. Ceramics International 26: 897-900.

[186] Hayashi K, Mashima T, Uenoyama K. 1999. The effect of hydroxyapatite coating on bony ingrowth into grooved titanium implants. Biomaterials 20: 111-119.

[187] Overgaard S, Lind M, Glerup H, Bunger C, Soballe K. 1998. Porous-coated versus grit blasted surface texture of hydroxyapatite-coated implants during controlled micromotion: Mechanical and Histomorphometric results. The Journal of Arthroplasty 13: 449-458.

[188] Chang BS, Lee CK, Hong KS, Youn HJ, Ryu HS, Chung SS, Park KW. 2000. Osteoconduction at porous hydroxyapatite with various pore configurations. Biomaterials 21: 1291-1298.

[189] Soballe K, Hansen ES, Rasmussen HB, Jorgensen PH, Bunger C. 1992. Tissue ingrowth into titanium and hydroxyapatite-coated implants during stable and unstable mechanical conditions. Journal of Orthopaedic research 10: 285-299.

[190] Froimson MI, Garino J, Machenaud A, Vidalain JP. 2007. Minimum 10-year results of a tapered, titanium, Hydroxyapatite-coated hip stem: An independent review. The Journal of Arthroplasty 22: 1-6.

[191] Rothman RH, Hozack WJ, Ranawat A, Moriarty L. 1996. Hydroxyapatite-caoted femoral stems. A matched-pair analysis of coated and uncoated implants. Journal of Bone and Joint Surgery Am 78: 319-324.

[192] Dalton JE CS, Thomas KA, Kay JF. 1995. The effect of operative fit and hydroxyapatite coating on the mechanical and biological response to porous implants. Journal of Bone and Joint Surgery Am 77: 97-110.

[193] Callaghan JJ. 1993. The clinical results and basic science of total hip arthroplasty with porous-coated prostheses. Journal of Bone and Joint Surgery Br 75: 299-310.

[194] Frenkel SR, Simon J, Alexander H, Dennis M, Ricci JL. . 2002. Osseointegration on metallic implant surfaces: effects of microgeometry and growth factor treatment. Journal of Biomedical Materials Research 63: 706-713.

[195] Sumner DR, Turner TM, Purchio AF, Gombotz WR, Urban RM, Galante. 1995. Enhancement of bone ingrowth by transforming growth factor-beta. Journal of Bone and Joint Surgery Am 77: 1135-1147.

[196] Einhorn TA. 1998. The cell and molecular biology of fracture healing. Clinical Orthopaedics and related research 355S: S7-S21.

[197] Heppenstall RB, Goodwin CW, Brighton CT. 1976. Fracture healing in the presence of chronic hypoxia. Journal of Bone and Joint Surgery Am 58: 1153-1156.

[198] McKibbin B. 1978. The biology of fracture healing in long bones. Journal of Bone and Joint Surgery Br 60B: 150-162.

[199] Perren SM. 1979. Physical and Biological aspects of fracture healing. Clinical Orthopaedics and related research 138: 175-196.

[200] Simmons DJ. 1985. Fracture healing perspectives. Clinical Orthopaedics and related research 200: 100-113.

[201] Hulth A. 1989. Current concepts of fracture healing. Clinical Orthopaedics and related research 249: 265-284.

[202] Frost HM. 1989. The biology of fracture healing: An overview for clinicians. Part II. Clinical Orthopaedics and related research 248: 294-309.

[203] Park JY, Davies JE. 2000. Red blood cell and platelet interactions with titanium implant surfaces. Clinical Oral Implant Research 11: 530-539.

[204] Carter DR, Beaupre GS, Giori NJ, Helms JA. 1998. Mechanbiology of skeletal regeneration. Clinical Orthopaedics and related research 355s: S41-S55.

[205] Claes LE, Heigele CA. 1999. Magnitudes of local stress and strain along bony surfaces predict the course and type of fracture healing. Journal of Biomechanics 32: 255-266.

[206] Giori NJ, Ryd L, Carter DR. 1995. Mechanical influences on tissue differentiation at bone-cement interfaces. The Journal of Arthroplasty 10: 514-522.

[207] Huiskes R, Weinans H, Grootenboer J, Dalstra M, Fudala B, Sloof TJ. 1987. Adaptive bone-remodeling theory applied to prosthetic-design analysis. Journal of Biomechanics 20: 1135-1150.

[208] Mow VC, Huiskes R,. 2005. Basic Orthopaedic Biomechanics and Mechano-Biology. Lippincott Williams and Wilkins, Philadelphia.

[209] Carter DR. 1987. Mechanical loading history and skeletal biology. Journal of Biomechanics 20: 1095-1109.

[210] Loboa EG, Beaupre GS, Carter DR,. 2001. Mechanobiology of initial pseudoarthrosis formation with oblique fractures. Journal of Orthopaedic research 19: 1067-1072.

[211] Gardner TN, Mishra S, Marks L. 2004. The role of osteogenic index, octahedral shear stress and dilatational stress in the ossification of a fracture callus. Medical Engineering & Physics 26: 493-501.

[212] Isaksson H, Corrinus C, Donkelaar V, Huiskes R, Ito K. 2006. Corroboration of mechanoregulatory algorithms for tissue differentiation during fracture healing: Comparison with In vivo results. Journal of Orthopaedic Research 24: 898-907.

[213] Gardner TN, Stoll T, Mishra S, Marks L, Tate MK. 2000. The infuence of mechanical stimulus on the pattern of tissue differentiation in a long bone fracture - an FEM study. Journal of Biomechanics 33: 415-425.

[214] Garcia-Aznar JM, Kuiper JH, Benito MJG, Doblare M, Richardson JB. 2007. Computational simulation of fracture healing: Influence of interfragmentary movement on the callus growth. Journal of Biomechanics 40: 1467-1476.

[215] Gomez-Benito MJ, Aznar JMG, Kuiper JH, Doblare M. 2005. Influence of fracture gap size on the pattern of long bone healing: a computational study. Journal of Theoretical Biology 235: 105-119.

[216] Andreykiv A, Van Keulen F, Prendergast PJ. 2007. Simulation of fracture healing incorporating mechanoregulation of tissue differentiation and dispersal/proliferation of cells. Biomechanics and Modeling in Mechanobiology 7: 443-461.

[217] Lacroix D, Prendergast PJ. 2002. A mechano-regulation model for tissue differentiation during fracture healing:analysis of gap size and loading. Journal of Biomechanics 35: 1163-1171.

[218] Lacroix D, Prendergast PJ. 2002. Three-dimensional Simulation of Fracture Repair in the Human Tibia. Computer methods in Biomechanics and Biomedical engineering 5: 369-376.

[219] Liu X, Niebur GL. 2007. Bone ingrowth into a porous coated implant predicted by a mechano-regulatory tissue differentiation algorithm. Biomechanics and Modeling in Mechanobiology 7(4).

[220] Lacroix D, Prendergast PJ, Li G, Marsh D. 2002. Biomechanical model to simulate tissue differentiation and bone regeneration: application to fracture healing. Medical & Biological Engineering and Computing 40: 14-21.

[221] Kelly DJ. 2003. Mechanobiology of tissue differentiation during osteochondral defect repair. PhD Thesis.

[222] Kelly DJ, Prendergast PJ. 2005. Mechano-regulation of stem cell differentiation and tissue regeneration in osteochondral defects. Journal of Biomechanics 38: 1413-1422.

[223] Epari DR, Taylor WR, Heller M, Duda N. 2006. Mechanical conditions in the initial phase of bone healing. Clinical Biomechanics 21: 646-655.

[224] Carter DR BG. 1999. Comment by Carter. Journal of Biomechanics 32: 1255-1256.

[225] Engh CA. 1998. Distal porous coating yields optimal fixation. Current Orthopaedics 12: 232-238.

[226] Fyhrie DP, Carter DR, Schurman DJ. 1988. Effects of ingrowth, geometry, and material on stress transfer under porous-coated hip surface replacements. Journal of Orthopaedic Research 6: 425-433.

[227] Skinner HB, Kim AS, Keyak JH, Mote CD. 1994. Femoral prosthesis implantation induces changes in bone stress that depend on the extent of porous coating. Journal of Orthopaedic research 12: 553-563.

[228] Kendrick JB, Noble PC, Tullos HS. 1995. Distal stem design and the torsional stability of cementless femoral stems. The Journal of Arthroplasty 10: 463-469.

[229] Munting E, Smitz P, Van Sante N, Nagant de Deuxchaisnes, Vincent A, Devogelaer J-P,. 1997. Effect of a stemless femoral implant for total hip arthroplasty on the bone mineral density of the proximal femur. The Journal of Arthroplasty 12: 373-379.

[230] Jasty M, Krushell R, Zalenski E, O'Connor D, Sedlacek R, Harris W,. 1993. The contribution of the nonporous distal stem to the stability of proximally porous-coated canine femoral components. Journal of Arthroplasty 8: 33-41.

[231] d'Imporzano M, Pierannunzii L,. 2006. Minimally invasive total hip replacement. Journal of Orthopaedic Traumatology 7: 42-50.

[232] Learmonth ID. 2005. Conservative hip implants. Current Orthopaedics 19: 255-262.

[233] Santori N, Albanese CV, Learmonth ID, Santori FS. 2006. Bone preservation with a conservative metaphyseal loading implant. Hip International 16: S16-S21.

[234] Keaveny TM, Bartel DL. 1995. Mechanical consequences of bone ingrowth in a hip prosthesis inserted without cement. Journal of Bone and Joint Surgery Am 77: 911-923.

[235] Waide V, Cristofolini L, Stolk J, Verdonschot N, Boogaard GJ, Toni A. 2004. Modelling the fibrous tissue layer in cemented hip replacments: Experimental and Finite element methods. Journal of Biomechanics 37: 13-26.

[236] Carter DR, Hayes WC. 1976. Bone Compressive Strength: The Influence of Density and Strain Rate. Science 194: 1174-1176.

[237] Leali A, Fetto J, Insler H, Elfenbein D. 2002. The effect of a lateral flare feature on implant stability. International Orthopaedics 26: 166-169.

[238] Kulkarni M, Wylde V, Aspros D, Learmonth ID,. 2006. Early clinical experience with a metaphyseal loading implant: Why have a stem. Hip International 16: S3-S8.

[239] Leali A, Fetto J. 2007. Promising mid-term results of total hip arthroplasties using an uncemented lateral-flare hip prosthesis: a clinical and radiographic study. International Orthopaedics 31: 845-849.

[240] Koch JC. 1917. The laws of bone architecture. American Journal of Anatomy 21: 177-298.

[241] Fetto J, Leali A, Moroz A. 2002. Evolution of the Koch model of the biomechanics of the hip: clinical perspective. Journal of Orthopaedic Science 7: 724-730.

[242] Albanese CV, Santori FS, Pavan L, Learmonth ID, Passaiello R. 2009. Periprosthetic DXA after total hip arthroplasty with short vs. ultra-short custom-made femoral stems. Acta Orthopaedica 80: 291-297.

[243] Westphal FM, Bishop N, Honl M, Hille E, Pulschel K, Morlock MM. 2006. Migration and cyclic motion of a new short stemmed hip prosthesis - a biomechanical in vitro study. Clinical Biomechanics 21: 834-840.

[244] Havelin LI, Espehaug B, Vollset SE, Engesaeter LB. 1995. Early aseptic loosening of uncemented femoral components in primary total hip replacement. Journal of Bone and Joint Surgery Br 77: 11-17.

[245] Walker PS, Culigan SG. 1999. The effect of a lateral flare feature on uncemented hip stems. Hip International 9: 71-80.

[246] Kim YH, Kim JS, Cho SH. 2001. Strain distribution in the proximal femur- An in vitro comparison in the intact femur and after insertion of reference and experimental femoral stems. Journal of Bone and Joint Surgery Br 83: 295-301.

[247] Kawahara H, Kokubo Y, Yayama T,Uchida K,Kobayashi S, Nakajima H, Hisashi Oki H, Negoro K,Mwaka ES, Norbert T, Orwotho NT, Baba H. 2010. Metaphyseal-loading anterolaterally-flared femoral stem in cementless total hip arthroplasty: Five- to eleven-year follow up evaluation. Artifical Organs 34: 377-383.

[248] Leali A, Fetto J, Insler H. 2006. Favourable midterm results of total hip arthroplasties with a lateral flare uncemented stem. Clinical Orthopaedics and Related Research 450: 138-144.

[249] Leali A, Fetto J. 2004. Preservation of femoral bone mass after total hip replacements with a lateral flare stem. International Orthopaedics 28: 151-154.

[250] Engh CA Jr, Claus AM, Hopper RH Jr, Engh CA,. 2001. Long-term results using the anatomic medullary locking hip prosthesis. Clin Orthop Relat Res 393: 137-146.

[251] Engh CA, Bobyn JD, Glassman AH. 1987. Porous-coated Hip replacement: The factors governing bone ingrowth, stress shielding, and clinical results. Journal of Bone and Joint Surgery Br 69: 45-55.

[252] Belmont PJ, Powers CC, Beykirch SE, Hopper RH, Engh CA Jr., Engh CA Sr. 2008. Results of the anatomic medullary locking total hip arthroplasty at a minimum of twenty years. A concise follow-up of previous reports. Journal of Bone and Joint Surgery Am 90: 1524-1530.

[253] Engh CA, Hooten JP, Zettl-Schaffer KF, Ghaffarpour M, McGovern TF, Macalino GE, Zicat B. 1994. Porous-coated total hip replacement. Clinical Orthopaedics and Related Research 298: 89-96.

[254] Engh CA Jr., Anderson C, Culpepper WJ, Engh CA Sr. 1997. Long-term results of use of the anatomic medullary locking prosthesis in total hip arthroplasty. Journal of Bone and Joint Surgery Am 79: 177-184.

[255] Engh CA, Bobyn JD 1988. The influence of stem size and extent of porous coating on femoral bone resorption after primary cementless hip arthroplasty. Clinical Orthopaedics and Related Research 231: 7-28.

[256] Kilgus DJ, Shimoka EE, Tipton JS, Eberle RW. 1993. Dual energy X ray absorptiometry measurement of bone mineral density around porous coated cementless femoral implants. Journal of Bone and Joint Surgery Br 75: 279-287.

[257] Folgado J, Fernandes PR, Jacobs CR, Pellegrini VD. 2009. Influence of femoral stem geometry, material and extent of porous coating on bone ingrowth and atrophy in cementless total hip arthroplasty: an iterative finite element model. Computer Methods in Biomechanics and Biomedical Engineering 12: 135-145.

[258] Sychterz CJ, Claus AM, Engh CA. 2002. What we have learned about long-term cementless fixation from autopsy retrievals. Clinical Orthopaedics and Related Research 405: 79-91.

[259] McAuley JP, Sychterz CJ, Engh CA Sr. 2000. Influence of porous coating level on proximal femoral remodeling. A postmortem analysis. Clinical Orthopaedics and Related Research 371: 146-153.

[260] Al Hertani W, Waddell JP, Anderson GI. 2000. The effect of partial vs. full hydroxyapatite coating on periprosthetic bone quality around the canine madreporic femoral stem. Journal of Biomedical Materials Research 53: 518-524.

[261] Nourbash PS, Paprosky WG,. 1998. Cementless femoral design concerns: Rationale for extensive porous coating. Clinical Orthopaedics and Related Research 355: 189-199.

[262] Barrack RL, Folgueras AJ. 1995. Revision total hip arthroplasty: The femoral component. Journal of American Academy of Orthopaedic Surgeons 3: 79-85.

[263] Mont MA, Hungerford DS. 1997. Proximally coated ingrowth prostheses. A review. Clinical Orthopaedics and Related Research 344: 139-149.

[264] Sluimer JC, Hoefnagels NHM, Emams PJ, Kuijer R, Geesink RGT. 2006. Comparison of two hydroxyapatite-coated femoral stems. The Journal of Arthroplasty 21: 344-352.

[265] Britton JR, Prendergast PJ. 2005. Preclinical testing of femoral hip components:An experimental investigation with four prostheses. Transactions of the ASME 127: 872-880.

[266] Jasty M, Bragdon CR, Maloney WJ, Haire T, Harris WH. 1991. Ingrowth of bone in failed fixation of porous-coated femoral components. Journal of Bone and Joint Surgery Am 73: 1331-1337.

[267] Aspenberg P, Herbertsson P. 1996. Periprosthetic bone resoprtion:particles versus movement. Journal of Bone and Joint Surgery Br 78: 641-646.

[268] Hori RY, Lewis JL. 1982. Mechanical properties of the fibrous tissue found at the bone-cement interface following total joint replacement. Journal of Biomedical Materials Research 16: 911-927.

[269] Kadir MRA, Kamsah N. 2009. Interface micromotion of cementless hip stems in simulated hip arthroplasty. American Journal of Applied Sciences 9: 1682-1689.

[270] Farron A, Rakotomananan RL, Zambelli PY, Leyvraz PF. 1995. Total knee prosthesis. Clinical and numerical study of micromovements of the tibial implant. Rev Chir Orthop Reparatrice Appar Mot 80: 28-35.

[271] Hacking SA, Bobyn JD, Toh KK, Tanzer M, Krygier JJ. 2000. Fibrous tissue ingrowth and attachment to porous tantalum. Journal of Biomedical Materials Research 52: 631-638.

[272] Stadelmann VA, Pioletti DP. 2007. Activation pathways of osteoclasts are up-regulated by micromotions at the bone–implant interface. Computer Methods in Biomechanics and Biomedical Engineering S1: 93-94.

[273] Pioletti DP, Muller J, Rakotomanana LR, Corbeil J, Wild E. 2003. Effect of micromechanical stimulations on osteoblasts: development of a device simulating the mechanical situation at the bone–implant interface. Journal of Biomechanics 36: 131-135.

[274] Overgaard S, Linkd M, Glerup H, Bunger C, Soballe K. 1998. Porous-coated versus grit-blasted surface texture of hydroxyapatite-coated implants during controlled micromotion. The Journal of Arthroplasty 14: 449-458.

[275] Yuan X, Ryd L, Huiskes R. 2000. Wear particle diffusion and tissue differentiation in TKA implant fibrous interfaces. Journal of Biomechanics 33: 1279-1286.

[276] Jasty M, Bragdon CR, Haire T, Mulroy RD, Harris W H. 1993. Comparison of bone ingrowth into cobalt chrome sphere and titatnium fiber mesh porous coated cementless canine acetabular components. Journal of Biomedical Materials Research 27: 639-644.

[277] Bobyn JD PR, Cameron HU,Weatherly GC. 1980. The Optimum Pore Size for the Fixation of Porous Surfaced Metal Implants by the Ingrowth of bone. Clinical Orthopaedics and related research 150: 263-270.

[278] Galante JO, Jacobs J. 1992. Clinical performances of ingrowth surfaces. Clinical Orthopaedics and Related Research 276: 41-49.

[279] Bobyn JD, Pilliar RM,Cameron HU,Weatherly GC,Kent GM. 1980. The effect of porous surface configurations on the tensile strength of fixation of implants by bone ingrowth. Clinical Orthopaedics and Related Research 149: 291-298.

[280] Manley MT, Kotzar G, Stern LS, Wilde A. 1987. Effects of repetitive loading on the integrity of porous coatings. Clinical Orthopaedics and Related Research 217: 293-302.

[281] Pilliar RM, Cameron HV, Macnab I,. 1975. Porous surface layered prosthetic devices. Biomedical Engineering 10: 126-131.

[282] 2008. Canadian joint replacement registry.

[283] Pynsent PB, Carter SR, Bulstrode CJK. 1996. The total cost of hip-joint replacent; a model for purchasers. Journal of Public Health Medicine 18: 157-168.

[284] Barrack RL, Castro F, Guinn S 1996. Cost of implanting a cemented versus cementless femoral stem. The Journal of Arthroplasty 11: 373-376.

[285] Yates P, Serjeant S, Rushforth G, Middleton R. 2006. The relative cost of cemented and uncemented total hip arthroplasties. The Journal of Arthroplasty 21: 102-105.

[286] Britton JR, Lyons CG, Prendergast PJ. 2004. Measurement of the relative motion between an implant and bone under cyclic loading. Strain 40: 193-202.

[287] Gomez-Benito MJ, Aznar JMG, Doblare M. 2006. Formulation and computational aspects on the simulation of fracture healing. Monografías del Seminario Matemático García de Galdeano 33: 121-128.

[288] Geris L. 2007. Mathematical modelling of bone regeneration during fracture healing and implant osseointegration. PhD Thesis.

[289] Chen G, Niemeyer F, Wehner T, Simon U, Schuetz MA, Pearcy MJ, Claes LE. 2009. Simulation of the nutrient supply infracture healing. Journal of Biomechanics 42: 2575-2583.

[290] Huiskes R SP, Heck JV, Slooff TJJH. 1985. Interface stresses in the resurfaced hip : Finite element analysis of load transmission in the femoral head. Acta Orthop Scand 56: 474-478.

[291] McNamara LM, Prendergast PJ. 2007. Bone remodelling algorithms incorporating both strain and microdamage stimuli. Journal of Biomechanics 40: 1381-1391.

[292] Scannell PT, Prendergast PJ. 2006. Influence of stem material properties on bone remodelling and interfacial tissue formation in uncemented hip replacements. In.

[293] Turner AWL, Gillies RM, Sekel R, Morris P, Bruce W, Walsh WR. 2005. Computational bone remodelling simulations and comparisons with DEXA results. Journal of Orthopaedic research 23: 705-712.

[294] Gupta S, New AMR, Taylor M,. 2006. Bone remodelling inside a cemented resurfaced femoral head. Clinical Biomechanics 21: 594-602.

[295] Scannell PT, Prendergast PJ. 2009. Cortical and interfacial bone changes around a non-cemented hip implant: Simulations using a combined strain/damage remodelling algorithm. Medical Engineering & Physics 31: 477-488.

[296] Geris L, Vandamme K, Naert I, Sloten JV, Duyck J, Oosterwyck HV. 2008. Application of mechanoregulatory models to simulate peri-implant tissue formation in an in vivo bone chamber. Journal of Biomechanics 41: 145-154.

[297] Liu X NG. 2008. Bone ingrowth into a porous coated implant predicted by a mechano-regulatory tissue differentiation algorithm. . Biomechanics and Modeling in Mechanobiology 7: 335-344.

[298] Dopico-Gonzalez C, New AM, Browne M. 2009. Probabilistic finite element analysis of the uncemented hip replacement-effect of femur characterisitcs and implant design. Journal of Biomechanics 43: 512-520.

[299] Dopico-Gonzalez C, New AM, Browne M. 2008. Probabilistic analysis of an uncemented total hip replaceemnt considering implant anteversion. Journal of Biomechanics 41: S434.

[300] Checa-Esteban S, Prendergast P. 2010. Effect of cell seeding and mechanical loading on vascularization and tissue formation inside a scaffold: A mechano-biological model using a lattice approach to simulate cell activity. Journal of Biomechanics 43: 961-968.

9.2 APPENDIX B: MESH CONVERGENCE STUDY – PROXIMA

The tissue differentiation patterns obtained at an intermediate stage of 10 iterations for different mesh combinations (Maximum element size, Minimum element size) shown below. As seen from the figure, the tissues formed across the combinations are comparable.

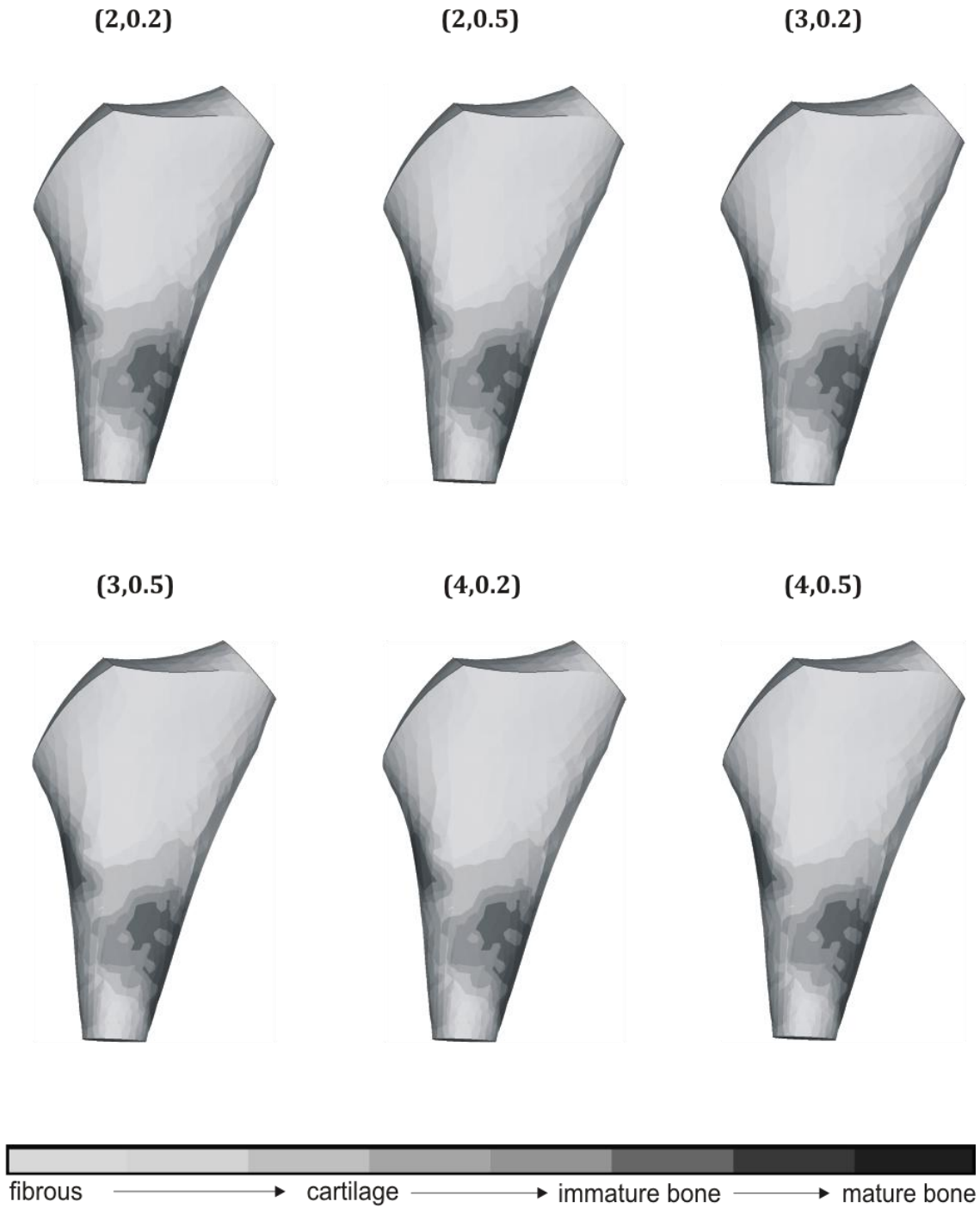

9.3 APPENDIX C: PROXIMA, IPS, AND COMPARISON TO CLINICAL DATA FOR THE DETERMINATION OF K

The metaphyseal loading implants, Proxima (left) and the IPS (right) with the lateral flare marked (arrows). Note that the lateral flare of the Proxima is more pronounced.

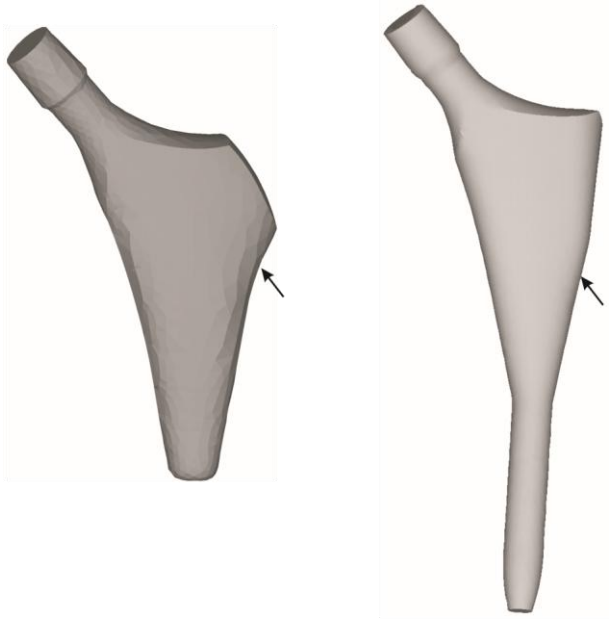

Shown below, the tissue differentiation pattern obtained for the chosen value of K=2 when compared to osseointegration patterns of the IPS reported in literature [237-239]. Note that the arrows denote the regions of bone formation, mostly under the lateral flare on the medial and lateral sides. The results match very well with the radiographic results.

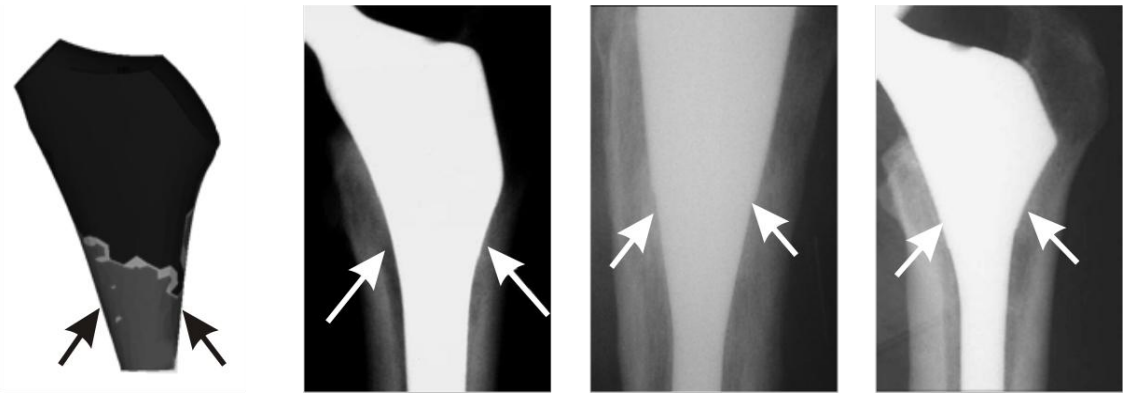

9.4 APPENDIX D: FEMORAL CUT – BONE STRAINS

Length of femur cut from stem tip (mm)	**Maximum principal bone strain (με)**
20	2482
40	2236
60	2189
80	1840
100	1602
120	1324
140	1310
160	1302
180	1290
Complete femur	1281

9.5 APPENDIX E: MESH CONVERGENCE STUDY – AML

The tissue differentiation patterns obtained at an intermediate stage of 10 iterations for different mesh combinations (Maximum element size, Minimum element size) shown below. As seen from the figure, the tissues formed across the combinations are comparable with the exception of the (4, 0.5) combination which demonstrates a slightly different pattern. Considering the tissue thickness of the tissue layer was 0.750mm, the (3, 0.5) combination was found to be apt.

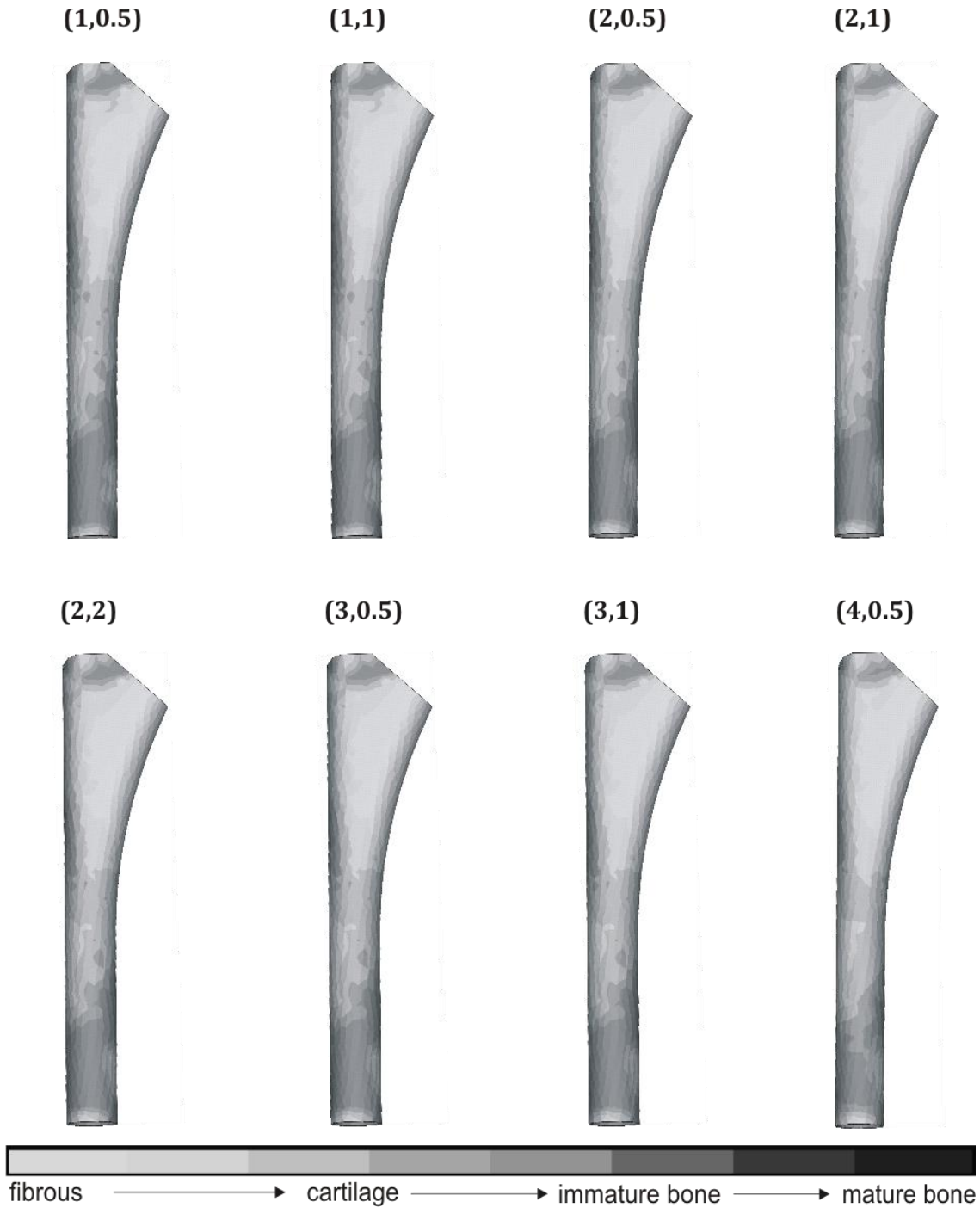

9.6 APPENDIX F: LIST OF PUBLICATIONS

9.6.1 CONFERENCES:

1. Puthumanapully P.K., New A.M., Browne M. (2008) **"Do multi-layer beads on porous coated implants influence bone ingrowth? A finite element study"** the 16th Congress of the European Society of Biomechanics, Lucerne, Switzerland.

2. Puthumanapully P.K., New A.M., Browne M. (2009**) "Osseointegration of a short stemmed femoral prosthesis as predicted by a mechanoregulatory algorithm"** The 55th annual meeting of the Orthopaedic Research Society, Las Vegas, NV.

3. Puthumanapully P.K., New A.M., Browne M. (2009) **"Simulating bone ingrowth in porous coated implants"** Exploring the biological/biomechanics interface. Arup campus, Blythe valley park, Solihull, UK.

4. Puthumanapully P.K., New A.M., Browne M. (2009) **"Do size and shape matter? Osseointegration in a short stemmed femoral prosthesis as predicted by a mechanoregulatory algorithm"** The 22nd Annual Congress of International Society for Technology in Arthroplasty, Big Island, Hawaii.

5. Puthumanapully P.K., Browne M. (2009) **"Predicting bone ingrowth and tissue differentiation around a long stemmed porous coated hip implant using fracture healing principles"** The 22nd Annual Congress of International Society for Technology in Arthroplasty, Big Island, Hawaii.

6. Puthumanapully P.K., New A.M., Browne M. (2010) **"Design influences of a short-stemmed and long-stemmed uncemented implant on tissue differentiation at the interface: A computational study based on a mechanoregulatory hypothesis"** The 9th international symposium of computer methods in biomechanics and biomedical engineering, Valencia, Spain.

9.6.2 JOURNALS:

1. Puthumanapully P.K., New A.M., Browne M. (2008) **"Do multi-layer beads on porous coated implants influence bone ingrowth? A finite element study"** Journal of Biomechanics. Vol 41 (1) S290. 2008.

2. Puthumanapully P.K., Browne M. (2009) **"Tissue differentiation around a short stemmed metaphyseal loading implant employing a modified mechanoregulatory algorithm- a finite element study"** Journal of Orthopaedic Research (In Press).